THE FUNCTION OF FORESTED SWAMPS IN THE BOREAL PLAIN:

climate and storage shape ecohydrological interactions

---

by

ALEXANDER GIDEON HURLEY

A thesis submitted to the University of Birmingham for the degree of
DOCTOR OF PHILOSOPHY

School of Geography, Earth and Environmental Sciences
College of Life & Environmental Sciences
University of Birmingham
November 2019

UNIVERSITY OF
BIRMINGHAM

University of Birmingham Research Archive

e-theses repository

This unpublished thesis/dissertation is copyright of the author and/or third parties. The intellectual property rights of the author or third parties in respect of this work are as defined by The Copyright Designs and Patents Act 1988 or as modified by any successor legislation.

Any use made of information contained in this thesis/dissertation must be in accordance with that legislation and must be properly acknowledged. Further distribution or reproduction in any format is prohibited without the permission of the copyright holder.

Abstract

Swamps can promote hydrologic connectivity in the landscape mosaic of the sub-humid Boreal Plain (BP, west-central Canada). Yet, understanding of processes controlling and interactions arising from their ecohydrologic functioning, and their temporal variability throughout expressed BP climate cycles, is still limited for this drought-prone region. Such understanding is crucial in catchments where the sub-humid climate interacts with the prevalent deep, glacial deposits and vegetation to create extensive unsaturated zones; this gives rise to a tendency of vertical over lateral water flows due to expressed storage-threshold dynamics.

This thesis aimed to assess the capacity of swamps to redistribute water in such catchments, as well as characteristics necessary for and controls thereof under wet, mesic and dry climatic conditions. Further, potential interactions with adjacent systems, *viz.* forest growth along wetland interfaces, were investigated. The swamp was forested (deciduous canopies) and located in an aspen-dominated, mixed-wood headwater catchment within an upland-wetland-pond complex lacking an apparent drainage network, and isolated from larger-scale groundwater flows. As water redistribution is most likely limited to low-storage areas, this setting represents BP landscapes that may be particularly affected by climate warming increasing evapotranspiration ET.

Results showed that low storage and specific yields defined the swamp's ephemeral hydrologic regime, promoting frequent saturation (conducive for) subsurface and surface flows downgradient and to adjacent forests in all but the driest years. These conditions were internally-generated (i.e. required no upland water inputs), beginning in zones of lowest storage capacity at the swamp's upper end. This process was facilitated by dynamic storage-reduction through surface-near ice, as well as ET-limiting mechanisms that maintained high antecedent moisture. In particular, sub-canopy ET,

as the dominant efflux, was controlled by soil-plant-atmosphere feedbacks via soil-physical and structural changes in the deciduous over- and understory. Detailed hydrological assessments of the wetland-upland complex, combined with dendroecological and wood-anatomical analyses, further allowed concluding that the wetland provided groundwater supplements across its interface which modulated effects of hydroclimatic variability for white spruce, and potentially for trembling aspen.

This thesis provides novel understanding of BP swamp ecohydrology, including the first detailed ET assessment of a deciduous system, and highlights swamps as important landscape units. It is hoped that the focus on storage dynamics will inform further BP catchment conceptualizations, and allow landmanagers to direct anthropogenic disturbances away from these key water source areas.

Acknowledgments

I thank Nick Kettridge for his advice and support throughout this endeavor. His insights on scientific reasoning, ecohydrology and navigating a career in science have been highly appreciated as they have been formative. Similarly, Kevin Devito's enthusiasm for and encouragement of pursuing scientific advances in the Boreal Plain have driven me to become a more well-rounded scientist and person, which I am grateful for - the times spent in Canada are thoroughly cherished. Without both of their support, work completed here would not have been possible. Through them, financial support was provided via Natural Environment Research Council studentship funding, Syncrude Canada Ltd and Canadian Natural Resources Ltd (SCL4600100599) and Natural Sciences and Engineering Research Council (NSERC-CRD CRDPJ477235-14). I also thank Stefan Krause, who provided valuable advice, financial and research support in shaping this thesis and my career, notably for arranging training that led to dendroecological analyses presented here. For the latter, I also extend my utmost thanks to Ingo Heinrich for continuous support and encouragement. Rhoswen Leonnard is also thanked for her effort and dedication in showing me the ropes at Birmingham and in the field at URSA.

Numerous other scientists - and friends - have contributed to my thought process, aided in interpretation (or challenged mine), which frequently provided for highly stimulating conversations, as well as many good laughs. To everybody I shared time with in the office (325) and beyond: you have made the last years one of the most enjoyable periods of my life. Danny, Ben, Tanu, Doris, Sijeh, Ruben, Sam, Rhoswen (and all you others) - I will thoroughly miss you. Dan and Richard, thank you for introducing me to dendroecology (and the lab at GFZ). My utmost thanks also go out to my dear friends from various stages of my life, which provided support and encouragement throughout the last 4 years - shared times in Amberg, Bαyreuth and Birmingham have helped in shaping me into a resilient and curious person, as they have provided comic and emotional relief.

This work also provided opportunities to gain experience in supervising undergraduate and masters students for their research projects - thank you for your trust, your hard work, and the countless lessons you taught me. The hours you put in in the field are one reason this thesis was possible, and my utmost thanks go out to all of you. Similarly, all students at the URSA, regardless of what their role, made the time there most memorable, and the shared support shaped the vision I have for future collaborations. To Arynn, who shared every day in the field with me in 2017, and who became a dear friend, I owe more to the completion of this thesis than she will likely know - keeping me sane, challenging my views, sharing laughter; her and her partner were some of the kindest Canadians, which are notoriously kind, I will likely ever meet.

I also enjoyed the opportunities and trust afforded to me by Andrea Popp, Louise Slater and Shaun Harrigan for developing materials on open, reproducible science and sharing them with broad audiences - thank you.

Lastly, I cannot hope to express the extent of gratitude toward my closest support network, my family. Dear Mom, dear Dad, Sister, Brother, Nephew and Stephanie, this work was first and foremost possible through your unconditional support and love. As some of my favorite artists stated:

In this note that I am sending you, I need to show my gratitude. I'm truly indebted to you - thank you for pulling me through. Dear family and friends, I really need to thank you. You were there for me, so I will always be there for you. And this is how I show my gratitude.

– Pete Philly and Perquisite

In loving memory of and dedicated to my father,

Hiram Dale Hurley.

Contents

List of Tables

List of Figures

CHAPTER 1

Introduction

1.1 Rationale

The Boreal Plain (BP), as part of the circumpolar Boreal Forest, is a vital contributor to the global carbon and water cycles (Ireson *et al.*, 2015). Its sub-humid climate with strong inter-annual variability largely controls the frequency and magnitude of water availability (Devito *et al.*, 2012) and thereby determines ecosystem functioning by controlling ecohydrological processes within, and interactions between systems (Hanson *et al.*, 2008). These include, water storage and/or transmission (Spence *et al.*, 2011), biogeochemical processes (Jackson *et al.*, 2009), as well as plant water-use and growth dynamics (Hogg and Bernier, 2005), amongst others.

Several studies focused on the BP predict future warming and drying in the 21^{st} century (see Price *et al.*, 2013 for detailed discussion). The close balance between precipitation and (potential) evapotranspiration potentially entails directional (i.e. sign) as well as magnitude changes of local water balances in the future. Such changes could perturb ecohydrological dynamics within a given system, but, more so, may have especially adverse effects where interactions with downgradient or adjacent systems are impeded, for example, by receiving less water from source systems (Jackson *et al.*, 2009; Cohen *et al.*, 2016; Rains *et al.*, 2016). Ultimately, extensive functional changes could lead to shifts from typical Boreal Forest ecosystems to those resembling drier and less productive ecoregions further south, concurrent with decreased regional water yield (Hogg and Hurdle, 1995; Price *et al.*, 2013; Schneider *et al.*, 2016). This landscape-scale vulnerability is set against the high socio-economic value of (un)managed Boreal Forest landscapes (Kurz *et al.*, 2013; Ireson *et al.*, 2015), concerns of water security in light of increased water demand (Ireson *et al.*, 2015), as well as potential habitat and carbon loss in the BP (Price *et al.*, 2013). Consequently, identifying and assessing mechanisms generating water surplus and/or governing its redistribution, as well as resulting ecohydrological interactions, are ongoing research priorities in the BP (e.g. Devito *et*

al., 2016). In its landscape mosaic, fen and bog peatlands, as well as swamp cover reportedly increase hydrological connectivity and thereby runoff magnitudes (Gibson *et al.*, 2015; Devito *et al.*, 2017). While extensive research on ecohydrological feedbacks allowing water-surplus generation and ultimately connectivity exists for the two former wetland types (see Waddington *et al.*, 2015 for review), swamps have received considerably less attention, particularly in the BP, despite indications of their importance for and ubiquitous presence in Boreal headwater catchments (Buttle *et al.*, 2012) and the BP more widely (DeLancey *et al.*, 2019). This may be, in part, due to higher carbon stocks in peatlands generating more traction in the scientific community in light of climate change, and their typically small size complicating identification at larger scales (e.g. few ha, cf. Creed *et al.*, 2003; Devito *et al.*, 2005a; Locky *et al.*, 2005). Yet, ephemeral systems, such as forested swamps or streams, can constitute a sizable fraction of continental-scale drainage networks (e.g. 59 % combined length for ephemeral wetlands and streams in conterminous U.S, Nadeau and Rains, 2007).

The strong dependence of forested swamps on climate to provide their functioning, i.e. due to their ephemeral nature (Buttle *et al.*, 2012), renders them and dependent landscapes particularly vulnerable to altered hydrometeorological regimes (Cohen *et al.*, 2016). Next to current and future climate change, the BP (and virtually all other Canadian Boreal ecoregions (White *et al.*, 2017)), is subject to intensive disturbance from natural (e.g. Frey *et al.*, 2004), as well as human origin (Pickell *et al.*, 2013). Anthropogenical disturbances follow from land conversion and use (e.g. agriculture and forestry), resource exploitation (in-situ oil and gas extraction, open-pit mining), as well as extensive linear disturbances for exploration and access roads (note, the latter two comprise approximately 600000 km of linear disturbances in the Canadian Boreal Forest Pasher *et al.*, 2013), amongst others (ABMI, 2017). These disturbances can impair ecological, biogeochemical and hydrological functioning of individual areas or entire systems. For example, roads constructed perpendicularly to dominant flow paths

in peatlands have been shown to enhance shrubification and tree encroachment down-gradient (Willier, 2017), with cascading negative effects due to water table drawdown, such as increased fire risk (Wilkinson *et al.*, 2018) and carbon losses (Waddington *et al.*, 2015). Seismic lines cutting through peatlands, i.e. linearly cleared vegetation, can dramatically alter local energy budgets and biogeochemical cycling leading to increased green house gas emissions and altered hydrological dynamics (e.g. through soil compaction and subsidence), as well as affect predator-prey systems, most notably ungulate-wolf interactions (see Dabros *et al.*, 2018 and references therein).
Forested swamps should hence very likely be considered highly vulnerable to anthropogenical disturbance. This is due to their typically limited size, their vegetation cover resembling uplands (e.g. deciduous systems within larger stands of economically viable Trembling Aspen (*Populus tremuloides* [Michx.]) and ephemeral hydrological regimes, where characteristics and/or conditions are less likely to direct land-managers away from forested swamps. Under such circumstances, disturbances can remove entire swamp systems or, when considering ecohydrological dynamics, severely impair hydrologically sensitive areas (Clark *et al.*, 2009) resulting in the loss of e.g. important headwater areas (Devito *et al.*, 2005a).

The focus in this thesis afforded to forested swamps, as systems with ephemeral regimes, hence arises from the potential hydroclimatical sensitivity and vulnerability to disturbance, as well as a lack of coverage in literature, despite repeated implication of swamps as water-generating features in the sub-humid BP. The thesis will address a number of research gaps by contributing to the knowledge base on ecohydrological functioning and interactions on local to catchment-scale across physiographical settings found in the BP. It will thereby also provide implications for land management, as well as reclamation/restoration practices that can capitalize on knowledge of internal and external swamp processes.

1.2 Boreal Plain ecohydrology: a landscape mosaic of sinks and sources

The BP has low topographic local and regional relief, a poorly developed drainage network, and features heterogeneously distributed, glacial deposits comprising 1) fine-textured glaciolacustrine, 2) fine-textured and clay-rich moraine as well as 3) coarser-textured glaciofluvial and glaciolacustrine substrates (Vogwill, 2005; Fenton *et al.*, 2013). Following Devito *et al.* (2005b) and Hokanson *et al.* (2018a), the hydrological functioning of BP catchments can be categorized based on the hydrogeological properties of the three surficial geology types (landforms) above, which broadly control the magnitude and frequency of groundwater-surface water exchange, water table configurations, recharge and dominant flow pathways (Winter, 2001; Devito *et al.*, 2012).

Responses are locally modulated by climatic variability (expressed dry and intermittent wet cycles), topographic position as well as soil stratification and overlying vegetation (Devito *et al.*, 2005b, 2017), which largely determines available water storage capacity (i.e. antecedent moisture) through local evapotranspiration dynamics (Rodriguez-Iturbe, 2000; Carrera-Hernández *et al.*, 2011). BP ecosystems, as distinct landscape units, are hence associated with water source and sink functions (Devito *et al.*, 2012; Ireson *et al.*, 2015).

1.2.1 Forested uplands

The interacting effects of surficial geology (glacial substrate type) and overlying vegetation are readily illustrated by comparing forests on fine-grained moraine and coarse-grained glaciofluvial deposits (Ireson *et al.*, 2015; Devito *et al.*, 2017). The hummocky terrain of the former typically features aspen-dominated stands with high transpiration rates (Barr *et al.*, 2012); combined with the steeper local relief, storage capacities are

large and deep unsaturated zones frequently develop and are maintained through all but the wettest climate cycles (Redding and Devito, 2008; Devito *et al.*, 2012). On coarse-grained glacial landforms, hydropedological and hydrogeological properties allow for greater recharge and deeper water tables to which rooting networks typically lack access; this reduces vegetation water use and hence forests may act as regional water sources (Smerdon *et al.*, 2008; Devito *et al.*, 2017).

1.2.2 Wetlands

Wetlands feature surface-near or above-ground water tables equating to low soil or depression storage, which can cause rapid responses to water inputs (Keddy, 2010). However, open-water wetlands act as "evaporation windows" by directly exposing water to the atmosphere; evaporative losses can be exacerbated as these systems often form where the surface intersects larger-scale groundwater flow systems and hence catchment and regional runoff generation are drastically reduced (Smerdon *et al.*, 2005; Devito *et al.*, 2017). Contrastingly, swamp, fen and bog cover reportedly increases runoff by generating sub-surface or surface flow within and between individual landscape units (Spence *et al.*, 2011; Gibson *et al.*, 2015; Devito *et al.*, 2017)

1.2.3 Wetland-upland interfaces

Wetland-upland interfaces show dynamic spatial extent and variable process magnitudes (transport of matter and energy) in relation to wetland center water tables (Devito *et al.*, 1989, 1996; Waddington *et al.*, 2015; Hokanson *et al.*, 2018b), and are notably sensitive to wildfire disturbance (Lukenbach *et al.*, 2017). They typically feature distinct vegetation communities, such as "lagg" ecotones for bogs, which are defined by soil stratification, water table and soil moisture dynamics, as well as nutrient availability (Langlois *et al.*, 2015; Paradis *et al.*, 2015; Mayner *et al.*, 2018). Studies

in the BP indicate that saturated and unsaturated flow from wetlands to uplands can occur where storage contrasts across interfaces are large enough, resulting in water table configurations that mirror local topography (Taylor and Pierson, 1985; Devito *et al.*, 1997; Wells *et al.*, 2017); this may be exacerbated by transpiration of upland trees along interfaces, which can draw groundwater tables down further and locally increase (unsaturated) hydraulic gradients (Winter, 2001; Riddell, 2008). Multiple BP studies report potential for forested uplands to sustain transpiration of canopy and sub-canopy vegetation via water supplementation under such conditions (Snedden, 2013a; Brown *et al.*, 2014a; Petrone *et al.*, 2014), and recent work on tree water sources along a wetland-upland hillslope complex indicates root-mediated water redistribution across interfaces to individual trees higher upslope (Depante *et al.*, 2019). Increased moisture availability can also lead to altered (soil) micro-climates which may benefit growth of forest stands along interfaces due to a buffering against heat stress where groundwater has a cooling effect, or allow for greater root activity earlier in the season when groundwater temperatures are above those of soils (Raney *et al.*, 2016).

1.3 Research Gaps on forested swamps

The above clearly shows that local and regional hydrology is shaped by, and in turn affects, the spatial distribution and ecohydrological functioning of individual landscape units. In particular, the arrangement, absolute and relative cover and type of wetland is crucial in determining hydrological connectivity as a sum of local ecohydrological processes and interactions (Devito *et al.*, 2012). This mechanistic understanding (ecohydrological processes, feedbacks and interactions) is still largely lacking for BP forested swamps, i.e. systems where water tables appear periodically and contributions from other (groundwater) flow systems are mostly absent (ephemeral hydrological regime, Buttle *et al.*, 2012). This may be due to their transient character regarding water

surplus generation and transmission, and often considerably smaller size hindering detection and delineation as distinct landscape features (Creed *et al.*, 2003; Dalu *et al.*, 2016), especially where canopy structure and phenology are similar to adjacent systems (i.e. deciduous / coniferous). In addition, swamps feature considerably lower carbon stocks compared to e.g. bog and fen peatlands, which may attract less attention from the scientific community. Given their typically limited extent (e.g. 0.5 *ha* here, 2.6 *ha* in Devito *et al.*, 2005a), such systems are also referred to as small, forested wetlands here. The heterogeneous glacial deposits, low relief and sub-humid climate (in conjunction with evapotranspiration) result in diffuse valley-hillslope connectivity and a propensity for vertical over lateral flow (Devito *et al.*, 2005b; Klaus *et al.*, 2015) in BP landscapes, calling for detailed assessments of local to catchment-scale dynamics and interactions across the range of prevalent physiographical settings.

Work by Devito *et al.* (2005a) on runoff generation in aspen-forested catchments on hummocky till deposits in the BP highlighted small, forested swamps as dominant areas of surplus generation, promoting connectivity along wetland-upland complexes. They note, however, that complex surface and groundwater dynamics between wetlands and uplands, as well as the role of soil stratification (modified by soil frost) require additional attention. Further, BP climate cycles determine available water storage capacity along wetland-upland complexes (Devito *et al.*, 2012); how swamp ecohydrological functioning behaves under different stages of these cycles (wet, dry, mesic) in the long-term remains a prominent gap.

In light of the above, as well as detailed assessments of literature in Chapters 2 through 5, four broad research gaps were identified; these arise either do to a lack of coverage of specific physiographical settings within the BP and/or from gaps in understanding of ecohydrological processes, their dynamics and interactions in low-relief, sub-humid landscapes; a notable, recurrent theme is available water storage capacity. The identified gaps are as follows:

1. **Role of heterogeneous distribution and temporal dynamics of available storage for generating downgradient and lateral flows in swamp wetland-upland systems**. The mechanisms allowing forested swamps with ephemeral regimes to contribute to catchment and regional runoff, as well as generate lateral flows to adjacent uplands have not been addressed extensively in the BP. Hence it is not clear whether reported increases in regional water yield arise via internal processes alone, or depend on external inputs. Process-based understanding of swamp ecohydrology in its local and catchment context is especially required for extending and/or developing landscape conceptualization in areas (i.e. glacial landforms) where runoff is low and highly variable. (Chapter 2)

2. **Interaction of climate, vegetation and storage capacity in shaping hydrological regime**. The relationships between vegetation and atmospheric water demand as well as available and absolute storage capacity have not been assessed in deciduous swamps under sub-humid climates. Assessments of the intra- and inter-annual variability of evapotranspiration in relation to storage (soil layering) are a key requirement for determining antecedent moisture and are a priority for accurately estimating the partitioning of precipitation into other components (lateral flow / runoff). (Chapter 3)

3. **Controls on and feedbacks within dominant water flux pathways**. Evapotranspiration (ET) is the dominant water flux from northern wetlands, especially when lacking well-defined drainage networks (Waddington *et al.*, 2015). The role of sub-canopy vegetation in driving water losses in BP swamps, and particularly deciduous systems, has not been assessed, and it is hence not clear whether they exhibit similar ET-reducing feedbacks as do moss-dominated peatlands. Understanding of the flux-partitioning, as well as identification of soil-plant-atmosphere relationships will aid enhancing landscape concepts and allow the inclusion of swamps in process-based modelling exercises. (Chapter 4)

4. **Impact of wetland-forested upland interactions on tree growth**. The modulating effect of water supplementation on tree growth has not been assessed in wetland-upland forest complexes in the Boreal Plain, despite indication of water transport and access for trembling aspen. Knowledge of growth/productivity dynamics for dominant tree species in relation to climate, landscape position and composition (i.e. wetland vs. upland) will inform land management (e.g. selective harvesting) and can potentially aid restoration planning. (Chapter 5)

1.4 Aims

This thesis set out to generate novel understanding of ecohydrological processes and interactions that could be a) translated and applied in other climatically and geologically similar regions, and b) allow informing and improving landscape conceptualizations within the Boreal Plain to aid in current as well as future land management, and by extension also ongoing restoration efforts. The specific **aims** were to assess the functioning (with respect to water surplus and flow generation) of forested swamps with ephemeral hydrological regimes under current climatic conditions and within a specific physiographical setting that promoted generalization and process-identification, and to assess whether these functions result in verifiable impact on other systems (locally) and/or have implications at or beyond that scale (local to regional). The following objectives were pursued to address the identified research gaps (Section 1.3):

1. Assess the capacity, frequency and processes which potentially allow forested swamps to act as water sources that connect disjunct units in headwater catchments through climatic cycles, and identify dominant attributes that allow for this functioning. (Chapter 2)

2. Determine the interacting effects of available storage (dominant attribute) and ecosystem water use (major water loss pathway) on the hydrological regime of a

forested swamp (Chapter 3)

3. Assess in detail the temporal dynamics of the largest water efflux (sub-canopy ET) and elucidate whether feedbacks identified for peatlands exist in a similar fashion within the soil-plant-atmosphere continuum. (Chapter 4)

4. Identify whether climate-growth dynamics of dominant upland tree species differ with respect to hydrological position along a hillslope with and without access to groundwater supplementation from a swamp. (Chapter 5)

1.5 General approach and thesis structure

A small, exemplary swamp in an intensively instrumented catchment was the main subject of study; it was ideally situated in a regional high where previous work indicated that larger flow systems were unlikely to drive or influence hydrological dynamics, and its location on a transition between glacial landforms allowed for assessing the effects of contrasting (available) storage capacity. The general approach adopted here relied on combining (long-term) environmental data from various sources, as well as *in-situ* eco-physiological, wood-anatomical (tree growth) and hydropedological data to generate novel understanding of swamp ecohydrology in the BP. Empirical and numerical methods were both applied to allow integrating the individual soil-plant-atmosphere processes and their functioning.

The thesis is structured in three main sections, comprising a broad introductory, four original research chapters, followed by one synthesis chapter. The research chapters are presented in paper-style, as self-contained studies reviewing literature pertinent to address main and study-specific aims, an overview of materials and methods, as well as results and discussion thereof. The synthesis chapter summarizes main findings, and discusses broader implications and outlines avenues for further research. Fig. 1.1 shows the structure and relationships between individual chapters, as well as their main topics

of concern.

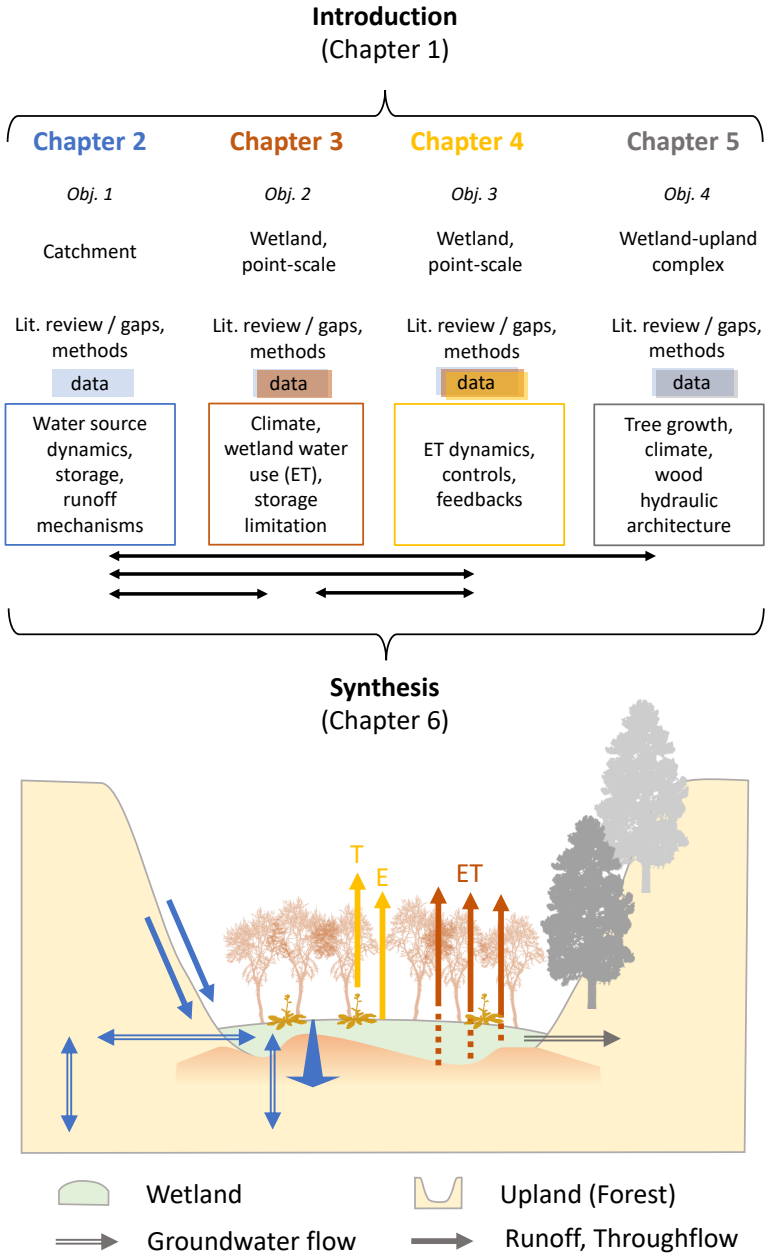

Figure 1.1: Structure of thesis and results chapters (top), relating chapters to each other (black arrows and braces), and relating back to objectives, giving a reference frame (scale of concern, e.g. "catchment"), data (color represents overlap between chapters) and main topics. The diagram (bottom) shows a hillslope-wetland complex (downgradient runoff indicated by perspective on arrow for surface runoff) as well as flows and/or main objects of investigation for each chapter, with colors matching the schema above. (Plant pictograms sourced from phylopic.org and onlygfx.com)

CHAPTER 2

Dynamic storage and connectivity in small, forested wetlands impact runoff in low-relief, aspen-dominated catchments of the sub-humid Boreal Plains

2.1 Abstract

hydrological connectivity in the sub-humid, low-relief Boreal Plain (BP) is largely controlled by storage-threshold dynamics where glacial deposits with high storage capacities exist. Vertical fluxes generally dominate over runoff, which can have return periods of several years to decades. In this landscape, shallow, forested wetlands of small spatial extent that are embedded in a matrix of high-storage, forested uplands were identified. Despite multi-year water deficits and high atmospheric demand coinciding with most of the annual precipitation, these wetlands - unlike uplands - must frequently saturate to be maintained. It was hypothesized that these systems promote lateral water redistribution to other landscape units as runoff downslope, or via subsurface flow to adjacent uplands, and hence may be key for maintaining the ecohydrological functioning of BP catchments. Multiple conceptual models of the potential functioning of these wetlands were drawn upon to identify the primary process that induces saturation, connectivity and runoff generation. Within an exemplary (typical configuration, size and lack of extensive disturbances), isolated and permanently perched catchment comprising a terminal pond, aspen-dominated uplands and a small ($< 1\ ha$) forested wetland (swamp), deep and shallow groundwater dynamics, as well as surface runoff from the wetland for a period covering wet, mesic and dry conditions (2005 - 2018) were assessed. This was done in conjunction with detailed measurements of soil stratigraphy ($n > 120$ locations) and texture within the wetland and across the interface to adjacent forests.

It was found that internally-generated saturation (i.e. precipitation-fed) was the primary process generating runoff. Neither extensive hillslope contributions (via infiltration excess, development of transient water tables or ridging at the slope base), nor a rise of deeper groundwater ("priming" for saturation excess) were observed. The proximity of a shallow, low-permeability clay layer was the main control on storage, saturated area formation and groundwater interaction. This layer rapidly increased

in depth toward uplands. Where wetland soils were only between 30 to 50 *cm* thick above clay, successive precipitation events of 10 to 15 *mm* across few days (typical for convective summer storms) satisfied storage. The highly variable distribution of (available) storage resulted in dynamic connectivity between individual areas, and at times the entire wetland, and was therefore the main control on frequency and magnitude of runoff responses. Hence, extent and geometry of saturated areas that effectively contributed and transmitted lateral flows downslope were fundamentally determined by climate as well as vegetation-controlled antecedent moisture and the largest available (i.e. limiting) storage along flow paths. This work increases understanding of runoff processes and hydrological connectivity across the physiographical range of the Boreal Plain, and highlights the capacity of low-storage systems (such as forested swamps), to provide and maintain functioning even under (future) dry conditions.

2.2 Introduction

Runoff (R), its generating mechanisms and dynamics are less-well assessed in low-relief, glaciated and sub-humid regions as compared to steeper, more humid ones (Buttle *et al.*, 2009; Bachmair and Weiler, 2011; Klaus *et al.*, 2015). Under sub-humid climates, precipitation (P) and evapotranspiration (ET) approximate each other, typically leading to a dominance of vertical over lateral fluxes (Grayson *et al.*, 1997), especially where catchments are subject to storage thresholds (Spence, 2010; Ali *et al.*, 2011) between water source and R-generating areas (i.e. across hillslope-valley-stream complex). Annual and seasonal climatic variability regularly shifts water balances into surplus or deficit, and thereby affects - and can reverse - vertical and lateral hydrological gradients (Winter, 1999; Jackson *et al.*, 2009). Consequently, R can span multiple orders of magnitude within and between years (e.g. Devito *et al.*, 2017).

This variability is set against increasing socio-economic dependence on resource and service provisioning by ecosystems that rely on water (Immerzeel and Bierkens, 2012; Falkenmark, 2013), and a sensitivity to changing climates given the close balance of $P - ET$ (Jackson *et al.*, 2009; Ireson *et al.*, 2015), potentially altering landcover distribution and thereby ecohydrology of landscapes. There is hence a need to better characterize the hydrological functioning of low-relief, sub-humid regions across a range of physiographical and hydro-climatic settings, with a focus on properties that influence storage-release dynamics (McNamara *et al.*, 2011) of catchments.

The Boreal Plains (BP), as part Canada's Boreal Forest, represents one such region, that supports a range of biodiversity and contributes to global carbon as well as water cycles; it will experience drastic shifts in future hydro-climatic regimes (Ireson *et al.*, 2015). Increasing land-use from agriculture, industrial operations and resource exploration/extraction both threaten as well as demand space and water security at present and in the near future (Rooney *et al.*, 2015). The BP is (1) set atop thick (45

to 240 m), heterogeneous and stratified glacial deposits ranging from finer glaciolacustrine and moraine to glaciofluvial substrates (Vogwill, 2005), (2) features varying, yet low, degrees of drainage network integration, and (3) displays a range of interaction between local to regional groundwater systems (Devito *et al.*, 2005b; Smerdon *et al.*, 2008; Thompson *et al.*, 2015a) and hydrological connectivity between hillslopes and valley bottoms (Devito *et al.*, 2005a; Redding and Devito, 2008). The identification and assessment of runoff and its generating processes for a number of physiographical settings - and perhaps most importantly - their conceptual application to other regions is therefore possible. Contrasting and spatially variable storage capacities within and between catchments are often encountered as a result of recurring deposition and subsequent reworking of sediments (e.g. Fenton *et al.*, 2005). To a large degree this variability controls the distribution of hydrological units (*sensu* Devito *et al.*, 2005a): a mosaic of upland forests, wetlands and open water bodies. Resulting source and sink functions of BP catchments are fundamentally represented by these landscape units (Barr *et al.*, 2012; Hokanson *et al.*, 2018a), and hydrological responses (i.e. R) strongly contrast between wetland and aspen-dominated catchments of higher ET demand (Brown *et al.*, 2014b; Devito *et al.*, 2017).

On regional scales across the BP, wetland cover (peatlands and swamps) increases runoff coefficients (Barr *et al.*, 2012; Gibson *et al.*, 2015; Devito *et al.*, 2017). Recent work focused on R generation from wetland (dominated) basins in landscape positions and configurations allowing permanent groundwater and/or upland contributions to either decrease available storage (promoting R) or supplement R directly (Wells *et al.*, 2017; Goodbrand *et al.*, 2018). However, aspen-dominated catchments typically develop atop finer-grained substrates such as found in hummocky landscapes - a frequent glacial landform in the BP (Fenton *et al.*, 2013) - formed by stagnant ice moraines (Eyles *et al.*, 1999). These feature high storage capacities due to their texture, topography and vegetation water-use interacting, which can exceed net atmospheric inputs

during a given year. This can frequently prevent hillslope-valley connectivity (subsurface and surface), explaining larger variability in R magnitude and frequency from aspen hillslopes (Redding and Devito, 2008) and aspen-dominated catchments (Devito *et al.*, 2005a).

Variability of storage in catchments can generate hydrologically active areas where capacities are lowest (Phillips *et al.*, 2011). Where topography and soil stratigraphy permit (Meerveld and McDonnell, 2006; Ali *et al.*, 2011), these areas may connect and contribute to R at the catchment outflow, more frequently than hillslopes with greater storage do. These low-storage areas are typically found in topographic lows (i.e. valley bottoms, e.g. Devito *et al.*, 2005a), either where finer sediments accumulated, or through variations in the depth of coarser materials atop finer, confining strata.

In aspen-dominated (i.e. hummocky-moraine) and coarser hydrological response areas (typically pine-dominated) (Devito *et al.*, 2005b; Hokanson *et al.*, 2018a), low-storage areas typically represent small, forested wetlands with deciduous canopies (e.g. Devito *et al.*, 2005a). These wetlands and their role in generating R in aspen-dominated catchments are still underrepresented in literature, likely due to their limited extent and similar phenology to adjacent uplands (i.e. 'cryptic wetlands', Creed *et al.*, 2003). Devito *et al.* (2005a) identified the extent of surface saturated areas in low-storage zones (wetlands, ephemeral draws) as a dominant control on R generation across four years in an aspen-forested catchment. They further highlighted the complexity of hillslope-valley interactions in contributing groundwater to these based on water table dynamics across one summer. Here, the aim is to extend their work by assessing the frequency and magnitude of R in an aspen-dominated catchment with exemplary characteristics, i.e. a valley-bottom wetland, high water storage capacities in adjacent uplands, and few linear disturbances typical for the Boreal Plain (access roads, seismic lines). In particular, the heterogeneous storage distribution within the catchment was determined and the roles of climate variability (on seasonal to multi-decadal

scales) and soil stratigraphy in dynamically controlling saturated area development and connectivity between hillslopes and valleys, as well as between shallow and deeper (i.e. regional) groundwater were identified.

Klaus *et al.* (2015) noted the difficulties of identifying and quantifying water source for R in low-relief, forested catchments due to complex interactions of groundwater flow systems (Winter, 1999). Hence, a regionally perched catchment on a topographic high (Hokanson *et al.*, 2018a) in the Utikuma Region Study Area (Devito *et al.*, 2016) was chosen, under the assumption that this would make process identification more feasible. The experimental design and analyses were informed by a set of working hypotheses based on previously identified R generating mechanisms in other low-relief, stratified and/or sub-humid regions depicted and described in Fig. 2.1.

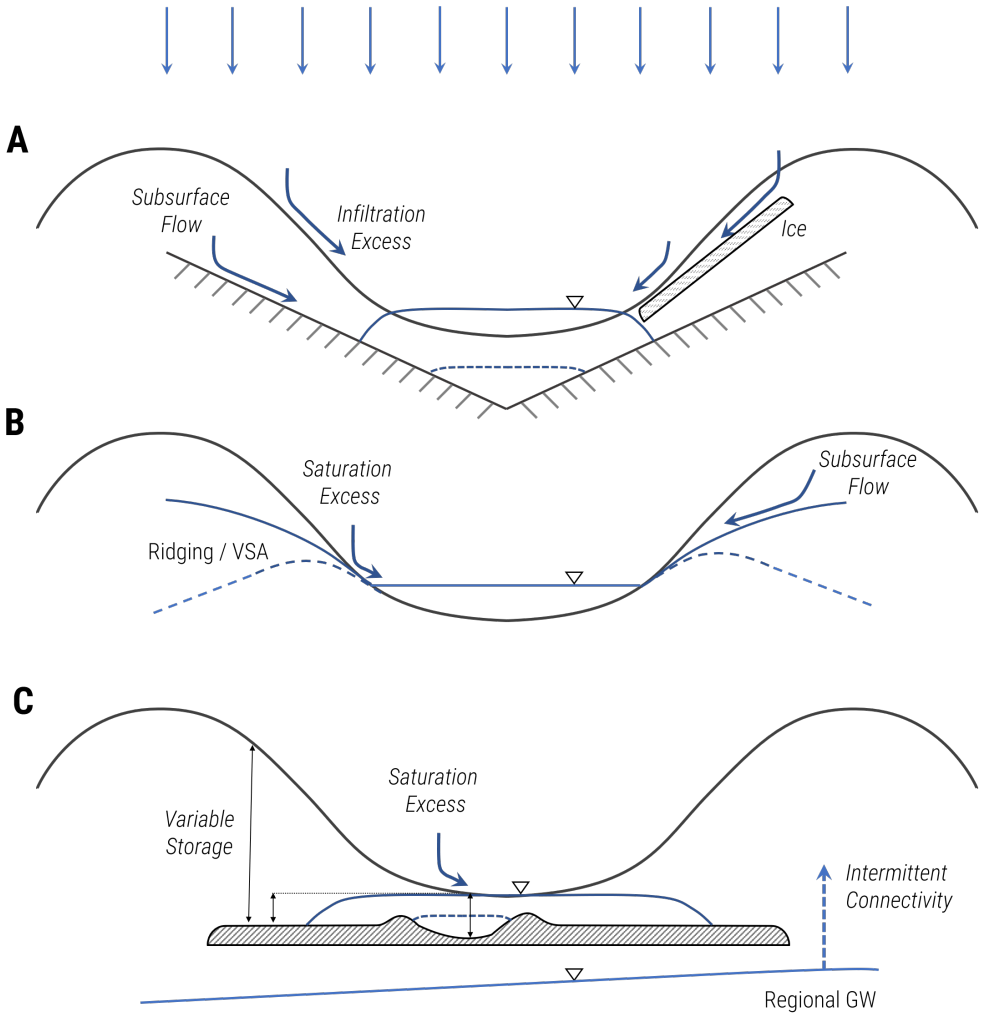

Figure 2.1: Overview of mechanisms promoting surface saturation and/or resulting in lateral flow directly in relation to water tables before (dashed) and after precipitation (solid) in a hillslope-valley complex; note, for the sake of visualization, regional groundwater in C is in solid and dynamics are indicated by a dashed arrow. A) depicts processes of hillslope contributions in stratified systems over bed-rock (Spence and Woo, 2003) or along soil conductivity contrasts (organic vs. mineral layer; Wells *et al.*, 2017), and/or ice (Hayashi *et al.*, 1998; Carey and Woo, 2001a), as well as infiltration excess due to soil properties or ice (e.g. Hayashi *et al.*, 1998). B) shows dynamics of the variable source area (VSA) concept (Hewlett and Hibbert, 1967; McDonnell, 2003), as well as lateral flow contributions from (transient) water tables (e.g. Goodbrand *et al.*, 2018). C) indicates interactions with larger-scale groundwater flow systems (Winter, 1999) and their capacity to saturate and "prime" the valley for R generation, as well as the role of storage heterogeneity in (represented through absolute storage depth) in locally promoting saturation (e.g. Ali *et al.*, 2011; Devito *et al.*, 2005a; Phillips *et al.*, 2011).

It is hoped that this work will 1) shed additional light on the capacity (frequency, magnitude) of aspen-dominated catchments to generate downslope/downstream R (important for water security and potentially ecosystem resilience, 2) highlight the importance storage heterogeneity (represented by small, forested wetlands) and variability for R generation in low-relief landscapes, and 3) add to and contextualize conceptual

understanding of BP runoff dynamics across physiographical and hydro-meteorological settings.

2.3 Materials and methods

Data was collected at variable time intervals (depending on measurement type) between 1999 and 2018 as part of ongoing research in the Utikuma Region Study Area (URSA; Devito *et al.*, 2016). Hydrological, (micro-)meteorological and pedological surveying was focused in two intensive periods between 2004 to 2009 and 2013 to 2018 for this study; key sites were surveyed at least once per year in late July.

2.3.1 Study area

The wetland is around 0.5 *ha* large and situated in the lower end of a predominantly forested (ca. 95 %) headwater catchment (11.9 *ha*) extending south. It is located at 56.081432N, -115.537168W, around 400 km north of Edmonton (Alberta, Canada) in the low-relief, sub-humid Western Boreal Plains (mixed-wood ecoregion; Fig. 2.2).

Here, potential evapotranspiration (pET, 517 mm; Bothe and Abraham, 1993) generally exceeds precipitation (P, 481 *mm*; Marshall *et al.*, 1999) on annual basis; actual evapotranspiration varies with landcover and available storage (Devito *et al.*, 2016). High inter-annual variability leads to accumulation of multi-year moisture deficits, which are compensated during wet cycles approximately every 10 to 15 years (Mwale *et al.*, 2009).

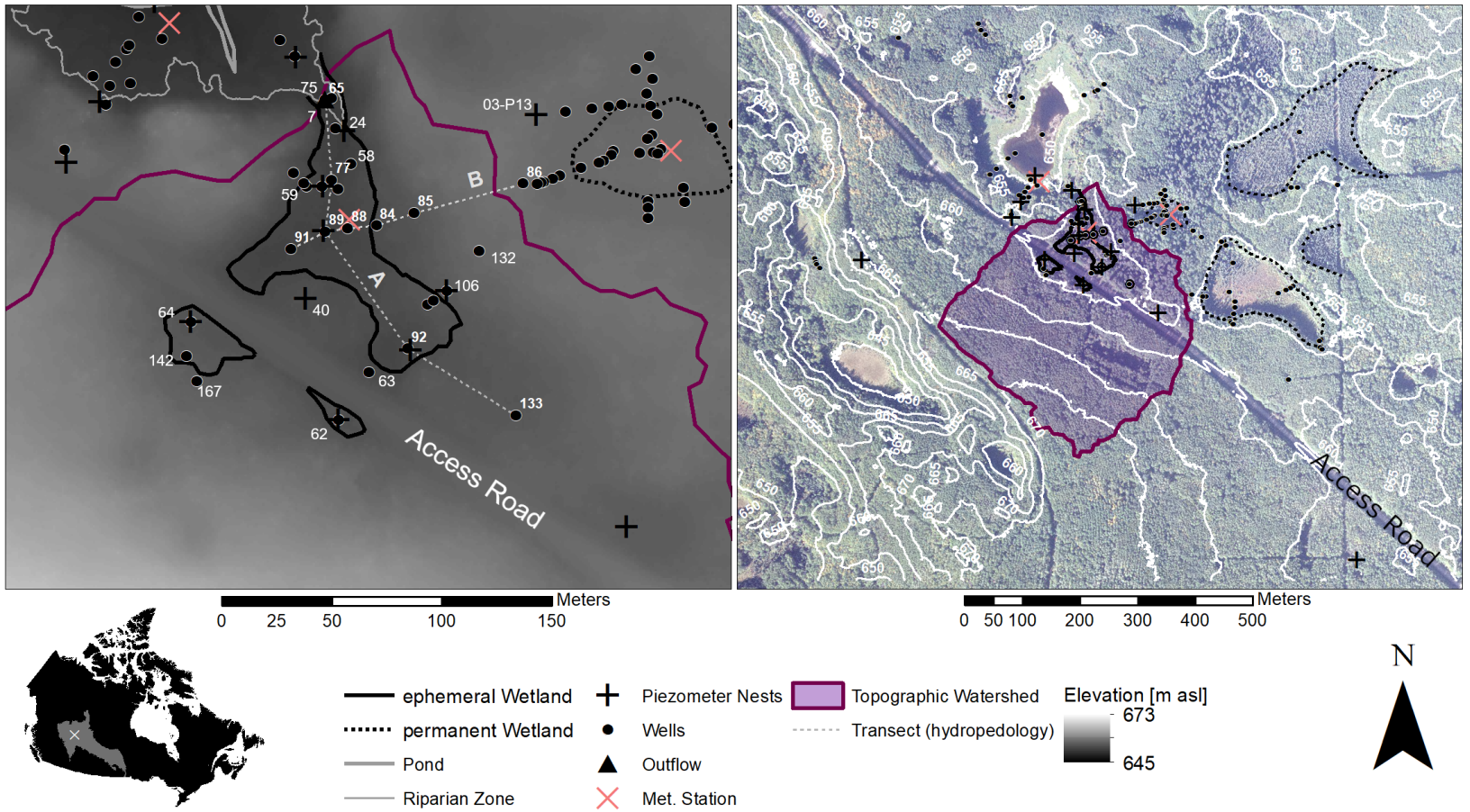

Figure 2.2: Overview of study site (a) and wider landscape (b), and the study site's regional context (c) within Canada and the Boreal Plains ecozone (grey). Two main transects (A, B; in a) were chosen to illustrate site characteristics and hydrological dynamics within the wetland and across its interface. Note, the wetland's extent in comparison to the topographic watershed (b), consisting predominantly of forested upland. The wetland's vegetation is markedly similar to its immediate surroundings (i.e. deciduous, broadleaf). Due to this, and the small extent, wetlands as such may be difficult to identify, rendering them 'cryptic'. Channelized drainage networks are virtually absent in the area.

The wetland lies on a transition zone between fine-grained sediments from a stagnant ice moraine and coarser glaciofluvial deposits (Fenton *et al.*, 2005), where shallow, perched groundwater systems prevail (Hokanson *et al.*, 2018a). It formed in a local, topographic low atop a surface-near, low-permeability confining layer (CL; approximately 0.30 to 0.80 m deep) of clay and silty clay (results sections 2.4.3 and 2.4.5.3 for details and cross sections). Sloping north (approximately 2 %), it intermittently discharges into a pond or its riparian area (dependent on stage); flows are typically non-erosive, but the catchment's outflow is situated at the beginning of a vegetated beaver channel, connecting the wetland to the pond at high stages. An industrial gravel road cut through the southern ends of the wetland and, due to the roads mounding, created ditch-like depressions that can briefly feature standing water after snow melt.

Hollows (with CL depth $\leq 0.30\ m$) are typically only covered by ferns, moss and/or (leaf) litter; areas of greater CL depth have dense sub-canopy growth with shrub and herb layers consisting of red-osier dogwood *(Cornus sericea* L.), low-bush cranberry (*Viburnum edule* [Michx.] Raf.), prickly rose (*Rosa acicularis*), stinging nettle (*Urtica dioica* L.), as well as grasses (*Poaceae*) and are dominated by river alder (*Alnus incana* subsp. *tenuifolia* [Nutt.]), willow (*Salix* spp.) and paper birch (*Betula papyrifera* Marshall). Sparsely distributed hummocks with largest CL depth (within the wetland's bounds) can feature trembling aspen (*Populus tremuloides* Michx.) or white spruce (*Picea glauca* [Moench] Voss) with similar sub-canopy communities. Tab. 2.1 shows stem densities of the forested wetland. Aspen-dominated, mixed-wood forests on luvisolic soils (Soil Classification Working Group, 1998) atop silt and loam deposits of several meters cover adjacent uplands. The wetland was classed as a flat swamp (NWWG, 1997) based on dominant vegetation, soil characteristics (mainly humisols, humic gleysols at greater CL depths; Soil Classification Working Group, 1998) and hydro-regime. For purposes of this study it is referred to as a small, forested wetland.

Table 2.1: Stem density of dominant tree species in wetland estimated from 5 mensuration plots ($10 \cdot 10\ m^2$).

Species	**Common**	$stems \cdot ha^{-1}$
Alnus incana subsp. *tenuifolia*	River Alder	1600
Salix spp.	Willow spp.	1200
Betula papyrifera	Paper Birch	960
Picea glauca	White Spruce	360
Populus tremuloides	Trembling Aspen	200

2.3.2 Micrometeorological data

Air temperature (2 m, Hobo U23-001) and P (tipping buckets, Onset Model RG2m) were recorded continuously at two meteorological stations (outside wetland, Fig. 2.2). With a set of additional hand gauges, P measurements were cross-referenced for quality control. Data were supplemented with measurements from nearby URSA sites (Devito *et al.*, 2016), establishing a record from 1999 to 2018, and further validated against data from the Canadian departments of Environment as well as Agriculture and Forestry (stations in Red Earth Creek, 70 km north; and Peavine, 50 km south-west). Snow water equivalent was estimated as the sum of winter precipitation occurring below $2°C$ air temperature (at 2 m). A third meteorological station within the wetland recorded climate data from 2014 to 2018, and additional hand gauges ($n = 28$) were used to establish throughfall depths; these data are not reported here.

2.3.2.1 Estimation of pET

Daily pET was calculated based on Hamon's method (after Lu *et al.*, 2005) as below, and summed to annual totals:

$$pET \ = \ 0.1651 \cdot \frac{L_d}{12} \cdot k \cdot 216.7 \cdot \frac{e_s}{T + 273.3} \tag{2.1}$$

Where k is a calibration coefficient ($k = 1$ here), L_d is day length (hours) and T is the monthly, mean air temperature ($^{\circ}C$). The monthly, mean saturation vapor pressure e_s (mb) is defined as:

$$e_s = 6.1078 \cdot \exp\left(\frac{17.26939 \cdot T}{T + 238.3}\right) \tag{2.2}$$

2.3.3 Hydrological and hydro-pedological measurements

2.3.3.1 Groundwater

A network of 133 polyvinyl-chloride (PVC) wells (ID = 0.051 m, fully screened) and 108 piezometers (ID = 0.025 - 0.051 m, screen lengths 0.2 to 2 m) were installed in the wider area, covering different topographic positions within the wetland and adjacent uplands (as well as other wetland systems), with some up to 28 m deep intersecting regional groundwater. Two well transects (A, B; Fig. 2.2) are used to illustrate the role of topography, surficial geology and water table dynamics in surface runoff generation. Data from additional sites (i.e. wells or piezometers) are used to elucidate interactions (vertical, lateral) between shallow and deeper groundwater systems.

Boreholes were drilled either manually with hand or power-drill augers, or with a drill rig and solid-stem augers. Screened pipe sections were wrapped in well sock. Borehole annuli were filled with sand for screened intervals and then bentonite chips and parent material to the surface. Detailed borehole logs (visual description, texture) were kept for each location and sub-samples were used to determine grain size distributions with a Micrometrics Corporation Sedigraph 5100; coarser grain sizes were measured via sieving. Slug tests were done in 20 piezometers (18 mineral, 2 organic soils) covering dominant soil texture types (i.e. silts, clays and peat) after Hvorslev (1951) by Riddell (2008).

Wells and piezometers were surveyed using a Leica NA720 to establish a datum above sea level and water levels were measured manually with a Solinst TLC Model 107 at variable intervals (event-based or bi-weekly during growing seasons, longer intervals for remaining periods) and depending on sampling year. Depths of solid ice were assessed with steel rods in three locations around wells or piezometers (up to a depth of around 0.40 m) and supplemented with ice depths recorded within them. Pressure transducers (Hobo U20-001-02, Solinst Black/Gold Levelloggers, Solinst Barologgers) were installed in key wells in upper, middle and lower (i.e. outflow) areas of the wetland, as well as in one hillslope well to establish continuous water level records; temporal coverage varies between 13 to 3 years.

2.3.3.2 Surface water

Discharge (Q, ls^{-1}) was estimated by averaging repeated measurements of volume increase over time in a graded cylinder in a natural confinement (beginning of beaver-dug channel) at the wetland's outflow. A stage-discharge relationship between these and manual water level measurements from outflow sites (65, 75) was used to estimate surface runoff (R) from continuous records in the same sites. The relationship was based on a power equation and its parameters were estimated using a non-linear least squares regression in `R` (R Core Team, 2018); it took the form of:

$$Q = a \cdot exp(b \cdot WL_{65}) \tag{2.3}$$

were Q is discharge (ls^{-1}), $a = 8.36 \cdot 10^{-16}$ (ls^{-1}), $b = 36.51$ (m^{-1}) and WL_{65} the level at site 65 (m, adjusted by 650). Q measurements did not coincide with highest water tables; due to the exponential base, Q estimates were unrealistically high at upper water level ranges. A well-defined P event was chosen, totaling 81 mm over 3 days in 2005 (including largest P event of 68 mm on record), and (1) the total water volume the wetland received was estimated, (2) a runoff coefficient of $R/P = 1$ for the

subsequent 7 days of observed discharge (based on above-groundwater levels) assumed, and (3) corresponding average discharge rate was calculated. This rate was used to constrain the stage-discharge relationship. R was then calculated for the topographic catchment and wetland area.

2.3.4 Assessment of subsurface stratigraphy

The subsurface stratigraphy was assessed at 127 locations with two methods depending on expected CL depth: 1) augering and manual texture analyses for greater depths (e.g. wetland-upland interface, uplands); 2) steel rod penetration until refusal within the wetland. All locations were surveyed alongside groundwater monitoring wells and georeferenced.

Point-based elevation of the CL ($m\ asl$) was set by subtracting measured depths from a LiDAR-derived DEM (1 m resolution). A smooth surface was then interpolated using ArcMap 10.4 Geospatial Analyst, where parameters were adjusted to ensure good fit and conformity with assumptions of the empirical semivariogram function. A raster of CL depths (DTC) was then calculated as the difference between surface DEM and interpolated CL elevation.

2.3.5 Storage estimation and surface saturated areas

Water storage capacity (in equivalent water depth) was estimated spatially-explicit as the product of DTC (1 m resolution) and effective porosity ($n_e = 0.2$), assumed equal to specific yield. The latter was estimated from water level responses to precipitation following Devito *et al.* (2005a) in wetland wells along transect A (65, 77, 89, 92), as the inverse of the mean response (b), i.e. slopes (unitless; Fig 2.S3) modeled via ordinary

least squares (OLS) regression in `R` (R Core Team, 2018) after:

$$n_e \; = \; 1/\frac{1}{n}\sum_{i=1}^{n} b_i \tag{2.4}$$

Luvisolic soils, such as found in uplands of adjacent hillslopes, are more porous, and consequently, feature greater storage capacities (especially in light of P-pET deficits, Redding and Devito, 2010; Brown *et al.*, 2014b), rendering estimates of potential SSA beyond the wetland highly conservative despite using a fixed value for n_e for different landcovers, topographic positions and soil types.

Saturated areas were mapped along four transects, one longitudinal (i.e. along main axes from pond to southern end), and three lateral, from the wetland center into adjacent uplands at approximately 5 m intervals. Refer to Fig. 2.11b for transect layouts. Transects were assessed approximately fortnightly between 2014 and 2018 and multiple measurements were taken to account for micro-topography (i.e. hummocks $vs.$ hollows) where warranted.

2.4 Results

2.4.1 Hydroclimate

Precipitation (P) averaged 417 mm for the period of 1999 to 2018, which was approximately 50 to 70 mm below the long-term average. Around 70 % of total P occurred between April and September; snow water equivalent averaged approximately 119 mm (Tab. 2.2).

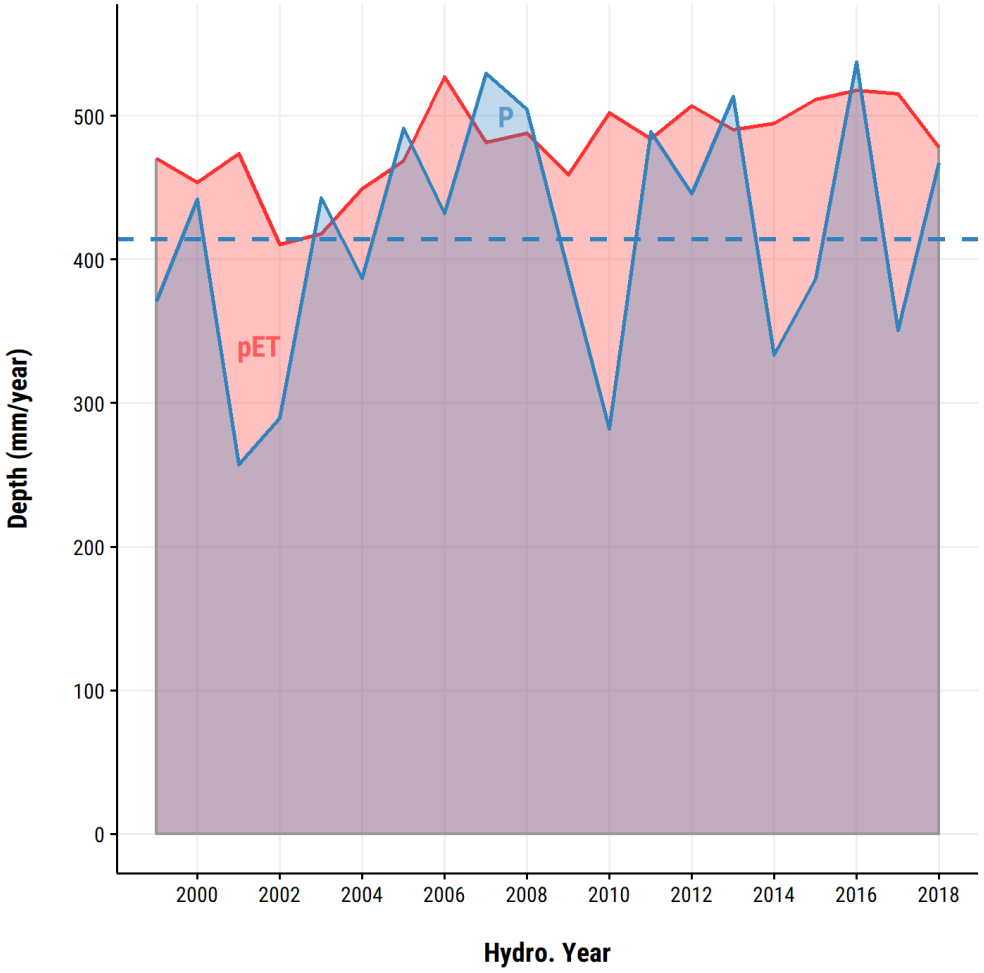

Figure 2.3: Annual P (blue) and pET (red) for the study region. The dashed, line is the the study period average (417 mm).

On an annual basis, P ranged from 257 mm (2001) to 537 mm (2016), and generally was below pET, which averaged 480 mm and was less variable (Fig. 2.3). Years of excess P (i.e $P - pET > 0$) occurred at variable intervals (1 to 4 years). Minimum and maximum pET were 410 and 527 mm in 2002 and 2006, respectively.

2.4.2 Runoff dynamics

Runoff (R) was episodic on inter-annual basis, with three subsequent years (2005 - 2007), as well as 2014, producing annual runoff coefficients (R/P) ranging from less than 8 to 54 %, and peaked in 2014 at 26 $mm \cdot day^{-1}$ (with respect to wetland; Tab.

Table 2.2: Averages of monthly precipitation and 'potential' snow water equivalent (SWE). Note, 1) SWE is considered potential, as it was estimated based on local air temperature dynamics (i.e. snow when air temperature $< 2°C$), and 2) that sum of percentages exceeds 100, as SWE is assumed to accumulate across winter months (Oct-April).

	Nov	Dec	Jan	Feb	Mar	Apr	SWE	May	Jun	Jul	Aug	Sep	Oct
P (mm)	20	17	27	19	20	25	119	44	67	67	53	37	21
%	5	4	7	5	5	6	29	11	16	16	13	9	5

2.3). Below R is reported based on the wetland as the effective catchment area, but note, that the 96 % forested, topographic catchment produced R of 2 to 8 $mm \cdot year^{-1}$. R was not correlated to total, annual precipitation or precipitation anomalies (i.e. cumulative mean departures, as used by Hokanson *et al.*, 2018a for explaining Boreal Plains groundwater dynamics) across one to three years (Fig. 2.S1), or snow accumulation (Fig. 2.S2); most noteworthy, peak R coincided with a deficit year where P was 110 mm below average. Within a given year, R typically occurred after snow melt (i.e. snow fully absent) in May, June or July in response to P when wetland water tables were already surface-near, or when P increased water tables sufficiently (Fig. 2.4). Available water storage capacity attenuated R, as is illustrated by comparing years 2005

Table 2.3: Annual P, R (wetland and topographic catchment) and corresponding runoff coefficients. Note that rows (i.e. years) marked with asterisks only have sparse manual stage measurements, and hence calculating metrics was not possible.

Year	P	R_c (mm)	R_c/P (%)	R_w (mm)	R_w/P (%)
2005	491	2	< 1	42	8
2006	432	2	< 1	39	9
2007	530	5	1	117	22
2008	504	0	0	0	0
2009*	391*	0*	0*	0*	0*
2010	282	0	0	0	0
2011	489	0	0	0	0
2012	446	0	0	0	0
2013	513	0	0	0	0
2014	334	8	2	179	54
2015	387	0	0	0	0
2016	537	0	0	0	0
2017*	351*	0*	0*	0*	0*
2018	467	0	0	0	0

and 2006. R recurred intermittently from May into June in 2006, and only in July in

2005. In 2005, both June and July P were above-average, with 77 and 106 mm, causing peak R of 4 $mm \cdot day^{-1}$ and 7 $mm \cdot day^{-1}$ on July 3 and 24, respectively. The latter was linked to the largest, individual storm event (80 mm, July 21-23), raising water tables sufficiently (after they had receded into/below CL under well base at the outflow). Similarly, above-average P in May 2006 (94 mm) allowed meeting and exceeding storage in response to 34 mm (9 days, late May) with max R of 5.6 $mm \cdot day^{-1}$ and an individual P event of 15 mm on June 3 resulting in 6.2 $mm \cdot day^{-1}$. Contrastingly, a wetter July in 2006 (137 mm) did not result in R that month, as the water table had already receded increasing available storage, and no individual storms of magnitudes comparable to July 2005 occurred.

In 2007, P totaling 49 mm between May 3 to 5, raised water tables near the outflow, and together with earlier snow melt, primed the wetland for R in late May and throughout June, with peaks of 8 (May 30), 10 (June 20) and 12 $mm \cdot day^{-1}$ (July 1). Successive storms (approximately 7 to 14-day intervals) in May and June ensured wetland water levels remained high or increased sufficiently before events causing lateral flows; for example, 24 mm P fell a week before a total of 35 mm (across 2 days) causing the July 1 peak R response.

In 2014, R likely began in late April or early May. However, the pressure transducer used for the stage-discharge relationship was raised in winter 2013/14 to prevent freezing until May 24, after which continuous data became available. Manual discharge measurements on May 1, 9, 13 and 24 indicate R of approximately 0.5 to 1.5 $mm \cdot day^{-1}$. R continued through June 21; a minor second period occurred from June 25 to 27. R increased from May 25 following P of around 6 mm to 4.2 $mm \cdot day^{-1}$ on May 29, and finally peaked at 26.4 $mm \cdot day^{-1}$ on June 11 after a week of successive P totaling about 29 mm.

Tab. 2.4 elucidates the role climate and storage have on controlling runoff: all R -generating years have excess water (P-pET) available when SWE is taken into account,

Table 2.4: Peak R and cumulative, excess water (i.e. net P) until peak based on different time periods, for Spring (1 May), winter (SWE; 1 November, previous year), previous fall (15 September, previous year). The last week of April was included in 2014's spring value in parenthesis, as R initiated May 1 that year, and a 34 mm P-event in that week likely saturated the wetland. Note (1) that stage measurements were available from 2005, (2) June 21 was chosen for non-R generating years as it is the mean Julian day of all observed R responses, and (3) values marked with asterisks indicate maximum values established from instantaneous, manual measurements and may be an underestimation of actual peak R.

Date	**peak R (mm)**	**P-pET Spring (mm)**	**P-pET (SWE)**	**P-pET (Fall)**
21 Jun, 1999	-	9	91	91
21 Jun, 2000	-	48	70	34
21 Jun, 2001	-	-40	4	-23
21 Jun, 2002	-	-52	-6	-27
21 Jun, 2003	-	-25	62	60
21 Jun, 2004	-	-54	-8	1
24 Jul, 2005	6.9	24	155	171
04 Jun, 2006	6.2	31	62	25
01 Jul, 2007	12	27	210	203
21 Jun, 2008	-	-31	116	98
25 Jul, 2009	6.14*	-77	66	87
21 Jun, 2010	-	-75	-37	-58
21 Jun, 2011	-	-33	81	46
21 Jun, 2012	-	-50	41	33
21 Jun, 2013	-	-27	122	132
11 Jun, 2014	26.4	-32 (-7)	89	103
21 Jun, 2015	-	-44	60	39
21 Jun, 2016	-	31	106	69
13 May, 2017	1.19*	5	49	38

and except for 2014, also feature excess water through rain starting in Spring (May 01). Despite, the spring deficit for 2014, R in this year was greatest, which required available storage to be met. The amount and timing of P in the previous year (during fall and winter), can 1) fill storage and 2) freeze and create solid ice which may serve to reduce storage. While 2007 saw the largest amounts of excess fall P and SWE until peak R, it was preceded by a deficit year (2006). Contrastingly, 2014 had started with P excess from 2013 (Fig. 2.3). Solid ice depths varied substantially between years, based on late fall P (not lost to atmosphere and available for freezing), and spring temperatures. Detailed ice dynamics are reported for a dry (2014), average (2015) and the wettest year (2016), but note, that surface-near, solid ice was observed at the outflow (sites 65, 75, 7) within 0.05 m of the surface during runoff in Spring 2005 (Riddell, 2008). Detailed assessments from 2014 indicated solid ice at 0.03 m below

ground on April 24, coinciding with a 33 mm P event. Ice receded to 0.20 m May 14 and exceeded 0.50 m by May 24. Further usplope, (lower catchment, 77), ice was recorded at 0.03 m depth April 24, 0.10 m by May 1 and exceeded 0.30 m by May 24. Contrastingly, in 2015 ice depths were around 0.07 m throughout the wetland by April 25, dropped to 0.22 m (outflow) and 0.14 m (lower catchment), and eventually exceeded depths of 0.40 m by May 14. A warm and dry period in Spring of 2016 resulted in ice dropping to 0.11 m to 0.20 m at the outflow by April 21, and exceeding 0.40 m by April 26; lower catchment ice (at 77) was around 0.08 m by April 26, and exceeded 0.40 m shortly after. Hillslopes typically formed discontinuous frost, as P went into storage and soils did not saturate. However, Riddell (2008) reported solid ice on the wetland-upland interface in 2005, which may have served to route snow melt in this area into the wetland, rather than allowing percolation.

Analogous to shallower ice depths in the lower catchment compared to the outflow, water levels at 77 typically were closer to or above the surface more frequently (Figs. 2.4 and 2.12). Lateral flows generated there often disappeared into available soil storage further downslope, and hence did not contribute to R at the outflow.

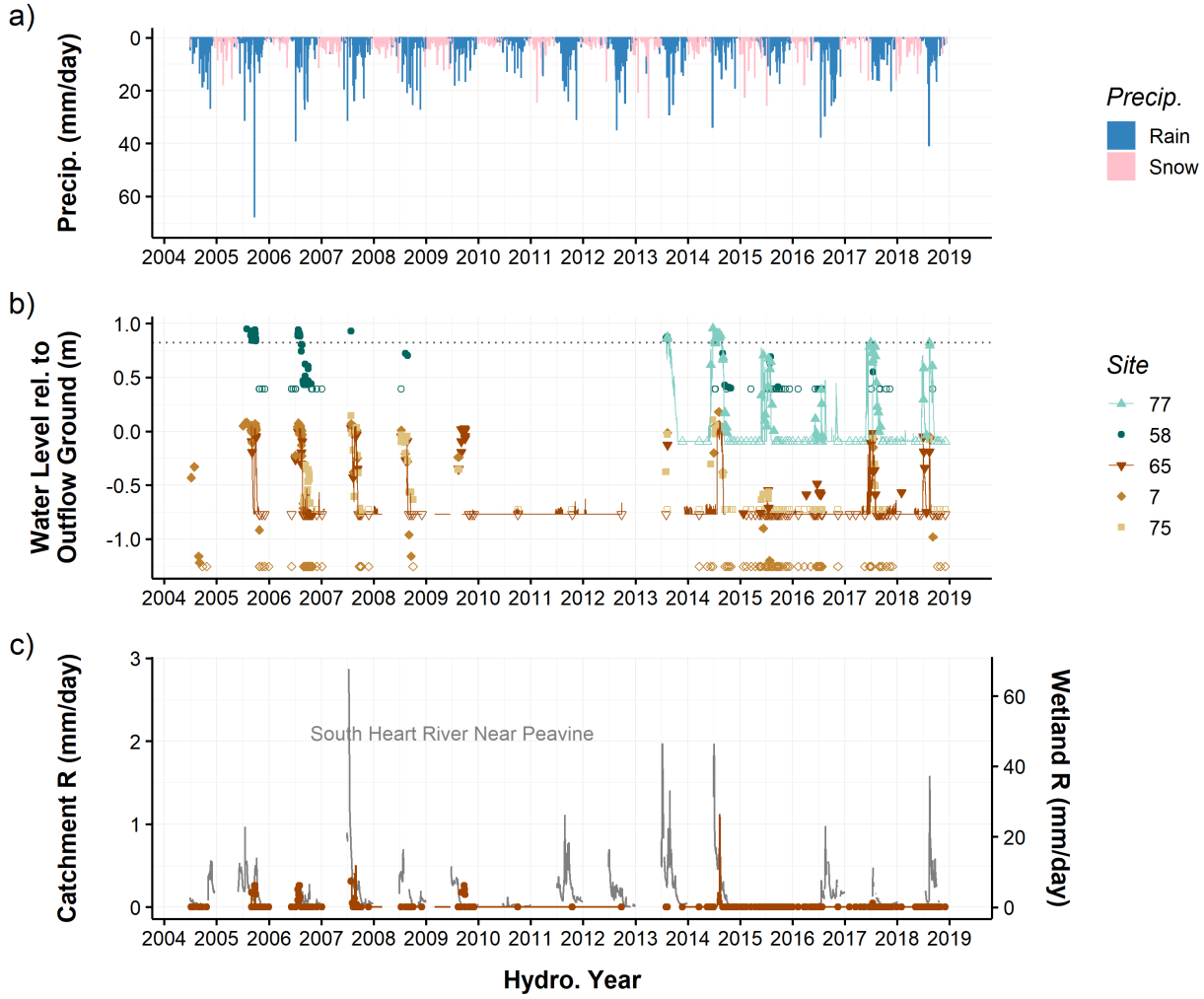

Figure 2.4: Timeseries of precipitation (a), water level dynamics (b) and runoff (c; axes using topographic catchment and wetland area as effective catchment, respectively). Water levels at the outflow (surface elevation of site 65 as relative datum) are in brown hues, uplsope in blues (dashed line for surface elevation at 77). Continuous records (solid lines) at key sites were supplemented with manual measurements (from nearby wells). Open symbols are dry wells. (c). With the wetland's conceptualization as a runoff-generating unit, amounts from the topographic vs. effective catchment area (i.e. only wetland) were approximately 23.5 times larger (cf. left and right axes, respectively). The South Heart River (station 56 km south west, catchment area 1710 km^2) shown for reference.

2.4.3 Confining layer characteristics and morphology

The CL featured low, saturated hydraulic conductivities ranging from 10^{-9} to 10^{-10} ms^{-1} (Riddell, 2008). It consisted mainly of silty clay and clay substrates which were generally blue to grey in color at the upper end of the stratum, and gradually turned to beige and brown, with signs of oxidation at greater depths. The CL was between 3

to 5 m thick in the wetland's center, and showed some outcrops (lens-like) around its margins that ranged 0.2 to 0.5 m (e.g. near site 106).

Depth to confining layer (DTC) was shallowest along transect A in the upper (ca. 0.30 m), middle areas (0.30 to 0.40 m, also western end of transect B), and gradually dipped off toward the outflow (ca. 0.60 to 1.00 m); at depths below ca. 0.50 to 0.80 m soil substrate shifted from predominantly organic material to higher fractions of silt. A series of subsurface depression was distributed along the wetland (2.5 bottom panels), akin to bowls or pans. Interface CL (i.e. bordering uplands) displayed variable morphology and either dipped of (mirroring surface topography) or remained more or less level. Hence, CL depths generally increased rapidly along hillslopes due to relief. The wetland areas beyond the road (south end), had shallower DTC on the western flank, following local topography, which then dipped off toward south and south-east.

On the eastern flank, a shallow and thin clay layer (ca. 0.20 m deep and thick in the Bt horizon of luvisolic soil) was found extending beyond the wetland's bounds (Fig.2.5); it was highly oxidized, fractured, and likely ineffective in preventing percolation, illustrated in water levels more than 1.00 m below ground in Fig. 2.7.

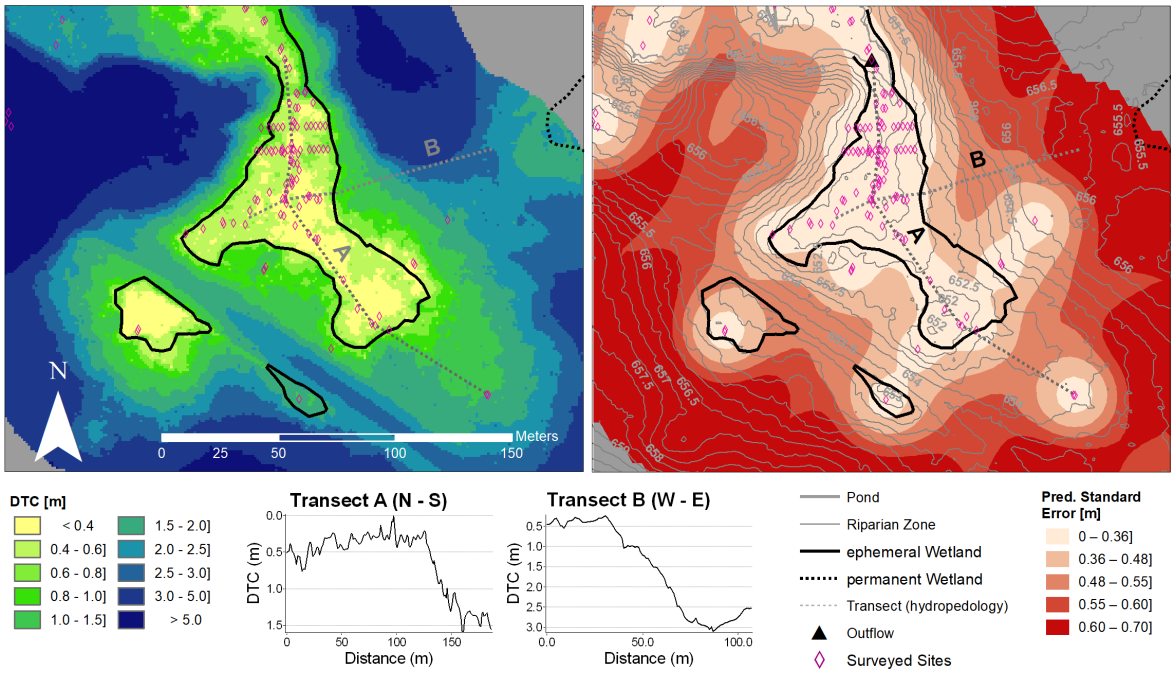

Figure 2.5: Depth to confining layer (DTC; left) as the difference between DEM and interpolated CL elevation (Section 2.3.4 for details), corresponding standard errors indicating prediction accuracy (right), and DTC along transects A and B on bottom panels. Purple diamonds are sites where the CL was encountered during surveying or installations (i.e. a sub-set of all assessed sites). Note, while multiple wells are along transect B (into upland), none of them reached or penetrated the CL at depths between 0.8 to 2 m and hence were excluded here from interpolation. The resulting descrepancy with observations is addressed in Fig. 2.10.

2.4.4 Interaction with deeper groundwater and hillslopes

2.4.4.1 Vertical configuration

Regional groundwater (Fig. 2.6a) never intersected the shallow - and effectively perched - wetland's groundwater system (Figs. 2.5 and 2.10 for elevations of wetland CL and Hokanson *et al.* (2018a) for regional context of site, see 'CO-Perched') and is unlikely to do so within the current hydro-climatic setting. Vertical gradients (Fig. 2.6b) generally indicated recharge conditions near the outflow (site 24) and toward the southern end (40). The latter infrequently showed surface-near, upward gradients, potentially linked to CL morphology and/or influxes from (ditches) beyond the damming road.

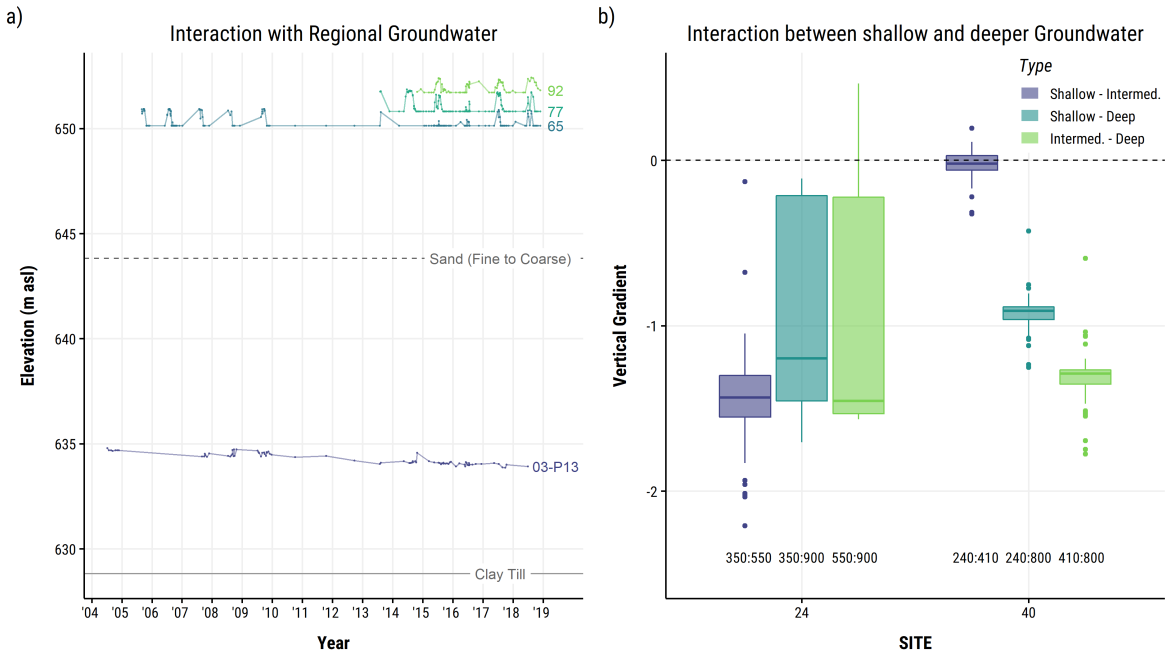

Figure 2.6: Differentiation between a) shallow and regional groundwater (in sand aquifer above glacial clay till; cf. horizontal lines) and b) vertical gradients within shallower groundwater. Negative gradients indicate downward water movement (i.e. recharge). Note, piezometer installation depths (in cm) are given below respective boxes (showing interquartile ranges [IQR] and medians; outliers are beyond $1.5 \cdot IQR$). Refer to Fig. 2.2 for location of sites.

2.4.4.2 Horizontal configuration

Water tables indicated flow into adjacent hillslopes in (Fig. 2.7a). The surface-near (0.20 m), fractured clay at 106 (Fig. 2.5) does not act as an effective confining layer, as levels stay well below those in the wetland. Water levels toward the southern hillslope (i.e. across and beyond road) indicated intermittent contributions after snow melt from the cut-off wetland portion (site 62 in Fig. 2.7c; 62 in Fig. 2.7b). Higher hillslope wells (167, 142) showed potential ridging at the hillslope base. This may be related to the ditch-like morphology due to the road, and likely compacted ground impeding lateral flows. Snow accumulation from drift and subsequent melt in these sites (62, 64) also led to saturation. However, due to shorter records in 167 and 142 a potential hillslope contribution could not be fully excluded over the study period - yet it is likely infrequent given the depth/absence of a confining layer, as well as in light of understanding from adjacent hillslopes of similar soil texture and stratification (e.g. transect B, 2.10b).

Refer to Section 2.4.5.3 for cross sections and water table configurations in space for exemplary sites and conditions.

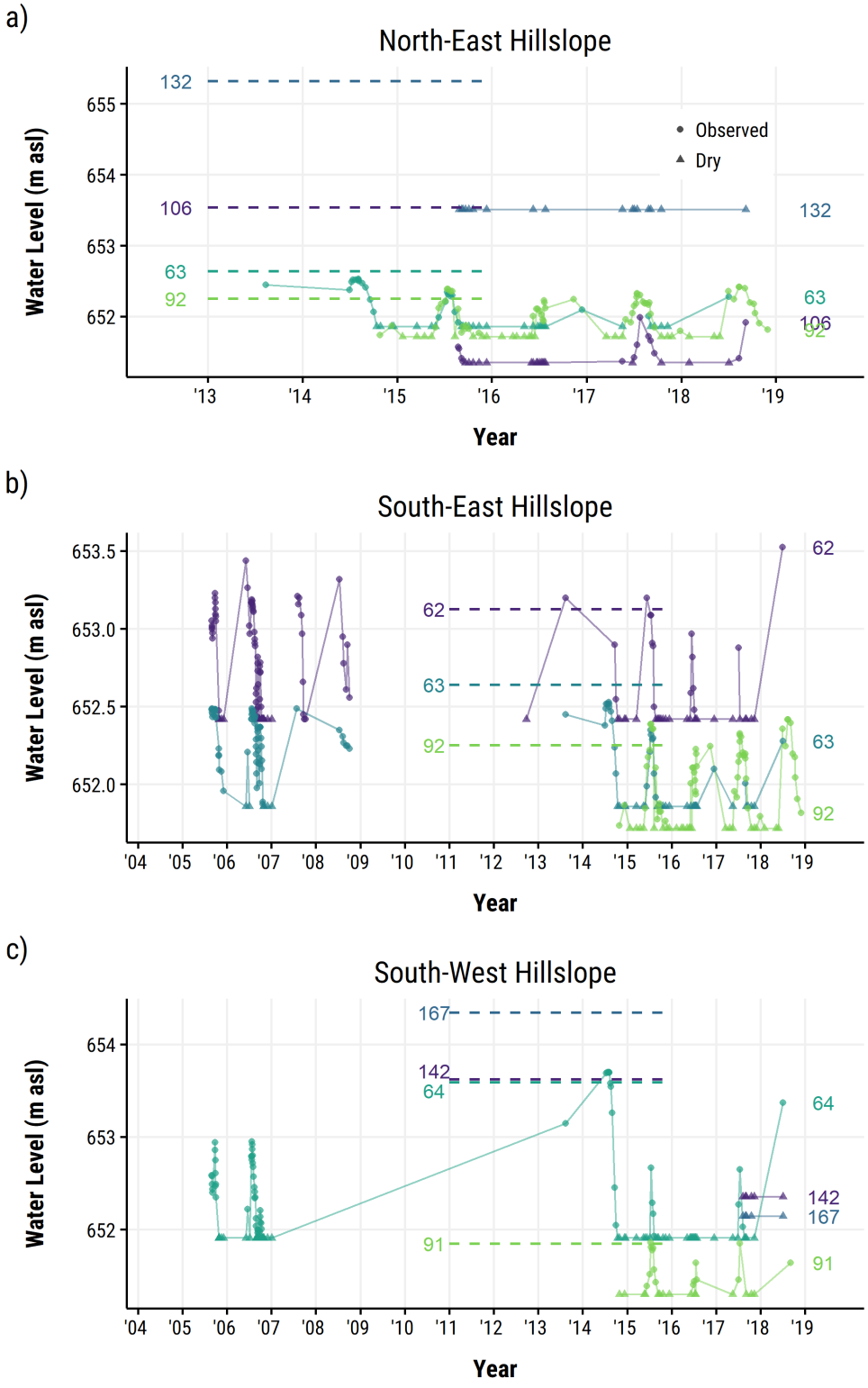

Figure 2.7: Water table dynamics from wetland to uplands. Site locations (colored labels) are shown in Fig. 2.2, dashed lines are respective ground surfaces.

2.4.5 Thresholds in surface connectivity

2.4.5.1 Spring melt and precipitation responses

2017 was chosen to illustrate spring melt and water table responses to precipitation, using sites along transect A, as well as one interface site (59) half-way along the wetland (Fig. 2.8). Snow was virtually absent from the area by April 30. Solid ice was observed at all wetland sites (Section 2.4.2 for ice dynamics) and the interface; ice was last observed May 15 (depths around 0.20 m) and absent by late May (i.e. > 0.40 m).

Ice thaw coincided with successive P events May 12 trough 18. Two days of 13 and 16 mm on May 11 and 12, respectively, increased water levels in the upper (92), lower (77) and outflow (65) areas of the wetland. Note, continuous records for site 89 begins after briefly after this period; yet manual observations (not shown in Fig. 2.8) indicated a rapid increase from 0.40 m to the surface.

At 77 a surface-near ice layer caused a perched water table prior the May 12 to 18 events, evidenced by saturated soils, standing water at the site, as well as manual ice and water level measurements. During thaw, and with simultaneous P inputs on May 11 and 12, levels rose rapidly by ca. 0.40 m, while standing water disappeared. Subsequently, levels increased near to surface until May 23; this was only initially accompanied by P inputs until May 18. A 9 mm event on May 23 resulted in saturation and lateral flows initiating. These flows did not continue to the outflow (65), but rather went into soil storage.

This period of sustained increase, and following the May 23 event, was the only time water levels were observed in the hillslope well 19-59 (west of 77) in 2017, indicating flow toward the interface and into the hillslope.

Starting May 27, water levels decreased at all wetland sites. Levels reached the

surface at 92 after successive P events in mid and late June. This site featured water tables closest to or above the surface most frequently (Fig. 2.12). P responses were typically delayed from higher to lower sites, with levels at 65 below the well or absent as summer progressed. The shape of site 92's response in late June to 1 July may be indicative of (downslope) subsurface flow, attenuating a more flashy response, as seen in 89 and 77.

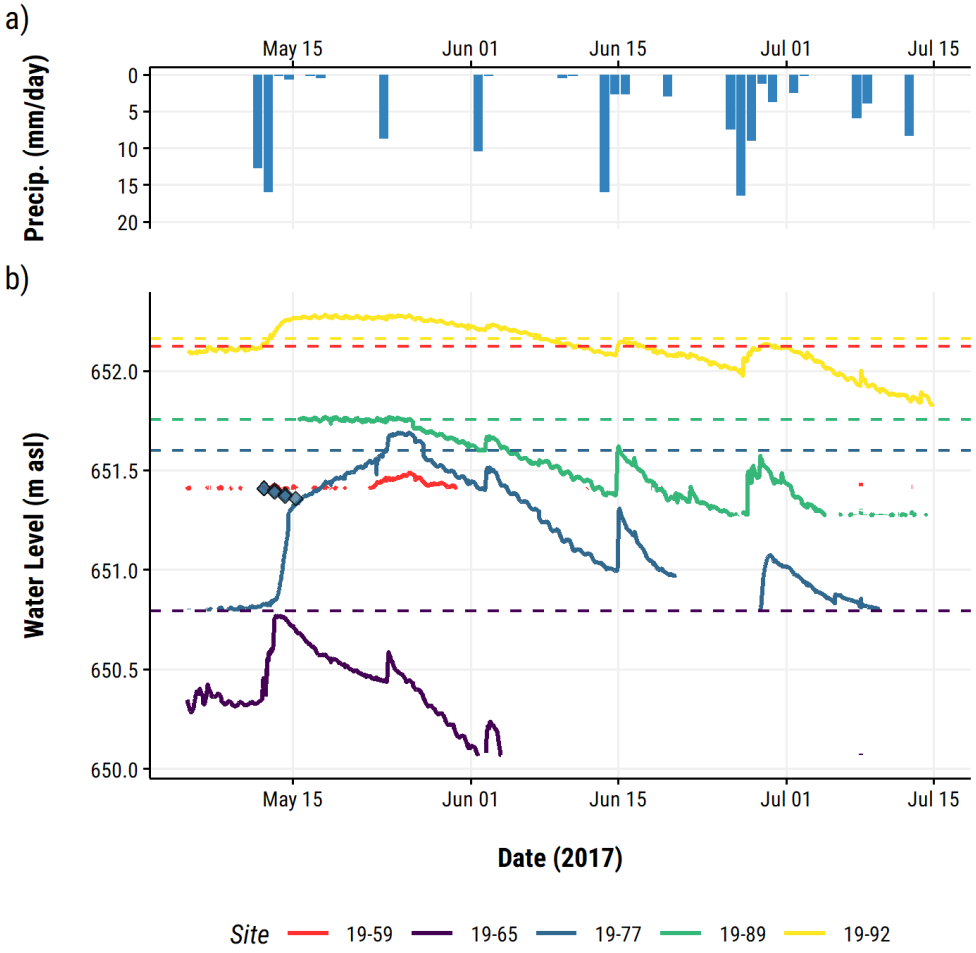

Figure 2.8: Precipitation (a) and corresponding water table dynamics (b) for wells along transect A, and site 59 (wetland-upland interface near 77; red) for an exemplary period in May - June (2017); blue diamonds indicate solid ice at 77. During and after ice thaw (May 15), water tables indicated lateral flow from higher to lower wetland areas, as well as flow into adjacent hillslopes (i.e. 77 to 59). Note, a brief period of missing data for 77 (mid to late June) and that dynamics of 89, 77 and 65 are also represented in Fig. 2.9.

2.4.5.2 Downslope connectivity

Water table dynamics showed characteristic behavior from upslope to downslope sites with resulting water table configurations that indicated subsurface, lateral flow, potential connectivity and threshold-type behavior (Fig. 2.9). Increases in 89 after P were typically trailed by responses in 77, during which water table configurations indicated lateral, (subsurface) flows downslope (i.e. arrows pointing right in Fig. 2.9a). Dynamics in 77 and 65 were disjunct, with lacking responses in the higher site (77) due to ice in early May (Fig. 2.9b). The subsequent increases in 77 were absent downslope in 65, potentially indicating continued losses (due to lateral or vertical fluxes, and/or evapotranspiration). However, larger P inputs resulted in responses in both sites until June. Later, these were absent in 65, as the water table dropped off into the CL from 77 to 65, or due to thresholds imposed by the confining layer's morphology (lower panels in Fig. 2.5 and Fig. 2.10a), causing a disconnect toward the outflow.

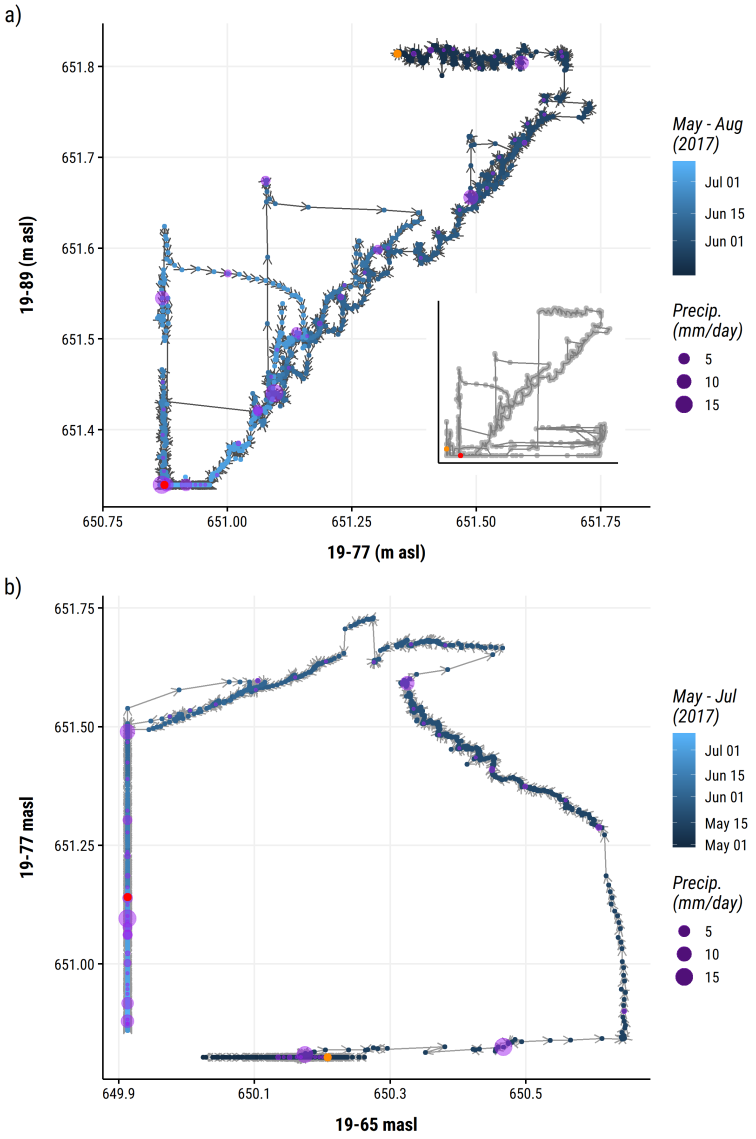

Figure 2.9: Water table dynamics between a topographically higher (y-axis) and lower site for a) 89 and 77 (mid to lower wetland) where inset shows extended series with disjunct dynamics due to ice prior May 15, and b) 77 and 65 (lower to outflow). Color and arrows indicate time; orange and red dots are start and end, respectively.

2.4.5.3 Configurations in wet and dry periods

Transect A showed a disconnect between the wetland and the hillslope toward 133 (or rather indicated flow toward upland), and only intermittent connections between the lower area at 77 and the outflow at 65 (Fig. 2.10). Depending on time of year, and antecedent conditions (available storage capacity and ice presence), markedly different P amounts resulted in water table rises or (surface-near) saturation at the outflow.

However, in addition to increased storage capacity (shift from wetland soils toward more silt at outflow), CL morphology may impose additional thresholds as it may have locally provided depression storage. Under dry antecedent conditions (after exceptionally dry and warm April and early May 2016) 56 mm P raised water tables only marginally, compared to P of around 30 mm under wet conditions and with ice present. Note that in 2016, the wetland saturated top-down from 92 to 77 (inferred from water table position relative to ground). Transect B (Fig. 2.10b) also showed saturation from the wetland outward under these conditions. Wet antecedent conditions led to ridging at the hillslope base (interface site 84) under small inputs (around 30 mm), indicating that brief yet frequent flow reversals may occur (likely promoted through ice in wetland and potentially at interface). Exceptionally wet conditions caused a short-lived water table configuration indicative of hillslope contributions (around 80 mm within 2 days before June 12, 2018, 106 mm total). However, given the large storage capacities of fine(er)-grained uplands (silt and sandy silt), this configuration may have been an outward movement of a ridge initially developed closer to the interface.

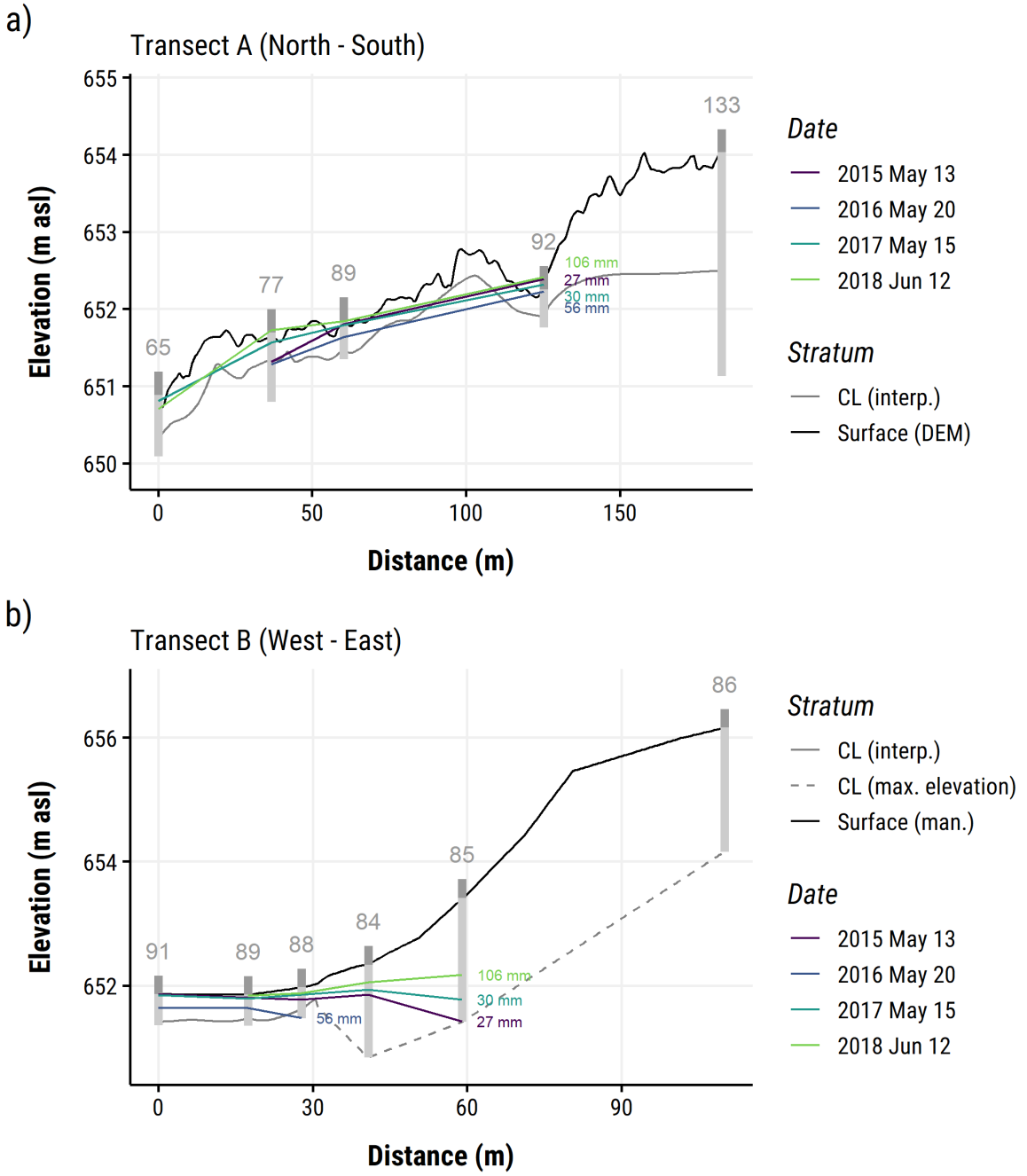

Figure 2.10: Transects of micro-tropograhy and CL along the main wetland axes (a) and into north-east upland (b). Above and below-ground sections of wells are in dark and light grey, respectively; well elevations are from manual surveys and were used for graphing water tables (colored lines) after a given P amount (total of 15 preceding days) under different antecedent conditions. Water tables were only graphed up until wells where water was observed (i.e. 133 and 86 always dry), except for site 91 on Jun 12, 2018, where data was missing. Manual elevations were used for the surface in b), due to more than 0.5 m mismatch with DEM (likely due to micro-topography, and a number of large snags/logs). Interpolated CL in b) showed stark discrepancies with observations in interface (84) and hillslope sites (85, 86). Hence, a maximum potential elevation for the CL was assigned at each of these well's bases. Also note the different scale between panels.

2.4.6 Surface saturated areas

Fig. 2.11 shows the potential extent of surface saturated areas (SSA) in response to a given amount of P, based on estimated storage capacity. Note, that the potential SSA displayed in Fig. 2.11 are solely based on storage depth estimates, and do not take into account any lateral flow that may serve to reduce storage locally further downslope. Shallow DTC areas along the wetland's main axes saturate under little P input; successively larger P events are required to increase the extent of active SSA. Across panels, note the top-down saturation and the discontinuity (i.e. larger storage) near the outflow; Fig. 2.12 highlights the tendency to saturate from higher to lower topographic areas in the wetland, rather than from the outflow (connection to surface water body) upward. Estimates indicate total P of around 120 to 140 mm are required to connect active SSA in the wetland to the outflow.

SSA extend beyond the wetlands bound toward the north-eastern hillslope as a result of including the shallow CL near 106 in interpolation; due to the fractured nature of clays and water table dynamics (Fig. 2.7) it is cautioned that these areas would most likely only contribute to SSA under large-magnitude P events (>20 mm) under sufficiently wet antecedent conditions (i.e. soil at field capacity). Field assessments (crosses in Fig. 2.11b) showed fair agreement of estimated and actual SSA in mid-May after 28 mm P.

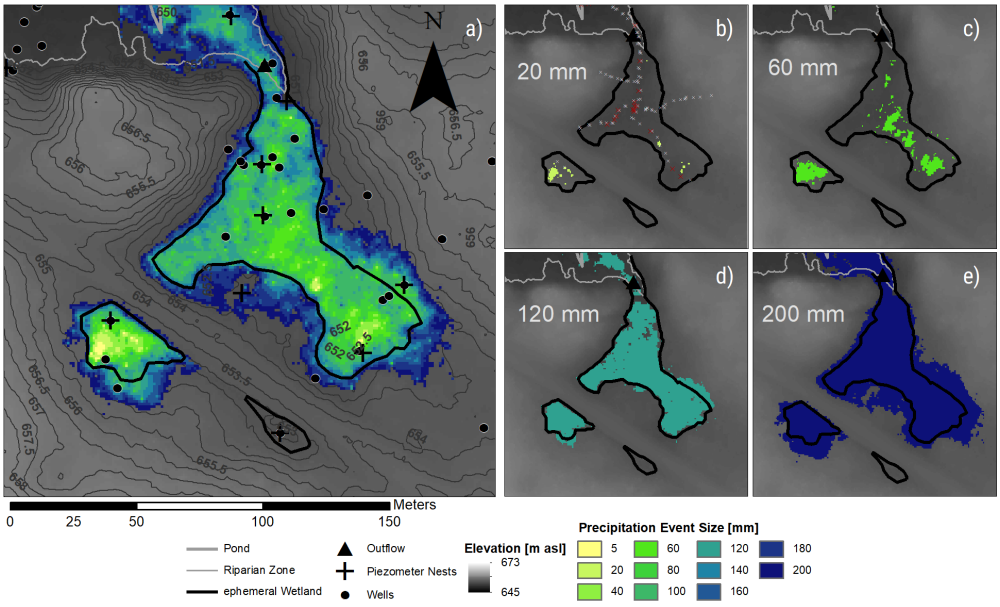

Figure 2.11: Potential extent of surface saturated areas (SSA) due to P events meeting soil moisture storage capacities (in equivalent water depth of mm). Calculations are based on depth to confining layer (Fig. 2.5) and an estimate of wetland-averaged porosity (Section 2.3.4). Panel a) shows the distribution of SSA under all event sizes, while the remainder feature events that may occur individually, over multiple days in conjunction with antecedent conditions and/or during snow melt. Panel b) also shows the location of surveyed SSA (red crosses) along a set of transects spanning the wetland and adjacent uplands (grey crosses) after a total of 28 mm precipitation (15-day window prior May 14, 2015).

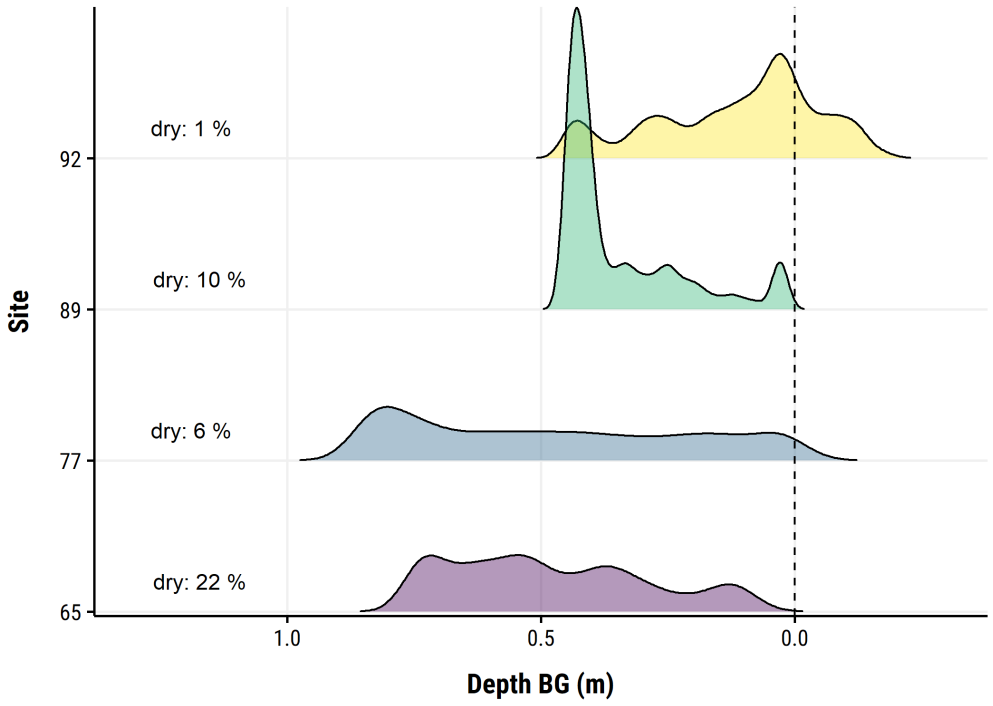

Figure 2.12: Empirical frequency distribution of water tables relative to respective ground surface. Distributions are based on continuous records between May 2016 and August 2018. and were trimmed toward the well base to prevent 'zero inflation' when dry (percentage time plotted). Sites are ordered based on elevation, from top of wetland to outflow.

Fig. 2.13 shows probabilities for time periods (month[s] in a; 15-day periods across years in b) to deliver a given amount of P (intervals match those of Fig. 2.11), resulting in potential SSA. Most precipitation typically occurs during late spring and summer. In conjunction with SWE, which is between 100 to 120 *mm* approximately every second year (Fig. 2.13a), estimated storage capacities throughout most of the wetland could have typically been met frequently between May and June. Note that large events in late summer (Jul - Sep; e.g. 106 *mm* between Jun 11 to 12, 2018, Fig. 2.10) did occur. Within 15-day windows (Fig. 2.13b), depths of 100 *mm* were exceeded approximately every 5 to 7 years, and 60 to 80 *mm* approximately within 3 to 5 years.

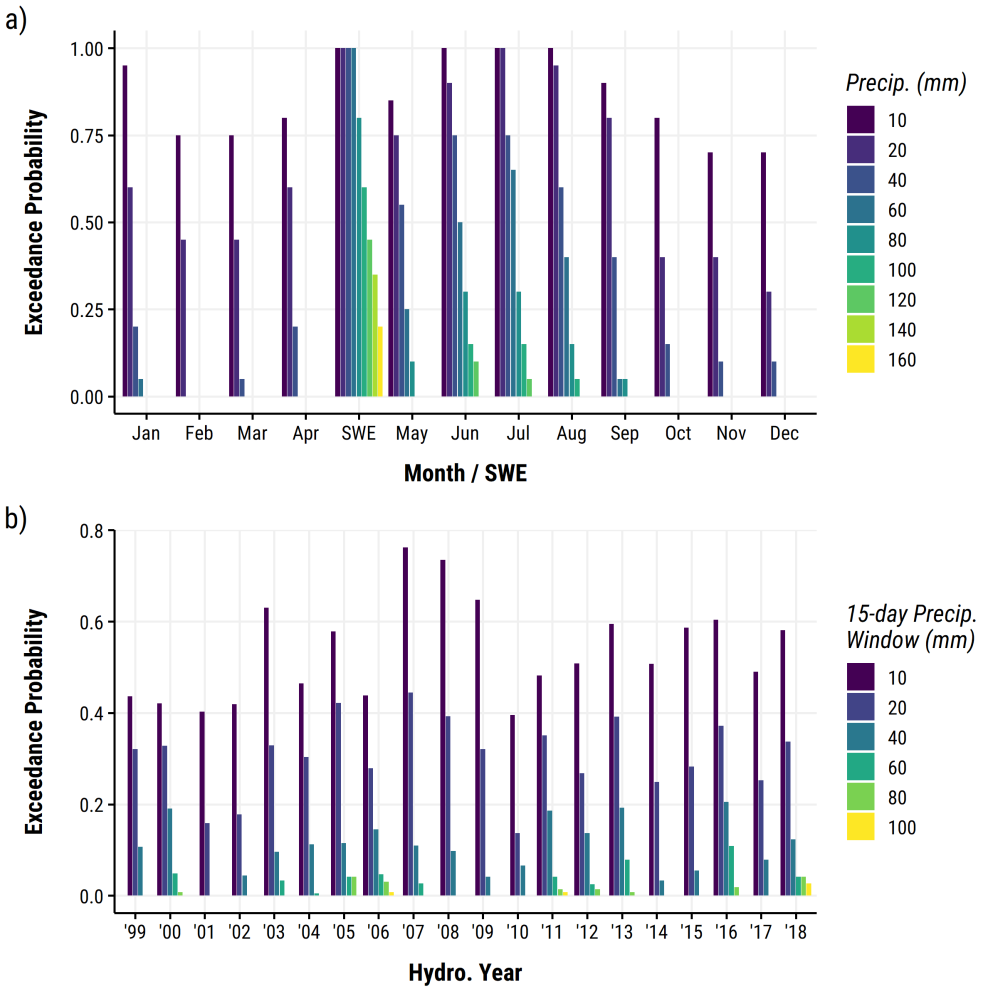

Figure 2.13: Probabilities of reaching or exceeding a given amount precipitation summed over months and estimated snow water equivalent (SWE, Oct - Apr) (a) or over a 15-day period for each respective year of the record (b), promoting saturation within the wetland.

2.5 Discussion

Runoff and subsurface flow generation in the Boreal Plains is not predominantly controlled by topography (Devito *et al.*, 2005b; Smith and Redding, 2012). That is, landscape position, geology, vegetation and climate can take precedent in driving dynamics (Tóth, 1963; Winter, 1999). Accordingly, the focus was on assessing storage and connectivity (as flow-process connectivity *sensu* Bracken *et al.*, 2013) in light of the sub-humid climate, between the wetland and adjacent uplands, constituting the majority (96 %) of the study catchment.

2.5.1 Runoff dynamics

The (topographic) catchment generated R between 2 to 8 $mm \cdot year^{-1}$ (on 6 out of 13 years), depending on climate (bulk P of current and previous fall/winter), weather patterns (timing and magnitude of storms) and ice. The range in R responses is similar to values reported for aspen-dominated catchments in Boreal Plains by Devito *et al.* (2005a), as well as Barr *et al.* (2012), with comparatively low flows (30 $mm \cdot year^{-1}$). Given the expected sink function of aspen (or deciduous and mixed-wood) forests (Brown *et al.*, 2014b), Devito *et al.* (2017) noted their comparative study on regional scale in the BP indicated virtually no runoff from catchments with deciduous cover above 70 %.

2.5.2 Runoff-generating mechanisms

The perched catchment (Riddell, 2008; Hokanson *et al.*, 2018a) and the geographically-isolated nature (*sensu* Mushet *et al.*, 2015) of its wetlands allowed identifying the dominant runoff mechanism by exclusion of hypothesis posed in Section 2.2.

Lateral (surface) flows contributing to catchment R were only generated within the wetland during this study. R initiated via saturation excess when hydrologically active areas connected to the outflow.

Water table configurations indicated that internally-generated saturation combined with infrequent contributions from interfaces via ridging, and potentially from locally recharged groundwater under uplands, created conditions for R. This required overcoming heterogeneous storage along (subsurface) flow paths (Phillips *et al.*, 2011; Spence *et al.*, 2011) imposed predominantly by CL morphology and soil texture (organic vs. mineral).

Surface flows from uplands on adjacent luvisolic hillslopes contributing to R at the catchment outflow were not observed and are unlikely or very small in magnitude (Whitson *et al.*, 2004; Redding and Devito, 2008) for periods of at least multiple years to decades. Subsurface contributions (interflow) from uplands can occur (Whitson *et al.*, 2004; Redding and Devito, 2010), but it is highly likely they would be restricted to snow melt or rain over solid ice that formed on wetland interfaces (e.g. as indicated for 2005 by Riddell, 2008).

However, more clay-enriched Bt horizons, if unfractured (van der Kamp and Hayashi, 2009), could promote surface-near lateral flow on similar soils found within the wider landscape on moraine deposits. Regional water tables neither rose to intersect the ground surface, nor above the confining layer during the study period, and are highly unlikely to do so given the prevalent sub-humid climate and landscape position (regional high, Hokanson *et al.*, 2018a)

Responsive (organic) wetland soils, and a shallow mineral CL were prerequisite for providing conditions suitable for efficient subsurface, downslope transport in a "two-layer" flow system (Carey and Woo, 2001a; Devito *et al.*, 2005a), with rapid groundwater responses and lateral flows above a lower-K_s mineral layer. Surface-near ice was crucial for temporarily decreasing storage capacities and "priming" the wetland

for surface runoff, most evident in 2014 - one of the driest years - generating highest R on record. The efficiency of the wetland in its R-generating function is reflected in a maximum runoff coefficient of 54 %, compared to 2 % of the wider catchment. Given its small extent, its function, and that of low-storage areas in valley bottoms in general (Devito *et al.*, 2005a), is therefore considered of disproportionate importance in generating downslope (or downstream) R in aspen-dominated catchments.

2.5.3 Hydro-climatic controls on runoff

Climate is decisive in R generation by determining atmospheric fluxes (precipitation, actual ET) as well as ice dynamics (Carey *et al.*, 2010). Wet antecedent conditions considerably increase the probability of surface runoff generation by reducing storage capacity and/or raising water levels closer to the surface prior to melt or P, serving to hydrologically connect active areas (e.g. Jencso *et al.*, 2009; Phillips *et al.*, 2011).

P in spring and summer was only infrequently high enough to meet storage within the wetland, as small and intermediate P events ($<10\ mm \cdot day^{-1}$) were most probable. Hence, the timing of P may well be considered more important than absolute magnitude and intensity (Devito *et al.*, 2005a; Wells *et al.*, 2017). Yet, in three consecutive years generating R (2005 to 2007) P-pET indicated surplus water until peak R in May, June and up to July in one case. Note, however, in conjunction with previous-fall P or SWE this balance was in excess on a frequent basis. Despite this, most years did not produce any R, highlighting the role of available storage in buffering responses to P.

Solid ice layers can considerably reduce available storage and thereby promote the generation of lateral flow and eventually surface R (e.g. Carey and Woo, 2001b) in areas with greater CL depths (higher storage) under partially saturated conditions (regarding entire soil column). This process was evident, for example, in Spring 2017 (Fig. 2.8). The development of such layers requires 1) either adequate saturation and/or moisture

levels prior winter, and freezing temperatures coinciding with little insulation (from snow or litter), and/or 2) adequate water inputs during winter, typically in form of intermittent snow melt and refreeze cycles (see Woo and Winter, 1993). Disturbances that alter snow interception, drift and sublimation processes, such as stand-replacing fire, harvesting or insect infestations (leading to mortality), could therefore severely alter soil ice dynamics - either enhancing or decreasing R generating capacity, dependent on how its depth, coverage and persistence is affected. Thompson *et al.* (2017) highlights that climate models consistently predict an increase in winter precipitation, typically in form of rain; this may serve to increase the propensity of solid ice layers to form, if temperatures remain low enough despite projected warming (Price *et al.*, 2013). Note, that solid ice may also affect surface energy balance dynamics, resulting in reduced evapotranspiration, as observed for the Pauciflaura Basin (Van Huizen *et al.*, 2020), further enhancing the likelihood of R generation under average P conditions.

Nearly 14 years of ground- and surface water data presented here cover multiple wet and dry periods. This includes responses to rare, large events (e.g. >30 $mm \cdot day^{-1}$), which created hydrological gradients indicating interface and/or upland contributions to the wetland on infrequent basis. Note that successive, excessively wet years, such as 1996 and 1997 (both above 600 mm, see Hokanson *et al.*, 2018a), would likely be able to fully saturate the wetland (even in absence of ice), as well as potentially adjacent, forested uplands (see Redding and Devito, 2008). These may be expected on cycles of up to 25 years (Mwale *et al.*, 2009), and are likely to increase R by an order of magnitude (e.g. Devito *et al.*, 2005a). The wetland therefore ranges in character from intermittently to ephemerally connected (Cohen *et al.*, 2016), and in function from storing, to transmitting and generating (Black, 1997).

2.5.4 Dynamic storage and connectivity

Holecek (1988) developed the storage-effective discharge (SED) model to assess effects of disturbance (logging) on R in an experimental aspen-dominated catchment in the Boreal Plains. It recognizes the variability of storage in time and successfully reproduces observed, highly non-linear R responses to P. The SED achieves this by reducing a catchment into a single (theoretical) storage unit and thereby represents a stark oversimplification of its characteristics. However, it is this reductionist view of dynamic storage, in conjunction with hydrological connectivity as a dominant driver of R generation (Spence, 2007, 2010; Kirchner, 2009), that allows contextualizing the contrasting behavior of the catchment's forested uplands (deep storage zones) and the small wetland (shallow storage), and the catchment itself in wider Boreal Plains landscapes.

Hydrologically connected areas can efficiently contribute to stream flow (or discharge at catchment outlet) via subsurface flows and surface R. However, heterogeneous storage capacities (especially when higher at down-slope locations), or discontinuous low-permeability layers (e.g. bedrock cracks or heterogeneous clay lenses) along flow paths, can result in impedance or buffering of R responses (Kuraś *et al.*, 2008; Jencso *et al.*, 2009).

Generally, the range of dynamic storage varied greatly in space (upland vs. wetland, DTC, ice) and in time (seasonally, inter-annually). A comparatively-high storage zone was located in the wetland just before the catchment's outflow, as the CL dropped down to around 0.60 to 0.80 m. Consequently, this attenuated R responses under dry antecedent conditions or in the absence of ice. Subsurface flow may occur more frequently within the wetland, especially in spring, and/or during intense and prolonged precipitation events during which water tables in the lower catchment rise (sites 77 to 65) .

Connections in the wetland formed top-down, when local storage deficits where

overcome as perched water tables developed. Meeting these thresholds did not necessarily require full saturation at a given point (i.e. water tables at/above surface). Rather, thresholds were defined by CL morphology, where flows follow the interface of the low-permeability layer (or bedrock, Devito *et al.*, 1996; Freer *et al.*, 2002; Meerveld and McDonnell, 2006) and higher K_s soil, and then spilled into zones with larger storage deficits (Spence and Woo, 2003; Ali *et al.*, 2011; Phillips *et al.*, 2011). As for Ali *et al.* (2011), more efficient downslope transport of water was expected once sub-surface depression storage along flow paths was met (i.e water table above depression "outlet", but at/below surface). Fig. 2.9a may be indicative of this process, where mid-wetland water tables (site 89) remained stable (or hydraulically limited, Anderson *et al.*, 2010) through continued upslope input and downslope spill (evident in the water table increase at 77). An analogous surface process is found in the prairie pothole region of North America, where fill-and-spill dynamics (via surface and subsurface flow) between individual wetlands govern catchment connectivity, and ultimately also result in complex, storage-threshold controlled, non-linear R (e.g. van der Kamp and Hayashi, 2009; Shaw *et al.*, 2012, 2013; Vanderhoof *et al.*, 2016). However, regional water tables are typically closer to the surface, and in conjunction with low-permeability soils, control the distribution of hydrologically active and contributing areas. In contrast, the variable DTC led to large range of available storage in the catchment (modified by vegetation water demand and climate); the development of saturated areas (and perched groundwater tables) was therefore typically limited in extent to low-storage areas in the wetland and its interfaces.

Spatio-temporal variability of wetland-upland connectivity along interfaces is a common result of heterogeneity in local properties (e.g. topography, geometry, and *P-ET* modulated by vegetation) and can drastically alter subsurface dynamics (Doss, 1993; Grayson *et al.*, 1997; Rosenberry and Winter, 1997; Spence, 2010). Overall, a

groundwater sink-function of forested uplands, rather than contributions to the wetland, was frequently observed, especially in dry years or later in summer when atmospheric demand was largest (Brown *et al.*, 2014b). Similar dynamics have been documented and reproduced in other field-based and modelling studies within the Utikuma region (Ferone and Devito, 2004; Smerdon *et al.*, 2008; Thompson *et al.*, 2015a) as well, and are in agreement with broader landscape conceptualizations of the Boreal Plains (Devito *et al.*, 2005b, 2017; Smith and Redding, 2012).

Prolonged connectivity and therefore contributions from adjacent uplands to catchment R may occur during "re-wetting" cycles (Mwale *et al.*, 2009; Devito *et al.*, 2012), or intense and prolonged precipitation events in spring or early summer (Taylor and Pierson, 1985; Todd *et al.*, 2006; Thompson *et al.*, 2015a). However, ridging at interfaces and potential groundwater contributions from local recharge under upland hummocks occurred in response to successive, large P events (rare) or under wet antecedent conditions with intermediately-sized P.

2.5.5 Dynamic storage in a landscape context

This study focused on R generation from one exemplary, aspen-dominated catchment, with a small, forested wetland. Both upland forest and wetland can be considered distinct hydrological units (Devito *et al.*, 2005b). However, viewing the catchment as a dynamic storage unit (*sensu* Holecek, 1988), allows understanding of R generation to be readily translated to other physiographical settings within Boreal Plains landscapes. This requires taking into account the role of surficial geology, landscape position vegetation and climate in dictating storage availability, and ultimately, R responses (Devito *et al.*, 2005b, 2017; Barr *et al.*, 2012; Gibson *et al.*, 2015). Fig. 2.14 illustrates the role aforementioned factors play in mediating R responses. This concept is drawn upon to contextualize results from BP studies of Wells *et al.* (2017), indicating high and non-linear R, and Goodbrand *et al.* (2018), indicating intermediate and less variable

R.

Wells *et al.* (2017) report high potential for frequent and large R generation from a headwater catchment (Pauciflora Basin). Their system had 26 % wetland (fen) cover, which received groundwater consistently from one hillslope, and intermittently from the opposing valley flank. This served to reduce available storage in their wetland (as opposed to non-groundwater-fed systems). Soils in adjacent hillslopes also featured a "two-layer" flow system with a surface-near, high-K_s layer; note, that the hillslope-wetland complex is in function and configuration similar to this wetland-pond complex. Further, conditions were markedly wetter than on average for Boreal Plains landscapes, evident in 4 consecutive years of P-pET excess. Hence, dynamic storage was typically low, and comparatively large areas became connected on a frequent basis in response to individual P events, despite expressed non-linearity. The combination of landscape position, soils, and climate resulted in conditions highly conducive for R generation, and must be considered somewhat uncommon for the Boreal Plains given its climate. However, as mentioned previously, in substantially wet years ($P - pET \gg 0$), similar behavior may arise in typically less-connected areas, such as this study's catchment, when (transient) water tables form in hillslopes or storage capacities are fully met and lateral contributions ensue (Grayson *et al.*, 1997; Redding and Devito, 2010).

Goodbrand *et al.* (2018) studied a peatland within the Pine Fen Creek Catchment on coarse, glaciofluvial deposits and its role in controlling stream response (i.e. R). Their system was situated in a topographic low, intersecting the regional sand aquifer. The continuous groundwater supply also served to reduce available storage, by keeping wetland water tables surface-near. However, P-pET was typically closer to average values observed across the Boreal Plains and climatic variability did result in dry conditions (P-pET). Therefore, the wetland in the catchment displayed functions ranging from groundwater storing to transmitting, as well as R generating. While similar range in function was inferred for this wetland, magnitude and frequency are

both far below that of Goodbrand *et al.* (2018)'s peatland. Again, excess-P years, or a rise in regional water table (unlikely) could shift the behavior of this catchment closer to that of theirs.

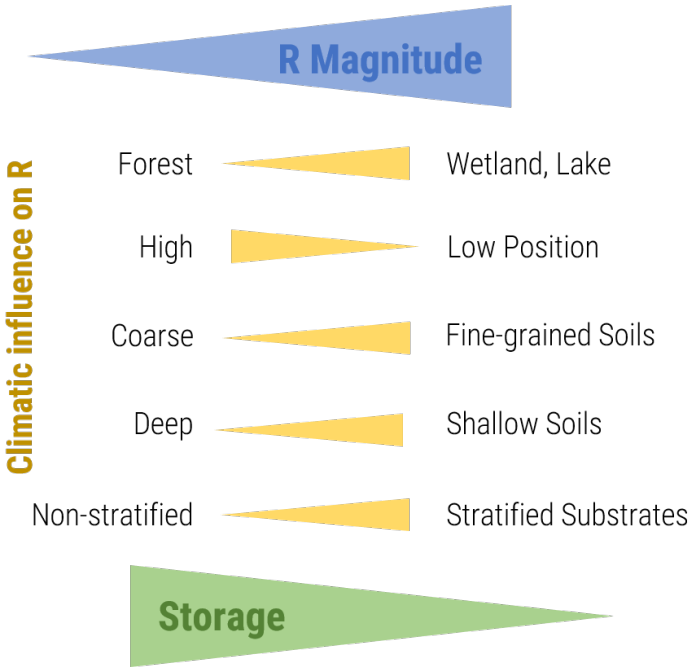

Figure 2.14: Conceptualization of climatic controls (here difference between precipitation and evapotranspiration) on runoff and how they vary based on surficial geology, soil texture and vegetation, based on Devito *et al.* (2012), Devito *et al.* (2017) and Smith and Redding (2012). Effect sizes are represented by width of triangle along its main axis. Climatic variability (and especially P-pET across time scales) is a strong modulator of R responses. Dynamics presented here are found in the contrasting wetland and forested upland (individual hydrological units, Devito *et al.* (2005b)), but readily translate to contrasting response areas, defined by geology (Devito *et al.*, 2005b; Hokanson *et al.*, 2018a), or other sub-humid regions.

2.5.6 Prevalence of small, forested wetlands as low-storage units and ecohydrological relevance

There are multiple perched peatlands (ombrotrophic bogs) in the immediate vicinity, even at topographically higher landscape positions (e.g. to north-east and east), which are also linked to the presence of a shallow CL. While their topography and geometry likely does not allow for surface R, James (2017) found hydraulic gradients indicative of subsurface flow into adjacent uplands, similar to e.g. Hayashi *et al.* (1998). On larger scales, the heterogeneous geology of the Boreal Plains due to the deposition

of substrates of contrasting texture, and subsequent re-working via (glacio-)fluvial and aeolian processes, certainly resulted in similar configurations (i.e. low-permeability substrate located in a coarser matrix), despite in different landscape positions, geometries and topographic gradients. In light of large range in dynamic storage resulting in the R -generating function in the catchment's wetland, it is hypothesized that low-storage zones, such as the wetland, have a decisive role in maintaining the ecohydrological functioning of adjacent and downstream/downslope systems, especially in a high-storage landscape matrix, as found for aspen-dominated areas (Devito *et al.*, 2005b; Ireson *et al.*, 2015), such as terminal ponds, or adjacent forests. For the latter, extensive aspen root systems could benefit from lateral flow across the wetland-upland interface (Snedden, 2013a; Depante *et al.*, 2019).

2.5.7 Functioning under future climate and research priorities

The Canadian Boreal is predicted to experience dramatic change within our century (Price *et al.*, 2013), including shifts from less snow accumulation to more summer precipitation, as well as increases in both winter and summer temperatures in the Boreal Plains (Ireson *et al.*, 2015) (note, that humidity is also expected to increase, therefore trends in actual ET are not fully established).

The prevalent sub-humid climate implies a close balance between atmospheric fluxes, which in turn determines water table configurations in and across individual hydrological units in their respective physiographical setting. A shift from their current status ($P - pET \approx 0$) could result in a fundamental change in hydrological behavior (Jackson *et al.*, 2009), especially if vertical or lateral flow gradients are dramatically altered or reversed. Such vulnerability resulting from altered hydro(meteoro)logic regimes has been noted previously for the water-limited Boreal Plain, with potentially dramatic state shifts for the entire ecoregion (Hogg and Hurdle, 1995; Schneider *et*

al., 2016). However, systems with low intrinsic storage, and/or where storage availability is highly dynamic (e.g. due to ice or dependency on intermittent connectivity), will likely be most resilient to shifting hydrometeorlogical regimes, as their functioning is internally-driven and will likely continue to arise even during dry conditions, as evidenced for the forested wetland here.

Vertical fluxes typically dominate Boreal Plains water balances (Barr *et al.*, 2012; Devito *et al.*, 2017). R generation in aspen-forested catchments, through zones of low intrinsic but highly variable storage, decidedly depends on establishing and maintaining excess water and saturation. A detailed assessment of actual ET, resolved across structural components of wetland and upland canopies in such catchments, is currently lacking and therefore presents a major research priority; this will help to better understand potential impacts of altered regimes (e.g. causing reversal of hydraulic gradients) and aid landscape management, for example, by delineating areas of high importance for R generation (Devito *et al.*, 2005a). This will also allow elucidating the role of potential feedback mechanisms (as observed in other northern wetland systems Waddington *et al.*, 2015), such as e.g. self-shading and ET-reduction via root anoxia, that allow forested wetlands to generate and potentially prolong saturated conditions.

2.6 Conclusion

This work built on Devito *et al.* (2005a), and provided new insight on the role of longer-term climatic variability, ice and the dynamic nature of connectivity between hydrologically active areas (in wetlands) and adjacent upland hillslopes in aspen-forested catchments in the Boreal Plains.

R was generated on 6 of 13 years of detailed water level measurements. R initiated solely as saturation excess flow in a small, forested wetland (swamp) above the catchment's outlet, making up only 4 % of total area. This was driven by the heterogeneous

and stratified distribution of glacial substrate resulting in a) contrasting storage between the forested upland and wetland, and b) as well as within the wetland, imposed through local differences of CL depth and morphology.

Climatic variability served to drastically modify available storage via antecedent moisture and ice, resulting in dynamic connectivity within the wetland, and during short periods, with adjacent hillslopes, creating conditions suitable for R generation. For example, peak R for the entire study period occurred in a net-deficit year ($P - pET < 0$) where surface-near solid ice along the main flow path in the wetland reduced absolute storage capacities, which were subsequently met by intermediately-sized P events. In particular, the wetland saturated top-down following surface topography and sub-surface CL morphology, where high storage areas - especially toward the outflow - buffered R responses to P. Hillslope contributions were limited to subsurface flows (as indicated by hydraulic gradients), and most likely rare and brief in duration. More frequently, the wetland water tables were above those in uplands, indicating outward flow. Together with R, this water redistribution must be considered instrumental for maintaining downgradient systems, such as the isolated pond here, but potentially even (margins of) upland forests.

The strong focus on heterogeneous storage distribution between and within hydrological units, as well as climate as a dynamic control, also allowed contextualizing previous work on R generation in Boreal Plains catchments within respective physiographical settings.

The study further highlighted the need to better characterize ET - as the dominant flux - and controls thereof within the wetland, as it determines available storage before P events, and thereby fundamentally controls flow gradients and R on catchment-level. A better understanding of this flux in relation to storage distribution will ultimately also allow sound management of aspen-dominated catchments where a balance between the exploitation of forestry resources and downstream water availability needs to be

met.

2.7 Acknowledgments/Contributions

This chapter was established collaboratively with Prof. Kevin Devito and Prof. Carl Mendoza (University of Alberta, Edmonton, Canada). Measurements prior spring 2016 (water levels, soil stratigraphy, climate/weather data) were kindly provided via their monitoring data base, established through various members of their research groups. The design of the study and this chapter were developed jointly with Prof. Kevin Devito and Dr. Nick Kettridge (supervisor). All analyses, and interpretation/writing were done by myself, A. Hurley.

2.8 Supplemental Material

2.8.1 Figures

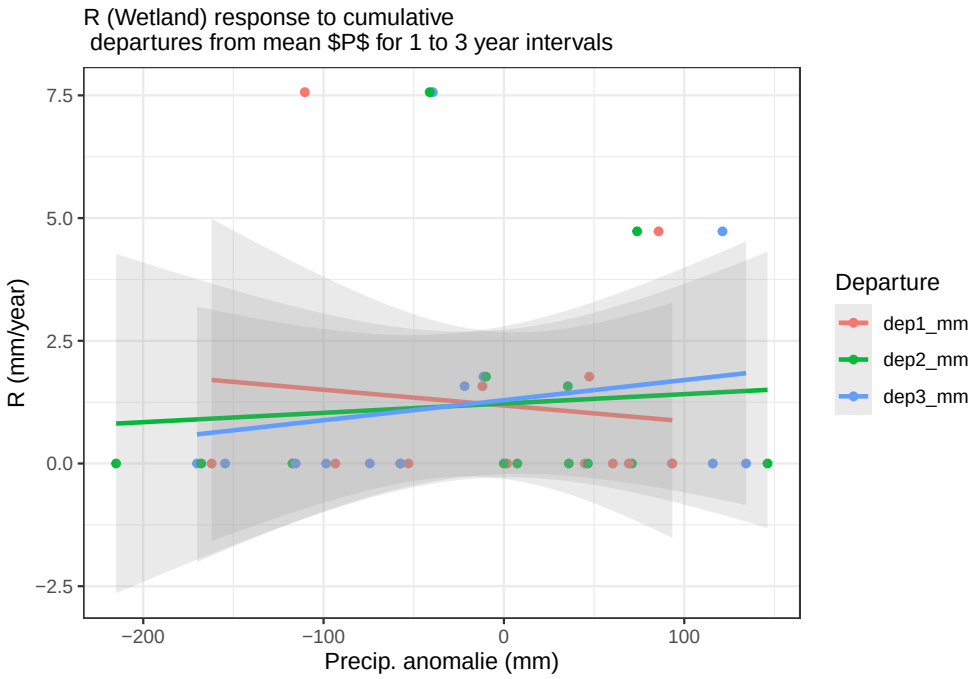

Figure 2.S1: Relationship between annual runoff and precipitation anomalies (cumulative departures from mean) for 1 to 3 years. For more frequently connected systems, relationships between R and mean departure are more pronounced and indicative of storage threshold and lag dynamics in the BP (Devito *et al.*, 2012). Here, no clear relationship could be discerneced, likely owing to the contrasting high storage upland and low storage valley-bottom wetland; the latter was the R generating area, and was likely greatly influenced by short-term climate (previous year) and weather (ice dynamics)

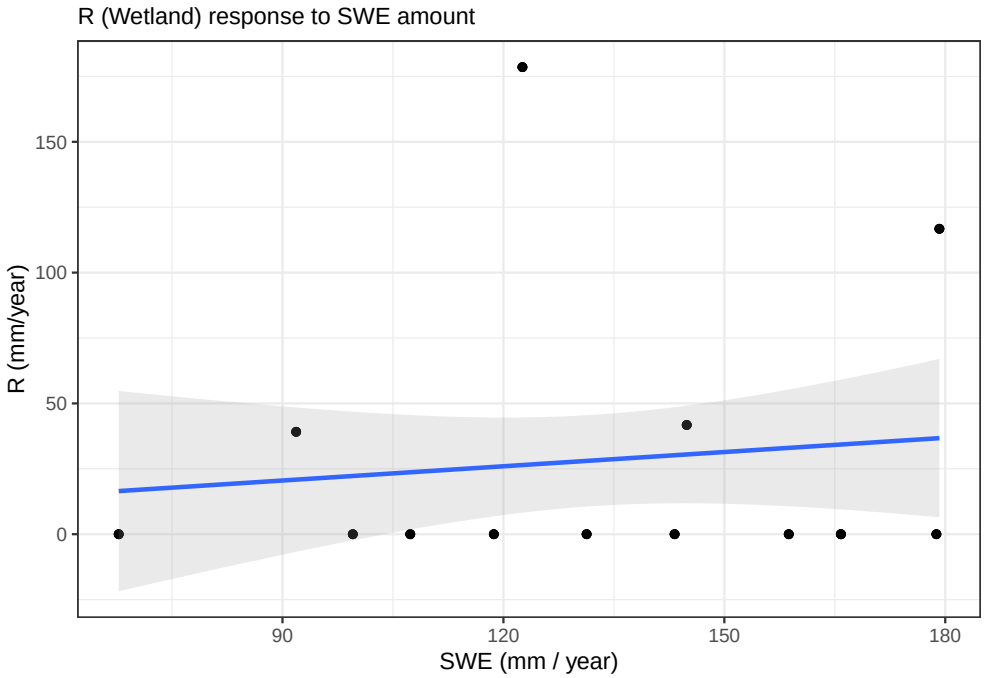

Figure 2.S2: Relation off runoff to snow water equivalent (SWE). No clear relationship was discerned, indicating the strong control available storage capacity (i.e. previous year deficit) and current climate dynamics (ice) have on R generation. Note, that SWE was determined by a temperature threshold, and it did not take into account canopy and sub-canopy snow drift or ablation.

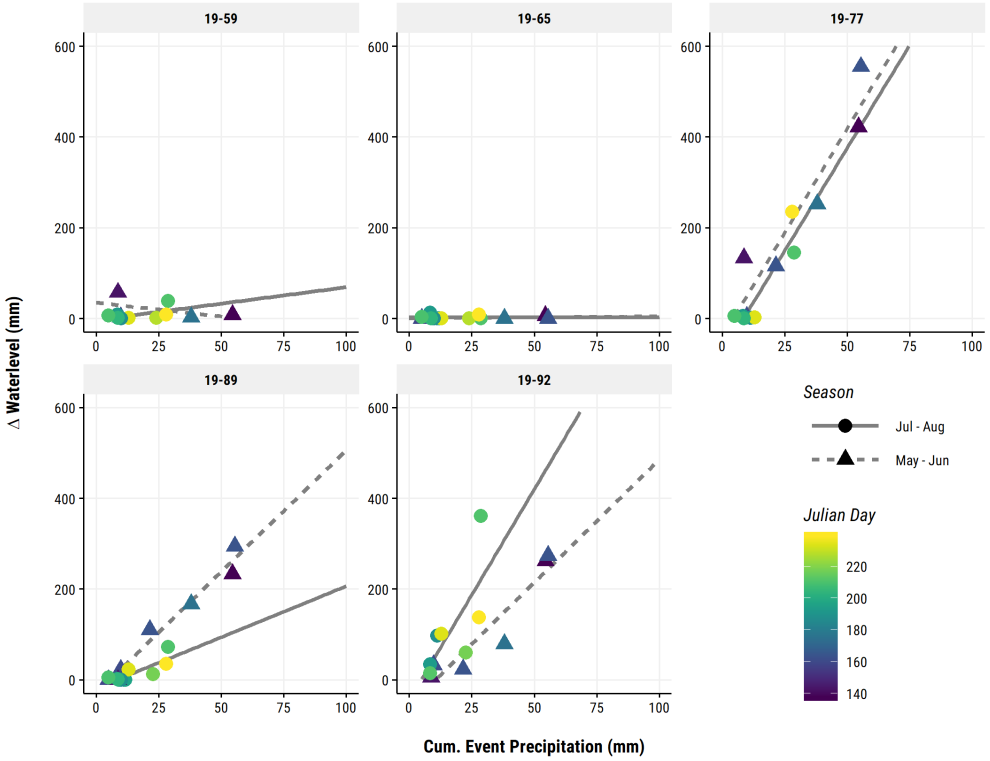

Figure 2.S3: Water table responses to precipitation for multiple wetland sites along transect A, and one hillslope well. Lines represent fits from OLS regression. Separate models were fit for spring and summer to account for dampened event responses due to seasonally increasing ET and interception. Slopes from wetland wells were averaged and their inverse was used as an estimate for specific yield in storage depth estimation.

2.8.2 Tables

Table 2.S1: Results from OLS regression between total P event size (mm) and water table increase. Inverse of mean of slopes was used as specific yield for storage depth estimation. Note, that dropping Site 65, which has considerably higher depth to CL, changes the estimate from $s_y = 0.20$ to $s_y = 0.15$. Given that the model was not significant, the inclusion its value is considered as conservative and taking into account the increased storage toward interfaces and the outflow.

Site	**season**	β	**std.error**	**statistic**	**p.value**
19-65	Spring	0.043	0.0583	0.738	0.514
19-77	Spring	9.21	1.65	5.58	0.00507
19-89	Spring	5.35	0.421	12.7	5.34e-05
19-92	Spring	5.42	1.01	5.35	0.00589

CHAPTER 3

Evapotranspiration from a small Boreal swamp indicates the generation of a water surplus in a sub-humid climate

3.1 Abstract

Forested swamps redistribute water across the drought-prone Boreal Plain (BP), typically due to shallow, responsive soils with low storage. Yet, compared to bog or fen peatlands with similar roles, little is known about their ecohydrological functioning and ensued partitioning of inputs into runoff and other fluxes throughout the highly-variable BP climate. Here, the role of absolute and available storage capacity on the atmospheric water balance and resulting hydrological regime of a shallow, forested, swamp (soils < 1 m depth) were investigated over 20 years including wet, mesic and dry climate cycles, constituting the first assessment of evapotranspiration (ET) from a deciduous BP swamp. Empirical and numerical methods were used to measure atmospheric fluxes from all wetland (structural) components across two growing seasons (2016, 2017), and subsequently simulate them for an idealized system on daily basis for a range of absolute storage found across the swamp. Results allow concluding that shallow swamps can generate water surplus (for runoff) even during most dry years, typically during shoulder seasons (spring, autumn), and that sub-canopy ET was the dominant efflux. Further, relationships between annual ET and precipitation indicated that maximum ET was realized during years with approximately mean, annual precipitation, but was at least 20 % lower than inputs (accounting for interception) and increasingly limited by shallower storage (lower ET, maxima at higher annual precipitation). Simulations with unconstrained storage showed that climatic conditions and water-use of the current vegetation community would only allow for a maximum ET of approximately 85 % of precipitation, with maxima located at a similar value ($ET \approx 307$ $mm \approx$ precipitation). Using ET as a proxy for productivity, these results indicate that the swamp ecosystem is adjusted to conditions imposed by storage limitation, and conditions wetter or dryer than average result in decreased productivity and/or potentially loss of organic soil matter, locking the system in a low productivity state.

3.2 Introduction

The Boreal Plains ecozone consists of a mosaic of forests, wetlands and open-water bodies (Ducks Unlimited Canada, 2011). This landscape is a disproportionately important carbon store (Vitt *et al.*, 2000), provides habitat to a plethora of native and migratory species (Ducks Unlimited Canada, 2000), and is of high economic interest for multiple natural and renewable resource industries (Ireson *et al.*, 2015). Many of these functions and services are derived from the direct or indirect use of surface and/or labile groundwater. Under future climate change increased temperatures and altered precipitation (P) regimes expected for this region (Price *et al.*, 2013; Ireson *et al.*, 2015) will shift the magnitude of individual water balance components over time (e.g. Thompson *et al.*, 2017), and ultimately, may even push ecosystems into alternate states (Schneider *et al.*, 2016). Due to the prevalent sub-humid climate, as well as low-relief landscapes made up of deep, heterogeneous glacial deposits, vertical fluxes (evapotranspiration, ET; percolation) tend to dominate water balances (Grayson *et al.*, 1997; Devito *et al.*, 2005a, 2005b). Boreal Plains wetlands, can serve as water transmitting, contributing or collecting/storing systems (Black, 1997; Spence *et al.*, 2011), and this function fundamentally depends on partitioning of P into ET and remaining fluxes. Indeed, peatland and swamp land cover reportedly increases Boreal Plains catchments' capacity to shift partitioning in favor of higher runoff (R) generation (Gibson *et al.*, 2015; Devito *et al.*, 2017). However, respective functions are mediated by local and regional geology as well as topography, landscape position, vegetation (in adjacent systems) and antecedent moisture conditions (Winter, 1999; Devito *et al.*, 2005a; Goodbrand *et al.*, 2018). Given the region's low $R : P$ ratios (and absolute R depths) and its high variability (Mwale *et al.*, 2010; Devito *et al.*, 2017), understanding the ecohydrological dynamics of these wetland landscape units is instrumental for ensuring that water security needs and demands of stakeholders are met, and to support management in maintaining adequate resilience of ecosystems.

While ecohydrological dynamics in northern (boreal) peatlands are extensively covered in the literature (see Waddington *et al.*, 2015 for review), few studies have focused on swamps (as forested wetlands) with shallow organic soils (i.e. average peat depth $< 0.4\ m$) in the Boreal, and in the Boreal Plain in particular, despite constituting frequent landscape features (Ducks Unlimited Canada, 2011; DeLancey *et al.*, 2019). Their implication as water sources in the landscape warrants detailed investigation of their water balance dynamics and how it is affected by the expressed dry-wet cycles which the Boreal Plain is subject to currently (Mwale *et al.*, 2009; Devito *et al.*, 2012), and to assess potential impact of future climate change (Price *et al.*, 2013; Ireson *et al.*, 2015).

Boreal peatlands, with deep organic soils up to multiple meters, reportedly have feedback mechanisms that allow reducing atmospheric water losses (Waddington *et al.*, 2015), e.g. by soil structures that increase tension under drying conditions resulting in larger surface resitance and lower ET (Kettridge and Waddington, 2014), or by having responsive water tables that drop below plant-accessible depths (Lafleur *et al.*, 2005), and quickly rise close to or above the surface following P inputs. As storage deficits are kept low, or replenished quickly, peatlands frequently generate hydraulic gradients that enable water redistribution as R or subsurface flow (Wells *et al.*, 2017; Goodbrand *et al.*, 2018). In addition, the cold Boral Plain climate, with average annual air temperatures near $0°C$, promote the formation of solid ice layers (under wet antecedent conditions) that last well-into spring, past snow melt and considerably decrease the storage capacity of wetlands (Petrone *et al.*, 2008; Smerdon and Mendoza, 2010), priming them for R.

Low storage, in turn, is also fundamental to the functioning of swamps, which typically feature shallow and highly-decomposed organic soils (NWWG, 1997). This is the result of intermittent or ephemeral hydrological regimes, with rapid and frequent fluctiations of moisture and water levels in organic soils, typically over a flow-impeding

layer (i.e. of low hydraulic conductivity). Due to regular exposure of soils to air, decomposition rates and consequently bulk densities are high (Philben *et al.*, 2014), giving rise to low specific yields, promoting "flashy" hydrological responses. Climate, local micro-meteorology, hydrogeology and vegetation jointly determine the magnitude of P and ET on intra- and inter-annual timescales, and hence whether the atmospheric balance of a swamp generates a deficit or a surplus available for subsequent processes (Winter, 1988; Porporato *et al.*, 2002; Padrón *et al.*, 2017) in a given year. Importantly, the shallow soils themselves must extert a strong control on the magnitude annual ET fluxes can reach, as their is less capacity for soils to uphold ET under extended demand (Jung *et al.*, 2010), and also a higher propensity for P to be partitioned into R when the low storage is frequently exceeded (Milly, 1994). Considering factors noted above, the landscape position and local topography, of course, mediate the ratio between P and ET by allowing for influxes or losses via subsurface and surface pathways. The physiographic characteristics (Winter, 1999) and spatial arrangement (e.g. Brannen *et al.*, 2015) of individual swamps then both affect their water balance, and dictate their cumulative effect on catchment or regional-scale water fluxes (e.g. Phillips *et al.*, 2011; Smith and Redding, 2012) to varying degrees. For example, where topography permits, swamps can be configured similar to swales ('ephemeral draws', e.g. Devito *et al.*, 2005a), or constitute margin systems adjacent to peatlands with deeper organics (e.g. Ferone and Devito, 2004).

Recent work by Dixon *et al.* (2017) highlighted the tendency of shallow peat soils underlain by confining geology (1-D simulations of idealized soil columns) to express water conservation as an emergent property under the Boreal Plains climate. Further, they suggest that the intermittent hydro-regime likely entails conditions which do not favor the accumulation of carbon, thereby maintaining the low-storage character over time; they conceptualize the functioning of these shallow soils to give rise to the typical swamp morphological forms described above. Building on their work, this study aimed to provide first insights on the atmospheric water balance of a shallow swamp

(i.e. forested wetland) in the Boreal Plains. In particular, the aims were to answer the following questions:

1. What is the atmospheric water balance of a shallow swamp and can water surplusses be generated frequently under the sub-humid climate and entailed P variability?
2. How does storage affect the maximum attainable ET under a fixed atmospheric demand?
3. What are the resulting hydrological regime and atmospheric balance magnitudes?

To answer these questions, the atmospheric fluxes of a small swamp were assessed and used to predict ET for the period of 1999 to 2018. Flux estimates were established over two growing seasons (2016, 2017) for the sub-canopy, shrub and tree stratum (varying coverage) and contrasted with water inputs. Given the typically small extent of margin swamps and ephemeral draws/swale-type swamps (e.g. studied swamp less than 0.5 ha), the stratified measurement approach was deemed most appropriate to assess fluxes, as opposed to e.g. relying on eddy-covariance-derived estimates, which would likely be confounded by fluxes from adjacent ecosystems. To limit the impact of lateral flows and groundwater exchange (inputs and losses) on atmospheric balance estimates, a system was selected in a catchment that is permanently perched 15 to 20 m above regional groundwater (Hokanson *et al.*, 2018a), due to an extensive low-conductivity clay layer on which the swamp formed. This study is, according to surveyed literature, the first to provide estimates of swamp ET and resulting atmospheric balances across nearly two decades in the BP; it is hoped that the results and their interpretation provide valuable insights on the impact of storage on the ecohydrological functioning of swamps for natural systems under current and potentially future conditions, as well as provide additional context for recently-identified, newly-established shallow wetland systems on reclaimed landscapes in Alberta (Little-Devito *et al.*, 2019).

3.3 Materials and methods

3.3.1 Study area and site overview

The 0.5 *ha* wetland is located within a predominantly aspen-forested, zero-order catchment (approximately 11.9 *ha*, topographically delineated). The wetland is the main (and typically exclusive) source area for intermittently-generated runoff, flowing downgradient toward a terminal pond north of its outlet. Located in North-Central Alberta (56.081432N, -115.537168W), it is part of the Western Boreal Plain mixed-wood ecoregion where P (444 mm for last 32 years; Hokanson *et al.*, 2018a) approximates potential ET (pET, 517 mm; Bothe and Abraham, 1993), yet is generally lower most years. Hence, water deficitis ($P < pET$) accumulate across multiple years, and are typically replenished after 10 to 15 years (Devito *et al.*, 2005b; Hokanson *et al.*, 2018a). Actual ET varies with landscape position, hydrological connectivity and vegetation type (amongst other factors) of hydrological units (Devito *et al.*, 2012, 2017).

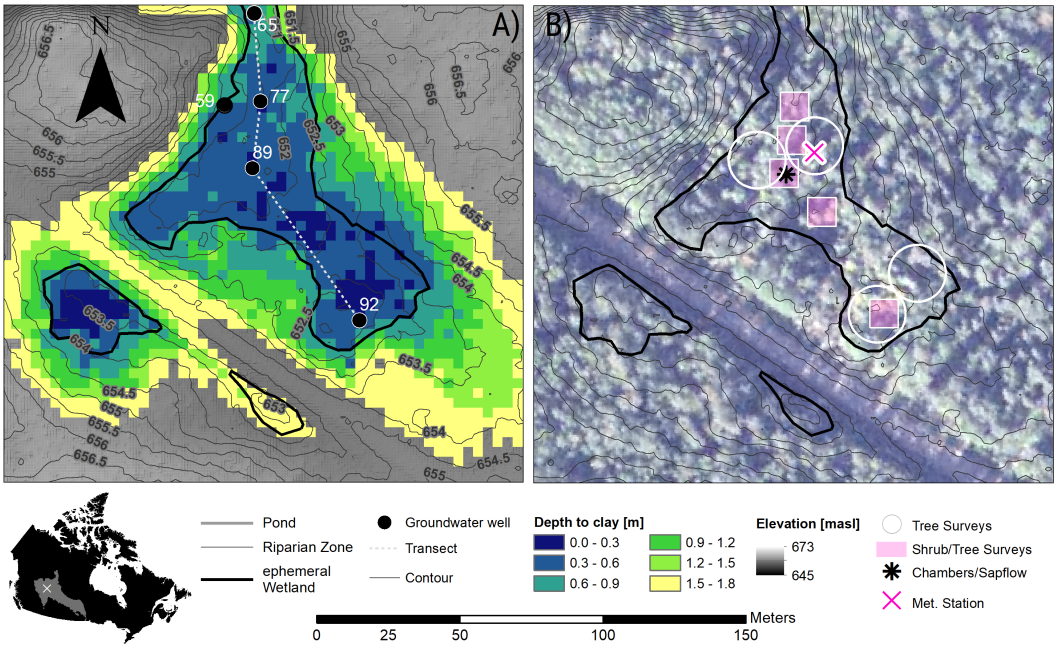

Figure 3.1: Overview of (A) study site and (B) Details on chamber systems and ET estimation are in section 3.3.2; details for micrometeorological and hydro(pedo)logical measurements are in sections 3.3.2.1 and 3.3.3, respectively.

The wetland established in a local topographic low atop a low-permeability clay layer (CL, $K_s \leq 10^{-8}$) at a depth of approximately 0.20 to 0.80 m (see Chapter 1, Fig. 3.1) in a transitional zone of coarse(r) glaciofluvial and fine-grained ice morain deposits (Fenton *et al.*, 2013). The stratification prevents interaction between local surficial and deeper, regional groundwater (approximately 15 to 20 m deep) in a sand aquifer, effectively perching the wetland and headwater catchment (Hokanson *et al.*, 2018a).

Vegetation was layered in three strata, which were also subject to study for estimating water fluxes: (1) sub-canopy, (2) shrubs and trees less than 2 m (referred to as shrubs hereafter), and (3) taller trees (> 2 m). Vegetation cover and tree densities were established in 5 mensuration plots (Fig. 3.1). These were established to reflect the variability of the vegetation strata following CL depth (greater toward outflow), providing more coverage (i.e. higher density of plots) at the most representative community composition in the wetland's center.

The tree stratum was dominated by river alder (*Alnus incana* subsp. *tenuifolia* [Nutt.], also speckled alder), willow (*Salix* spp.) and paper birch (*Betula papyrifera* Marshall) with a maximum height of approximately 5 m (Tab. 3.1). The shrub stratum consisted predominantly of red-osier dogwood *(Cornus sericea* L.), low-bush cranberry (*Viburnum edule* [Michx.] Raf.), prickly rose (*Rosa acicularis*) and beaked hazelnut (*Corylus cornuta* [Marsh.]) of up to around 1.5 m, as well as young trees (see above). The sub-canopy stratum (predominantly herbs and mosses) had stinging nettles (*Urtica dioica* L.), grasses (*Poaceae*), dewberry (*Rubus pubescens*), common horsetail (*Equisetum arvense*), twinflower (*Linnaea borealis*) and kidneyleaf violet (*Viola Renifolia*), amongst others, typically up to 0.50 m. The wetland was classed as a flat swamp (NWWG, 1997) given its vegetation and soil characteristics (humisols and humic gleysols; Soil Classification Working Group, 1998) and observed hydro-regime.

Table 3.1: Stem density of dominant tree species in wetland estimated from total counts of 5 mensuration plots (10 m^2).

Species	**Common**	$stems \cdot ha^{-1}$
Alnus incana subsp. *tenuifolia*	River Alder	1600
Salix spp.	Willow spp.	1200
Betula papyrifera	Paper Birch	960
Picea glauca	White Spruce	360
Populus tremuloides	Trembling Aspen	200

3.3.2 Estimation of atmospheric water balance

Instrumentation for micro-meteorological and hydro(pedo)logical assessments (details belows) was placed in the system's center, corresponding with conditions considered most representative of the forested swamp (reducing edge effects, approximately covering average soil conditions and most dominant vegetation structure and community composition).

3.3.2.1 Micrometeorological and climate data

Local and ancillary data was used for estimating (via simplified Penman-Monteith model, see Section 3.3.2.2) as well as predicting (Section 3.3.2.2) ET fluxes at longer time scales. Air temperature and relative humidity were recorded at 2 m by an Onset HOBO U23-001 Pro V2 logger in the wetland's center from June 2015 to August 2018 every 20 min and averaged to hourly values; this data is referred to as "on-site" throughout this study. Three ETgages (Model E, resolution of 0.254 mm on HOBO event logger, with protective cover only) were installed in the northern, center and southern sections of the wetland to provide a comprehensive estimate of micro-meteorological conditions below the tree canopy. Their surfaces evaporate water from a highly-porous ceramic plate (surface at approximately 0.6 m), and were used as an indicator for potential evapotranspiration, as well as to estimate aerodynamic resistances,

and to constrain shrub transpiration (assumed no transpiration when $ET_{ETgage} = 0$). Note, that ETgages only recorded data across the growing seasons in 2016 and 2017 (May - Aug).

To extend estimates of atmospheric water balance beyond the range of on-site data daily P, hourly T_{air} and relative humidty (rH) were obtained from records of Red Earth Creek Station approximately 70 km north of the site (Environment ad Climate Change, Canada, Station ID: 10183; LaZerte and Albers, 2018), and the DayMet climate service (Thornton *et al.*, 2017; Hufkens *et al.*, 2018) for 1999 to 2018; these ancillary data sets are referred to as "*REC*" and "*daymet*", respectively. Linear relationships between climate and derived variables (vapor pressure deficite, *vpd*) from these ancillary and on-site data (overlap from 2015 to 2017) were used to estimate local climate and micro-meteorological data from 1999 to 2018 (Fig 3.S2). Due to high prevalence of missing P records in the ancillary data, and the availability of local P data, the latter was used for water balance calculations. For comparison with actual ET, Hamon's potential ET was calculated with air temperatures from the *daymet* records, applying equations listed in Lu *et al.* (2005).

3.3.2.2 Evapotranspiration

Sub-canopy (ET_{sc}), shrub (T_{shrub}) and tree (T_{tree}) fluxes were assessed at different times and frequencies across the growing seasons of 2016 and 2017, for which local, micro-meteorological data was available (Tab. 3.2). Fluxes were estimated using automated chambers, leaf conductance and sap flow, respectively, and extrapolated to represent wetland-scale fluxes (where necessary) at hourly resolution. Empirical relationships between daily flux estimates and daily maximum *vpd*, were established and used to predict ET_{total} for periods with on-site micro-meteorological data and, longer-term climate records (see Section 3.3.2.1, *REC* and *daymet* data).

Table 3.2: Overview of measurement periods for individual wetland strata. Note, while shrub stomatal conductance (g_s) was established from four intensive measurement days, additional values were obtained on a weekly to fortnightly basis in 2017 to address potential temporal dynamics, and they were further constrained by the *ET* estimates from ETgages across both growing seasons in 2016 and 2017 (see text).

Stratum	Year	Min. Date	Max. Date	Frequency/Coverage
trees	2017	27 Jun	24 Aug	20 min frequ.
shrubs	2016	28 May	10 Aug	4 day coverage
	2017	18 May	22 Aug	weekly frequ.
sub-canopy	2016	17 May	07 Aug	1 h frequ.

Sub-canopy ET ET_{sc} was taken as the flux from bare soil, litter, moss and vascular vegetation up to a height of approximately 0.5 m and estimated in representative locations (near wetland center) using five pneumatically-controlled Perspex chambers following a modified approach of McLeod *et al.* (2004) from May 17 to Aug 07, 2016. Chambers were mounted onto carefully-placed soil collars (0.05 cm to 0.07 cm deep, area of 0.2 m^2). The chambers were placed in the wetland's center (deemed most representative, see above) in an approximately circular arrangement (2 m apart), covering different sub-canopy and overstory (i.e. shading) conditions. Instantaneous ET_{sc} was calculated from the initial increase of water vapour concentration ($\Delta\rho_{H_2O}/\Delta t$, $kg \cdot m^{-3} \cdot s^{-1}$) in the chamber (volume [V]; approximately 0.05 to 0.06 m^3 depending on micro-topgraphy) during closure over 2 min every hour using a Licor LI-840 infrared gas analzyer (for details see Kettridge and Waddington, 2014; Kettridge *et al.*, 2017):

$$ET_{sc} \;=\; 3600 \cdot \frac{\Delta\rho_{H_2O}/\Delta t \cdot V \cdot C}{A} \tag{3.1}$$

with A as surface area (m^2) and C a factor accounting for vapor absorption on chamber material (unitless; set to unity resulting in conservative estimates). The factor 3600 converts estimates to $mm \cdot h^{-1}$, assuming that 1 $kg \;=\; 10^{-3}$ m^3 water.

A fan ensured air was adequately mixed during measurements. Therefore, conditions in the closed chamber differed from those in the ambient environment. To assess whether ambient differed discernibly from chamber ET_{sc}, a modified Penman-Monteith

model (after Oke, 1992) was used to calculate fluxes under ambient conditions:

$$ET_{sc} = \frac{\rho_{sat} - \rho_{air}}{r_{total}} \tag{3.2}$$

with ρ_{sat} being the saturated vapor concentration of the evaporating surface (here the soil, calculated from surface temperatures measured with type-K thermocouples), ρ_{air} the vapor concentration in the pertinent volume at a given height (0.5 m in chamber, via type-E thermocouple; 2 m for ambient, via rH and temperature logger) in $kg \cdot m^3$, and total resistance r_{total} $(s \cdot m^{-1})$

The above model was forced with chamber and ambient humidity gradients, and $r_{s-chamber}$ (surface) and r_a (aerodynamic) acting in series (additive), giving r_{total}. $r_{s-chamber}$ was inferred by inverting and re-aranging the model under fluxes and conditions imposed during chamber closure, assuming previously determined $r_{a-chamber}$ of 62.6 $s \cdot m^{-1}$ for the same system (Kettridge *et al.*, 2017: SI1). r_a was derived from total resistance estimated from mean evaporation of 3 ETgages on hourly basis by applying the same approach imposing ambient humidity gradients and a fixed r_{s-etg}. The latter was estimated during a laboratory calibration, where E, T_{air} and rH were recorded, while a fan was directed at the evaporating surface to reduce r_{a-etg} to negligble values, giving $r_{s-etg} = 63.4 \pm 2.2\ s \cdot m^{-1}$. There was no discernable difference between mean ET_{sc} from both approaches ($\Delta\mu$ 95 % CI [-0.026, 0.002] $mm \cdot h^{-1}$, $t(260) = -1.65$, $p = 0.1$; Fig 3.S4 for comparison). Chamber and Penman-Monteith fluxes were hence considered representative of ET_{sc}, indicating - on average - similar aerodynamic resistances inside and out of the chamber. Chamber ET_{sc} was therefore used for further analyses.

Shrub transpiration The modified Penman-Monteith equation was also applied to estimate T_{shrub} with on-site data. The humidity gradient forcing the model was established between the transpiring leaf surface, and ambient T_{air} (at 2 m); leaf temperatures

for the entire on-site period were predicted via a linear relationship between recorded leaf temperatures during g_{sc} measurements (see below) and corresponding T_{air}. Note that T_{shrub} was assumed zero when $E_{ETgage} = 0$.

Aerodynamic resistance (r_a) was estimated as described in Section 3.3.2.2. Average shrub resistance ($r_{s-shrub}$) was estimated from repeat measurements of stomatal conductance (g_{sc}; inverse of stomatal resistance $r_{sc-shrub}$) of dominant plant species and individuals across 25 randomly selected 1 m^2 plots (5 each within the 5 tree mensuration plots). Measurements were done with a Decagon SC-1 porometer on three leaves for each individual between 10:00 to 18:00 MST, and repeated on a total of four consecutive days (July 26 to 29, 2016). $r_{s-shrub}$ was obtained as Allen *et al.* (1998):

$$r_{s-shrub} = \frac{r_{sc-shrub}}{LAI} \tag{3.3}$$

with LAI ($m^2 \cdot m^{-2}$) as leaf area index. Average shrub LAI was estimated on the 25 plants for g_s measurements (see above) on dominant individuals, i.e. the respective individual was the sole shrub present or cover from any other shrubs was negligible. Three to 5 leaves (dependent on visually-determined size variability) were removed from each individual, placed and scanned on a white-board with an area reference (square of 1 cm^2) to infer average leaf size, which was then multiplied by the number of leaves (n_{leaf}). n_{leaf} was either a direct count or an estimate based on n_{leaf} for 3 branches and extrapolated for individuals between 1.5 to 2 m. LAI was then averaged across plots and assumed representative of the entire wetland at or close to the seasonal LAI maximum as surveys coincided with peak-NDVI (Section 3.3.2.2). Further, to allow estimating annual shrub transpiration, seasonal LAI dynamics were determined from a bell-shaped function fit to $NDVI$ across day-of-year (for last 10 years) scaled from zero to unity.

Additional g_{sc} data were obtained in 2017 between May 27 and 26 July on approximately weekly basis from 6 individuals (in and next to the wetland center) to check

for potential temporal dynamics. Across all measured data (2016, 2017) the average response of g_{sc} to *vpd* was small (Fig. 3.S5), and hence the derived $r_{s-shrub}$ from the intensive, 4 day period in 2016 was deemed representative for the wetland, but was subject to further scaling (via $NDVI$) described in Section 3.3.2.2. Note that g_{sc} can decrease with higher *vpd*, this response is sensitive to temperature and soil water status, amongst others, (Jones, 2013). As the entire data collection covered a range of these conditions, using a community and seasonally-averaged value for $r_{sc-shrub}$ was deemed reasonable and acceptable for the answers sought from this modelling exercise; for further discussion see Section 3.5.3.

Tree transpiration Daily T_{tree} was estimated from sap velocity v_s derived with the heat ratio method after Burgess *et al.* (2001) (for sensor placement and wounding corrections; see equations in aforementioned manuscript for details) applying sensors following Davis *et al.* (2012) from July 27 to August 24, 2017. Measurements were taken every 20 min and averaged to hourly values for each individual, and species (temporal coverage given in Tab. 3.2). v_s was estimated in 4 individuals of the two dominant tree species each (n = 8), river alder (*A. incana* subsp. *tenuifolia* [Nutt.]), willow (*Salix spp.*). For paper birch (*B. papyrifera* Marshall), the next common species, v_s was assumed as the average of the two former. Note, that two *Salix spp.* sensors were excluded from analyses due to large and random noise (likely linked to a mismatch of sensor and sapwood depth). All trees were located in the wetland center. Volumetric sapflow V_s was derived as:

$$V_{s,i} = v_{s,i} \cdot A_{s,i} \tag{3.4}$$

where the index i denotes the species-specific, average v_s and total, cross-sectional sapwood area A_s, as a fraction of wetland basal area; V_s was then summed and scaled to the wetland area, giving T_{tree} as equivalent water depth. Total basal area was derived from *dbh* surveys in four representative 78.54 m^2 plots, where all stems above 2 m height were measured; linear relationships between diameter-at-breast height (*dbh*) and

sapwood area were established for *A. incana* and *Salix spp.* and allometric equations from Bond-Lamberty *et al.* (2002) were applied for *B. papyrifera* to subsequently estimate total A_s. Refer to Section 3.3.2.2 for details on the scaling method applied to T_{tree} predicted beyond the measurement period (July 27 to August 24, 2017).

Seasonal scaling approach As T_{tree} and T_{shrub} estimates (via proxy measurements and process-based models) did not cover the entire growing season, a scaling approach was implemented to account for phenological (i.e. leaf area) changes throughout the year and applied to predicted fluxes. For this, the annual amplitude and trajectory of MODIS NDVI Collection 5 (250 m resolution, product: MOD13Q1, band: 250m_16_days_NDVI), scaled from zero to unity, was used based on data for 2008 to 2018. Data was obtained using *MODISTools* (Tuck *et al.*, 2014) for a near-by, largely undisturbed, deciduous forest (Fig. 3.2), as the pixel including the wetland also covered water bodies and wetlands with coniferous or evergreen cover (contrasting the deciduous, broad-leaved vegetation in the study system). A sigmoidal function following logistic growth was fit (non-linear least squares regression in R (R Core Team, 2019)) between day-of-year (DOY) zero and the DOY corresponding to the last LAI survey day (shaded band in figure); the lower asymptote was used as the average minimum across the entire year (baseline for scaling). A LOESS fit was then established across all DOYs and adjusted to the baseline asymptote, as the smoothing chosen to follow the growing season trajectory resulted in under-estimation across the shoulder seasons. This LOESS fit's peak was used as the maximum value for scaling the fit NDVI data from zero to unity, and used as a DOY-specific scaling factor multiplied with the predicted T_{tree} flux, as well as LAI_{shrub} (to adjust surface resistance).

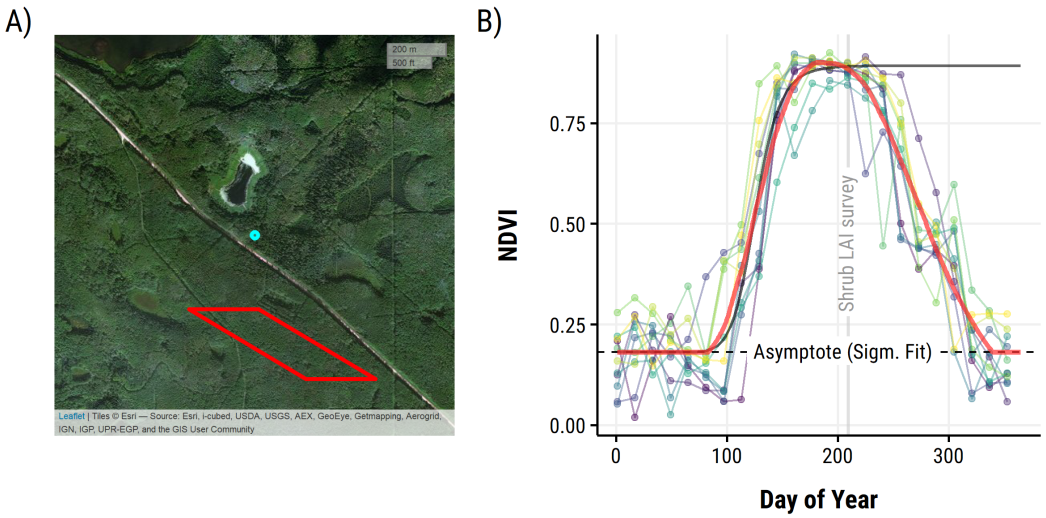

Figure 3.2: A) Extent of MODIS NDVI pixel (red polygon) and location of wetland (cyan point). B) MODIS NDVI data for ten years used to establish a scaling factor for LAI and T_{tree} between the asymptote-adjusted minimum and maximum LOESS-fit values (red line). The asymptote baseline was established from a sigmoidal fit (logistic growth function; black) across day-of-year 0 to 210, corresponding to the shrub LAI survey dates. Remaining point and line colors are years 2008 to 2018.

It is noted, however, that NDVI may saturate before peak LAI (Wang *et al.*, 2005), and hence the scaling may slightly under-estimate maximum T rates after the peak indicated in Fig. 3.2.

Model selection for ET_{total} prediction Daily ET_{total} was estimated as the sum of individual fluxes predicted via linear (OLS) relationships between daily maximum *vpd* and ET for each assessed strata (*vpd* accounted for at least 59 % of variance of each respective flux). Measurements were done during the periods in Tab. 3.2. A set of candidate models was established by fitting increasingly complex functions (polynomial orders 1 to 10); these were then tested for their skill in predicting "out-of-sample" ET. A final model was selected based on assessments of AIC (Akaike's Information Criterion) and BIC (Bayes' Information Criterion), as a measure of appropriate complexity, and a 10-fold cross-validation on a 80:20 split training and test data set using *caret* (Wing *et al.*, 2019) in *R* (R Core Team, 2019). For each candidate model, the root mean square error ($RMSE$) for prediction on the test set (i.e. 20 % hold out

during cross validation) was recorded. The model with the lowest $RMSE$ and an appropriate degree of complexity (i.e. ΔAIC and $\Delta BIC < 2$ units) was selected for final prediction. This procedure was applied to on-site data, and the chosen models were used with REC and *daymet*; predicted fluxes were then compared against measured data to assess their explanatory power (i.e. R^2) and whether they performed well for predicting ET beyond the range of on-site data.

Prediction errors for individual sums were propagated for each day, and cumulatively across a given hydrological year as:

$$\delta e_{total} = \sqrt{\sum (\delta e_i)^2} \tag{3.5}$$

where e is the prediction standard error for each stratum i on a given day, or the (cumulative) error from all days for $i = 1, 2..i-1$ and the current day i.

Throughfall Long-term, local P was measured by two to three tipping bucket rain gauges located at or within approximately 30 km of the study site from 1999 to 2018; during cold seasons P, was measured via spill-over from antifreeze-loaded reservoirs. Throughfall ratios z_{TF} were established 1) for the growing season months as the ratio of covered $vs.$ open-site P of 2017 using 27 hand gauges placed throughout the wetland representing variability in canopy openness and vegetation types; and 2) as the ratio of SWE of forested/treed wetlands in the area (less than 1 km distance) and open-site SWE. "Closed" SWE was established from snow-depth surveys along multiple transects using a linear relationship between SWE snow depth from all paired observations. Snow density (ρ_{snow}; required for model time steps) was estimated via a linear relationship between paired observations of SWE and ρ_{snow} (depth integrated). Note, that further references to annual P are based on these throughfall-adjusted values, contrasting incoming, i.e. available, water with atmospheric losses.

3.3.2.3 Water balance model

The atmospheric water balance of the wetland was simulated on daily basis using a "bucket"-model as:

$$\Delta S_t = \begin{cases} 0, & \text{if } T_{air,t} < 0 \\ 0, & \text{if } P_t = 0 \text{ and } S_{t-1} = 0 \text{ and } SWE_{t-1} = 0 \\ z_{TF} \cdot P_t - ET_{total,t} + M_t, & \text{if } S_{t-1} < S_{max} \end{cases} \tag{3.6}$$

with $(\Delta)S$ being (change) in storage, z_{TF} the throughfall ratio (adjusted to growing season and cold season months), P as precipitation, ET_{total} the predicted, daily ET across all strata, M as melt from snow water equivalent (SWE storage), T_{air} as daily average air temperature at 2 m ($^{\circ}C$) and S_{max} the maximum storage capacity; subscripts t and $t-1$ denote the current and previous time step, respectively. ET_{total} was set to zero when $T_{air} < 0$ or when S was depleted; whenever the latter mechanism operated, ET_{total} is referred to as constrained, as opposed to the unconstrained flux predicted from *vpd* (see Section 3.3.2.2). Excess water ($S > S_{max}$) was removed via runoff. Snow accumulation was assumed for P when $T_{air} < 0$. All units are in depths of water equivalent (mm).

M was taken as the daily melt from SWE following Anderson (1976):

$$M = \begin{cases} D_{f,t} \cdot (T_{air,t} – T_B), & \text{if } SWE > 0 \\ 0, & \text{otherwise} \end{cases} \tag{3.7}$$

where T_B ($0^{\circ}C$) is the base melt temperature after and D_f is the degree-day factor ($mm \cdot day^{-1} \cdot^{\circ} C^{-1}$) after (Bedient *et al.*, 2008):

$$D_{f,t} = 0.011 \cdot \rho_{snow,t} \tag{3.8}$$

with ρ_{snow} being the depth-averaged snow density ($kg \cdot m^{-3}$) for each time t, estimated from a linear relationship between SWE and ρ_{snow} (see section 3.3.2.2).

Model runs, boundaries and initial conditions The bucket model was run for the hydrological years of 1999 to 2017, and initiated with empty storage. Water balance dynamics were established for an "idealized" system represented by properties at the wetland's center (chamber site), where the low-conductivity clay layer was approximately 0.3 m deep. Based on the site-averaged estimates of specific yield (approximated by effective porosity $n_e = 0.2$; Section 3.3.3), that equated to a maximum storage capacity of $S_{max} = 60\ mm$. As the focus of this study was to determine swamp hydrological regimes, as well as the capacity to generate water surplus under current climates, only atmospheric fluxes and runoff were considered. That is, subsurface flows, runon, as well as recharge were not modelled. The large storage contrasts as well as the regionally-perched character (confining clay layer with $K_s < 10^{-9}$, Riddell, 2008) of the assessed wetland, however, minimize the impact of external water inputs, and the chosen model complexity is hence considered appropriate for this study's aims.

To investigate the impact of storage variability and sensitivity to boundary and initial conditions, the model was further evaluated across a range of S_{max} (10 to 80 mm, 10 mm intervals) and initial storage S_0 (0 to S_{max}, 10 mm intervals). These ranges approximately reflect the storage variability found throughout the wetland resulting from heterogeneous CL depth (hollows, hummocks, etc.) as well as varying climatic (antecedent) conditions given by the sub-humid Boreal Plain climate (Devito *et al.*, 2012).

3.3.3 Hydrological measurements

A series groundwater wells ($\varnothing = 0.051\ m$, fully slotted), intersecting the low-conductivity clay layer at each location, were monitored over the 2017 growing season with Solinst

Gold Levelloger (corrected for atmospheric pressure) from May to August. Wells were located along a longitudinal transect (Fig. 3.1) from the wetland outlet in the North running upgradient toward the South; an additional well (19-59) was situated at the wetland-upland interface near 19-77. Water levels were cross-referenced with (approximately) fortnightly manual water level measurements (Solinst TLC Model 107 dipmeter), which were complemented with manual ice depth surveys (steel rod penetration depth).

Water storage capacity (in equivalent water depth) was estimated as the product of the depth to the low-conductivity clay layer (depths ranging from 0.1 to 0.8 m) and effective porosity ($n_e = 0.2$), assumed equal to specific yield. The latter was estimated from water level responses to precipitation (Devito *et al.*, 2005a) in wetland wells along transect A (65, 77, 89, 92), as the inverse of the mean response (b), i.e. slopes (unitless; Fig 3.S6) modeled via OLS regression (Tab. 3.S2) in `R` (R Core Team, 2018):

$$n_e = 1/\frac{1}{n}\sum_{i=1}^{n} b_i \tag{3.9}$$

3.4 Results

3.4.1 ET Prediction

3.4.1.1 Model selection

A comparison between all fitted linear relationships between vpd and ET fluxes (sub-canopy, shrubs, trees) with polynomial orders ranging from 1 to 10 indicated that lower orders (between 1 to 3) out-performed higher orders in their predictive skill ($RMSE$). Similar indications were given by information-loss and complexity trade-off given by

Table 3.3: Final models selected for predicting stratum-specific fluxes with respective parameter estimates for polynomial terms, and corresponding statistics (SE is standard error). Model equations represented linear models of the form $Y = \beta_0 + \beta_1 x_1^1 ... + \beta_n x_n^n + \epsilon$.

Stratum	Order	β_0 (interc.)	β_1	β_2	β_3	R^2	SE	t-statistic	P-value	df
trees	3	-0.02	0.72	-0.32	0.05	0.71	0.09	122.22	0	4
shrubs	2	0.02	0.87	-0.16	NA	0.59	0.24	111.02	0	3
sub-canopy	2	0.04	0.89	-0.20	NA	0.67	0.22	435.05	0	3

ΔAIC scores (Fig. 3.3). Note that lowest $RMSE$ for T_{tree} was achieved at polynomial order 9, which was deemed unnecessarily complex (as indicated by the lowest ΔAIC at order 3). Final selected models are given in Tab. 3.3. Choices were informed by above metrics, as well as to implicitly include the ecohydrological feedback of decreasing or asymptotically-saturating fluxes at the highest ranges of *vpd* (Chapter 6, Jones, 2013), notably by choosing polynomial order 2 over order 1 for the sub-canopy ET_{sc}. Refer to Fig. 3.S7 for implications of model choice on predicted fluxes.

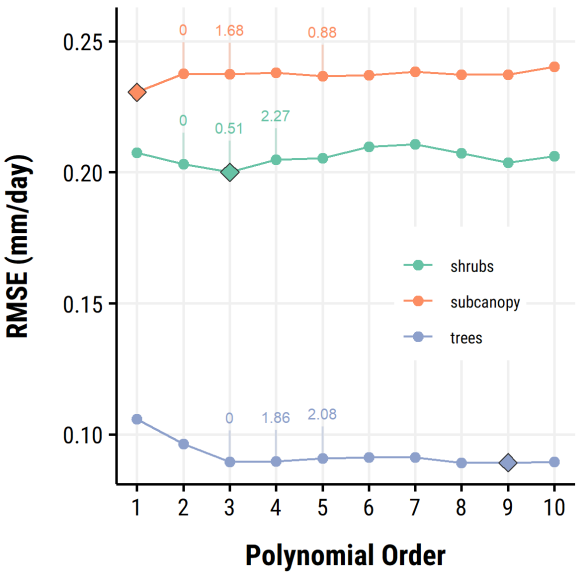

Figure 3.3: Comparison of models based on RMSE (lowest value denoted by diamond) and three lowest ΔAIC scores (text labels) for all candidate models (polynomial order 1 to 10).

3.4.1.2 Comparison between on-site and ancillary data

ET_{total} was predicted as the sum of stratum-specific fluxes (Fig. 3.S7). A comparison across on-site (for short-term), *REC* and *daymet* (for long-term) data sets indicated good fit for all records (note, the latter two were used to estimate on-site conditions). Predictions based on on-site data agreed best with fluxes from measured/modelled values (R^2 of 0.66, 0.52 and 0.76 for ET_{sc}, T_{shrub} and T_{tree}, respectively; Fig. 3.4A-C), indicating that the chosen prediction approach was suitable to generate flux estimates. When comparing predictions based on *vpd* derived from *REC* (nearby station) and *daymet* (1 *km* gridded) data, agreement decreased slightly for ET_{sc} (≈ 2 %) and T_{shrub} (≈ 4 %). A stronger reduction was found for T_{tree} (48 %, *REC vs daymet*); however, *daymet* predictions approximated measured data better on average, evident in a slope closer to unity compared to *REC* (1.26 ± 0.26 *vs.* 1.50 ± 0.17, respectively) and lower (absolute) intercept (-0.01 ± 0.12 vs. -0.27 ± 0.08). Predicted ET_{sc} was slightly higher for *REC* and *daymet* with 0.24 ± 0.05 (intercepts for both), but slopes were fairly close to unity (1.09 ± 0.06 and 1.11 ± 0.06, respectively). On average, T_{shrub} predictions from *REC* and *daymet* followed modelled fluxes closely (slopes 0.95 ± 0.13 and 0.93 ± 0.13; intercepts -0.03 ± 0.12 and 0.02 ± 0.11, respectively). Overall, *daymet* was deemed more suitable for flux predictions, and was applied for estimating the atmospheric water balance. Using this data set, maximum fluxes reached 2.84 ± 0.71, 2.80 ± 0.69 and 2.80 ± 0.69 $mm \cdot day^{-1}$ from 2015 through 2017, respectively (Fig. 3.4D). ET_{sc} was the largest flux from the system, averaging 0.45 ± 0.01 $mm \cdot day^{-1}$, followed by T_{shrub} (0.31 ± 0.01 $mm \cdot day^{-1}$) and T_{tree} (0.17 ± 0.01 $mm \cdot day^{-1}$), based on predictions given in Fig. 3.4D.

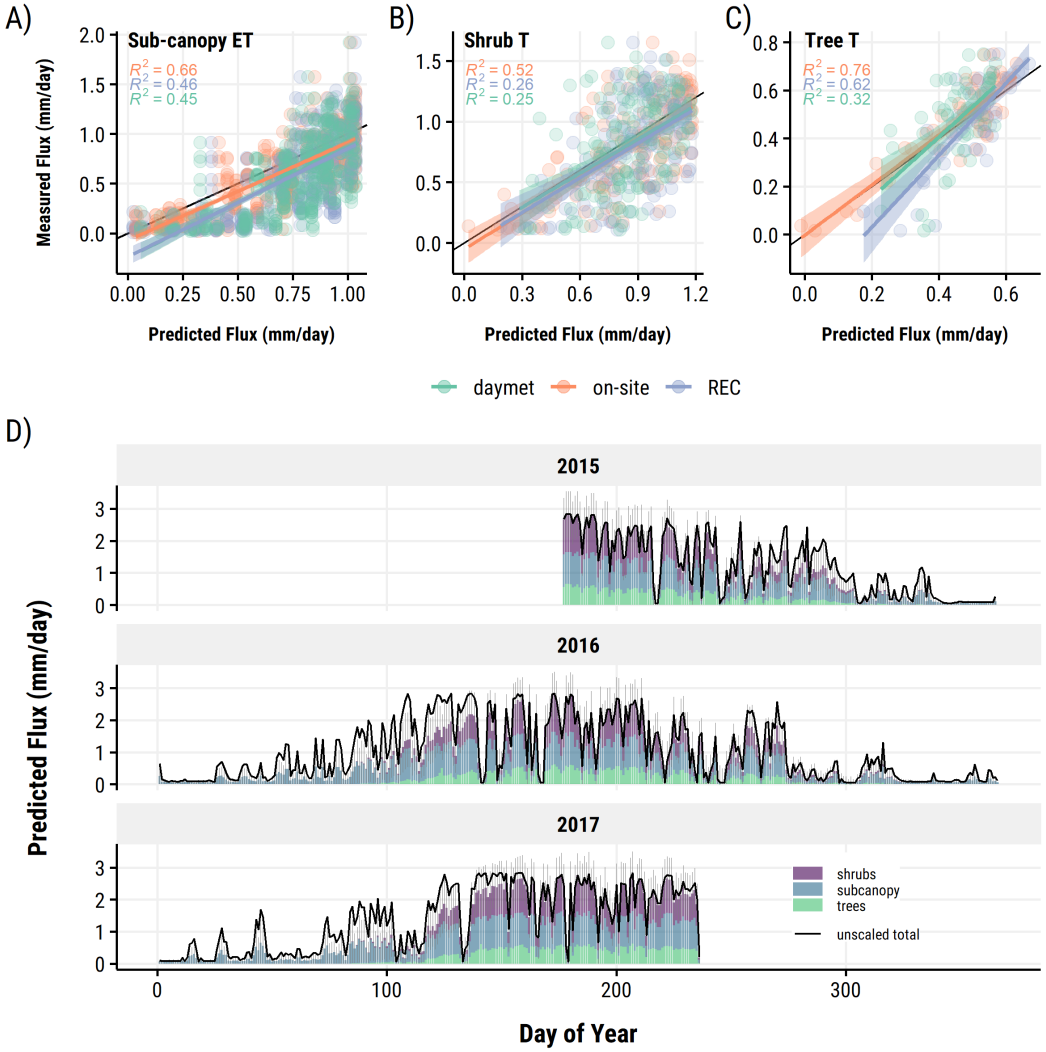

Figure 3.4: Comparison of predictive performance between measured/modelled data, and $on-site$, $daymey$ and REC climate records for all strata (A - C), and D) ET_{total} predicted for the on-site data period, with scaled and unscaled totals; gray bars are cumulative standard errors of scaled fluxes. Note, that ET_{total} was not set to zero where $T_{air} < 0$ here - this is for illustrative purposes only, and fluxes were assumed unconstrained.

3.4.2 Multi-year water balance

Across the 19 years (1999 - 2018), P averaged 361 $\pm$ 16 $mm \cdot year^{-1}$ (min.: 225, max: 467 mm; Fig. 3.5, also Fig. 3.8 and Fig. 3.S1). Predicted ET_{total} - as an imposed or storage-unconstrained flux (Fig. 3.5) - was 297 $\pm$ 5 $mm \cdot year^{-1}$ (min 251: , max: 328 $mm \cdot year^{-1}$). By contrast, once storage limitation was introduced (model run with $S_{max} = 60$ mm, $S_0 = 0$ mm), ET_{total} averaged 262 $\pm$ 7 $mm \cdot year^{-1}$ (min 206: ,

max: 307 $mm \cdot year^{-1}$).

Storage was typically close to or saturated by the end of winter and/or around early spring, as a result of "carry-over" from the preceding year, or due to snow melt moving into storage; the latter process delayed storage depletion, for example, in 2011 and 2013, where P events were of relatively small magnitude across spring (compared to other years; cf. steepness of cumulative P in Fig. 3.5). Larger, intermittent P events (steep increases in cumulative P in Fig. 3.5) bring the system close to or up to saturation for brief periods, due to its low specific yield (or effective porosity $n_e = 0.2$).

Vice versa, storage is rapidly depleted across late spring and summer, when ET_{total} is typically highest due to increased atmospheric and vegetation water demand. Where both annual P, as well as the frequency and size of P events are low simultaneously, storage is close to or fully depleted for prolonged periods, evident in e.g. 2001, as well as a large discrepancy between storage-constrained and unconstrained ET_{total} in multiple years (cf. red and green curves in Fig. 3.5). Disregarding 1999 as a "spin-up" year, storage was fully depleted in 12 of 19 years (for varying durations).

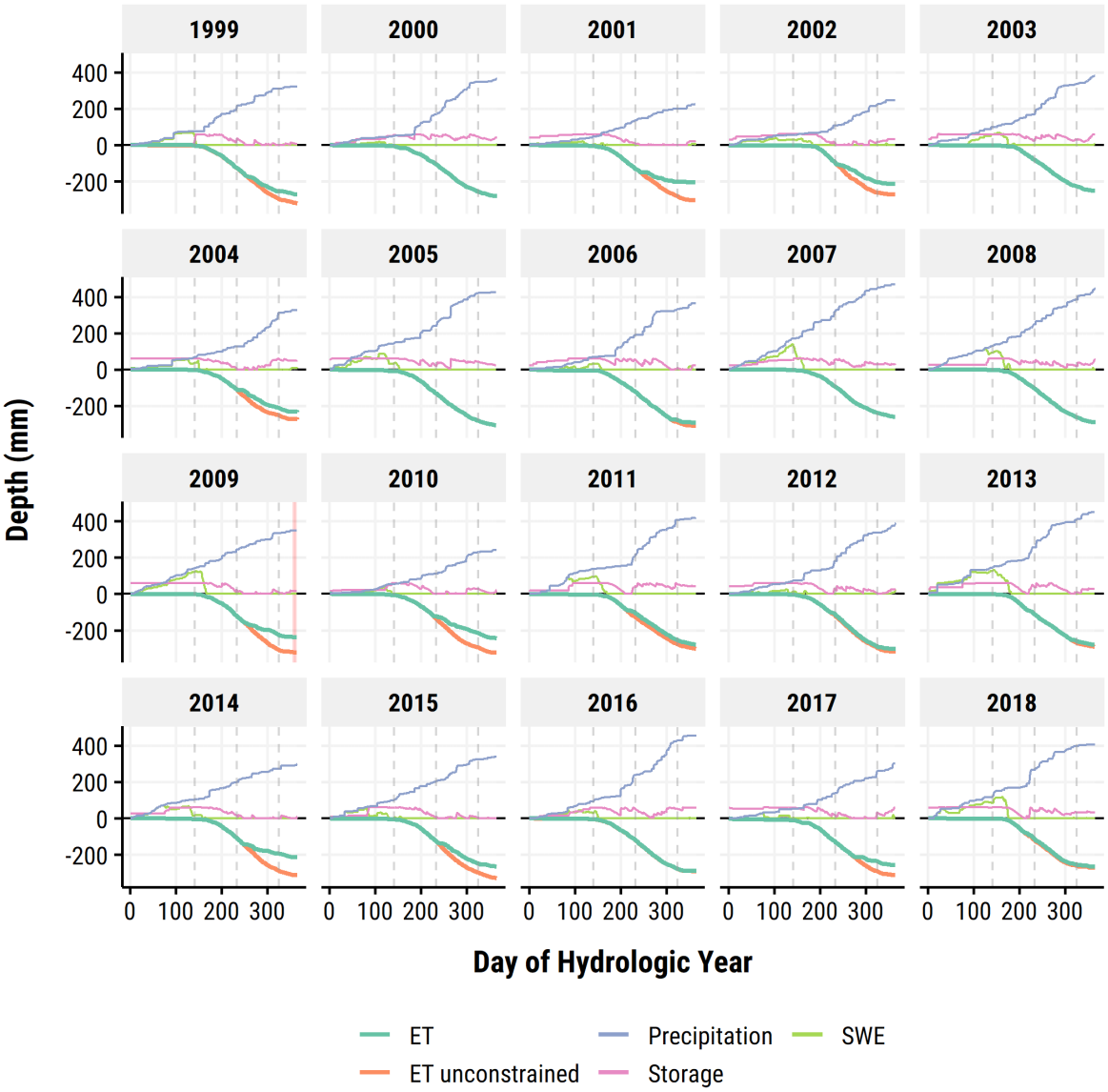

Figure 3.5: Water balance components across hydrological years with available data in the *daymet* record for a model run with $S_{max} = 60$ and $S_0 = 0$ (assumed average wetland conditions); all depths are cumulutaive, except for storage and SWE and red shading indicates missing P data. ET_{total} (line thickness indicates cumulative errors) is set to zero when storage is depleted (constrained); the impact of this storage dynamic is evident in the spread between constrained and unconstrained fluxes. Dashed, vertical lines indicate onset of spring, summer and autumn.

Water tables were monitored along a transect with different depths to a flow-impeding, low-conductivity clay layer (approximately 0.25 to 0.80 m from 19-92 to 19-65) and specific yields (Fig. 3.6). Considering this, the simulations with average-wetland conditions ($S_{max} = 60$, $n_e = 0.2$), and predicted ET_{total} reproduced the over-all water table trajectories (i.e. increase and recession periods) to a satisfactory degree;

most notably, the timing of saturation between simulated storage and observed water levels (near May 15, 2017) and the relative magnitudes of increases following P correspond well.

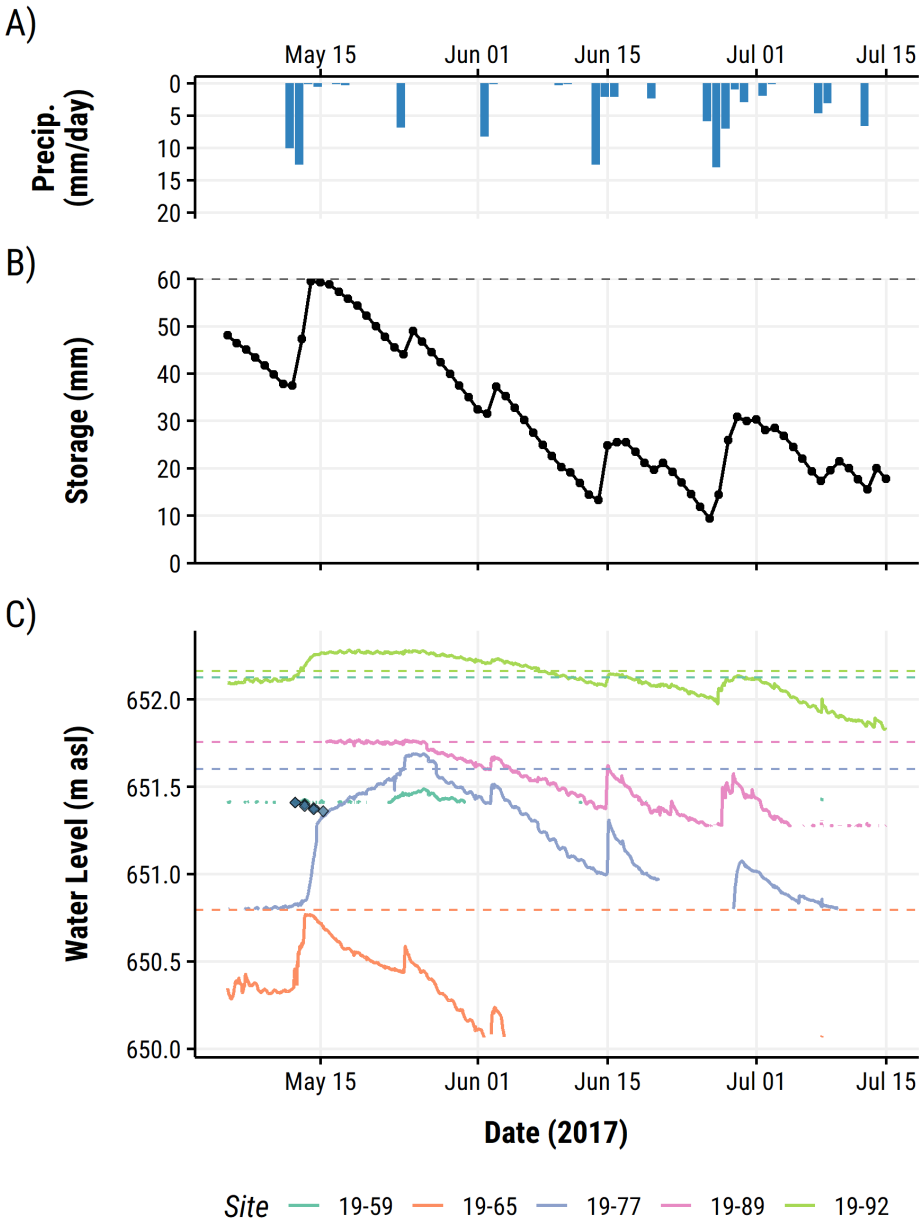

Figure 3.6: A) Daily P, B) corresponding, simulated storage ($S_{max} = 60\ mm$, $S_0 = 0\ mm$) water level response across wetland wells, from topographically high to lower positions (sites 19-92, 89, 77, 65), and a hillslope well (19-59). Dashed lines are respective ground surface elevation (note colors), and diamonds represent the elevation of a solid ice layer at 19-77. Note, that lateral fluxes are disregarded for storage dynamics.

The joint impact of annual total P, P event size and storage is reflected in the

atmospheric water balance across years, with boot-strapped means of -63 $mm \cdot year^{-1}$ (95 % CI: [-99, -31] $mm \cdot year^{-1}$), 64 $mm \cdot year^{-1}$ (95 % CI: [27, 101] $mm \cdot year^{-1}$), 98 $mm \cdot year^{-1}$ (95 % CI: [74, 123] $mm \cdot year^{-1}$) for potential ET, unconstrained, and storage-constrained ET_{total}, respectively (Fig. 3.7).

Except for 2010, all years produced a water surplus on annual basis when storage limited ET_{total} (Fig. 3.8). Storage-unconstrained ET produced positive atmospheric water balances less frequently (14 out of 19), and in most years at lower magnitudes. By comparison, when imposing potential ET (Hamon's method), only 7 of 19 years produce a slightly positive water balance (between 0 to 50 mm).

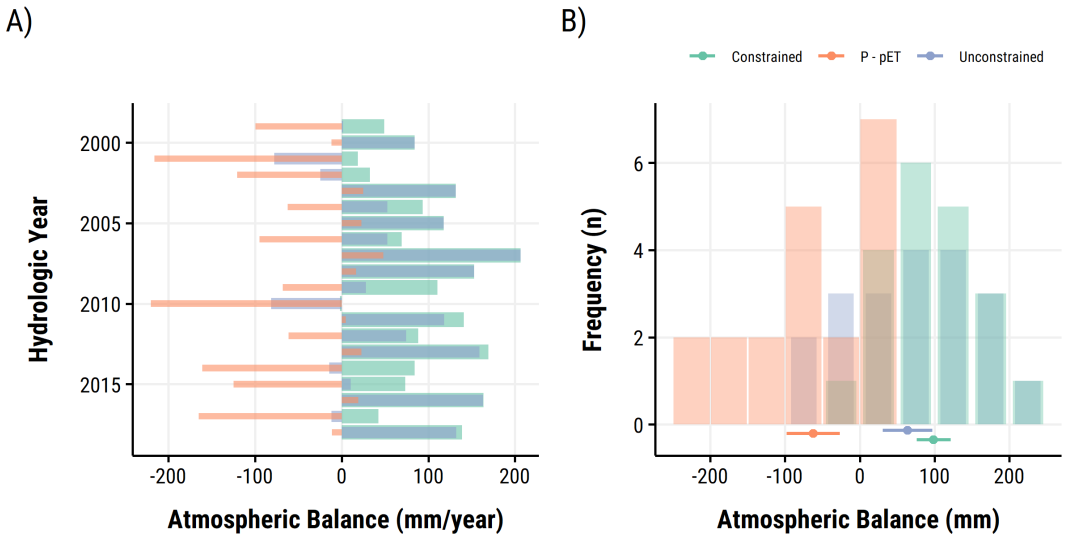

Figure 3.7: Atmospheric water balance for $S_{max} = 60$ and $S_0 = 0$ with constrained and unconstrained ET_{total}, as well as potential ET (Hamon's method) established (A) across years and (B) their respective frequencies. Point and linerange represent boot-strapped means and their 95 % CIs.

Storage limitation has a decisive impact on the atmospheric water balance (see above) by altering ET_{total} in relation to annual P, inferred by model runs at varying storage capacities (S_{max} 40 to 80 mm; Fig. 3.8). For systems with storage-limitation, the majority of years, even under dry conditions (i.e. below average P 361 $\pm$ 16 $mm \cdot year^{-1}$), produce surplus, with lower storage capacities producing more positive atmospheric balances at the same annual P (Fig. 3.8). Unconstrained ET_{total} reaches a higher maximum than for all other storage capacities (20 to 40 mm higher, Tab. 3.4),

Table 3.4: OLS model metrics and equations for 2^{nd}-order polynomials fit to ET_{total} and annual P, corresponding to Fig. 3.8. Equations are quadratic and take the form of parabolae: $y = max_{ET} - \beta \cdot (x_{optim} - x)$. Increasing storage is associated with higher maximum ET_{total} (i.e. max_{ET}), which is achieved at ever smaller annual P (i.e. x_{optim}).

Storage	R^2	SE	t-statistic	P-value	Equation
40	0.60	20.82	12.63	4.4e-04	$y = 266.05 - 0.00134 \cdot (465.75 - x)^2$
50	0.61	20.37	13.53	3.1e-04	$y = 279.1 - 0.00115 \cdot (489.15 - x)^2$
60	0.59	20.09	12.43	4.7e-04	$y = 284.5 - 0.00117 \cdot (478.03 - x)^2$
70	0.54	20.33	9.87	1.4e-03	$y = 286.16 - 0.00136 \cdot (446.78 - x)^2$
80	0.49	20.02	8.25	3.1e-03	$y = 287.95 - 0.00164 \cdot (418.05 - x)^2$
Unrest.	0.16	20.37	8.98	2.6e-04	$y = 305.7 - 0.000966 \cdot (297.72 - x)^2$

at considerably lower annual P (298 mm vs. at least 418 mm). ET_{total}, converges to similar values at higher P, and hence atmospheric balances begin to approximate each other in wettest years (above study average of 361 $\pm$ 16 $mm \cdot year^{-1}$). The strongest difference between storage-limited and unconstrained ET_{total} occurs before and up until average P is reached.

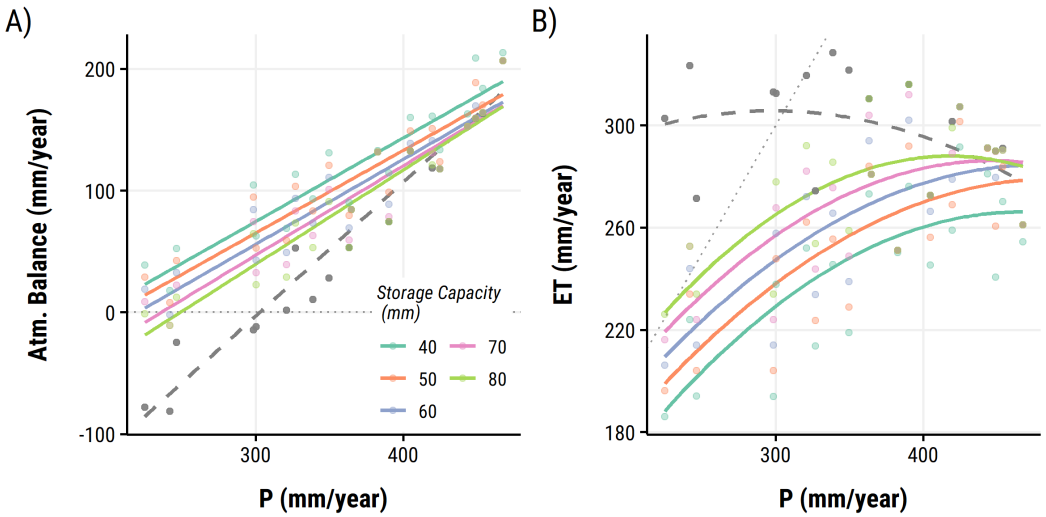

Figure 3.8: Impact of storage on A) water balance and B) ET_{total} in relation to annual P. Points on the dotted line represent $P = ET$; the gray dashed line and points are for unconstrained (infinite storage) ET and all models were run with $S_0 = 0$ mm. Lower storage allows for surplus water generation at lower annual P (Tab. 3.4), and, most notably, shifts maximum ET_{total} toward higher P.

3.4.3 Wetland functioning and model sensitivity

Model runs with varying storage capacity from 80 down to 10 mm (Fig. 3.9) were used to infer the ecohydrological functioning of increasingly shallow systems, as well as for a proxy of spatial variability within a system. In line with results above (i.e. largest surplus with lowest storage), systems with lower storage capacities (S_{max}) were saturated longest (above 10 %), while higher storage progressively diminished hydroperiods down to around 5 % (differences decreased with larger storage; Fig. 3.9A). Correspondingly, low storage is readily depleted under the imposed ET_{total} regime, and hence periods of complete dry-out are more pronounced as storage decreases with around 22 % of the 19 year record for $S_{max} = 10$ mm, down to below 5 % for $S_{max} = 80$ mm (Fig. 3.9B).

The average return period for saturation and storage depletion varied analogously to respective durations discussed above. Increasing storage is less frequently met or depleted under the imposed atmospheric demand, while decreasing storage is associated with higher turn-over. For example, the average return period for saturation for $S_{max} =$ 80 mm (approximately 42 days) was 147 % larger than for the smallest simulated storage $S_{max} = 10$ mm (17 days); for storage depletion, that difference was around 436 % ($S_{max} = 80$ mm: 118 days, $S_{max} = 10$ mm: 22 days).

The applied storage model was more sensitive to its boundary than initial conditions, as the relative impact of changing S_{max} was considerably larger than that of initial storage (typically within few percent). Basing interpretations of atmospheric water balances on a model run with $S_0 = 0$ was therefore considered adequate.

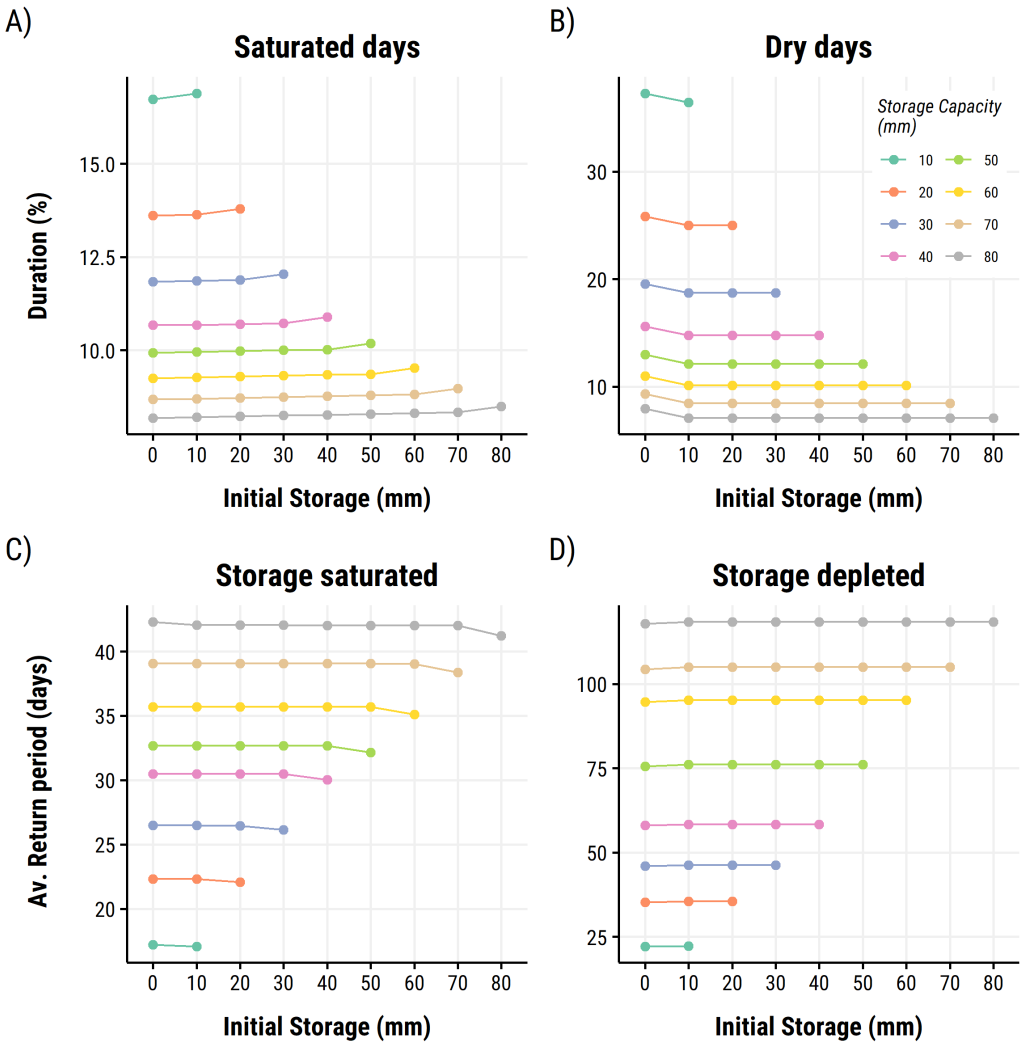

Figure 3.9: Duration (A, B) and return period (C, D) of saturation (A, C) and dry-up (B, D), commonly referred to as hydro-regime and hydro-period, respectively, in relation to different S_{max} and S_0 (i.e. boundary and initial conditions). Durations (i.e. periods) are calculated based on totals across the entire record from 1999-2018.

3.5 Discussion

Annual, atmospheric water balances were estimated for an idealized, shallow swamp using predicted ET_{total} and varying maximum storage capacities (S_{max}). The following sections discuss the role of storage, highlight potential implications of the results for landscape ecohydrology, as well as wetland establishment and permanence. Model assumptions and limitations are briefly reviewed and discussed.

3.5.1 Long-term functioning in relation to climate and shallow storage

3.5.1.1 Climate dynamics

The simulations indicated a high potential for frequent water redistribution via runoff (as modelled here) as well as sub-surface flows, to e.g. downgradient or adjacent systems (not explicitly considered). This potential was realized solely through internal processes, i.e. current climatic conditions set against the swamp's water demand, as on average only around 73 % of available P (adjusted for interception) were used to drive the swamp's ET. Positive atmospheric balances were frequently achieved on annual bases, as well as within a given year, where storage exceedence occurred frequently during shoulder seasons, especially around snow melt in spring. During, summer - typically the period of highest demand (Devito *et al.*, 2012; Brown *et al.*, 2014a) - the variability of P events had a major influence on whether soils saturated fully. Large, intense storms are generally more effective than smaller events over an extended period (Noy-Meir, 1973; Milly, 1994), a dynamic also found in observational studies of Boreal Plain wetlands (Devito *et al.*, 2005a; Wells *et al.*, 2017), albeit mediated by antecedent conditions (i.e. antecedent storage capacity).

The atmospheric surplus taken equivalent to R was in magnitude similar to that of Boreal Plain catchments dominated by peatlands and swamps (> 60 % cover), as reported by Devito *et al.* (2017), where R ranged between 60 to 119 mm; they further estimated via extrapolation that catchments fully covered with peatlands and swamps would would have a median annual ET of 301 $\pm$ 70 and R of 137 $\pm$ 57 mm ($\pm$ for 95 % CIs), agreeing well with estimates for the idealized swamp ($S_{max} = 60\ mm$) with ET_{total} of 262 $\pm$ 7 $mm \cdot year^{-1}$ taking into account interception losses.

ET from catchments in the Boreal Plain is typically water-limited, rather than by

available energy (Budyko *et al.*, 1974), i.e. their ratio of annual potential ET to P is above unity (Devito *et al.*, 2017). This would typically imply increasing ET_{total} with higher annual P, up until saturation (i.e. asymptotic leveling) where energy supply is fully exploited, as shown e.g. with the mathematical framework by Zhang *et al.* (2004) utilizing a similar approach to Budyko *et al.* (1974), and observed for other water-limited systems (e.g. Mediterranean catchments, Montaldo and Oren, 2018). Findings here show a similar initial increase, and suggest either an analogous leveling off of ET_{total} above a threshold P, or a decrease, as argued here. While interpretations are sensitive to the functional form chosen to fit the data, the quadratic fit adopted in Fig. 3.8 is conceptually sound: ET_{total} is largely dependent on daily maximum *vpd*, which is bound to be low(er) at higher annual P, as those conditions typically entail colder summers (Mwale *et al.*, 2009), with large storms and cyclonal weather patterns (i.e. temporally extended). Note, however, individual, high-intensity P events could allow for a saturating, rather than a decreasing trajectory, but given the low probabilities of such events (< 0.03 for 30 mm events in growing season; Devito *et al.*, 2005a) the quadratic, rather than a saturating function, provides a more likely trajectory for ET_{total} estimated here in relation to annual P.

3.5.1.2 Storage impacts

Atmospheric surplus generation was observed frequently for the modelled swamp and magnitudes showed a strong dependence on annual P as well as storage capacity S_{max}. Storage limitation (simulations with 80 to 40 mm S_{max}) showed a considerable shift of both maximum ET_{total}, which decreased with storage, and the climatic conditions (as annual P) at which maximum ET was achieved. This is due to the higher frequency and longer periods at which storage is depleted (Fig. 3.5). This feedback, while not encoded as a soil-plant-atmosphere process, is well documented in the literature, and observed for northern peatlands when water tables drop below a threshold-depth (e.g. Lafleur

et al., 2005; Waddington *et al.*, 2015 for review of such feedbacks). Dixon *et al.* (2017) further showed through a modelling exercise that low storage (shallow peat of up to 0.5 m over confining geology) result in frequent drop of water into mineral soil layers entailing a shut-down of ET, effectively conserving water (shifting atmospheric balances toward more positive values). A meta-analyses based on data from 1604 catchments in different climate regions showed that storage capacity was a minor factor in the partitioning of annual P into water balance components (ET, R) compared to climate and topography (Padrón *et al.*, 2017). The strong shifts in the ratio of ET to P reported here, however, are clearly related to maximum storage capacity. The disparity is easily reconciled when considering 1) the scale of investigation adopted here and in Padrón *et al.* (2017), as catchments typically are more variable and seldomly have storage capacities below 80 mm as found for (sections) of the studied swamp, and 2) while comparative in nature, the meta-analyses does not allow estimating effects of storage under a given climate for varying degrees of maximum capacity in the same location.

The limitation of ET_{total} due to storage further agrees with results from observational mesocosm (Pangle *et al.*, 2014) and regional ET dynamics (e.g. Jung *et al.*, 2010), as well as conceptual/lumped (e.g. Milly, 1994; Atkinson *et al.*, 2002) and fully explicit coupled land-surface and hydrological modelling studies (e.g. Milly and Dunne, 1994; Condon and Maxwell, 2017). For example, Milly (1994) employed a mathematical framework to show that ET was sensitive to a maximum soil water storage until a threshold, above which ET was maximized (Section 3.5.2 for further discussion); under these conditions either water or energy supply (lesser of both) would become limiting. Under limited storage, the author also found runoff increased, i.e. it approached P with storage tending toward zero - this is in accord with higher frequency of saturation (indicative of conditions for saturation excess flow) and more positive atmospheric balances in present study.

Other wetland systems with ephemeral regimes, such as seasonally-flooded ("vernal") pools have been shown to behave, partly, opposite (Brooks and Hayashi, 2002): those systems with the greatest, absolute storage, including surface depression, show the longest periods of saturation and/or inundation, while shallower storage is more readily depleted. The present study showed that shallow systems were saturated most frequently and in sum longest, while deeper storage was associated with less frequent dry-out (similar to Brooks and Hayashi, 2002). The longer saturation period for deep depression storage is easily reconciled with results here if one considers 1) the impact of perimeter:area ratios, where small systems can face relatively larger losses via interfaces, and 2) the greater heat buffering capacity and thermal inertia of water, and its dampening effect on evaporation (Allen *et al.*, 2016) found in systems with greater (absolute) storage. Hence, it is important to consider not only the absolute storage capacity, but also how stored water affects fluxes, as in this case, via thermodynamic dampening of ET or, for example, where rates of surface or subsurface fluxes are enhanced via transmissivity feedbacks in surface-near layers (Bishop *et al.*, 2004) close to or at saturation. Investigating swamps across a spectrum of hydrological regimes is therefore recommended to gain more insight on the dynamics of storage limitation and the partitioning of P.

3.5.2 Implications for local and landscape ecohydrology

The approach adopted here - all assumptions considered - allowed estimating the frequency at which the swamp produced a water surplus, as well as the optimal amount of annual total P to maximize ET under a given storage constraint. Dixon *et al.* (2017) found that shallow organic soil profiles (organics up to 0.5 m over confining geology) tend toward water conservation and lower productivity states (i.e. here suggested by total annual ET) as their capacity to sustain ET through the absence of P is less than for soils with larger storage, especially when taking into account upward transport from

underlying mineral soils. Milly and Dunne (1994; and later subsequently Milly, 1994) discuss control of storage on the atmospheric balance in light of vegetation water use, and suggest that ecosystems, on average, tend to maximize their use of water and minimize R in light of available storage. Results here suggest that optimal ET (as a proxy for maximum productivity) for unconstrained storage very closely approximates annual P, in line with suggestions of Milly and Dunne (1994). This may indicate that storage variability is fundamental in defining the limits of productivity of shallow-storage systems, as discussed by (Dixon *et al.*, 2017). It then follows, that for a given maximum storage capacity, years with annual P above and below this optimum are detrimental to productivity either through lack or excess of water, especially considering short-term variability throughout the growing season (Porporato *et al.*, 2002).

A caveat that must be considered here, however, is that the vegetation community and soil surface driving ET was fixed over time for each considered maximum storage capacity. In reality, vegetation communities would change over time based on cumulative water and oxygen stress (Rodriguez-Iturbe *et al.*, 2001; Brolsma and Bierkens, 2007), induced by the respective hydro-regime and period (Euliss *et al.*, 2004; Rodriguez-Iturbe *et al.*, 2007). A successive shift from low-productivity systems (indicated by low maximum annual ET) for low storage systems, to higher productivity systems could be achieved by the accrual of storage, i.e. through accumulation of organic soils (e.g. paludification, Rydin *et al.*, 2006), and would likely require successive years with annual P close to and above those that maximize ET to allow for adequate productivity, yet provide conditions suitable (i.e. wet enough) for organic mass to accumulate. However, the low storage leads to frequent wet and dry periods, with short return times, favoring decomposition of organic material (Philben *et al.*, 2014), and the recurring stress (drought and deluge), may result in low-storage systems being locked in a low-productivity state imposed by the Boreal Plain climate, as reported by Dixon *et al.* (2017).

Little-Devito *et al.* (2019) provide evidence for recent wetland establishment through their examination of factors controlling opportunistic (unplanned) wetland initiation in reclamation-managed landscapes (i.e. post mine closure) in the Athabasca Oil Sands region ($\approx 300\ km$ north east). They found that, in the absence of groundwater inputs, wetlands were only able to form where both storage and slope were sufficiently low (<3 %; reducing drainage). While mature states of these newly-formed wetlands are difficult to predict, it further highlights that autogenic wetland formation is possible under current climatic conditions (as opposed to after last glaciation; Vitt *et al.*, 2000). Results here indicate that shallow-storage systems can provide water surpluses even toward the dryer end of observed climatic variability. Hence it is likely that they, as well as these opportunistic wetlands, represent features that are resilient to future warming and potentially increased atmospheric water demand (Ireson *et al.*, 2015). This is in accord with Schneider *et al.* (2016), which suggest that, while there is potential for wetlands with shallow organic soils and intermittent or ephemeral regimes to face carbon-losses and state shifts to forest ecosystems throughout this century, the expected higher annual P (5 to 12 % Price *et al.*, 2013) will likely allow shallow swamps to maintain current hydrological regimes (and hydro-periods) and they should therefore remain stable features of Boreal Plains landscapes for the foreseeable future.

Natural (e.g. Frey *et al.*, 2004) and anthropogenical (e.g. Pickell *et al.*, 2013) disturbances are ubiquitous features of the Boreal Forest, including the Boreal Plain (Timoney, 2003; ABMI, 2017). Vertical fluxes (P, ET) dominate water balances in this region in general (Brown *et al.*, 2010, 2014a; Devito *et al.*, 2017), as is the case for the assessed swamp. Disturbances affecting energy and mass exchange across vegetation strata (sub-canopy, shrubs, trees) hence have the potential to dramatically alter the ecohydrological functioning of such systems on local, and by implication, potentially catchment scale. Such effects may result from internal and/or external disturbances, with immediate ("pulse") or lasting ("press") impacts (*sensu* Grosse *et al.*, 2018), as

well as interacting effects between disturbed and non-disturbed strata (Black and Kelliher, 1989). For example, canopy defoliation following insect infestation (Malmström and Raffa, 2000) may have immediate effects in a given year on radiative (transmission, albedo) and turbulent energy exchange (eddy dynamics, transpiration, interception), which may be carried over to subsequent years due to legacy effects on tree productivity (e.g. Jones *et al.*, 2004). Similarly, snow breakage in the tree stratum may reduce canopy cover across multiple years with similar outcomes for atmospheric water balances. Linear disturbances, such as roads and seismic lines, are common features of the Boreal Plain (ABMI, 2017; Dabros *et al.*, 2018) and typically entail full or partial removal of vegetation strata, with analogous (yet more severe) effects on energy and mass flux dynamics as above, as well as compaction of soils, potentially altering surface and subsurface hydrology (Willier, 2017). The disturbance magnitude will vary with location (internal, external), orientation and construction date of such linear features. A potential drastic loss of ecohydrological functioning can be expected where these features cut through (the majority) of a small, forested wetland, or where e.g. systems are cut off from lateral flows, facilitating shrubification and tree encroachment, i.e. conversion to uplands, (Wilkinson *et al.*, 2018), or experience increased flooding due to 'damming' (Bocking *et al.*, 2017). External disturbances that remove atmospheric sheltering and shading from e.g. adjacent upland forests (Petrone *et al.*, 2014; Plach *et al.*, 2016), may also alter water balance of wetlands, especially in small systems where boundary layer dynamics and incident radiation are largely externally controlled.

3.5.3 Critical review of model and data limitations

The modelling approach applied here was based on the classic bucket concept (e.g. Manabe, 1969) with one store. Certainly, more sophisticated approaches have been applied, for example, with multiple, inter-connected stores (Atkinson *et al.*, 2002; Farmer *et al.*, 2003; Elshorbagy *et al.*, 2005), or fully-coupled surface-subsurface models (Milly

and Dunne, 1994; Condon and Maxwell, 2017), capturing a wider range of process-complexity. The focus here was to determine the hydrological regime of an exemplary swamp as imposed by the sub-humid climate and fluxes originating from its land/vegetation cover. This was done to identify (and re-affirm, Chapter 2) whether swamps are able to provide water redistributing functions solely based on autogenic processes under current conditions. The study system was chosen to minimize impacts from sub-surface and surface fluxes, and hence served to emphasize the role of (absolute) storage capacity, which is a strong control on hydrological responses in the Boreal Plain due to its heterogeneous glacial substrates (Devito *et al.*, 2005b; Ireson *et al.*, 2015). Nevertheless, a detailed discussion of implications of the adopted approach is provided in the supplementary information of this chapter (Section 3.7.1)

3.6 Conclusion

This study is the first to use empirically-derived estimates of P and ET of a deciduous swamp system, to arrive at atmospheric water balances across nearly 20 years. Results indicate a frequent potential to generate a water surplus on annual basis, even under relatively dry, sub-humid conditions. The system provided saturated conditions necessary for R generation during snow melt and/or shoulder seasons, as well as somewhat less frequently in response to growing-season P events. Confidence in these results is based on a carefully-selected study site limiting confounding groundwater-surface water processes, a thorough discussion of limitations and implications of the chosen approach, and good agreement with other ET and R peatland and swamp-dominated catchments in the Boreal Plain. As Dixon *et al.* (2017) suggested through modelling of idealized soil columns, swamps can act as water sources in these landscapes, and as this study confirms, even without groundwater or surface water inputs.

Given future climate projections of higher winter and summer temperatures, as well

as increased P (Price *et al.*, 2013; Ireson *et al.*, 2015), it seems likely that swamps will still produce atmospheric surplus on annual basis, especially considering that storages between 40 to 80 mm produced positive atmospheric balances close to the driest observed years. However, the timing when saturation (i.e. intra-annually) is reached may be altered depending on the timing, type (snow vs. rain) and magnitude of P events. Due to the intermittent hydro-regime swamps are subject to, with recurring wet and dry-cycles, however, extensive carbon gains remain unlikely, and their state appears to be stable (Schneider *et al.*, 2016; Dixon *et al.*, 2017); therefore, this function will likely be continuously provided - albeit potentially at different magnitudes and frequencies.

A set of model runs across a range of maximum storage capacities further showed that the magnitude and frequency of surplus generation was strongly controlled by the extent to which ET is constrained by storage depletion: lower storage capacities entailed lower maximum attainable ET (across all assessed years), and under which annual P it was realized. If (maximum) ET can be taken as a proxy for productivity, this implies that maximum productivity decreases progressively as storage is reduced, while this maximum is obtained at higher annual P - potentially indicating that the interplay between saturation and dry-out under storage constraints alters the ecohydrological optimum of swamp systems. As the atmospheric demand was estimated based on a fixed vegetation community, however, a detailed modelling exercise including soil-plant-atmosphere as well as stress and competition between plants would provide an interesting opportunity for further research to address this newly identified knowledge gap.

3.7 Supplemental Material

3.7.1 Impact of process complexity on model dynamics

This section critically reviews implications of the chosen approach, as well as the potential impact of disregarding the following processes and data limitations on results and interpretations: 1) subsurface and surface flow, 2) infiltration capacity, 3) soil-plant-atmosphere feedbacks and 4) erroneous estimation of input data, 5) climate-storage impacts.

3.7.1.1 Subsurface and surface flow

Additional inputs to the system could sustain ET for longer periods, rendering it into a sink (i.e. negative atmospheric balance). Surface runoff from aspen-forested uplands, however, are rare with return periods of multiple decades (Redding and Devito, 2008); similarly, sub-surface flow from these uplands is rare due to accumulated moisture deficits (Devito *et al.*, 2005a, 2012), but can occur during large P events ($> 15\ mm$) under wet antecedent conditions (Redding and Devito, 2008). Excluding this process from consideration was thus reasonable. Flow from the swamp into adjacent uplands (and downgradient), however, can occur frequently with (partial) saturation; such water table configurations are common in the Boreal Plain [Ferone and Devito (2004);Wells *et al.* (2017); Chapter 2] and other dry, glacially-derived landscapes (van der Kamp and Hayashi, 2009 for review). However, water losses via this pathway - and through deep percolation - would exacerbate the storage limitation, as available water for ET is depleted quicker, and hence, on annual basis, the atmospheric balance would become more positive. Disregarding these processes is therefore conservative with respect to the interpretations here.

3.7.1.2 Infiltration capacity

Soil moisture-dependent infiltration (Blume *et al.*, 2016) was not accounted for here, and hence water removal as R only occurred when maximum storage capacity was exceeded. Arguably, this process is important when partitioning P into R and ET (e.g. Condon and Maxwell, 2017). However, implementing the potential for infiltration excess would act to increase the effect of storage limitation, as less water would be available for ET, depleting storage more rapidly. An assessment of rainfall intensity and infiltration capacities of typical swamp soils, as well as an implementation of infiltration processes, would increase the confidence in estimates of the atmospheric balance; magnitudes and directional shifts in relation to maximum storage capacities, however, are considered robust.

3.7.1.3 Soil-plant-atmosphere feedbacks

There are several feedback mechanisms that control and affect ET fluxes (e.g. Oke, 1992; Jones, 2013). For the sake of brevity and relevance, only the effect of extreme storage ranges (proxy for soil water potential and oxygen availability) and plant responses to atmospheric water demand are discussed. Low soil water status, concomitant with low soil water potential, can impede root water uptake as well as moisture transport through soil, and hence decrease ET rates (Buckley, 2005a; An *et al.*, 2018). While these processes have been implemented in other studies in some form (e.g. Abatzoglou *et al.*, 2018; Porporato *et al.*, 2002), the effect here would also shift the atmospheric water balance toward more positive values. However, given that rates are reduced prior to a full shut down, the effect would likely be less positive, if notable at all on annual basis.

Saturation can lead to low oxygen availability for roots, leading to reducing conditions and thereby altering osmotic potential (Whitlow and Harris, 1979) resulting in

decreased transpiration; "oxygen stress" has been implemented by e.g. Brolsma and Bierkens (2007). The vegetation community in the assessed swamp is certainly adapted to such conditions (Group *et al.*, 1997), and periods of total saturation were relatively short during growing seasons; the impact on annual scales would likely be small. Yet, reduced transpiration close to or at saturation would result in more positive atmospheric balances as incoming P either goes into storage or is removed via saturation excess.

Transpiration is sensitive to *vpd*, with high atmospheric demand entailing closure of stomatal apertures; however, this is species and temperature dependent, amongst others (e.g. Jones, 2013; Buckley, 2005a). Here, this process was indirectly encoded by the empirical approach (and model selection) adopted to predict ET from daily maximum *vpd*. While direct measurements were employed for the sub-canopy, as well as tree stratum (i.e. direct capture of physiological response), the shrub stratum was modelled via a modified Penman-Monteith approach. The impact of *vpd* on stomata here is represented via surface resistance (related to stomatal resistance and leaf area). Repeated measurements of stomatal resistance across species showed little sensitivity to *vpd* over-all; note however, that this response was derived from measurements on sunny days across two years under variable conditions (air temperature, soil moisture, etc.). For annual time-scales, representing surface resistance with an average value was hence deemed adequate. Estimated T_{shrub} could hence represent an over-estimation of actual fluxes, and therefore corresponding atmospheric balances are considered conservative in relation to surplus generation.

Note, that additional inter-related effects such as phenological responses to extended drought (e.g. leaf area decrease) or impact of soil temperature on root activity, are acknowledged, but not further discussed here; the reader is referred to e.g. Jones (2013) or Eamus *et al.* (2016) for further details.

3.7.1.4 Estimation of input data (P and ET_{total})

Over- or underestimation of interception ratios would have a major impact on the magnitude of total annual ET by altering water availability (further mediated by constrained storage). However, the observed range of P gives an indication that even with higher interception, the (idealized) swamp would likely still produce water surpluses; the impact of maximum storage capacity would remain similar in relative terms. Note, that on annual time-scales, the impact of over- or under-estimate snow interception would additionally affect the timing and temporal extent at which available storage is supplemented, and thereby when saturation (excess) can be reached. This study would benefit from additional collection of rain throughfall data to cover multiple years, as well as higher temporal resolution to account for P intensity; the data set for snow interception has good temporal coverage and estimated snow storage and melt factors are considered adequate. Additionally, model outputs could be assessed for their sensitivity to throughfall ratios in a formal manner; however, this was considered beyond the scope of this study.

Rates of ET_{total} were estimated as the sum of predicted fluxes from three strata (sub-canopy, shrubs, trees). Including more species and achieving higher temporal coverage for T_{tree}, including wet and dry cycles, would certainly increase the confidence in the estimates established here. While low values for T_{tree} have been estimated in treed peatlands at comparable rates (e.g. Thompson *et al.*, 2014; Warren *et al.*, 2018), those systems had water tables that were typically close to or at the surface permanently (leading to low tree productivity and transpiration); the swamp here, contrastingly, has short hydro-periods, and therefore, in theory, could support higher rates. Angstmann *et al.* (2012), however, reports average daily ET rates for a mixed-wood stand in poorly drained conditions of approximately 0.8 $mm \cdot day^{-1}$, which corresponds to maximum values reported here. Confidence in ET_{sc} and T_{shrub} data and implications have been discussed in previous sections.

3.7.1.5 Climate-storage feedbacks

Solid ice formation under high antecedent moisture can drastically reduce available storage. If such ice persists into and after snow-melt, the generation of R is promoted (Devito *et al.*, 2005a; Redding and Devito, 2011). While soil thermodynamics were not considered here, they would shift atmospheric balances toward more positive values; hence, generated estimates are considered conservative with respective to this process.

3.7.2 Figures

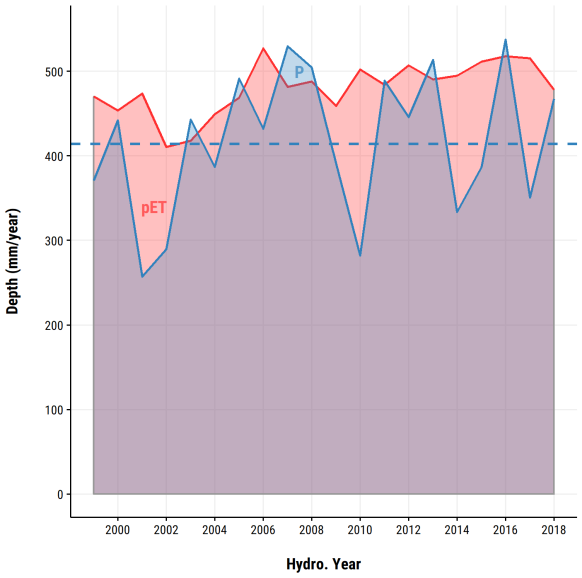

Figure 3.S1: Annual P (blue) and pET (red) for the study region. The dashed, line is the the study period average (417 mm).

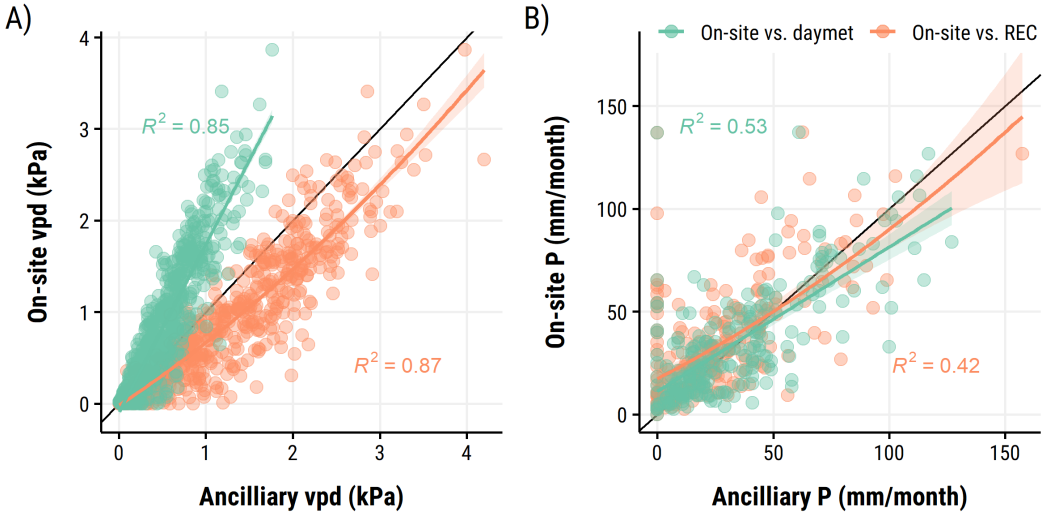

Figure 3.S2: Relationship between local and ancillary climate data sets for a) *vpd* for the overlapping period of 2015 - 2017 and b) P for 1999 - 2018. The linear model fit for daymet data displayed in a) was used to predict *vpd* for 1999 - 2018, as, despite a slightly better fit, more data was missing in the REC records.

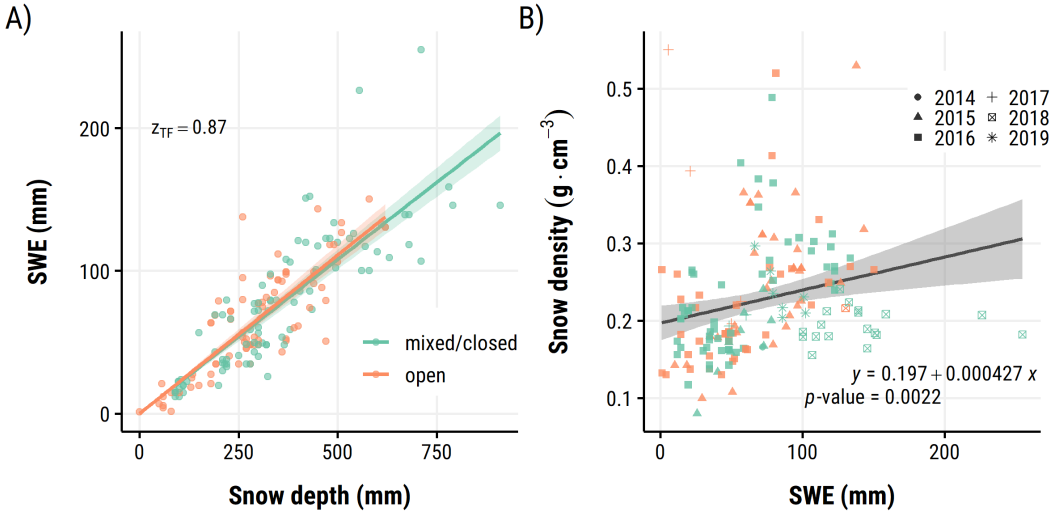

Figure 3.S3: Snow survey data from the wider catchment area, including adjacent wetlands and their uplands. A) SWE vs. snow depth and closed and open sites; the throughfall ratio z_{TF} (text label) was estimated from paired data (i.e. across the same dates). Note, the close correspondence across canopy closure (see linear models). B) The linear relationship between SWE and snow density used for estimating the degree-day factor D_f for snow melt; the model was fit for all data across sites and years, as the observed SWE vs. snow depth relationship was fairly consistent across canopy closure.

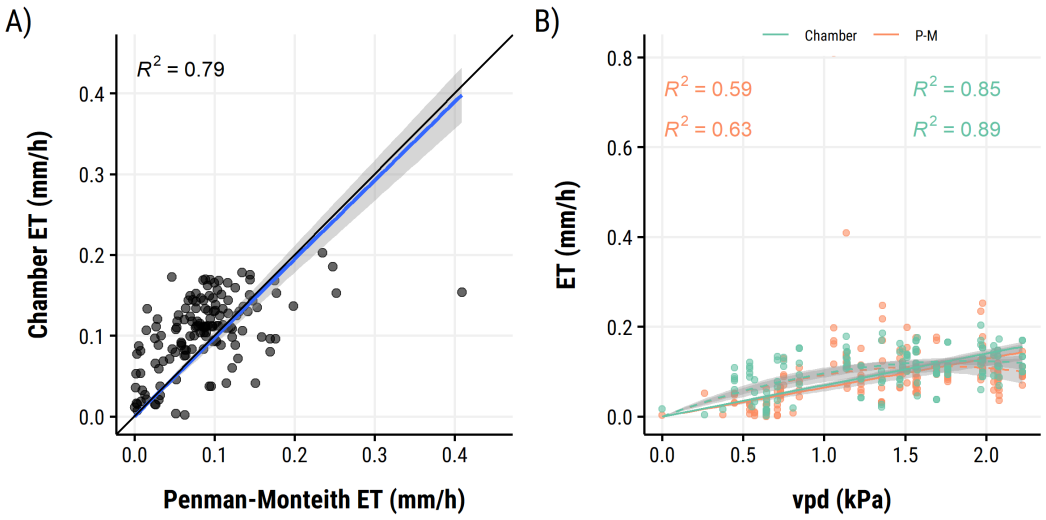

Figure 3.S4: a) Penman-Monteith vs. measured Chamber ET; b) corresponding relationships with *vpd*.

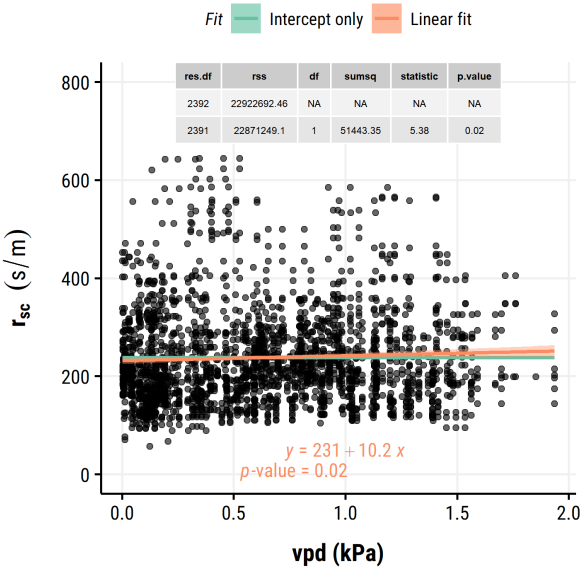

Figure 3.S5: Community and growing-season (2016, 2017) averaged response of stomatal resistance r_{sc} to *vpd* and two models (intercept only, linear) fit to the data (for 1100 to 1600 MST, where demand is typically highest). The table shows results from an ANOVA comparing both models. Note, while there is a statistically discernible increase (slope in equation), it is arguably small across the observed range of *vpd* over time; hence, the average (i.e. intercept only) was used for analyses.

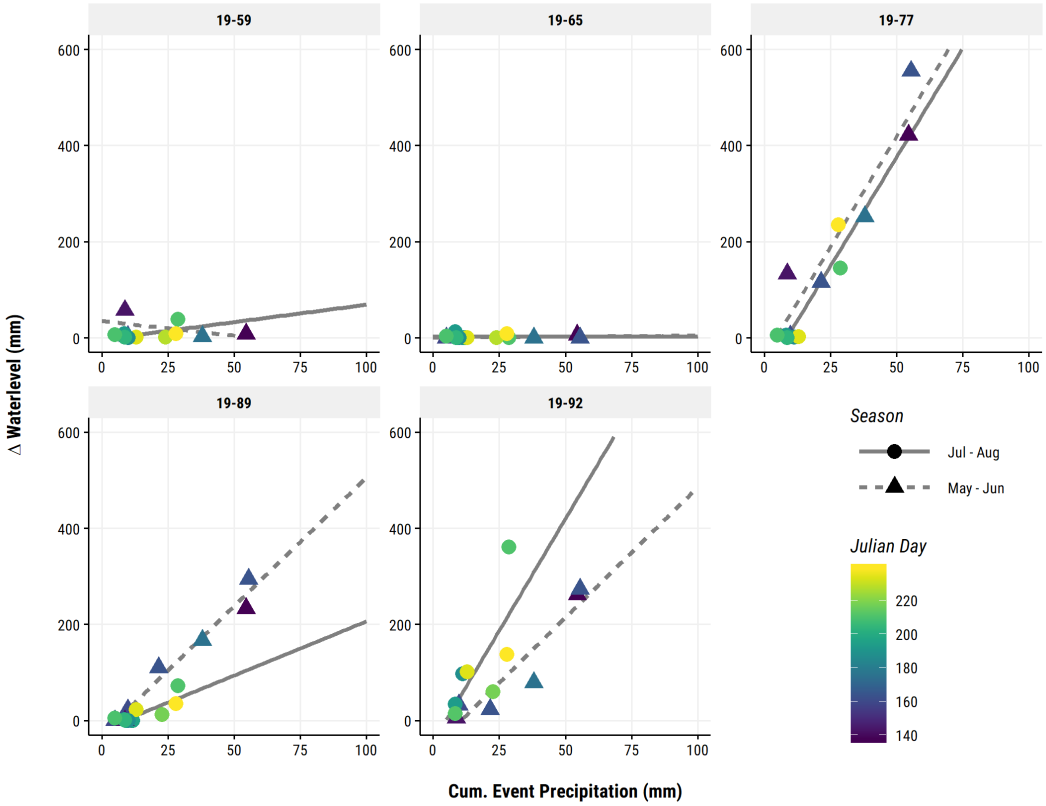

Figure 3.S6: Water table responses to precipitation for multiple wetland sites along transect A, and one hillslope well. Lines represent fits from OLS regression. Separate models were fit for spring and summer to account for dampened event responses due to seasonally increasing ET and interception. Slopes from wetland wells were averaged and their inverse was used as an estimate for specific yield in storage depth estimation.

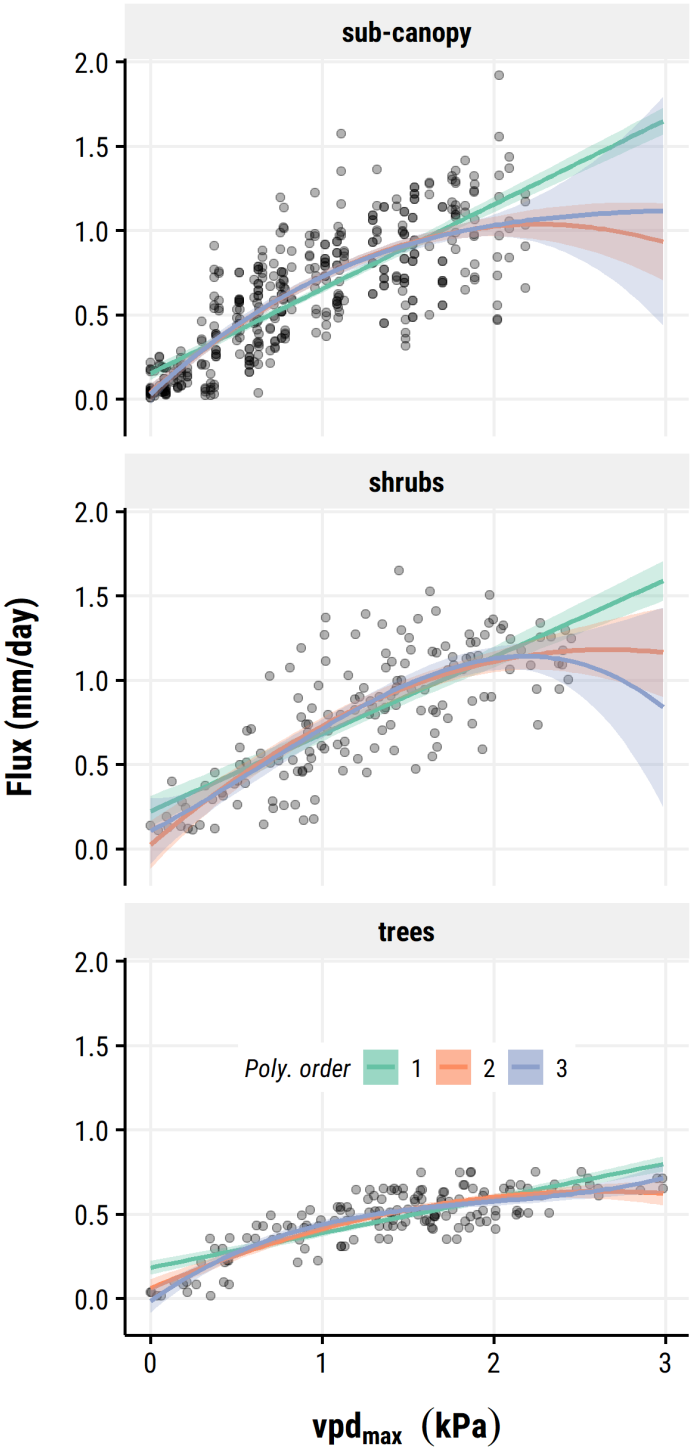

Figure 3.S7: Fluxes from all strata estimated via direct measurement or modelled via Penman-Monteith (shrubs) with linear relationships of increasing polynomial order fitted across daily maximum *vpd* recorded on-site. Fits are displayed beyond the observed range of *vpd* to indicate implications for prediction. Refer to Tab. 3.S1 for model performance metrics, and Tab. 3.3 for selected models.

3.7.3 Tables

Table 3.S1: Model diagnostic and selection metrics for the relationship between *vpd* and the respective ET/T flux and stratum. Models are ordered by stratum and lowest (most negative) AIC.

stratum	order	r.squared	std_error	statistic	p.value	df	AIC	BIC
trees	3	0.71	0.09	122.22	0	4	-280.89	-265.74
	4	0.71	0.10	91.17	0	5	-279.03	-260.85
	5	0.71	0.09	73.63	0	6	-278.81	-257.60
	6	0.71	0.10	60.95	0	7	-276.82	-252.58
	8	0.72	0.09	46.43	0	9	-276.06	-245.76
	7	0.72	0.10	52.04	0	8	-275.15	-247.88
	9	0.72	0.10	41.00	0	10	-274.09	-240.75
	10	0.72	0.10	37.02	0	11	-273.24	-236.87
	2	0.69	0.10	167.95	0	3	-272.77	-260.65
	1	0.62	0.11	243.85	0	2	-242.01	-232.92
shrubs	2	0.59	0.24	111.02	0	3	4.94	17.20
	3	0.59	0.24	74.72	0	4	5.45	20.76
	4	0.59	0.24	55.82	0	5	7.21	25.59
	5	0.59	0.24	44.36	0	6	9.21	30.65
	6	0.59	0.24	36.76	0	7	11.13	35.63
	7	0.59	0.24	31.31	0	8	13.11	40.68
	8	0.60	0.24	27.54	0	9	13.97	44.60
	9	0.60	0.24	24.60	0	10	14.89	48.58
	1	0.56	0.25	195.35	0	2	15.11	24.30
	10	0.60	0.25	22.04	0	11	16.68	53.43
sub-canopy	2	0.67	0.22	435.05	0	3	-81.40	-65.14
	5	0.67	0.22	175.88	0	6	-80.52	-52.07
	3	0.67	0.22	289.68	0	4	-79.72	-59.40
	6	0.68	0.22	146.77	0	7	-79.60	-47.09
	4	0.67	0.22	217.87	0	5	-79.20	-54.82
	8	0.68	0.22	110.38	0	9	-77.77	-37.13
	7	0.68	0.22	125.55	0	8	-77.71	-41.14
	10	0.68	0.22	88.59	0	11	-76.12	-27.35
	9	0.68	0.22	97.93	0	10	-75.91	-31.21
	1	0.64	0.23	753.43	0	2	-42.22	-30.03

Table 3.S2: Results from OLS regression between total P event size (mm) and water table increase. Inverse of mean of slopes was used as specific yield for storage depth estimation. Note, that dropping Site 65, which has considerably higher depth to CL, changes the estimate from $s_y = 0.20$ to $s_y = 0.15$. Despite the model for Site 65 having p ¿ 0.05, it was included in the final estimate, as the higher specific yield accounts for increasing storage toward interfaces and the outflow (along the transect), and is therefore more representative for average wetland conditions.

Site	season	estimate	std.error	statistic	p.value
19-65	Spring	0.043	0.0583	0.738	0.514
19-77	Spring	9.21	1.65	5.58	0.00507
19-89	Spring	5.35	0.421	12.7	5.34e-05
19-92	Spring	5.42	1.01	5.35	0.00589

CHAPTER 4

Small forested wetland microclimate limits sub-canopy evapotranspiration to promote ecosystem persistence in the sub-humid Boreal Plain

4.1 Abstract

Small, forested wetlands (SFW) with ephemeral hydrological regimes are susceptible to climatic variability and change, as well as disturbances. In the Boreal Plains (BP), these often represent isolated swamps embedded in uplands, where they can serve as water-redistributing units. Their persistence demands adequate extents and periods of saturation. In the sub-humid BP evapotranspiration (ET) is a major negative water flux, especially in landscapes with coarse to intermediate substrates (sands and silts). Partitioning ET between structural components (sub-canopy, overstory), and pathways (E, T), is therefore key in assessing the capacity of SFW to maintain their functioning, and to identify potential (future) vulnerabilities. This chapter focused on determining controls on sub-canopy ET (ET_{sc}), as part of this major flux, in an exemplary SFW. The chosen system is on a moraine-outwash transition zone dominated by aspen forest, geographically isolated and perched 15 to 20 m above regional groundwater. Micro-meteorological and hydro-pedological drivers of ET_{sc}, as well as the interplay between atmospheric and radiative forcing throughout the growing season of 2016 were assessed. (ET_{sc}) averaged 0.87 ± 0.06 $mm \cdot day^{-1}$, similar to other closed-canopy Boreal wetlands; it was considerably lower than that of more open systems in general, and of those in the same region in particular. This was driven by the distinct micro-meteorological conditions the SFW established throughout its growing season, sheltering the sub-canopy from incident radiation, and impeding exchange with the atmosphere above. Incident, shortwave radiation ($K\downarrow$) and (daily maximum) vapor pressure deficit (vpd) and were strong predictors ET_{sc} Increased total resistance (r_{total}) to ET_{sc} coincided with periods of high demand, indicating vegetation control, depletion of soil water stores and/or changing evaporation mechanisms (i.e to diffusion from deeper soil layers). This work highlights the capacity of SFW to decrease ET_{sc} (i.e. self-regulate) by establishing distinct micro-climates and likely through plant- and soil-atmosphere feedbacks, implying the potential to maintain higher levels of moisture

over time. In light of the above dynamics, and the low storage intrinsic to SFWs, it is assumed that SFW are likely to maintain their ecohydrological functioning across a broad range of water availability. However, especially plant-structural or phenological processes that allow for this functioning may be increasingly impeded or even lost, if future hydrometeorological regimes entail surpassing physiological thresholds, or render these wetlands more vulnerable to external stressors (e.g. defoliation events allowing for greater atmospheric exchange).

4.2 Introduction

Small, forested wetlands (SFW) support the landscape-scale ecohydrological function of the Boreal Plain (BP), promoting regional runoff (Chapter 2, Devito *et al.*, 2017), and likely enhance productivity of adjacent forest ecosystems (Devito *et al.*, 2012; Brown *et al.*, 2014a; Depante *et al.*, 2019) within the regional sub-humid (i.e. water-limited) climate. Whilst the potential of SFW to frequently export water in response to intense summer precipitation and snow-melt is recognized, the capacity and mechanisms by which they maintain saturation subsequently is unknown. Yet, it is this continued saturation that enables formation of hydric wetland soils and establishment of typical species (and therefore habitats), ultimately resulting in aforementioned functioning in a dry climate. Further, SFW - especially with ephemeral hydrological regimes - may be vulnerable to altered climatic and (human) disturbance regimes (Dalu *et al.*, 2016), which could lead to functional shifts, for example, by altering carbon and/or water source-sink dynamics (Kettridge *et al.*, 2015, 2017; Waddington *et al.*, 2015; Schneider *et al.*, 2016). This is due to the dependence on receiving water at adequate times and amounts (e.g. Leibowitz and Brooks, 2008) in contrast to sustained evapotranspiration (ET) loss, which is the dominant water flux in sub-humid regions such as the BP (Jackson *et al.*, 2009; Devito *et al.*, 2017). Hence, further assessments of ET dynamics and drivers thereof are needed not only to increase current understanding

of SFW persistence, but also to anticipate potential changes in their ecohydrological functioning aross the 21st century, where increasing temperatures (likely enhancing ET) and altered temporal patterns of precipitation are expected (Price *et al.*, 2013; Ireson *et al.*, 2015).

Fatichi and Pappas (2017) note a paucity of studies reporting on partitioning of ET into flux mechanisms (evaporation, E; transpiration, T) from Boreal ecosystems, which also holds true for partitioning between overstory and sub-canopy. Yet, sub-canopy ET (ET_{sc}) can comprise a large proportion of total ET in boreal wetlands; for example multiple studies reported sub-canopy contributions to total ET above 60 % (Lafleur and Schreader, 1994; Thompson *et al.*, 2014; Kettridge *et al.*, 2017), in some cases reaching over 90 % (e.g. Warren *et al.*, 2018). The magnitude of ET_{sc}, and its contribution to total ET, heavily depend the micro-climate found within the space beneath the overstory. This micro-climate is the outcome of multiple, interacting characteristics, such as ecosystem structure (vertical and horizontal distribution of leaf area), vegetation type (vascular *vs.* non-vascular; broad-leaf *vs.* needle-leaf) and the degree of overstory closure, and groundwater depth (e.g. Baldocchi *et al.*, 2000; Lafleur, 2008; Iida *et al.*, 2009; Kettridge *et al.*, 2013; Limpens *et al.*, 2014; Thompson *et al.*, 2015c). These factors control, amongst others, how radiation is adsorbed and transmitted from overstories to sub-canopies, the amount of throughfall and stemflow reaching soils, stomatal conductance in response to humidity and soil moisture, as well as frequency and magnitude of eddies sweeping through the overstory and into the sub-canopy (McNaughton and Jarvis, 1983; Black and Kelliher, 1989). For example, Heijmans *et al.* (2004), identified overstory closure as well as sub-canopy structure (vascular *vs.* non-vascular) as a major control on ET_{sc}, with lowest rates occurring under closed black spruce overstories (forests) in sub-canopies with shrub cover, and markedly higher ET_{sc} for open wetland systems. Note that the vast majority of studies directed their efforts at northern bogs and fens with coniferous tree cover and evergreen sub-canopies (i.e. shrubs), or marshes.

Assessments of ET dynamics, their mechanistic (E *vs.* T) and structural partitioning (overstory *vs.* sub-canopy), as well as micro-climatic conditions in broad-leaf, deciduous Boreal wetlands are rare (Munro, 1979, 1986; Lafleur, 2008), and completely lacking for the BP. Here, such SFW often constitute swamps; these therefore represent unstudied landscape units in the BP ecoregion, which starkly contrast moss-dominated wetland systems typically subject to study (e.g. Waddington *et al.*, 2015). This lack of research may in part be due to a "cryptic" character, when overstories are phenologically close to that of adjacent forested uplands, which, in conjunction with a small size, can make SFW difficult to identify (Creed *et al.*, 2003); considerably smaller carbon stocks compared to peatlands may also attract less attention from the scientific community given the current urgency presented by climate change. In contrast to evergreen (and needle-leaf) systems, deciduous, broad-leaf swamps undergo extensive changes due to the seasonal development and subsequent shedding of leaves, resulting in a temporally variable micro-climate: Progressively increasing overstory leaf area affects ET_{sc} by reducing the transmittance of energy, momentum and mass through the overstory as aerodynamic resistance increases (Hollinger *et al.*, 1994; Dupont and Patton, 2012), as well as by providing seasonally-variable energy storage in foliage, water, wetland soils (Munro, 1979; Allen, 2016) and physical barriers to horizontal air flow (e.g. Oke, 1992). Deciduous swamps hence most likely feature micro-climates similar to (more) open sites during senescence (i.e. leafless period) or early growing season, and increasingly diverge from these conditions to produce a "sheltered" sub-canopy environment. This distinct micro-climate is, for example, evident in forest ecosystems, when comparing gaps with closed-canopy environments (Abd Latif and Blackburn, 2010). Given the phenological similarity between swamps and forested uplands with broad-leaf, deciduous vegetation, analogous dynamics are expected.

This study aimed to assess SFW ET_{sc} dynamics in detail as a first step in understanding their atmospheric water fluxes from wetland soils and vegetation in the sub-humid BP climate. In particular, it sought to address research gaps regarding

(1) what magnitudes and temporal patterns of ET_{sc} are, (2) to which degree the overstory and sub-canopy interact to establish a distinct micro-climate, and how it develops throughout a growing season; and (3) whether the micro-climate and any soil- or plant-atmosphere feedbacks limit ET_{sc}, thereby contributing to wetland persistence by extending hydroperiods in the sub-humid climate of the BP. Additionally, this understanding may also inform restoration and reclamation management, by highlighting key mechanisms that may be required to establish and/or maintain constructed wetland systems in the sub-humid Boreal Plain (Nwaishi *et al.*, 2015; Little-Devito *et al.*, 2019), as well as provide a baseline from natural analogues (i.e. systems with little disturbance) for comparison. The chosen study system was a flat swamp (NWWG, 1997), predominantly covered with deciduous, broad-leaf vegetation (overstory and sub-canopy) with high maximum overstory LAI. It is located on a moraine-outwash transition zone dominated by aspen forest, geographically isolated and perched 15 to 20 m above regional groundwater; shallow organic soils result in frequent cycles of saturation and subsequent drying. The isolation and perching were specifically sought as means to increase the strength of inferences on relationships between ET_{sc} and micro-meteorological, as well as hydro-pedological variables, as this ensured that observed dynamics arose solely through local soil-plant-atmosphere interactions, rather than being affected by e.g. larger-scale groundwater inputs (upholding ET_{sc} rates).

The seasonality of ET_{sc} drivers, and of vegetation itself, are assumed to jointly affect the magnitude of atmospheric water losses via sub-canopies of broad-leaf, deciduous SFW: a) ET_{sc} is expected to peak near the annual solar maximum, but before overstory LAI, with ET_{sc} rates intermediate to those of moss-dominated wetlands with fully-closed and fully-open overstories typical for the BP, owing to the seasonal development of both sub-canopy and overstory LAI; b) that micro-climates are increasingly less conducive to ET_{sc} compared to above-canopy or open-reference conditions, as driving gradients diminish; and c) that soil- and vascular plant-atmosphere feedbacks act to limit ET_{sc} under high demands or low moisture conditions. The latter may also be a

critical difference when comparing with more open wetlands (assumption b) dominated by morphologically-contrasting moss species; these result in different transport mechanisms for liquid water and vapor (capillary rise for *Sphagnum*, Goetz and Price, 2015; diffusion barrier for (burnt) feather moss Kettridge and Waddington, 2014; Kettridge *et al.*, 2019), as well as contrasting surface roughness affecting aerodynamic resistance (Rice *et al.*, 2001).

4.3 Materials and methods

4.3.1 Study area and site overview

The 0.5 *ha* wetland lies at the northern end of an aspen-dominated headwater catchment (11.9 *ha*), generating intermittent runoff to a down-gradient, terminal pond. It is located in North-Central Alberta at 56.081432N, -115.537168W, in the sub-humid Western Boreal Plain (mixed-wood ecoregion; Fig. 4.1b). Here, P (481 *mm*; Marshall *et al.*, 1999) approaches potential ET (pET, 517 mm; Bothe and Abraham, 1993), but is generally lower most years. Actual ET depends on landscape units and their cover, as well as their water storage capacity (Devito *et al.*, 2016), resulting in contrasting water source and sink functions of vegetated wetlands and forests or open-water bodies/areas (Devito *et al.*, 2012, 2017).

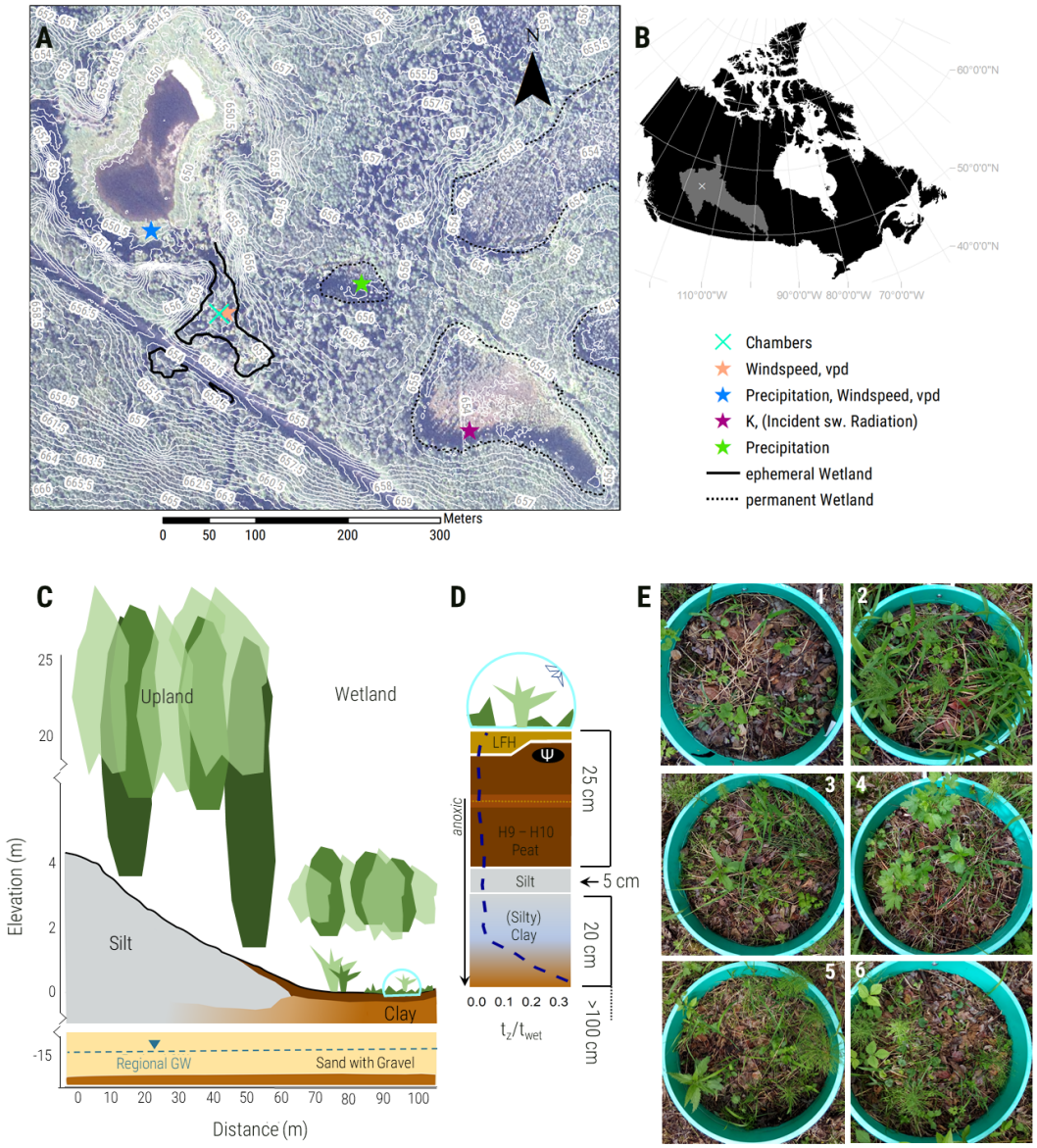

Figure 4.1: Overview of (A) study site and (B) region, (C, D) local characteristics, and (D, E) chamber system set-up. Micrometeorological data was collected at multiple open sites within the larger catchment, as well as within the wetland sub-canopy (A). Six chamber systems were deployed in representative areas in the sub-canopy space surrounding a groundwater monitoring well (max. distance $< 5m$). Note, tree and shrub stems were excluded for visual clarity and to emphasize the sub-canopy environment (C). A shallow, low-permeability clay layer (C, D) and highly-decomposed peat result in rapid water table responses to P; the blue, dashed line in D is the frequency distribution of water table depths (z) for all periods (t_z) at which a water level was observed (2016 - 2018). Frequent saturation leads to anoxic conditions in the majority of the soil column (D; orange, dashed line as mean, with standard error as band); reducing conditions are evident in blue-gray coloring of mineral soils at the clay's top. Soil water potential (Ψ) was measuread at approximately 5 cm depth. Ground cover in each chamber consisted of leaf litter, debris and vascular vegetation only (E; pictures from May 30, 2016). Details on chamber systems and ET estimation are in section 4.3.2; details for micrometeorological and hydro(pedo)logical measurements are in sections 4.3.3 and 4.3.4, respectively.

The wetland formed in a transition zone between coarser glaciofluvial and fine(r)-grained ice moraine deposits (Fenton *et al.*, 2005) in a local topographic low, atop a low-permeability clay layer (CL, $K_s \leq 10^{-8}$; approximately 0.30 to 0.80 deep, see Chapter 1, Fig. 4.1). The stratification led to permanent perching of local groundwater tables above a regional groundwater body approximately 15 to 20 m deep in a sand aquifer (Hokanson *et al.*, 2018a).

Stem density ($DBH > 0.05\ m$) in the wetland was approximately 4320 $stems \cdot ha^{-1}$. The vegetation community was structured threefold: 1) a dense overstory of river alder (*Alnus incana* subsp. *tenuifolia* [Nutt.], also speckled alder), willow (*Salix* spp.) and paper birch (*Betula papyrifera* Marshall) of 2 to 5 m height, 2) a sub-canopy comprising a shrub layer of red-osier dogwood *(Cornus sericea* L.), low-bush cranberry (*Viburnum edule* [Michx.] Raf.), prickly rose (*Rosa acicularis*) of up to around 1.5 m, 3) a herb and moss layer with stinging nettle (*Urtica dioica* L.), grasses (*Poaceae*), dewberry (*Rubus pubescens*), common horsetail (*Equisetum arvense*), twinflower (*Linnaea borealis*) and kidneyleaf violet (*Viola Renifolia*), amongst others, typically up to 0.50 m. Sparsely distributed hummocks can feature trembling aspen (*Populus tremuloides* Michx.) or white spruce (*Picea glauca* [Moench] Voss) with similar sub-canopy communities. Aspen-dominated, mixed-wood forests on luvisolic soils (Soil Classification Working Group, 1998) atop silt and loam deposits of several meters cover adjacent uplands (stem density approximately 1146 $stems \cdot ha^{-1}$).

The wetland was classed as a flat swamp (NWWG, 1997) given its vegetation and soil characteristics (humisols and humic gleysols; Soil Classification Working Group, 1998) and hydro-regime.

4.3.2 Estimation of sub-canopy ET

Sub-canopy ET (ET_{sc}) was defined as the water flux from bare soil (or litter), moss and vascular vegetation up to a height of approximately 0.5 m. (ET_{sc}) estimated for representative locations in the wetland's center (Fig. 4.1d and 4.1e) using six pneumatically-controlled Perspex chambers following a modified approach of McLeod *et al.* (2004). Chambers were arranged circularly (approximately 2 m apart), covering the apparent range of overstory closure. Measurements lasted from May 18 to Aug 04, 2016. Chambers were mounted on collars carefully inserted into the highly-decomposed, organic soil (0.05 cm to 0.07 cm deep, area of 0.2 m^2). Instantaneous ET_{sc} rates were estimated via the initial increase of water vapor concentration ($\Delta\rho_{H_2O}/\Delta t,\ kg \cdot m^{-3} \cdot s^{-1}$) in the chamber (volume; approximately 0.05 to 0.06 m^3 depending on micro-topography) during closure (2 min every hour) using a Licor LI-840 infrared gas analyzer (for details see Kettridge and Waddington, 2014; Kettridge *et al.*, 2017); a fan ensured air was adequately mixed during measurements:

$$ET_{sc} \ = \ 3600 \cdot \frac{\Delta\rho_{H_2O}/\Delta t \cdot V \cdot C}{A} \tag{4.1}$$

with A as surface area (m^2) and C a factor accounting for vapor absorption on chamber material (unitless; set to unity). The factor 3600 converts estimates to $mm \cdot h^{-1}$, assuming that 1 $kg \ = \ 10^{-3}\ m^3$ water. One chamber (ID = 3) failed to reach equilibrium conditions during 2 min closure under high atmospheric demand, indicating sealing issues (i.e. constant influx of ambient air), and was hence excluded from analyses.

4.3.2.1 ET_{sc} partitioning

ET_{sc} was partitioned into transpiration (T) and evaporation (E) using a simplified Penman-Monteith model assuming that the water flux is impeded by a resistance (r_{total},

$s \cdot m^{-1}$), analogous to electrical circuits (Oke, 1992; Kettridge and Waddington, 2014):

$$ET_{sc} = \frac{\rho_s^* - \rho_a}{r_{total}} \tag{4.2}$$

where ρ_s^* and ρ_a are saturation vapor concentration of the evaporating surface/leaf and vapor concentration of air ($kg \cdot m^{-3}$), respectively, and following the above assumption of 1 $kg = 10^{-3}$ m^3 water. Temperatures required for calculating both vapor concentrations where obtained from type T thermocouples installed just at the soil surface (logged with Campbell Sci. CR10X), and Type E thermocouples freely hanging inside each chamber (logged by auto-chamber controller). Note, that vapor gradients between air and both vegetation and soil surface were assumed equal.

Resistance originated from a series of aerodynamic (r_a) and surface resistance, the latter being made up of resistance from vascular vegetation r_{vasc} and topsoil (i.e. litter; r_{soil}) acting in parallel. The resistances are hence given by:

$$r_{total} = \frac{1}{\frac{1}{r_{vasc}} + \frac{1}{r_{soil}}} + ra \tag{4.3}$$

r_{total} for each day of the campaign was derived from the median of hourly resistance values by re-arranging the simplified Penman-Monteith model. Hours were restricted to 12:00 to 15:00 MST and the median across the entire season was applied in subsequent (daily) calculations. This allowed estimating T $vs.$ E despite large variability of r_{total} across and within individual days, e.g. due to short-lived convective afternoon storms, (see Eqs. (4.4) - (4.6)). r_{vasc} was estimated as the mean of three replicate measures (separate leaves) of stomatal resistance (r_{st}) on the dominant plant species (one individual, by percentage cover) in each chamber using a Decagon SC-1 leaf porometer across three days (26, 26, and 29 Jul 2016) under dry, sunny conditions. Note that in chambers 2 and 5 *Equisetum spp.* and *Poaceae* were most abundant and potentially dominant toward the end of the season. Their leaf morphology, however, does not lend

itself to measurements with the available porometer, and hence the second-most common species was used. For chambers 1 through 6, the following species were considered dominant and assessed: Chamber 1 - Wild Red Currant (*Ribes triste*); Chamber 2 - Wild Red Currant (*Ribes triste*); Chamber 3 - Stinging Nettle (*Urtica dioica*); Chamber 4 - Stinging Nettle (*Urtica dioica*); Chamber 5 - Stinging Nettle (*Urtica dioica*); Chamber 6 - Wild Red Raspberry (*Rubus strigosus*). r_{vasc} was then obtained as r_{st}/LAI (LAI from photograph classification; vascular *vs.* non-vascular) on a total of seven days from May 30 to Aug 13, 2016; intermediate LAI was linearly interpolated. Adjusted, mean r_{vasc} was then applied for respective chambers across each day of the campaign. r_a was set to 62 $s \cdot m^{-1}$ (from laboratory calibration in Kettridge *et al.*, 2017). r_{soil} was calculated by re-arranging above equation to:

$$r_{soil} = \frac{r_{total} \cdot r_{vasc} - r_{vasc} \cdot r_a}{r_a - r_{total} + r_{vasc}} \tag{4.4}$$

Drawing on the electrical circuit analogy, the ratio between T and E is:

$$\frac{T}{E} = \frac{r_{soil}}{r_{vasc}} = p \tag{4.5}$$

and it can be shown that respective contributions to ET_{sc} can be derived as:

$$\frac{E}{ET_{sc}} = \frac{1}{1+p} \quad or \quad \frac{T}{ET_{sc}} = \frac{1}{1+p^{-1}} \tag{4.6}$$

when assuming equal vapor concentration gradients for both fluxes.

4.3.3 Micrometeorological data

Micrometeorological measurements were done in multiple open locations, and in the wetland's center (Fig. 4.1). Windspeed was recorded at 2 m every 30 s (R.M. Young

05103 Wind Monitor), and averaged for 15 *min* intervals (internal processing in Campbell Sci. CR1000 or CR10X) in the wetland and in a clearing near a pond (NW of wetland). Air temperature and humidity were recorded at 2 m via an Onset HOBO U23-001 Pro V2 logger at the same locations; an additional device recorded at 0.5 m within the wetland. Precipitation was measured with tipping buckets (Onset Model RG2m) in two open locations (pond, peatland), and cross-referenced against handgauges in the same locations for quality assurance.

Half-hourly averages of incident shortwave radiation ($K\downarrow$) were recorded in an open peatland (E of wetland) at 5 m (Campbell Sci. CNR4-L with CRO1000). Wetland sub-canopy $K\downarrow$ was estimated from the fraction of transmitted light penetrating the wetland's tree canopy (i.e. overstory). For this, hemispherical, up-ward facing photographs were repeatedly taken 1 m above each chamber in accordance with Zhang *et al.* (2005) (on May 18, Jun 03 and 18, Jul 29). LAI, and subsequently transmitted light, were estimated with Gap Light Analyzer (v2.0, Frazer *et al.*, 1999). Subsequently, a non-linear regression was fit through the resulting daily means of transmitted light and an estimate for the senescence period (i.e. pre-leaf out) over time (Fig. 4.S2) using `R` (R Core Team, 2018) with the functional form of a logistic decay:

$$f(x) \;=\; a + \frac{b}{1 + c \cdot x^{d}} \tag{4.7}$$

An approximation of the Bowen ratio, as an indicator of whether sensible or latent heat fluxes dominated energy exchange in the sub-canopy, was calculated following Perez *et al.* (2008) on hourly basis:

$$B_{hour} \;=\; \gamma \cdot \frac{\Delta T}{\Delta e} \tag{4.8}$$

where γ is the psychrometric constant ($kPa \cdot^{\circ} C^{-1}$) and ΔT ($^{\circ}C$) and Δe (kPa) are the temperature and vapor pressure gradients between 0.5 and 2.0 m height.

4.3.4 Hydrological and hydro-pedological measurements

A groundwater monitoring well ($\varnothing = 0.051\ m$, fully slotted) in the center of the chamber systems was installed to a depth of 0.50 m, intersecting the low-permeability clay layer at 0.30 m, and wrapped in well-sock. A Solinst Gold Levelloger recorded pressure at the base of the well, which was corrected for atmospheric pressure to produce a record of water levels at 15 min intervals between May 15 2016 and August 18, 2018. This was cross-referenced with (approximately) fortnightly manual water level measurements (Solinst TLC Model 107 dipmeter) during the growing season; frequencies were lower during shoulder and winter seasons. Simultaneously, adjacent redox rods (ca. 0.30 m deep) were assessed for anoxic (i.e. reducing) conditions (Fig 4.1). Soil water potential was measured in the uppermost, non-debris layer of soil, at approximate depths of 0.05 to 0.07 m with Decagon MPS-2 sensors and EM50 loggers every 15 min in each chamber.

4.3.5 Statistical analyses

Analyses were done in `R` (R Core Team, 2018). Null Hypothesis were rejected at $\alpha \leq 0.05$ (corrected for multiple comparisons) for all statistical tests. Differences between ET_{sc} drivers, aggregated to different temporal scales (e.g. hourly, monthly) were assessed with student's t-tests (for means; unpaired, two-sample and two-sided, assuming unequal variance), and Kruskal-Wallis rank sum tests (for median ranks) when groups drastically differed from Gaussian distributions or had inconsistently shaped distributions.

The seasonal trajectories of effect sizes (β, i.e. regression slopes) for dominant ET_{sc} drivers were estimated via multiple, linear OLS regression with daily ET_{sc} as response, and vpd as well as $K\downarrow$ as dependents (no interaction term) across a stretching time windows (i.e. fixed at start, increased by available measurement days until end of

campaign). Fit models were assessed for their conformity with assumptions of OLS regression, and significant effect sizes ($\beta > 0$) were retained. A ratio between both slopes (i.e. β_{vpd} and $\beta_{K\downarrow}$), was obtained in similar fashion, but with standardized dependents (z-transformed). To identify changes in relative importances of *vpd* and $K\downarrow$, a change-point in effect size ratios ($\beta_{K\downarrow}$ / β_{vpd}) was identified using segmented linear models fit through ratios over time (after Muggeo, 2003, 2008).

Relationships between ET_{sc} and environmental variables were fit with OLS regressions ranging from intercept only to 4^{th}-order polynomials. Best fitting models were chosen based on their R^2 and AIC (Aikake Information Criterion) scores; note, that in one case (Fig. 4.5e) a model with (slightly) lower R^2 (i.e. lower order) was chosen, as interpretability was enhanced.

4.4 Results

4.4.1 Seasonal ET_{sc} dynamics and partitioning

Daily ET_{sc}, averaged among months, ranged from 0.42±0.04 $mm \cdot day^{-1}$ (Aug) to 1.04±0.05 $mm \cdot day^{-1}$ (Jun, Fig. 4.2); the seasonal average was 0.87 ± 0.06 $mm \cdot day^{-1}$. Lowest rates were observed in August; however, measurements were only taken on 3 days, likely leading to a mis-representation of dynamics. Seasonal maxima were reached in June before maximum sub-canopy and overstory leaf area (mid-Jul, Fig. 4.3 and Fig. 4.S2). Hourly ET rates peaked in the afternoon between 12:00 to 16:00 MST; peaks progressively shifted to later times of day through the growing season (disregarding August). May and June had markedly higher temporal variability owing to multiple cyclonal weather periods with lower temperatures and multi-day rain events (weather data not shown), as indicated by quantile bands in Fig. 4.2.

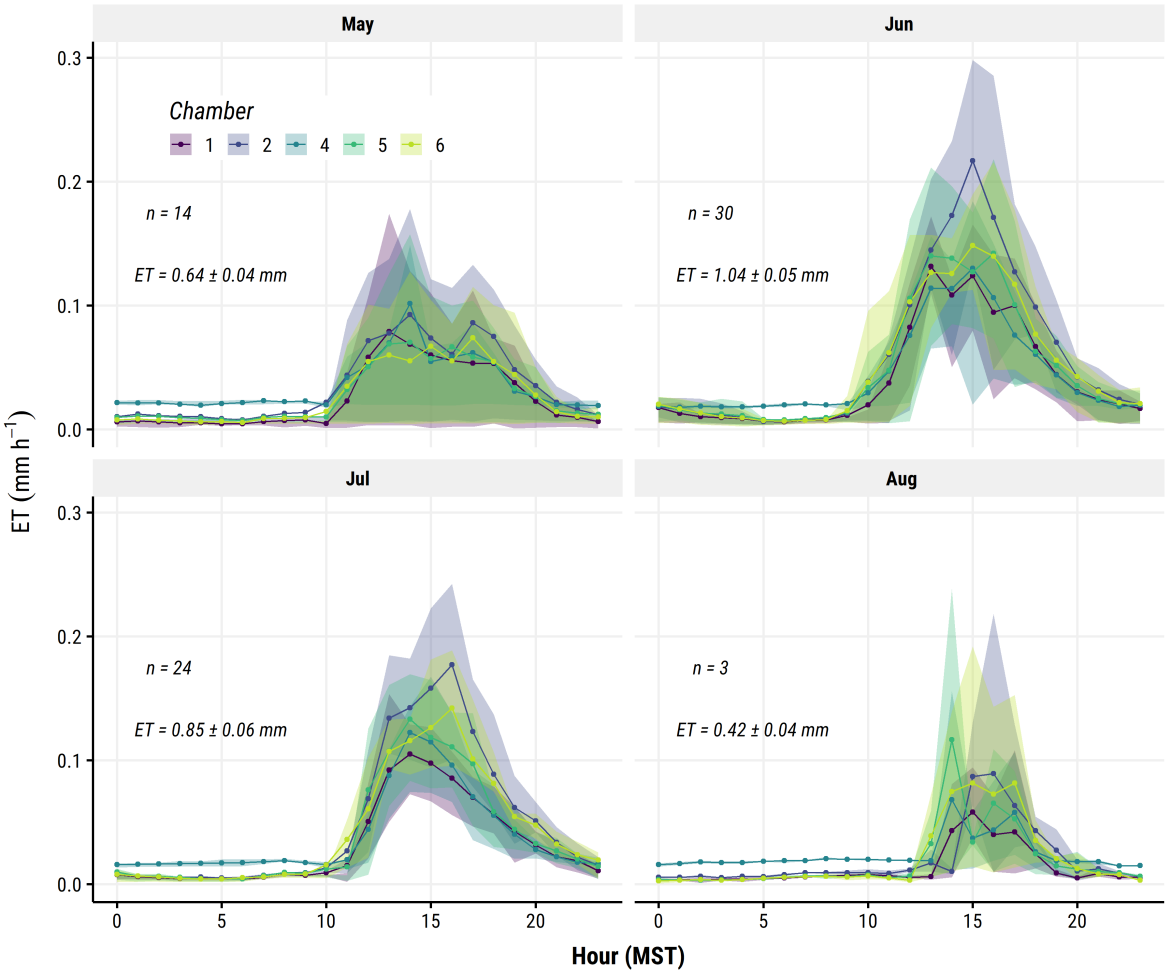

Figure 4.2: Diel ET_{sc} dynamics across growing season months (May to Aug) estimated from hourly measurements of five chamber systems (colors). Lines/dots are hourly means and ribbon bounds are 0.25 and 0.75 quantiles. Number of measured days (n) and daily average ET for all chambers and standard errors are given as text labels.

Through late May to August (inclusive) the contribution of T increased with LAI, however, the absolute magnitude of T varied markedly between chambers (Fig. 4.3, see large standard error bars). T reached up to and above 80 % for chamber 5, while it remained approximately below 25 % for most of the growing season in chamber 1; the remaining systems showed intermediate values between approximately 75 and 25 % (not shown). Early leaf senescence, likely due to water stress, in some leaves were observed in chambers 1, 2 and 5 in late July and August prior to or directly after reaching the seasonal maximum. Note, that mosses were absent in all chambers, and non-vascular cover were hence broad-leaf litter, small woody debris or dead grass

tussocks exclusively (see Fig. 4.1).

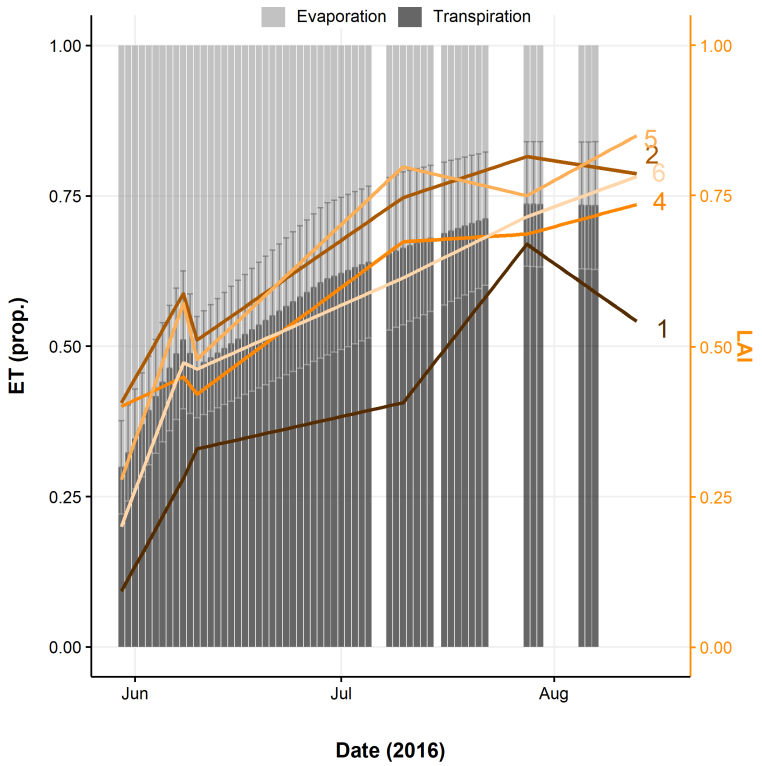

Figure 4.3: Daily ET_{sc} across the growing season partitioned into evaporation and transpiration (grey hues, left axis), as well as LAI (orange hues, right axis) of vascular vegetation in chambers (from classified photos). Missing values result from chamber downtime. Data shown from first available LAI measurement (30 May).

4.4.2 Wetland and reference site micro-climate

Median *vpd* showed a seasonal trend for both the SFW and open reference site ($\approx 150\ m$ distance), with increases in spring and early summer, followed by a decline toward August (Fig. 4.4a). Except for April (no discernible difference, $\Delta vpd = 0.03\ kPa$ $[-0.02,\ 0.09;\ 95\ \%\ \text{CI}]$, $t(1427) = 1.35$, $p \geq 0.05$), mean *vpd* was lower in the SFW, with differences increasing considerably from May ($\Delta vpd = 0.08\ kPa$, $t(1473) = 2.06$, $p < 0.05$) to August ($\Delta vpd = 0.21\ kPa$, $t(382) = 6.94$, $p < 0.01$; Tab. 4.S1 for full test statistics).

Windspeed decreased in both sites from May through August, with large median

and mean differences persisting throughout the season (Fig. 4.4b, Tab. 4.S2). Differences peaked in June ($\Delta WS = 0.22\ m \cdot s^{-1}$, $t(2093) = 27.48$, $p < 0.01$) and decreased slightly toward August ($\Delta WS = 0.17\ m \cdot s^{-1}$, $t(297) = 15.36$, $p < 0.01$), due to an overall decline in both sites.

Incident shortwave radiation ($K\downarrow$) is always lower in the wetland, owing to decreased transmittance from evergreen and senescent woody vegetation prior leaf-out. The discrepancy increased with LAI, and reached up to two orders of magnitude from approximately mid July on days with little cloud cover (Fig. 4.4c), coinciding with overstory LAI and corresponding decrease in transmittance (Fig. 4.S2).

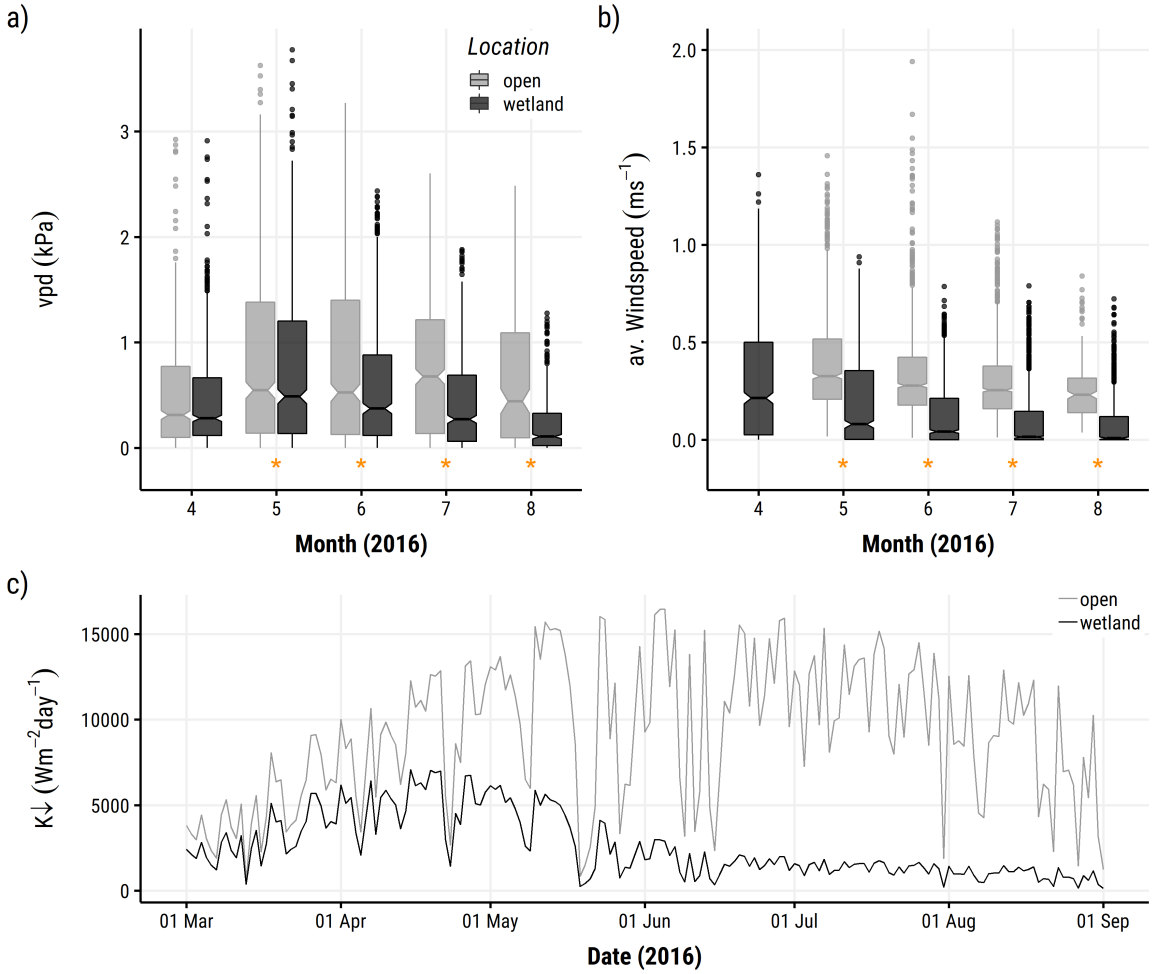

Figure 4.4: Comparison of micro-climatic ET drivers within the forested wetland (beneath overstory canopy, above sub-canopy) and a nearby clearing (terminal pond and its riparian zone, approx 150 m between stations) for (a) vpd, (b) windspeed and (c) incident shortwave radiation (measured at peatland to the east). Differences between monthly means were assessed using two-sided, non-paired t-tests assuming unequal sample variance; significant differences are denoted by asterisks (Tab. 4.S1 and Tab. 4.S2 for test results). Upper and lower limits on boxes represent 0.25 and 0.75 quantiles, Whiskers are 1.5 times the inter-quartile range above and below aforementioned quantiles; displayed points are beyond this range.

4.4.3 Controls on daily ET_{sc} totals

Daily maximum *vpd* (Fig. 4.5a) and incident, shortwave radiation ($K\downarrow$; Fig. 4.5b) were the strongest predictors of daily ET_{sc}, explaining 67 and 58 % of variance, respectively. Air temperature (at 2 m) also showed strong association with ET_{sc} (Fig. 4.5d, 49 % explained variance). The three variables were best represented by non-linear and non-monotonic relationships, indicating some degree of limitation at high values for *vpd*

and $K\downarrow$, as well as lower limits of air temperature within the observed range. High daily average air temperatures did not coincide with reduced ET_{sc}.

The chosen model for average soil moisture (VWC; Fig. 4.5e) and daily ET_{sc} had neither the highest explained variance (R^2) nor lowest AIC (Section 4.3.5). However, given the fairly poor fit found in all tested models, the 2^{nd}-order polynomial was deemed most interpretable, being in-line with physiological responses of vascular, terrestrial plants to soil water status. There was no conclusive evidence for analogous dynamics in relation to depth of groundwater levels (i.e. fully saturated conditions; Fig. 4.S1).

Neither daily average windspeed (WS; Fig. 4.5c) nor soil water potential (Ψ; Fig. 4.5f) showed any association with daily ET_{sc}.

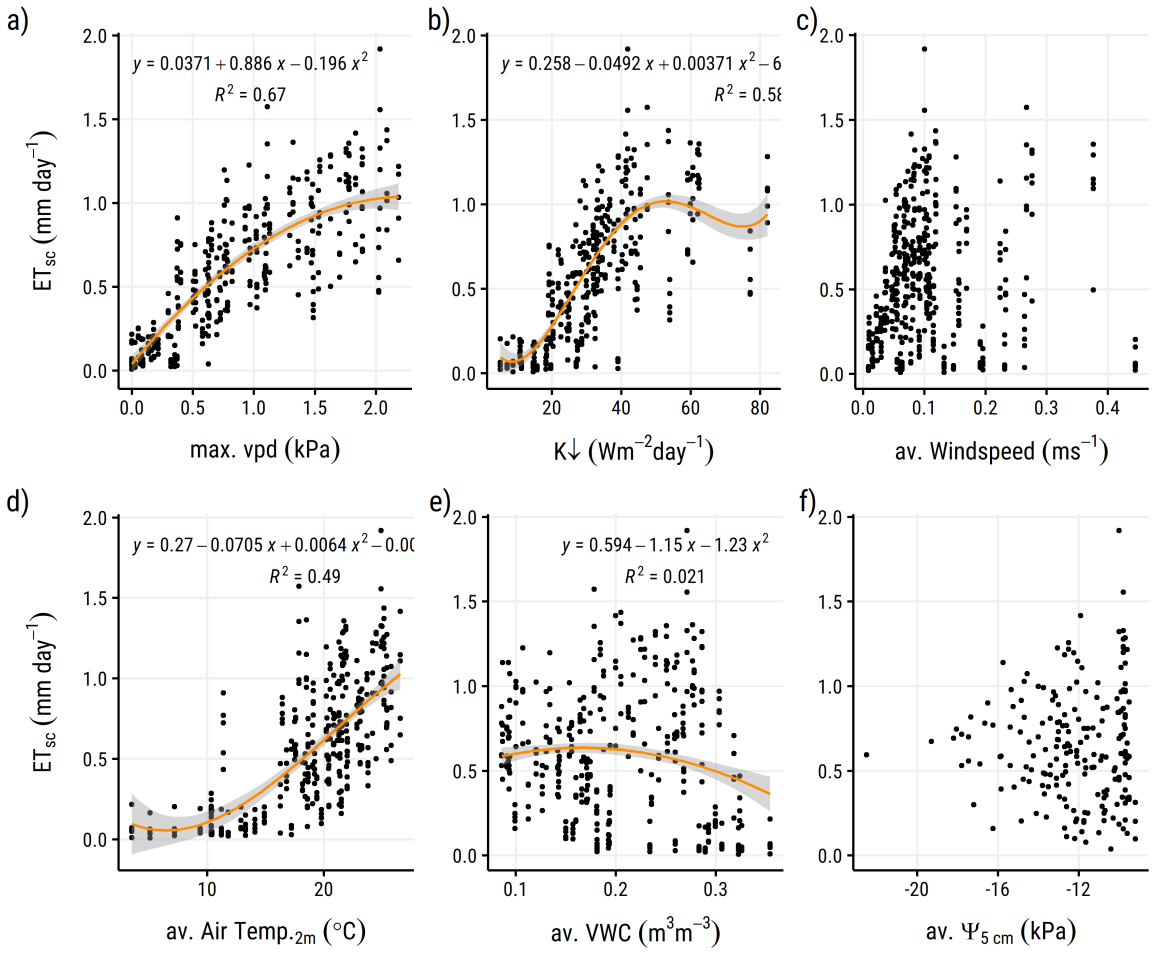

Figure 4.5: Daily ET_{sc} totals plotted against (micro-)meteorological (a - d) and hydro-pedological (e - f) variables. Best fitting (linear OLS) relationships (orange lines, gray shading for 95 % prediction CI) were chosen from a set of candidate models ranging from intercept-only to polynomials between first and fourth order using analyses of variance and AIC differences. Resulting equations and coefficent of determination (R^2) are given as text labels for each panel with significant relationships.

4.4.4 Seasonal development of ET_{sc} controls

The strength and relative importance of ET_{sc} drivers changed throughout the growing season, as inferred from multiple regression with vpd and $K\downarrow$ covering increasing time windows (i.e. fixed start, variable end date; Fig. 4.6). The effect sizes (β) for vpd increased progressively, while - $vice-versa$ - the effect size of $K\downarrow$ decreased, indicated by linear fits in Fig. 4.6a and Fig. 4.6b; however, a flattening of both trends is observable from July. In accordance, the effect size ratios ($\beta_{K\downarrow}/\beta_{vpd}$) decrease (slope

estimate $\beta = -0.07 \pm 0.01$, $t = -8.72$, $p = 2.03 \cdot 10^{-8}$), until a distinct changepoint (i.e. steadying) in ratios occurs on July 12 (± 1.9 *days*), approximately when overstory LAI was close to or at its peak (Fig. 4.S2). Subsequently, changes in ratios were effectively indistinguishable from null $\Delta\beta_{changepoint} = 0.07 \pm 0.01$, $t = 6.10$, $p \geq 0.05$).

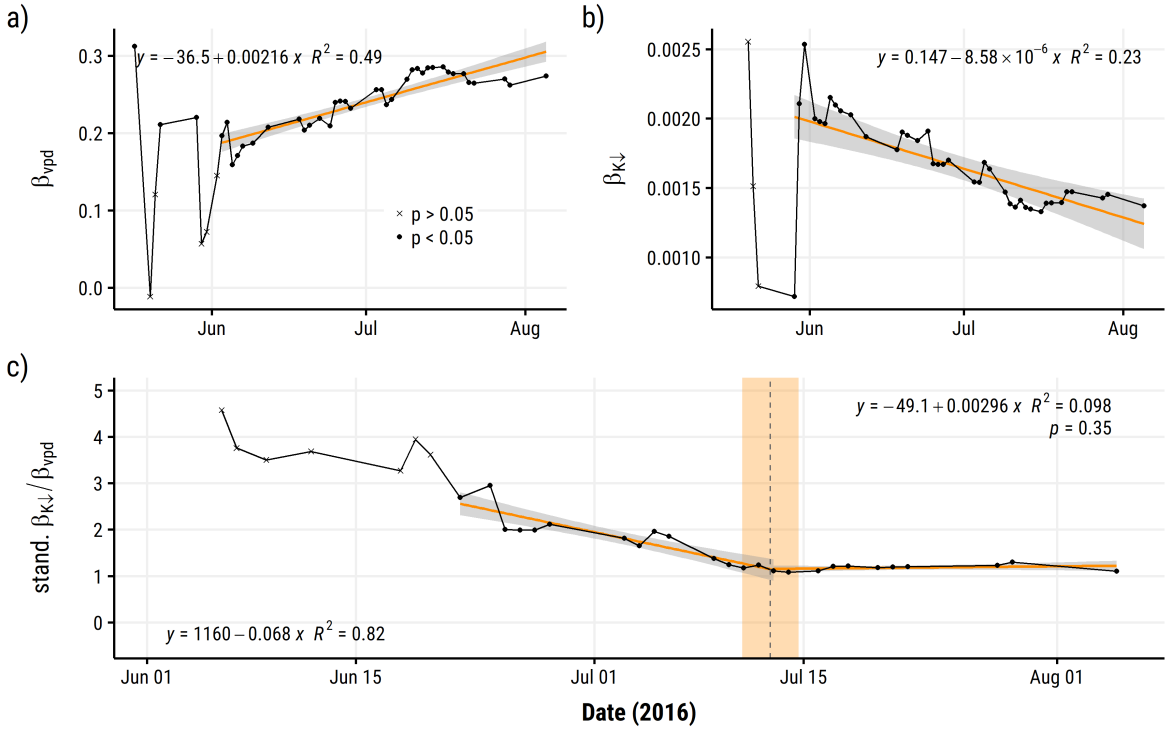

Figure 4.6: Seasonal trajectory of effect sizes (β) for dominant ET_{sc} drivers: (a) *vpd*, (b) inc. shortwave radiation ($K\downarrow$), and (c) their ratio. Respective β were estimated via multiple, linear OLS regression with daily ET_{sc} as response, and the two untransformed micro-climatic variables with strongest association (4.5) as dependents (no interaction term) across a stretching time windows (i.e. fixed at start, increased by available measurement days until end of campaign). Fit models were assessed for their conformity with assumptions of OLS regression, and significant effect sizes ($\beta > 0$) are denoted (see legend). The ratio (c) was calculated analogous, but with standardized dependents (z-transformed). To identify shifting relative importances of *vpd* and $K\downarrow$, a changepoint (dashed grey line) in effect size ratios was identified using segmented linear models fit through ratios over time (after Muggeo, 2003, 2008). Orange shading is the changepoint's standard error. Equations of final lines of β over time (orange lines, gray shading for 95 % prediction CI) and R^2 values are given by text labels; p-values are displayed only for non-significant relationships.

4.4.5 Controls on and dynamics of hourly ET_{sc}

ET_{sc} showed curvi-linear relationships with *vpd* specific to time-of-day (Fig. 4.7a). Before noon (left panel), ET_{sc} increased with *vpd* ($t(3) = 132$, $p < 0.01$), while later

in the day ET_{sc} followed a similar relationship under low *vpd*, but decreased under higher atmospheric demand over afternoon (peak $ET_{sc} \approx 0.16\ mm \cdot hour^{-1}$ for $vpd \approx 1.46\ kPa$; $t(3) = 511$, $p < 0.01$) and evening hours (peak $ET_{sc} \approx 0.11\ mm \cdot hour^{-1}$ for $vpd \approx 1.28\ kPa$; $t(3) = 603$, $p < 0.01$), indicating a potential limitation, as observed in Fig. 4.5a. High *vpd* coincided with high $K\downarrow$, most notable during afternoon hours (Fig. 4.7a).

ET_{sc} and soil water potential showed no discernible trend under low *vpd* (left panel), weakly negative at intermediate (center panel) and weakly positive relationships at high *vpd* (right panel; Fig. 4.7b). Given the skewed distributions of observations across the range of Ψ, the models are in violation of OLS regression assumptions, which should be borne in mind for further interpretation. Other regression approaches accounting for unequal variances (Heteroscedasticity, evident in the increasing spread with higher Ψ), such as weighted regression, were refrained from, as no inferences were sought with the model coefficients given the weak trends. The issues may be alleviated with deploying sensors able of covering a wider range ($\Psi > -10\ kPa$), or with additional data collection in drier periods. ET_{sc} was negatively related to VWC at low *vpd* (left panel; $\beta = -0.0230 \pm 0.00417$, $t = -5.51$, $p < 0.01$), and showed increasingly positive association at medium *vpd* (middle panel; $\beta = 0.0984 \pm 0.00837$, $t = 11.8$, $p < 0.01$) and high *vpd* (right panel of Fig. 4.5c $\beta = 0.147 \pm 0.0149$, $t = -9.91$, $p < 0.01$). While these relationships explain little variance (i.e. large scatter; R^2 between 0.01 and 0.025), the increase in slopes with *vpd* (i.e. panels in (Fig. 4.5c) is indicative of higher sensitivity to available soil moisture under high atmospheric demand.

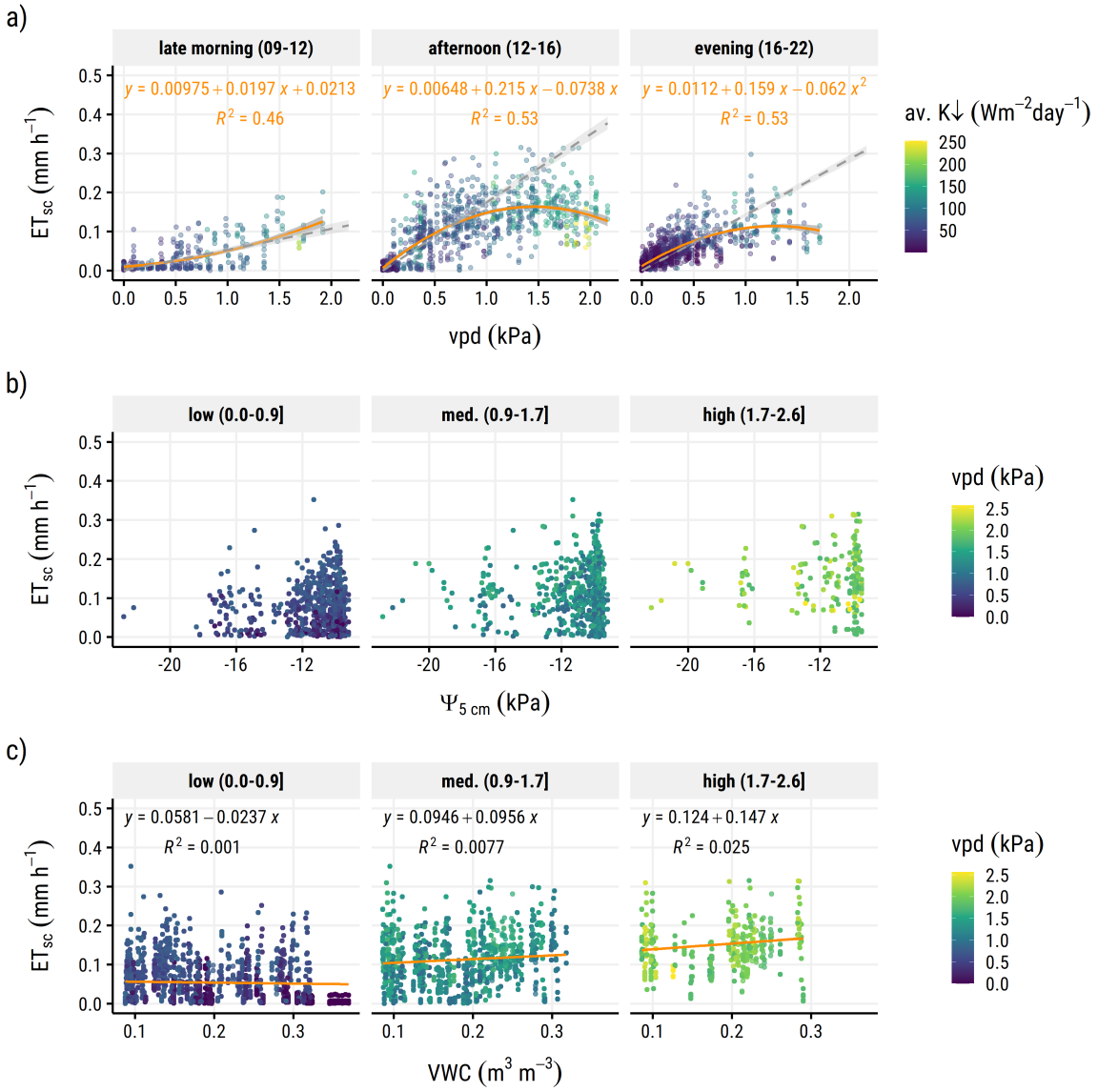

Figure 4.7: Hourly ET_{sc} rates *vs.* (a) vpd, (b) soil water potential, (c) and volumetric water content for different times of day (a) and atmospheric water demand (i.e. binned vpd; b, c). Refer to legends for colors. ET_{sc} for b) and c) are from 09:00 to 20:00 MST only. Best fitting (linear OLS) relationships (orange lines, gray shading for 95 % prediction CI) were chosen from a set of candidate models ranging from intercept-only to polynomials between first and fourth order using analyses of variance and AIC differences. Resulting equations and (R^2) values are given in each sub-panel; p-values are displayed if one or more relationships across sub-panels were non-significant. Note, that in a) linear (first order) models (for $vpd \leq 1$) are shown for comparison, and that no trend lines are given in the middle row as trends are small and estimated using OLS under violated assumptions (evident in heteroskedasticity - assumed appropriate as no inferences made with coefficients).

ET_{sc} showed characteristic, hysteretic dynamics with *vpd* (Fig. 4.8a), which indicate soil- or plant-atmosphere feedbacks. Three trajectories in response to P events (Fig. 4.8b) emerged: (1) Rain days resulted in low(er) hourly (and daily total) ET_{sc}

(e.g. DOY 182, 184, 185); (2) post-rain days showed steeper increases, with fairly close agreement of peak ET_{sc} and peak *vpd*, less pronounced hysteretic character and Bowen ratios indicative of the system switching to latent heat flux-dominated earlier in the day ($B < 1$, DOY 178, 183), as compared to (3) where consecutive dry days (e.g. DOY 179 to 181) showed flat trajectories with sensible heat flux dominating ($B \geq 1$) until approximately 10:00 to 12:00 MST. Note, that peak ET_{sc} did not coincide with maximum daily *vpd* (also Fig. 4.5a). Median r_{total} (Fig. 4.8c) increased throughout afternoons ($\chi^2(5) = 117.51, p < 0.001$), coinciding with times of highest atmospheric demand, from 136 $s \cdot m^{-1}$ at 13:00 MST to 221 $s \cdot m^{-1}$ at 17:00 MST (increase of 63 %).

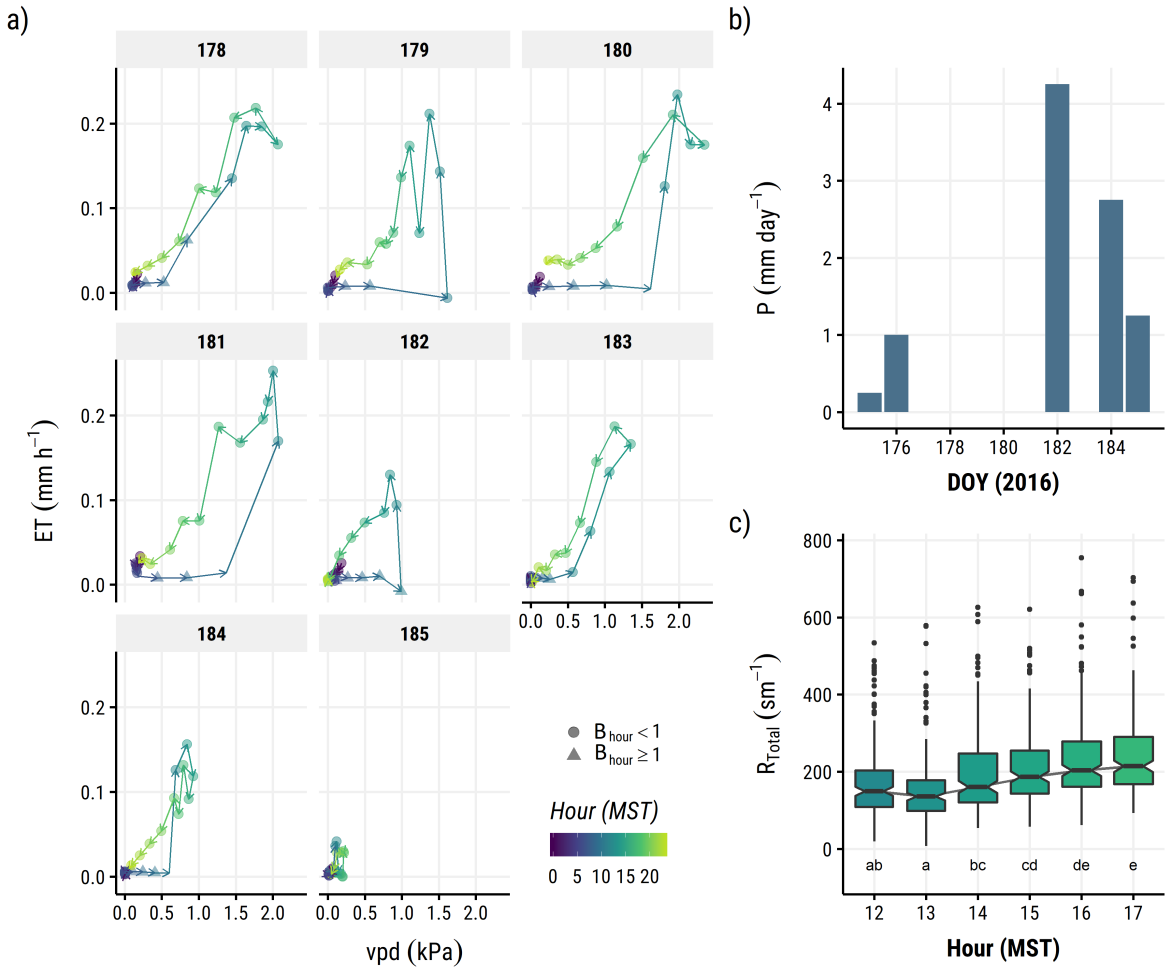

Figure 4.8: Hourly course of ET_{sc} in relation to (a) vpd (arrows and color indcate direction) for selected days, (b) corresponding daily precipitation and (c) total resistance to ET_{sc} at hours of highest demand (colors as in a; values from across season). Symbols in a) are an approximation of the Bowen ratio (after Perez *et al.*, 2008) indicating whether latent ($Bhour < 1$) or sensible heat fluxes dominated turbulent energy transfer toward the overstory; symbols are missing for non-finite values. Letters in c) indicate significantly different medians between hours (multiple-comparison Kruskal-Wallis test; α adjusted for multiple comparisons). Upper and lower limits on boxes represent 0.25 and 0.75 quantiles, whiskers are 1.5 times the inter-quartile range above and below aforementioned quantiles; displayed points are beyond this range. Data in a) is from chamber 5.

Across the growing season r_{total} increased with decreasing soil water potentials (Ψ_{5cm}), i.e. as soils dried (Fig. 4.9). The strengths of this relationship differed between chambers (slopes in regression equations of Fig. 4.9), but averaged approximately -3.6 $s \cdot m^{-1} \cdot kPa^{-1}$ ($[-4.5, \ -2.8]$ 95 % CI) in the observed range.

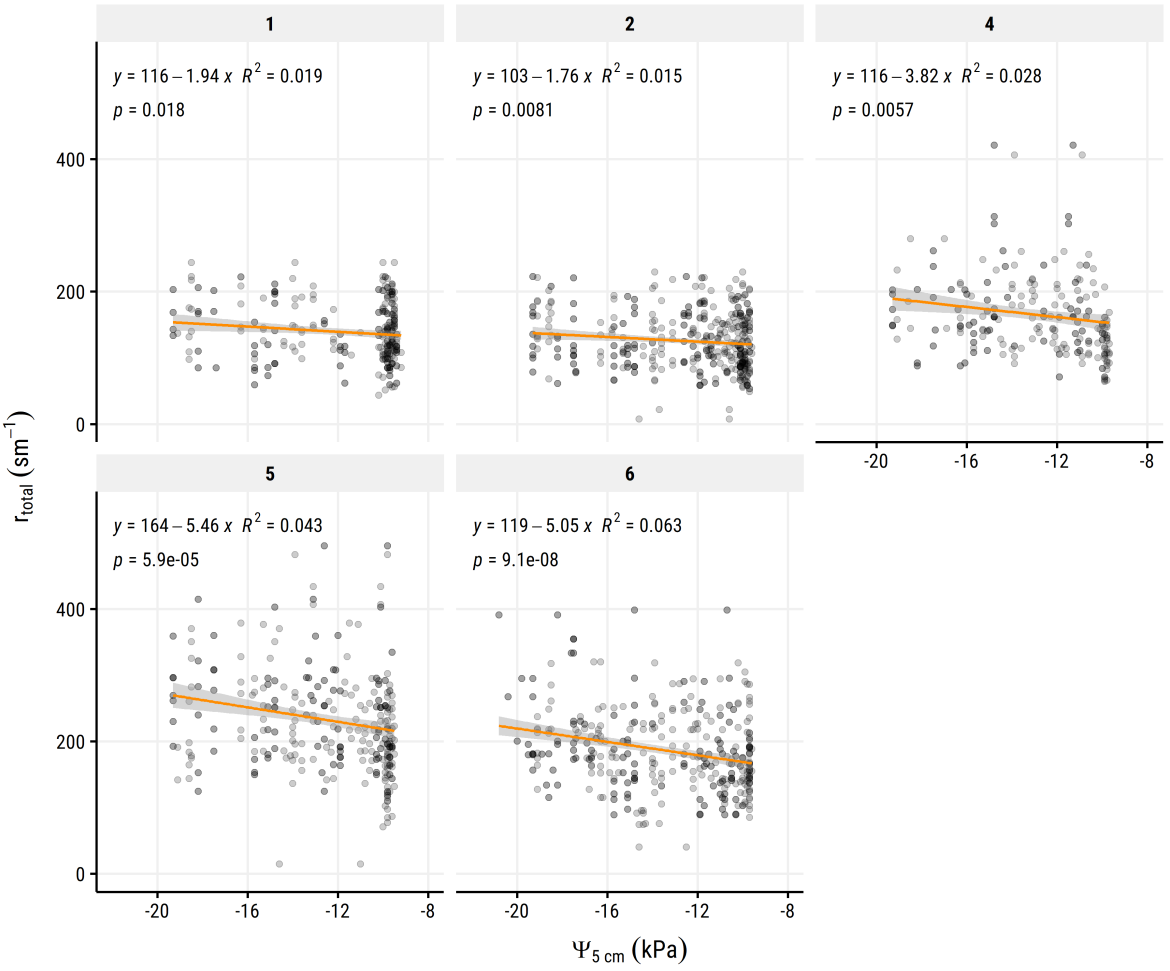

Figure 4.9: Total resistance (r_{total}) to ET_{sc} *vs.* soil water potential Ψ (5 *cm* depth) for all assessed chambers (hourly measurements, across entire campaign). Equations, R^2 and p-values of linear OLS models are displayed in each panel (fits are orange lines, gray shading for 95 % response CI). Note, that instrumentation did not measure $\Psi > -10$ *kPa*.

4.5 Discussion

4.5.1 ET_{sc} from a deciduous SFW in the Boreal Plain

Estimated ET_{sc} (0.87 ± 0.06 $mm \cdot day^{-1}$, Fig. 4.10) was approximately 2.2 to 4.3 times lower than reported for other typical BP wetland systems (e.g. Brown *et al.*, 2010; Kettridge *et al.*, 2013; Thompson *et al.*, 2014) (Fig. 4.10). The majority of forested boreal wetlands are bog or fen systems dominated by moss sub-canopy communities

(e.g. DeLancey *et al.*, 2019). Permanently high soil moisture and shallow groundwater, characteristic for these wetland systems, results in ample access to water to sustain ET_{sc}. Northern peatlands maintain these conditions through feedback mechanisms that reportedly reduce atmospheric water losses (relative to open water, Waddington *et al.*, 2015 for review), allowing for continued productivity even in water-limited regions such as the BP, where P approaches pET (Devito *et al.*, 2012). In contrast to vascular vegetation, mosses cannot actively regulate water loss (Rydin *et al.*, 2006), and E therefore largely depends on the morphological structure of prevalent species, with two distinct groups in the BP (e.g. Kettridge *et al.*, 2017) of contrasting transport mechanisms operating for liquid water and vapor: capillary rise for *Sphagnum spp.* (Goetz and Price, 2015) due to long stems, and layered, mat-like growth acting as a diffusion barrier for feather moss (Kettridge and Waddington, 2014; Kettridge *et al.*, 2019).

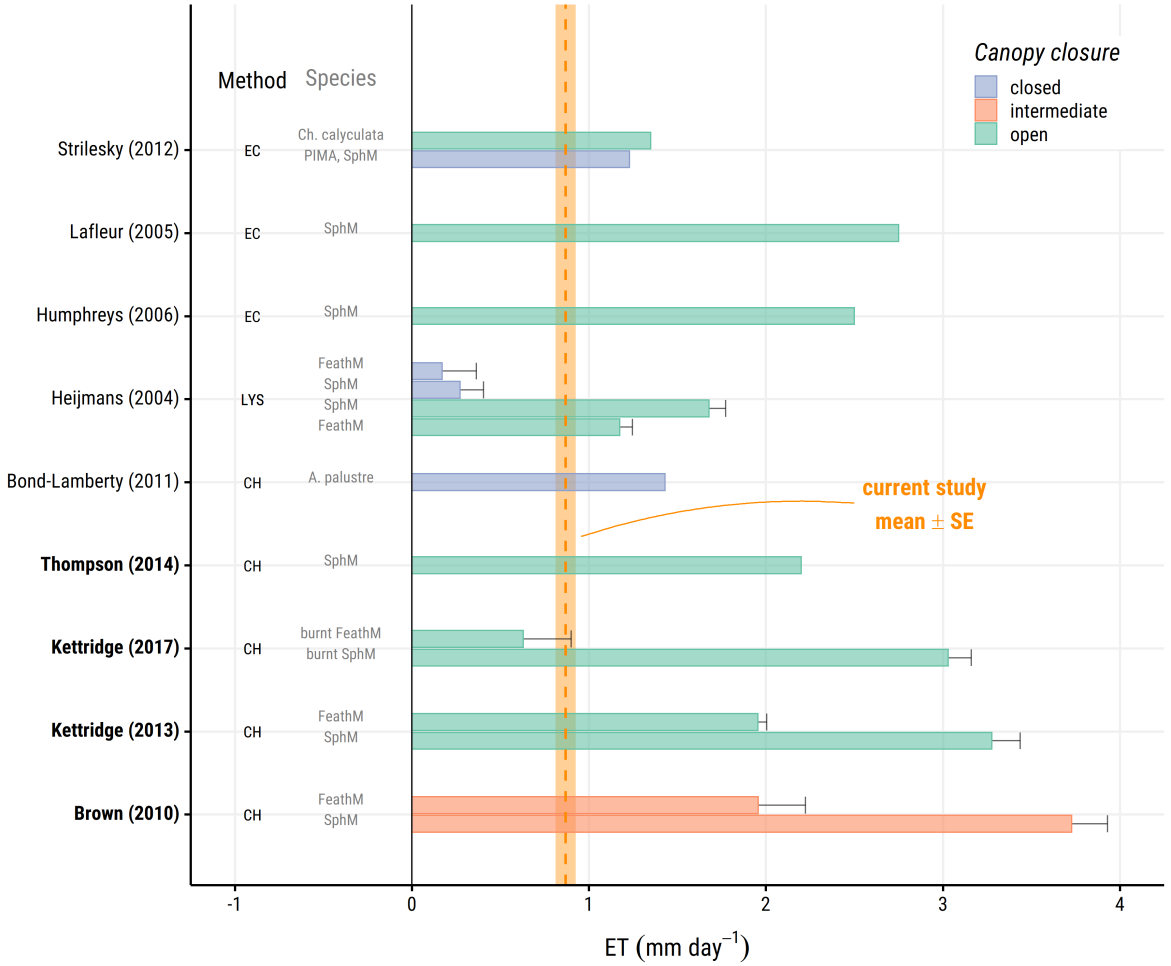

Figure 4.10: Comparison of ET_{sc} (*sensu* section 4.3.2) rates of northern/boreal bogs and fens (Boreal Plain studies in bold) from chamber (CH), lysimeter (LYS) and eddy co-variance (EC) measurements for three qualitative levels of canopy closure (based on reported canopy biomass density, percent cover or leaf area index); dominant sub-canopy species are given as text labels (SphM = *Sphagnum spp.*, FeathM = Feather Moss, PIMA = *Picea mariana* [< 0.5 *m* height], *Chamaedaphne calyculata*, *Aulacomnium palustre*. ET_{sc} rates were inferred from data figures and/or provided values (units converted where necessary). Bars indicate standard error, and where missing, ET_{sc} values were derived from lower resolution totals (e.g. seasonal) missing uncertainty measures. EC-based values are representative of systems with vegetation structure similar to this study's site and with little overstory transpiration. Compared to other systems typically linked to water surplus-generation and redistribution, ET_{sc} from the forested wetland assessed here was generally lower than in open wetlands for the Boreal Plain. Note that closed canopy sites from Heijmans *et al.* (2004) are black spruce forests.

For example, Brown *et al.* (2010) assessed sub-canopy fluxes from a Black Spruce peatland and found ET_{sc} of plots dominated by *Sphagnum spp.* (3.73 ± 0.20 $mm \cdot day^{-1}$) to be approximately 1.8 times higher than for feather moss plots (1.96 ± 0.27 $mm \cdot day^{-1}$). Feather moss communities display a substantial water-loss reduction in response to moderate wildfire (Kettridge *et al.*, 2017), a major component of the BP

disturbance regime (Johnson *et al.*, 1998; Kettridge *et al.*, 2015), allowing for subsequent recovery. It is most noteworthy that the deciduous SFW features ET_{sc} rates of similar magnitude (Fig. 4.10) to a system following such drastic disturbance (i.e. loss of sub-canopy community). These low ET_{sc} rates likely allow SFW, such as the deciduous swamp studied here, to maintain saturation and/or high moisture conditions long enough for characteristic wetland features to develop and persist through the marked climatic cycles (dry, mesic, wet, Mwale *et al.*, 2009; Devito *et al.*, 2012) of the BP. SFW in the BP, i.e. with ephemeral hydrological regimes, likely require sub-canopy conditions similar to those found in the system subject to study here. The isolated and perched nature of this SFW, as an extreme case of reliance on atmospheric water inputs, further highlights the system's self-regulation and capacity to persist in the sub-humid climate.

The SFW effectively shifts from open to closed-overstory conditions, with increasing sub-canopy leaf area throughout the season, evident in ET_{sc} and its drivers decreasing between June and July (Fig. 4.2 and Fig. 4.6). While increased sub-canopy LAI could have resulted in higher T, the SFW micro-climate likely acted suppressingly. This effect is expected and has been observed in a variety of wetland systems of different degrees of overstory closure, and in different climates (e.g. Strilesky and Humphreys, 2012, Fig. 4.10). While these results stem from different sub-canopy communities, environmental conditions (e.g. temperate systems for Strilesky and Humphreys, 2012) and methodological approaches, the direction of the effect, and its causes, do give insight into dynamics controlling ET_{sc} from SFW (in the BP). For example, Heijmans *et al.* (2004), also focusing on differences between *Sphagnum* and feather moss communities, identified overstory closure as well as sub-canopy structure (vascular vs. non-vascular) as a major control on ET_{sc}, with lowest rates occurring under closed black spruce overstories in sub-canopies with shrub cover (increasing aerodynamic resistance), and markedly higher ET_{sc} for open wetland systems.

The assessed ET_{sc} dynamics may further serve as a baseline and/or target (i.e. natural analogue), to compare against for restoration or reclamation managed sites. Recent work by Little-Devito *et al.* (2019) showed that low-storage wetlands initiated on reclaimed oil sand mines "opportunistically" (unplanned). These sites feature energy and mass exchange dynamics different to this study's system, as current vegetation communities and their structure are in early stages of successional development (Nwaishi *et al.*, 2015), with multiple potential endpoints. However, establishment of roughness elements, physical wind barriers and internal shading through canopy closure (Bourgeois *et al.*, 2016), as provided by the vegetation strata (trees, shrubs, sub-canopy) in the studied swamp here, are considered a key threshold for developing internal feedbacks that maintain ecohydrological functioning (e.g. R generation) in the region's sub-humid climate. Such mechanisms and feedbacks are addressed in the following sections, and analogous processes are frequently planned for in restoration or reclamation operations e.g. through placement of woody debris or micro- and mesotopography (Brown and Naeth, 2014; Forsch, 2014).

4.5.2 Role of SFW micro-climate

The above clearly emphasizes the role of the overstory and sub-canopy in developing, as well as self-regulating, a micro-climate less conducive for sustained, high ET_{sc}. The space above the sub-canopy and below the overstory ultimately defines vapor pressure and energy gradients between leaves and surrounding atmosphere. Dense overstories impede exchange of accumulated, moist air with the (typically) drier atmosphere above. Hence, ET_{sc} increasingly depends on the frequency and magnitude of eddies sweeping through the overstory and into the sub-canopy (Black and Kelliher, 1989) as the season progresses, which are typically infrequent or intermittent for deciduous systems (time scales of $< 1\ h$, Baldocchi and Meyers, 1988; Hollinger *et al.*, 1994). Further, localized convection via thermal plumes (e.g. generated through differential heating) may play

an increasing role under high LAI as well (Dupont and Patton, 2012). While initially turbulent exchange may be large (high roughness from woody stems), increasing LAI toward the seasonal maximum will decrease efficiency of momentum and mass (as well as energy) transfer to and from the sub-canopy, if stem and leaf density is sufficiently high (Oke, 1992).

Given the multi-layered structure and high LAI throughout the wetland's vertical profile, the drastic decrease in windspeed, as well as increasing discrepancy between reference and SFW *vpd* (Fig. 4.4), indicated progressively impeded turbulence, and consequently reduced ET_{sc} (Van Gardingen and Grace, 1991). The sub-canopy progressively became more sensitive to *vpd* across the growing season (Fig. 4.6c). Given the increasing shading and atmospheric sheltering, any eddies (or plumes) penetrating into the sub-canopy therefore re-establish vapor gradients that are diminished through ET_{sc} (assuming drier air above the overstory); advective displacement (i.e. via horizontal flow) of moist with drier air from the nearby opening may also uphold larger *vpd*, further explaining the increased sensitivity later in the season. Drawing upon theory from McNaughton and Jarvis (1983), and in light of non-equilibrium conditions (i.e. $vpd > 0$), the system should tend toward a higher relative importance of aerodynamic over radiative forcing in general, but will likely display a shift toward higher decoupling, owing to the decreased efficiency of turbulent exchange (e.g. Mackay *et al.*, 2007). Given that the degree of coupling largely depends on the ratio of canopy to aerodynamic conductance, a more detailed assessment of both represent an important avenue for future work.

4.5.3 ET_{sc} controls and soil-plant-atmosphere interactions

Daily maximum *vpd* and $K\downarrow$ were strong predictors of daily ET_{sc}. The observed non-monotonous relationships with daily ET_{sc} indicate some degree of limitation or control on water loss. This was also evident in (1) the analogous relationship between

hourly ET_{sc} and *vpd* (limited at around 1.5 kPa and likely enhanced under high $K\downarrow$, 4.7a), (2) a mismatch of peak *vpd* and ET_{sc}, as well as (3) increased sensitivity to soil moisture at higher atmospheric demands, and increased total resistance at lower soil water potentials (i.e. drier conditions). This could be imposed through either vascular vegetation or intrinsic soil properties.

Vascular plants, as opposed to mosses, may regulate (excessive) water losses by closing stomata under high atmospheric demand (i.e. *vpd*, Schulze and Hall, 1982; Black and Kelliher, 1989) or low soil water potentials (e.g. Buckley, 2005b), according with a saturating response of T against the respective driver(s). Considerably steeper and narrower hysteresis loops (Fig. 4.8a) after rain indicate little to no control exerted by stomata, i.e. wetted leaves readily evaporate under increased atmospheric demand similar to open water (Oke, 1992) or soil water potentials are adequately high and non-limiting (Buckley, 2005b). By contrast, the sub-canopy tended toward sensible heat flux in dry(ing) periods (flat hysteresis loops pre-noon), and periods of high atmospheric demand were typically met with higher total resistance (r_{total}), and lower ET_{sc}. The flatness prior noon may be indicative either of water conservation (likely until photosynthetic radiation reaches a threshold), replenishment of plant water stores over T and/or a delayed transfer of energy stored in soil (water) and the overstory subsequently driving ET_{sc} (Munro, 1979; Allen *et al.*, 2017). Any impacts of changing soil water conditions on E and T individually could not be inferred directly, as measurements did not allow partitioning ET_{sc} at sufficiently high temporal resolutions. However, the increased sensitivity to soil moisture (Fig. 4.7a) at high *vpd* at least hints at the potential regulation of stomatal conductance to prevent excessive water losses and physiological damage (e.g. Dixon and Johnson, 1993; Lafleur, 2008). There was no clear evidence for any impact of groundwater levels on ET_{sc} based on dynamics during the measurement campaign, as saturated or high-moisture conditions typically coincided with low atmospheric demand. However, reducing conditions in the soil column (cf Fig. 4.1) resulting from frequent wetting and drying may rapidly lead to anoxic

conditions following rain events; this can lead to stomatal closure (Pezeshki and DeLaune, 2012) and may represent another feedback by which the sub-canopy prolongs conditions suitable for wetland formation and persistence.

Deciduous vegetation, moss or bare ground/litter dominate the forest floor in the studied SFW; in early spring this hence entails a dominance of E over T, which shifts across the growing season (Fig. 4.3). An indication of a soil-atmosphere feedback was evident through r_{total} increasing with decreasing soil water potential (Fig. 4.9), which is likely most important early in the growing season (Fig. 4.3) when sub-canopy LAI is zero or low. E emanated from mosses or - in this case predominantly - through leaf litter from water transported via capillary rise, or through diffusion through the soil media (likely similar to a two-stage E process in porous media; Shokri *et al.*, 2009). Unless saturated to the top of the soil column (i.e. standing water), the layered and overlapping leaf litter may act as a barrier to vapor diffusion from continuous transport of pores underneath. In addition, the organic soil likely undergoes some degree of shrinkage as it dries and pore water pressure decreases (e.g. Price, 2003), increasing tensions and impeding diffusion upwards further. The early-season dominance of E over T warrants investigating surface resistance (i.e. r_{soil}) as a component of total resistance in controlling atmospheric water losses. A more detailed exploration with more highly resolving instrumentation (e.g. for soil water potential, Ψ), as well as additional measurements allowing for a more complex ET model provide further avenues of research.

4.6 Conclusion

ET_{sc} from the deciduous swamp assessed here was considerably lower than for open-canopy Boreal (Plain) wetlands, and somewhat below that of other closed wetlands. Systems similar to the SFW studied here, play an important role on local and regional

scales in redistributing water to adjacent systems (see Chapter 2, Devito *et al.*, 2017), similar to other BP wetlands (e.g. Gibson *et al.*, 2015: wells2017). Functioning in this capacity depends largely on maintaining high soil moisture or saturation. The distinct micro-climate which the SFW developed across the assessed growing season, led to conditions less conducive for high ET via the sub-canopy - indicating a self-regulated feedback that may prolong hydroperiods: T sustains overstory and sub-canopy growth, which in turn limit water losses through autogenic shading and aerodynamic sheltering. Given the low storage intrinsic to SFWs, and resulting hydro-regimes (Chapter 2, Chapter 3), these systems will likely be able to maintain their functioning across a range of hydrometeorological variability.

It must be noted, that no assessments of sub-canopy ET from deciduous, forested wetlands, in particular swamps, were found for the Boreal Forest, a paucity also noted in (Lafleur, 2008). This work therefore represents a first step toward quantifying the dynamics (and role) of atmospheric water fluxes in deciduous swamps, as small, forested wetlands, in the Boreal. Further, assessing the degree of coupling between sub-canopy (and overstory) in the SFW will shed additional light on the seasonally shifting sensitivity to radiative *vs.* aerodynamic forcing of ET. This is especially important in light of changing climatic dynamics that may drive the timing of vegetation development in overstory and sub-canopy (Laskin *et al.*, 2019), as well as affect plant physiological performance that may render Boreal trees more susceptible to secondary stress, such as insect infestations (defoliation), that may impede the proposed self-regulatory mechanism (Volney and Hirsch, 2005). This will inform whether isolated SFW, similar to this site, may be resilient to future warming and potentially increased atmospheric water demand (Ireson *et al.*, 2015) beyond a hydrological viewpoint.

4.7 Supplemental Material

4.7.1 Figures

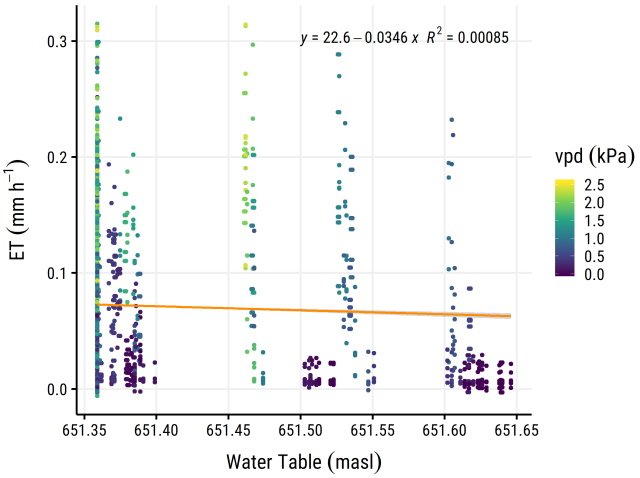

Figure 4.S1: Hourly ET_{sc} *vs.* water table elevation at a well located between chamber sites with *vpd* represented by color. The well base intersected the top of the low-permeability clay layer (at lowest elevation with clustered observations; well typically dry). ET_{sc} decreases with higher water tables. However, *vpd* is not equally distributed along all water levels (especially for higher levels close to surface), and therefore inferring potential interactions between water table elevation and ET_{sc} were refrained from.

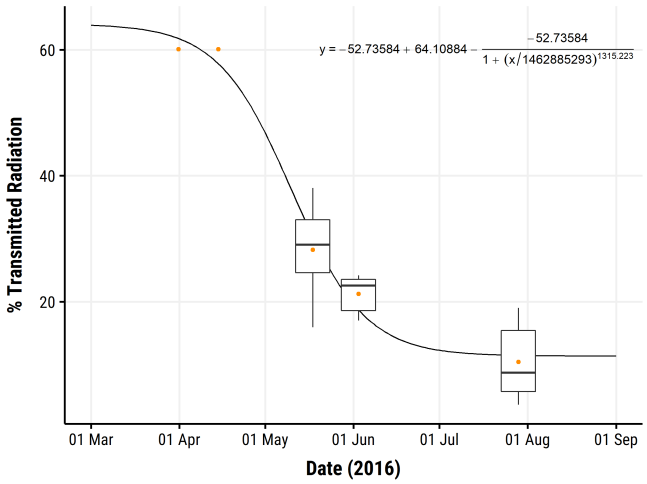

Figure 4.S2: Estimated light transmission through the overstory. Boxplots are based on transmitted light from repeated hemispherical photos across the chamber sites, and orange dots represent means. The contribution of leafless stems early in the season was estimated by classifying early-growing season images into vegetated vs. woody plant material. The black line and equation represent the best fit estimated via non-linear, least-squares regression through means. Maximum overstory leaf area and light extinction were approximately reached mid July. Upper and lower limits on boxes represent 0.25 and 0.75 quantiles, Whiskers are 1.5 times the inter-quartile range above and below aforementioned quantiles. Note, that time (x) was represented as a numeric value in seconds since January 1, 1970.

4.7.2 Tables

Table 4.S1: Comparison of hourly vpd (kPa) across months contrasting SFW micro-climate against an open reference site (150 m distance) with two-sided, non-paired t-tests assuming unequal sample variance. A difference between means was assumed at $\alpha < 0.05$; asterisks denote $p < 0.05$ (*), $p < 0.01$ (**), and $p < 0.001$ (***). Confidence intervals are for 0.025 (CI low) and 0.975 (CI high) quantiles of the estimated differences.

Month	av. diff.	av. SFW	av. open	adj. df	t-statistic	CI low	CI high	p
4	-0.03	0.45	0.48	1427	-1.35	-0.09	0.02	n.s.
5	-0.08	0.64	0.72	1473	-2.06	-0.16	0.00	*
6	-0.19	0.50	0.69	1340	-5.11	-0.26	-0.12	***
7	-0.18	0.39	0.56	1322	-6.19	-0.23	-0.12	***
8	-0.21	0.15	0.36	382	-6.94	-0.28	-0.15	***

Table 4.S2: Comparison of windspeed (ms^{-1}, 15 min averages) across months contrasting SFW micro-climate against an open reference site (150 m distance) with two-sided, non-paired t-tests assuming unequal sample variance. A difference between means was assumed at $\alpha < 0.05$; asterisks denote $p < 0.05$ (*), $p < 0.01$ (**), and $p < 0.001$ (***). Confidence intervals are for 0.025 (CI low) and 0.975 (CI high) quantiles of the estimated differences.

Month	av. diff.	av. SFW	av. open	adj. df	t-statistic	CI low	CI high	p
5	-0.21	0.19	0.39	1957	-19.54	-0.23	-0.19	***
6	-0.22	0.12	0.34	2093	-27.48	-0.23	-0.20	***
7	-0.20	0.09	0.29	2727	-32.07	-0.21	-0.19	***
8	-0.17	0.08	0.26	297	-15.36	-0.20	-0.15	***

CHAPTER 5

Species-specific climate-growth relationships of Boreal Plain upland trees indicate modulating interactions along the interface of a small, forested swamp

5.1 Abstract

Groundwater supplementation from wetlands to adjacent uplands may locally modulate climate-growth relationships, potentially acting as a buffer against hydrometeorological variability and entailed drought stress in moisture-limited regions such as the Boreal Plan (BP). This study aimed to identify if wetlands with ephemeral hydrological regimes (forested swamps) can provide water for mixed stands of two dominant upland tree species, *Populus tremuloides* Michx. (trembling aspen) and *Picea glauca* [Moench] Voss (white spruce) using dendroecological and wood-anatomical analyses. Ring width chronologies in a perched wetland-upland complex were established for the hillslope base (HSB), with intermittent groundwater supply, and for the hillslope middle (HSM), and correlated with precipitation (indices, P), maximum temperature, and vapor pressure deficit (*vpd*) for 1980 to 2015. In addition, xylem hydraulic architecture was assessed for *P. glauca*, and correlated with the same variables. *P. tremuloides* showed strong negative association with temperature and *vpd* and no significant correlations with P, indicating less or no water limitation along the hillslope, but strong down-regulation and/or increased respiration during unfavorable conditions. Potential explanations for the lack of P sensitivity, such as hydraulic redistribution via clonal root networks, are discussed. Radial growth of *P. glauca* increased with winter and spring P, while indications of heat-induced drought stress were given by negative correlations with temperature and *vpd*, agreeing with previous work. Water supplementation was indicated when combining ring widths and wood anatomy, showing increased growth in response to P, as well as lower size variability of water transport cells at the HSB, with divergent sensitivity to P early and late in growing seasons between sites. The strong correlations for *P. glauca* with multi-year P anomalies (Pearson's $r > 0.5$) also highlight the importance of (available) water storage capacity and local contrasts thereof in BP landscapes. Results indicate that water supplementation from swamps, as a

result of their low storage and frequent saturation even in dry years, may reduce negative impacts of climatic variability and water limitation in adjacent upland hillslopes. Additional work should increase confidence in proposed wetland-upland interactions by identifying tree water sources and potential differences in nutrient availability and age-specific climate responses.

5.2 Introduction

Canada's Boreal Plain (BP) ecoregion is part of the circumpolar Boreal Forest biome, which harbors approximately 14 % of all terrestrial biomass (Pan *et al.*, 2013), and it is hence a vital contributor to the global carbon cycle and climate (Kurz *et al.*, 2013; Lemprière *et al.*, 2013). Like other regions within the Canadian Boreal, the BP is of great socio-economic and ecological value (Ireson *et al.*, 2015), yet is subject to anthropogenical disturbance from resource exploitation, and increasingly frequent and severe natural disturbances, including droughts, fires and insect infestation (Volney and Hirsch, 2005; Soja *et al.*, 2007; Rooney *et al.*, 2015; White *et al.*, 2017). Two of the most common Boreal tree species, *Populus tremuloides* Michx. (trembling aspen) and *Picea glauca* [Moench] Voss (white spruce) show concerning and/or highly variable responses to recent climatic changes, which will be exacerbated in the near future (Hogg and Bernier, 2005; Price *et al.*, 2013). Girardin *et al.* (2016) report uncertain, but possibly decreasing, trajectories of aspen productivity in the BP during recent decades coupled with extreme drought-induced mortality (Hogg *et al.*, 2002; Michaelian *et al.*, 2011). Barber *et al.* (2000) found increased drought sensitivity with climate warming in the western Boreal for white spruce, while stand specific interactions with climate complicate generalizing patterns even for individual landscapes (Wilmking *et al.*, 2005). This prompts for continued efforts in characterizing climate-growth responses of forest stands and the mediating effect of local, site-specific conditions, which will aid in predicting forest dynamics across spatial scales in the near future (Soja *et al.*, 2007).

This is of particular interest, as vegetation cover in the BP landscape mosaic is a major determinant of water source (peatland and swamp wetlands) and sink (open water bodies and forests) dynamics, which in conjunction with local physiography of catchments, fundamentally control regional river runoff (Devito *et al.*, 2017). Future water security in the BP is, hence, closely tied to the distribution and functioning of

these landscape units.

Situated in the Western Prairie Provinces, BP forests are predominantly moisture limited (Hogg and Bernier, 2005), as precipitation (P) approximates, but is typically lower than, potential evapotranspiration (pET) annually (Bothe and Abraham, 1993; Devito *et al.*, 2017). Previous dendroclimatological research indicates that both *P. glauca* and *P. tremuloides* show decreased radial growth with lower P (or negative climate/soil moisture indices indicating deficits) during summer and autumn of the year prior, as well as during the current growing season (Chhin *et al.*, 2004a; Hogg *et al.*, 2013). This is because transpiration (and carbon fixation) is reduced via stomatal closure when soil moisture becomes depleted and/or because cavitation of water transporting conduits becomes more likely (e.g Sevanto *et al.*, 2014); further, moisture limitation may also impede wood formation by reducing cambial activity and decreasing cells' capacity to enlarge, as necessary turgor cannot be maintained (Hsiao and Acevedo, 1975; Zweifel *et al.*, 2006). Water limitation during these periods can be compounded by heat-induced stress for both species (Barber *et al.*, 2000; Hogg *et al.*, 2013). Consequently, increasing winter and summer temperatures during this century will most likely have detrimental effects on BP forest growth initially (Price *et al.*, 2013), and may ultimately result in drastic shifts of typical mixed-wood forests to markedly different ecosystem communities and structures, more representative of the drier Aspen Parkland, the ecoregion at the BP's southern border where $P < pET$ (Hogg and Hurdle, 1995; Schneider *et al.*, 2016).

The tight BP climatic water balance (i.e. $P \approx pET$) frequently produces extensive unsaturated zones beneath upland forests due to high growing season water demand coinciding with the majority of annual P ($\approx$ 70 % May - Sep) interacting with deep, glacial deposits (Devito *et al.*, 2005a; Carrera-Hernández *et al.*, 2011). By contrast, BP wetlands maintain water tables close to or at ground level via groundwater connectivity, favorable soil stratification, and/or internal feedbacks (Devito *et al.*, 2005a;

Waddington *et al.*, 2015). These may frequently create or maintain hydraulic gradients that promote lateral groundwater flows into adjacent uplands (Ferone and Devito, 2004; Devito *et al.*, 2005b; Wells *et al.*, 2017). Indeed, water use of (interface) upland trees has been reported for riparian zones of prairie potholes, semi-permanent wetlands in the semi-arid and sub-humid Great Plains (U.S.) and Prairie provinces of Canada (characteristic 'willow rings'; Hayashi *et al.*, 1998), as well indication of trembling aspen redistributing water from wetter areas (i.e. wetlands) via their extensive, clonal root system (Brown *et al.*, 2014b; Depante *et al.*, 2019).

Given the potential for drastic state-shifts of the BP mixed-wood forest, in response to productivity decreases, mortality, and impeded regeneration (Hogg and Bernier, 2005; Michaelian *et al.*, 2011), wetland interfaces may locally buffer against moisture limitation, and compounding heat-stress, providing "refugia", as observed for balsam fir and eastern white pine on fen edges in the temperate-boreal transition in the eastern U.S. (Raney *et al.*, 2016). However, whether and to which extent different physiographical settings, wetland types and forest communities interact to shape tree growth dynamics of mature stands have not been assessed for wetland-upland continua in the BP.

This study aimed to test whether such growth-modulating effects are found in mixed stands of two abundant upland tree species introduced above, *P. glauca* and *P. tremuloides*, along a perched wetland-upland hillslope transect, specifically in two hydrological positions representing the upland (hillslope middle, HSM), and a transitional site close to the wetland's interface (hillslope base, HSB). In this setting, forests lacked access to groundwater from larger scale flow systems, and typically develop extensive unsaturated zones following multi-year climatic water balances (Devito *et al.*, 2005a; Carrera-Hernández *et al.*, 2011; Hokanson *et al.*, 2018a). A shallow, forested swamp situated at the hillslope base was largely decoupled from the memory/lag of extensive vadose zone storage in adjacent uplands, as it has considerably smaller storage. This

configuration provided an ideal framework for testing the dependency on P and potential mediation via wetland water supplementation, and was specifically sought as it is likely that (perched) shallow storage systems will maintain their functioning even under projected temperature-driven increases of atmospheric water demand (Chapter 3; Chapter 4; Ireson *et al.*, 2015; Riddell, 2008; Dixon *et al.*, 2017). The study's focus was to address the following two questions: 1) What is the relationship between climatic variability and local tree growth for *P. glauca* and *P. tremuloides*? 2) Do growth responses differ between the wetland interface and upland hillslope on inter- and intra-annual time scales indicating varying relative importance of climate? To achieve this, growth chronologies of radial increments were developed for both species and set in relation to annual climate indices (indicating atmospheric water surplus or deficit), as well as main drivers of ecophysiological processes (temperature, vapor pressure deficit) (Jones, 2013) for periods during and prior ring formation. Further, wood anatomical analyses on intra-annual scales was used to infer if certain growth periods show site-specific responses to climate, as opposed to the integrated signal provided by ring widths alone. The latter was implemented in the first instance for *P. glauca*, which, as a conifer, has a simpler physiological structure, where the water transporting tracheids (more specifically their lumen) make up around 90 % of cells; their size distribution, hence, provides a direct link to plant-water dynamics via their hydraulic architecture (Sperry *et al.*, 2006; von Arx *et al.*, 2012).

5.3 Materials and methods

5.3.1 Study area

The study area is a predominantly aspen-forested headwater catchment ($\sim 11.9\ ha$) in the Boreal Plain Ecoregion, located in North-Central Alberta (56.081432N, -115.537168W).

The catchment formed on deep glacial substrates (45 to 240 m, Vogwill, 2005) in a transitional zone of coarse(r) glaciofluvial (outwash) and fine-grained stagnant ice moraine deposits (Fenton *et al.*, 2013). Soils are typically luvisols with large water storage capacity (Redding and Devito, 2010), also owing to several meters of silt and silty loam deposits below (Hokanson *et al.*, 2018a). Groundwater-surface water interactions with large-scale flow systems do not occur as the site is permanently perched by 15 to 20 m (Hokanson *et al.*, 2018a); the exclusion of these interactions is further amplified by an extensive low-permeability clay layer at variable depths. Where this layer is surface near (~ 1 m) a small, shallow swamp (~ 0.5 ha) with deciduous over and understory formed in the catchment's northern end. It frequently saturates and produces hydraulic gradients allowing lateral flows into adjacent hillslopes (see Fig. 5.S14), as often found in sub-humid glacial landscapes such as the Boreal Plain (e.g. Ferone and Devito, 2004; Devito *et al.*, 2005b) where P (444 mm for last 32 years; Hokanson *et al.*, 2018a) is close to and frequently below potential ET (pET, 517 mm; Bothe and Abraham, 1993). The wetland is typically the sole source of intermittent runoff generation (typically spring time or during wet years) to a downgradient terminal pond. An access road cut through the southern-most area of the wetland, slightly reducing its absolute area, as well as reducing potential for lateral surface and subsurface flow from the upper to lower catchment (i.e. northern outflow; see e.g. Fig 2.2 in Chapter 2). Climatic deficits (i.e. $P - pET$) typically accumulate across multiple years (Mwale *et al.*, 2009; Devito *et al.*, 2012) resulting in extensive unsaturated zone storage (Devito *et al.*, 2005b), with little lateral flow (surface or subsurface) contribution from upland areas (Redding and Devito, 2008; Smith and Redding, 2012) to the wetland.

5.3.2 Sampling strategy and wood material

Twenty trees were cored for wood material from *Populus tremuloides* Michx. and *Picea glauca* [Moench] Voss on the wetland's north-eastern interface at the hillslope

base (HSB) and the adjacent upland (hillslope middle; HSM), totaling $n = 80$ across two campaigns in August of 2016 and 2017. Trees were classed as HSB if they were between 5 to 10 m away from typical wetland vegetation communities, following the classification of the wetland as a flat swamp (NWWG, 1997), and in an area where wetland water tables are frequently approximately up to 0.5 m below ground. HSM trees were selected where the water table was at least 2 m below ground; typically these sites feature vadose zones of several meters, as indicated by previous investigations (see Chapter 2 and Riddell, 2008) and were between 30 to 50 m from HSB trees.

5.3.3 Wood processing and tree-ring analyses

Two replicate cores were extracted from each tree and processed following standard dendroecological practices (e.g. Speer, 2010). Subsequently, series were established via image acquisition and processing (WinDendro) or manual measurements (stage and microscope, Lintab), cross-dated, and averaged per tree, visually in TsapWin and statistically in COFECHA (Holmes, 1983).

A total of 12 (4 HSB, 8 HSM) *P. tremuloides* and 23 (12 HSB, 11 HSM) *P. glauca* individuals were excluded from analyses due to disintegration during storage or poor intra-series correlation (possibly due to reaction wood or crown damage visible in some of the dominant individuals). Series were detrended in *dplR* (Bunn *et al.*, 2017) to remove any age and growth-release trends by (1) fitting cubic splines with a frequency response of 85 % at $\frac{2}{3}$ of each series' length; (2) computing the ratio between observed and fitted values, and (3) by averaging detrended series using bi-weight robust means (Cook and Kairiukstis, 2013). Ring width indices (i.e. growth response time series) hence emphasized short-term variability over long-term climate trends. Influences of short-term variability on growth dynamics were assessed between 1980 and 2015. Note, that the years 1979 to 1983, as well as 2013 to 2014 were removed for *P. tremuloides*

Table 5.1: Mean and standard deviation of tree characteristics for analysed *P. glauca* and *P. tremuloides* at sites HSM and HSB.

Species	**Site**	**n**	**DBH (m)**	**σ DBH (m)**	**Height (m)**	**σ Height (m)**
Picea glauca	HSB	8	0.56	0.14	31.20	6.61
	HSM	9	0.36	0.17	28.67	11.02
Populus tremuloides	HSB	16	0.19	0.06	18.98	5.62
	HSM	12	0.45	0.12	30.29	7.32

indices, as intense, regional insect infestations (i.e. defoliation events) occurred, evidenced in small white rings with low density (Hogg *et al.*, 2002) (as seen on processed and scanned thin sections; not analysed or presented here). These former periods also coincided with a drought, which may have reduced precipitation-induced growth signals in dendroclimatological analyses, while 2013 is considered a regional wet period (Hokanson *et al.*, 2018a). However, as these infestations result in multi-year growth reductions, they were excluded from final indices. Chronology statistics indicating sample representativeness and common variability over time, *viz.* average inter-series correlation ($\bar{r}$) and expressed population signal (EPS), were calculated for each site and species with moving averages (30-yr window with 20-yr overlap) in *dplR* (Bunn *et al.*, 2017) across all available records. The EPS is defined as:

$$EPS(t) = \frac{t \cdot \bar{r}_{bt}}{t \cdot \bar{r}_{bt} + (1 - \bar{r}_{bt})} \tag{5.1}$$

where t is the number of tree series being averaged (considering one core per tree), and $\bar{r}_{bt}$ is the mean between-tree correlation. Based on these statistics, and available climate data, analyses were restricted to periods after 1980. Raw series and above statistics are found in Fig. 5.S1 and Fig. 5.S2 for *P. tremuloides* and *P. glauca*, respectively. Resulting chronologies for *P. tremuloides* and *P. glauca* and relevant statistics are found in Fig. 5.S3 and Fig. 5.S4; note, that while these constitute an important result *per se*, the chronologies are not the main focus of this study and are hence found in the supplemental information (Section 5.7) of this chapter. Additionally, these chronology statistics as well as the signal-to-noise ratio are found in Tab. 5.S1.

5.3.4 Wood anatomical analyses

Three *P. glauca* cores with the least visible damage per site were selected for wood anatomical analyses. After applying a non-Newtonian solution to prevent cell collapse, transverse cross-sections of 15 to 25 μm thickness were cut from the axially-oriented xylem cells using a WSL rotary microtome (Gärtner and Nievergelt, 2010). Thin sections were then rinsed repeatedly in water to remove the protective solution, stained with safranin and rinsed (and dehydrated) with ethanol until stain leeching ceased. Thin sections were then mounted on glass slides in glycerin, and scanned on a measurement stage with a confocal laser scanning microscope (Olympus FluoView FV300 CLSM). Resulting images had a resolution of 1.438 $pixel\ \mu m^{-1}$ and were stitched in Hugin (Pablo d'Angelo, `http://hugin.sourceforge.net/`) and processed in Roxas (von Arx and Carrer, 2014) and with algorithms in RAPTOR (Peters *et al.*, 2018), where lumen radial diameter was extracted on a minimum of 10, but typically 15 to 20 radial files per year ring. Radial files of different lengths were standardized (scaled and centered) by year and tree to produce tracheidograms based on percentiles (i.e. 20 relative position) similar to (Vaganov, 1990), allowing to compare equivalent portions regarding wood formation of tree rings on inter and intra-annual basis. These were averaged into four sectors for early- and latewood each, covering 25 % intervals of respective wood types; for each type, the first cells are labelled at percentile 100 in correspondence with typically having the largest size. Early and latewood were discriminated based on Mork's index (Denne, 1989), with a conservative threshold value of 0.5 (Park and Spiecker, 2005); hence, earlywood strongly emphasizes the first stages of the growing season. Resulting series were detrended where age trends were apparent (see above; frequency response of 50 %), providing chronologies covering 1988 to 2014.

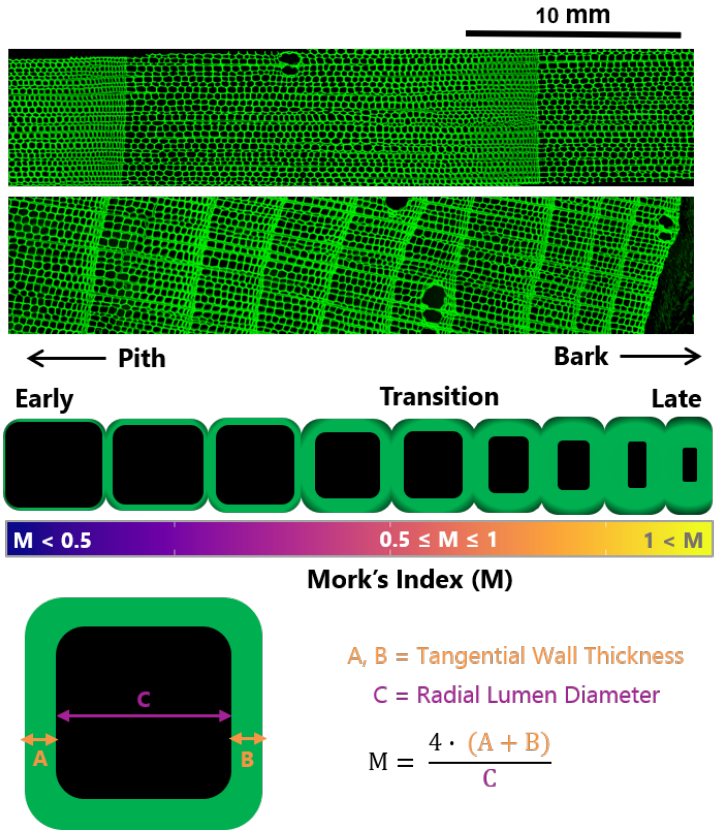

Figure 5.1: Exemplary scans of *P. glauca* for a fast and slow growing individual. Different number of cells per year were standardized to relative percentile position. The schematics below show idealized cells along a single radial file (and one single cell) and properties that were used for analyses (lumen radial diameter) as well as to discriminate early and latewood.

5.3.5 Climate data

Daily precipitation data was obtained in the area from 1999 to 2014 via multiple tipping-bucket rain gauges, which were modified during winter to record snow fall (anti-freeze liquid displacement). The local record was extended to 1980 with daily measurements from Ft. McMurray weather stations, which shows good agreement with general patterns (timings and totals; Devito *et al.*, 2012), and has considerably less missing records than other stations; data was obtained via Environment and Climate Change Canada weather service using *weathercan* (LaZerte and Albers, 2018). Water tables in BP catchments typically have lagged responses to precipitation up to three years (Hokanson *et al.*, 2018a) due to large storage deficits (Devito *et al.*, 2005b).

Hence, next to annual totals, indices representing cumulative departures from mean precipitation (455 *mm* for 1980-2015) were calculated for one to three-year windows for water years beginning November 1.

Mean daily temperature (t_{mean}) and vapor pressure deficit (*vpd*) were obtained from the gridded *daymet* service (1 *km* resolution; Thornton *et al.*, 2017) for the cell in which the catchment falls into from 1980 to 2015. Figure 5.2 gives an overview of the obtained, measured and derived (*viz.* mean departures) climate data.

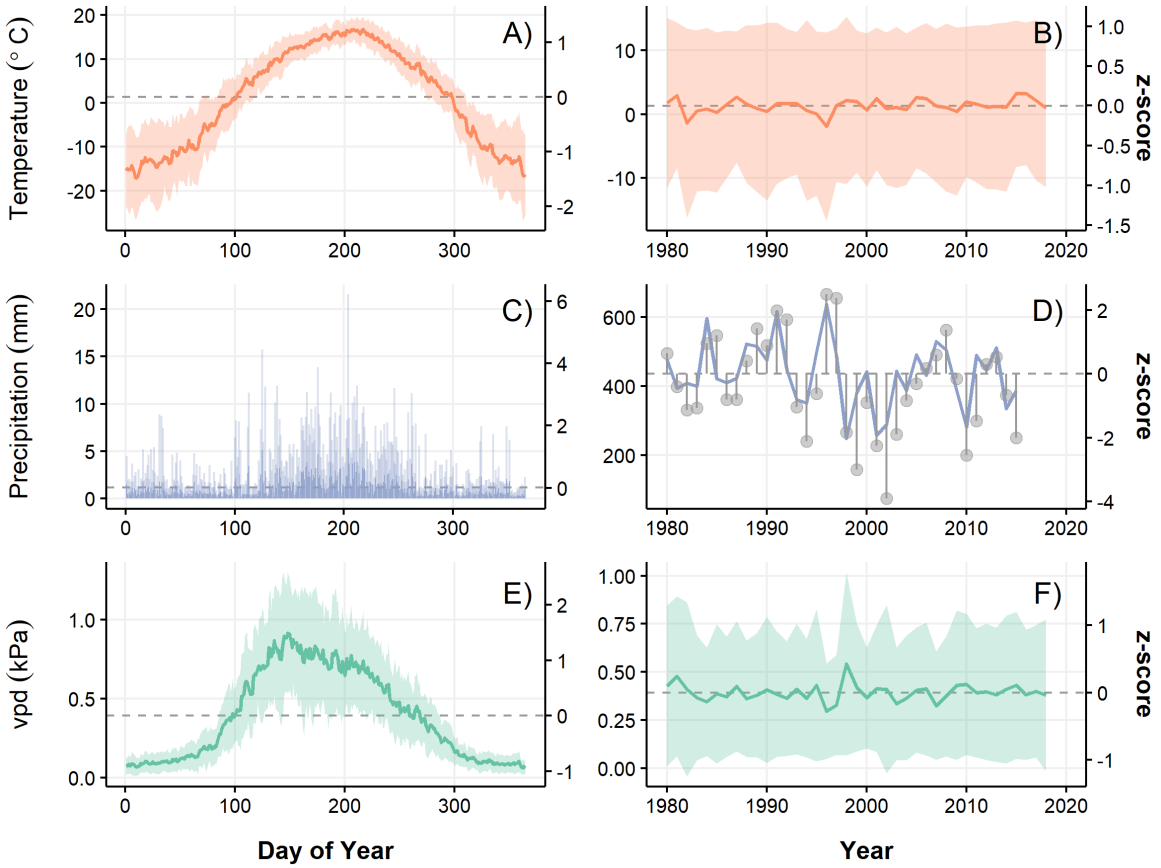

Figure 5.2: Climate data averaged across the investigated period (1980 - 2015) across a year (left) and the entire period (right). A) and B) are mean temperature (*daymet* service), C) and D) are precipitation (local and Ft. McMurray climate station), E) and F) are *daymet*-derived vpd. Shaded areas are standard deviations. The dots and line-ranges in D) indicate cumulative mean departures across 2 years. Z-scores are mean centered and scaled to units of standard deviation.

5.3.6 Dendroclimatological assessment and statistical analyses

The resulting ring width indices for both species, and standardized lumen radial diameter chronologies (*P. glauca*), were correlated with annual precipitation and mean departure indices. Further, running windows covering previous and current-year climatic conditions (P, t_{max}, vpd) were correlated with chronologies above, as well as earlywood sectors from *P. glauca*. To further infer the influence of water availability, the running window analyses was also implemented for latewood sectors and P. Note, that P totals summed over the respective window were applied. The analyses was implemented using methods provided by Jevsenak and Levanic (2018) with window sizes ranging from 30 to 270 days using Pearson's correlation. Differences between lumen diameter chronologies (HSB, HSM) in their variance point-estimate and variance homogeneity (indicating temporal stability) were established by applying χ^2-Test on Variance, as well as Levene's test for variance homogeneity using *EnvStats* (Millard, 2013). All hypothesis tests were implemented with $\alpha = 0.05$ for rejecting null hypotheses using R Core Team (2019). Note that the implied large number of simultaneous significance tests for moving-window correlations inevitably led to false-positives, as discussed by Jevsenak and Levanic (2018). This rate (i.e. type-I errors) can be reduced by decreasing the significance-threshold below e.g. $\alpha = 0.05$. However, the goal here was to capture ecologically-relevant key periods and their temporal stability, increasing interpretability. That is, continuity of correlations through time including specific windows/dates were taken as a strong indication of ecologically-relevant periods. Special attention was afforded to identifying spurious correlations (i.e. definitive false-positives) by considering species' life histories and growing season dynamics.

5.3.7 Ancillary data and observations

Continuous rooting-zone soil temperature and water potential for HSB and HSM were measured at 0.29 m and 0.26 m depth below ground, respectively, with Decagon MPS-2 and 5TE sensors connected to an EM50 data logger. The HSB sensors were placed in the north-eastern hillslope base, while HSM sensors were installed on the opposing hillslope; previous work showed that hillslope water level dynamics were roughly equivalent (see Chapter 2). Further, water tables were monitored manually at bi-weekly to fortnightly scales during the growing seasons of 2016 to 2018 along a wetland-HSB-HSM transect to provide insight on hydrological connectivity between the upland and wetland. These measurements indicated frequent lateral flow into hillslopes, and rare hillslope contributions to the wetland (see Fig. 5.S14), which matches experimental assessments of lateral flow thresholds on luvisolic hillslopes in the BP by Redding and Devito (2008).

5.4 Results

5.4.1 Ring width and climate dynamics

5.4.1.1 Inter-annual time-scale

Annual growth of *P. tremuloides* showed little sensitivity to annual P and cumulative departures from mean P. This was evident in correlations between ring width indices (RWI) and variables above showing inconsistent signs and magnitudes across sites (HSB, HSM) for current year (negative sign), *viz.* year of ring formation, as well as departures from 1 to 3 years (positive) as seen in Fig. 5.3. Only one correlation was statistically discernible: for HSB, RWI increased with previous-year P ($r = 0.42$, 95 %

CI: 0.08 - 0.68).

By contrast, *P. glauca* at both sites showed increased annual growth (i.e. RWI) with larger P as well as mean departures across all years, as inferred from correlations ranging from $r = 0.35$ (HSB, current) to $r = 0.57$ (HSB, 2-year departure) evident in Fig. 5.3. Correlations were stronger with P in years prior ring formation, as well as with departures up to three years. HSB growth dynamics showed marginally stronger positive correlations with P (and derived variables), but were not (statistically) different from HSM (see CIs in Fig. 5.3). A table with full correlation statistics (parameter estimates, p-values, etc.) is found in Tab. 5.S2.

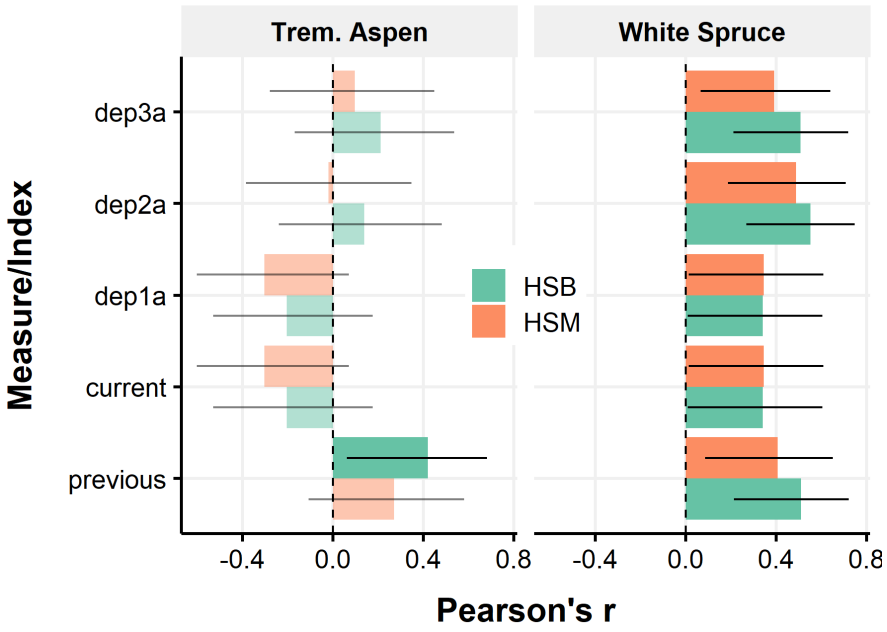

Figure 5.3: Pearson's correlations between ring width indices of both species and sites (HSB, HSM). Short-handles *dep* refer to cumulative departures from mean precipitation for 1 to 3 years. Opaque bars and lines have statiscically discernible correlations at $\alpha < 0.5$; lines are for 95 % CIs.

Analogous to the above, inter- and intra-species comparisons (pooled sites and between sites, respectively; Fig. 5.4) showed greater agreement of RWI dynamics (i.e. annual growth) within species (comparing sites, Fig. 5.4B and Fig. 5.4C): *P. glauca* RWI were more strongly related between sites ($r = 0.76$, 95 % CI: 0.53 - 0.98) than were

P. tremuloides RWI ($r = 0.59$, 95 % CI: 0.28 - 0.9). Further, *P. glauca* showed increased growth (i.e. larger RWI) with with greater water surplus (i.e. larger positive mean departures; see color in Fig. 5.4B, also Fig. 5.3). There was a considerably less pronounced pattern for *P. tremuloides* and the 2-year mean departure, also evident in and analogous to Fig. 5.3. In the inter-species comparison, more negative mean departures featured somewhat higher RWI (i.e. increased annual growth) for *P. tremuloides* in relative terms (pattern in Fig. 5.4A).

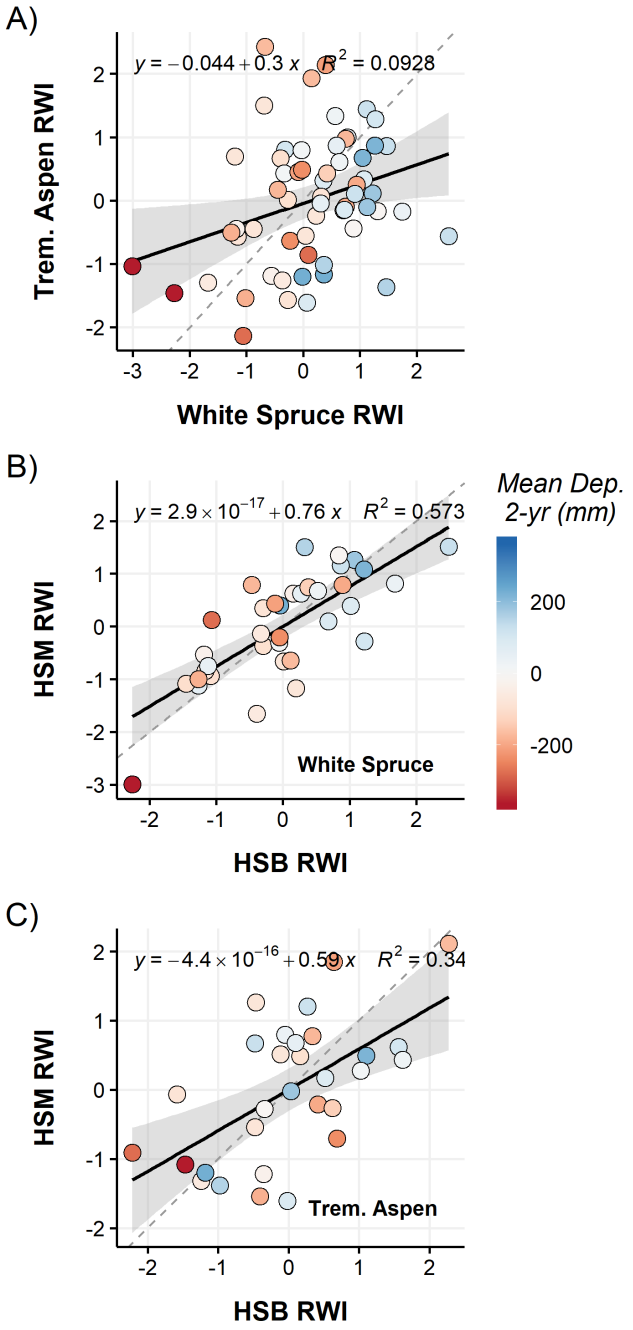

Figure 5.4: OLS relationships between (A) *P. glauca* (White spruce) and *P. tremuloides* (Trembling aspen) chronologies (i.e. ring width indices, RWI) across sites, as well as between sites for each respective species (B, C). RWI were standardized, and slopes hence represent Pearson correlation coefficients. Color is for 2-year, cumulative departure from the 1980-2015 P average. The dashed, gray line represents a 1:1 relationship.

5.4.1.2 Intra-annual time-scale

In line with Fig. 5.3, *P. tremuloides* RWI (i.e. annual growth) did not correlate with windows large enough to approximate annual P for either site. There was some indication of increased RWI with P occurring in the previous hydrological year covering February and April ($r_{HSB} = 0.41$ to $r_{HSM} = 0.47$; Fig. 5.5A and B) in both sites, as well as negative impacts on RWI in relation to P from early May to June ($r_{HSB} = -0.44$, $r_{HSM} = -0.37$).

Annual growth increased with temperatures across shoulder seasons and winter in both sites (Fig. 5.5C and D), evident in positive correlations. Strongest impacts were observed for late March and April P at HSB ($r_{HSB} = 0.59$), as well as of slightly lesser magnitude for periods covering late February to mid-May down to $r_{HSB} = 0.34$, and maximum correlation at HSM of $r_{HSM} = 0.50$ during December (with indications of positive association covering all of winter down to $r_{HSM} = 0.33$). Annual growth decreased with increasing growing season temperatures at both sites. Impacts were temporally more extensive at HSB, evident in correlations ranging from $r_{HSB} = -0.48$ to $r_{HSB} = -0.34$, and somewhat weaker for HSM with $r_{HSM} = -0.41$ to $r_{HSM} = -0.33$. RWI showed analogous patterns with *vpd*, albeit with temporally more extensive negative correlations during the year prior ring formation, with a minimum of $r_{HSB} = -0.55$ and $r_{HSM} = -0.52$ for May, including multiple periods covering the entire growing season for both sites. Increased RWI (i.e. enhanced growth) with higher *vpd* observed for winter time are most likely due to it being a temperature-dominated measure, indicating warmer periods during senescence (e.g. $r_{HSM} = 0.53$ for Nov to Dec).

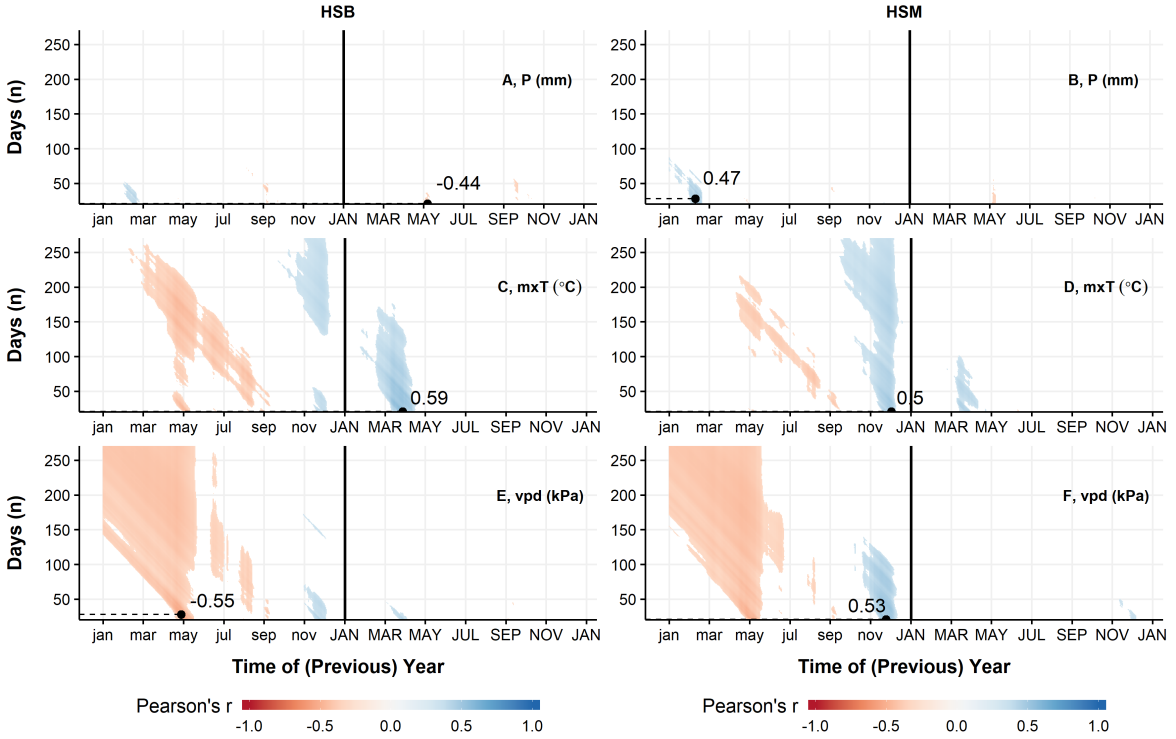

Figure 5.5: Pearson's correlations between ring width indices of *P. tremuloides* and *P, max. temp.* and *vpd* for both sites (HSB, HSM) using running windows of variable length (y-axis) and starting periods (x-axis). Points are highest identified correlation, and only statiscially discernible $\alpha < 0.05$ values are shown.

P. glauca RWI increased with P virtually covering all assessed periods prior the growing season in the ring forming year (Oct - May with $r_{HSB} = 0.65$, Aug - May with $r_{HSM} = 0.59$, Fig. 5.6A and B); there was also indication for these correlations commencing two years prior the ring formation (visual extrapolation), corresponding well with mean-departures in Fig. 5.3. RWI further increased with summer P during the ring forming year, with higher temporal coverage for HSB (Jun - Aug, $r_{HSB} = 0.60$), and to a lesser extent for HSM ($r_{HSM} = 0.40$, Jul). Note, that two minor periods covering May negatively impacted RWI for both HSB and HSM with $r_{HSB} = -0.47$ and $r_{HSM} = -0.36$.

Maximum temperature diminished RWI for both sites during the early growing season (May - Jul, ring forming year), as well as for HSB during the year prior (Fig. 5.5C and D) with $r_{HSB} = -0.42$ to -0.33, and $r_{HSM} = -0.54$ to -0.33. Contrastingly, RWI increased with maximum temperatures during July to Aug in both sites, with highest

correlations of up to $r_{HSB} = 0.46$ and $r_{HSM} = 0.59$.

RWI consistently decreased with *vpd* at both sites, as given by strong and temporally extensive negative correlations. For HSM, high *vpd* was associated with lower RWI across the entire growing season, with the strongest correlation found for late May to early July ($r_{HSM} = -0.64$). Analogous, but less extensive temporally, HSB *P. glauca* was most adversely affected by high *vpd* May through June ($r_{HSB} = -045$ to -0.33). In addition, high *vpd* during the growing season in the year prior ring formation showed strong, negative impacts on RWI across July ($r_{HSB} = -0.55$).

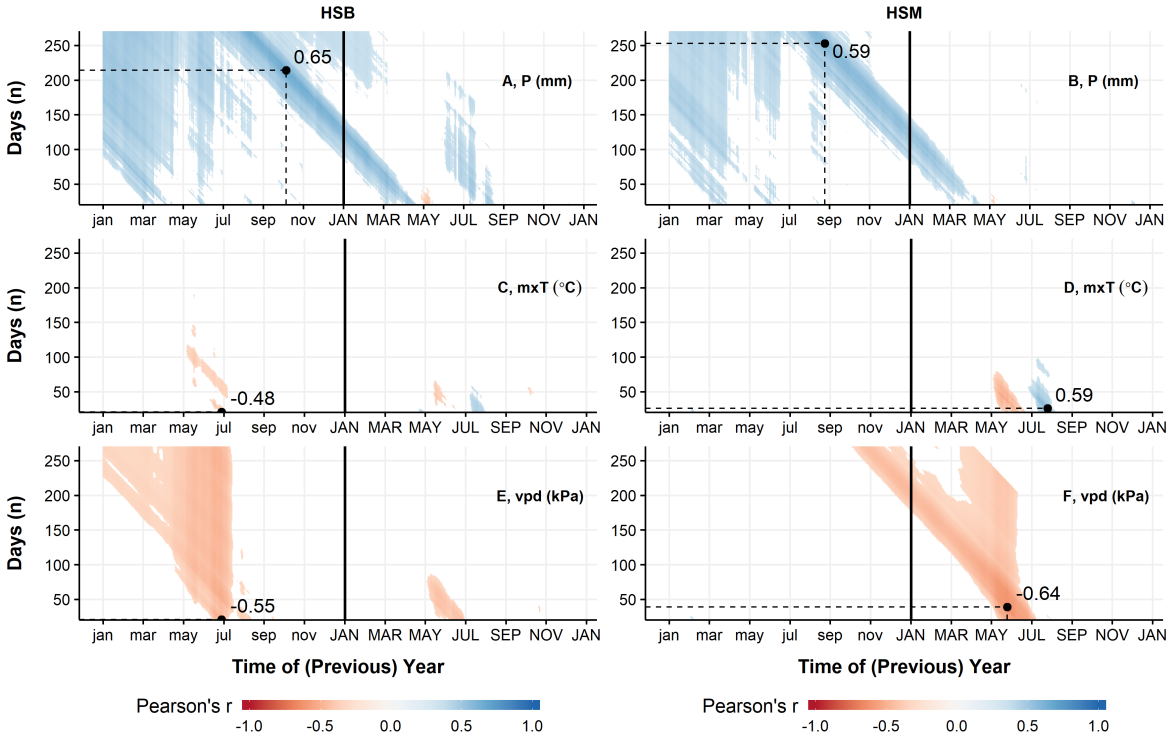

Figure 5.6: Pearson's correlations between ring width indices of *P. glauca* and *P, max. temp.* and *vpd* for both sites (HSB, HSM) using running windows of variable length (y-axis) and starting periods (x-axis). Points are highest identified correlation, and only statiscially discernible $\alpha < 0.05$ values are shown.

5.4.2 Lumen diameter and climate dynamics

5.4.2.1 Inter-annual time-scale

Lumen radial diameters of *P. glauca* were larger with greater current as well as previous-year P and cumulative mean P departures across earlywood and latewood sectors (Fig. 5.7). Patterns differed considerably between sites and wood type (early- *vs.* latewood): Relationships between P (and mean departures) and earlywood lumen diameters HSB were only discernible from zero for previous, as well as the 2-year mean departure (Fig. 5.7A) in the first portion of the annual ring (positions 76 - 100). Contrastingly, lumen diameters for HSM increased with with previous-year P as well as 2-year departures from section 76-51 onwards toward the earlywood-latewood boundary (and beyond; see Fig. 5.7B) with increasing magnitude for the 2-year departure, which was highest for 0-25, with $r = 0.53$ (95 % CI: 0.19 - 0.75). Only the lumen diameters in later earlywood portions of HSM were positively impacted by current-year P.

Latewood featured qualitatively and quantitatively similar patterns for HSM, with slightly stronger increases in lumen diameter in relation to previous year P, with the addition of a positive correlation (i.e. diameter increase) with the 3-year cumulative departure. Neither the latter two latewood sections of HSM, nor any HSB sectors, showed any influence of P on lumen diameters.

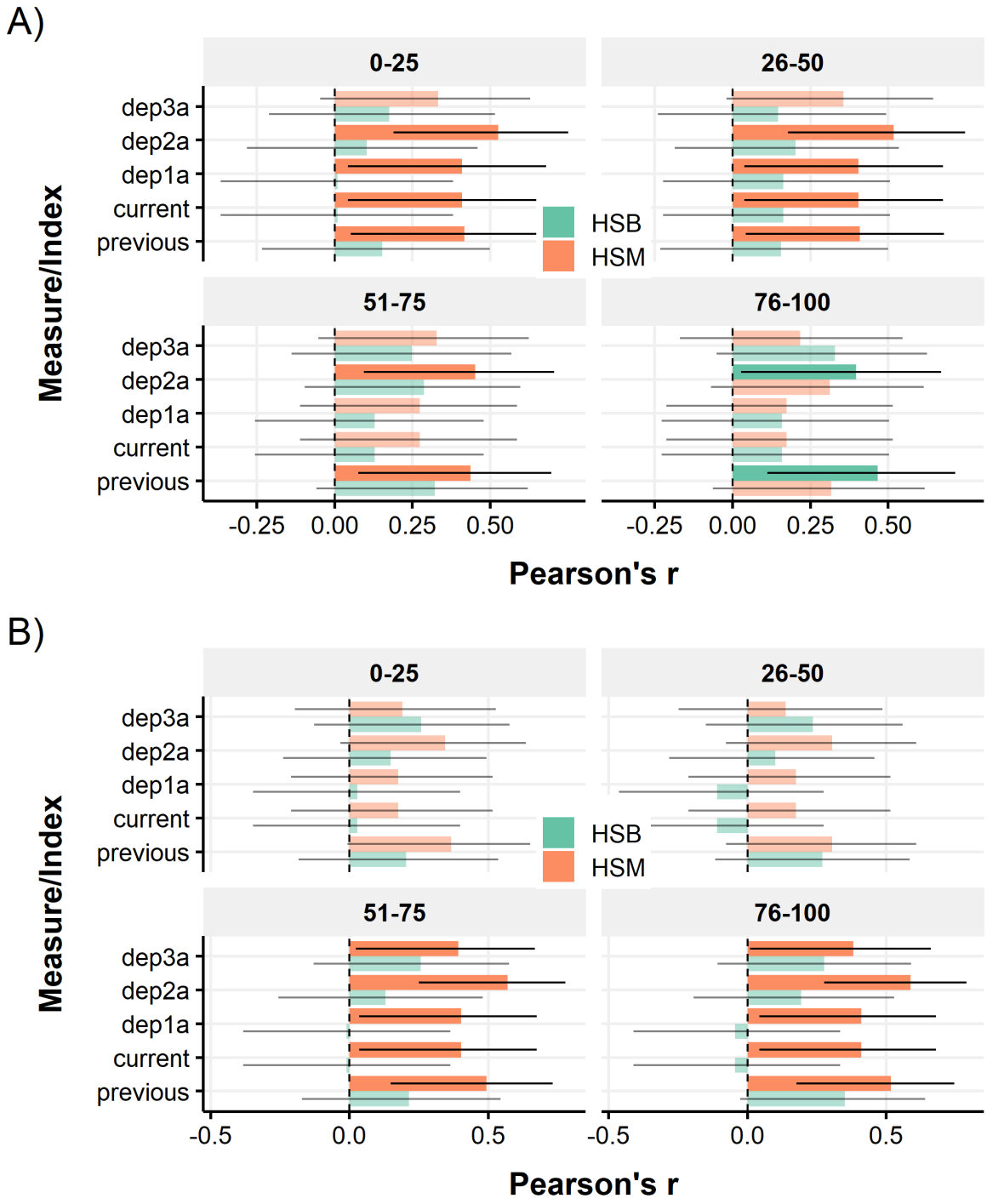

Figure 5.7: Pearson's correlation coefficients between standardized and averaged percentile positions of *P. glauca* for early (A) and latewood (B) at sites HSB and HSM. Short-handles *dep* refer to cumulative departures from mean precipitation for 1 to 3 years. Opaque bars and lines have statiscically discernible correlations at $\alpha < 0.5$; lines are for 95 % CIs.

A comparison between indices based on individual position percentiles between sites for *P. glauca* showed highest agreement (i.e. regression slopes on scaled data equivalent

to Pearson's correlation coefficients) for the 90^{th} ($r = 0.38$), as well as for the 65^{th} to 30^{th} percentiles, with ranges of $r = 0.38$ to 0.52, (Fig. 5.8A-D). Selected percentiles with high agreement in Fig. 5.8B and C showed more negative 2-year mean departures at higher index values for HSB (i.e. to the right of 1:1 line).

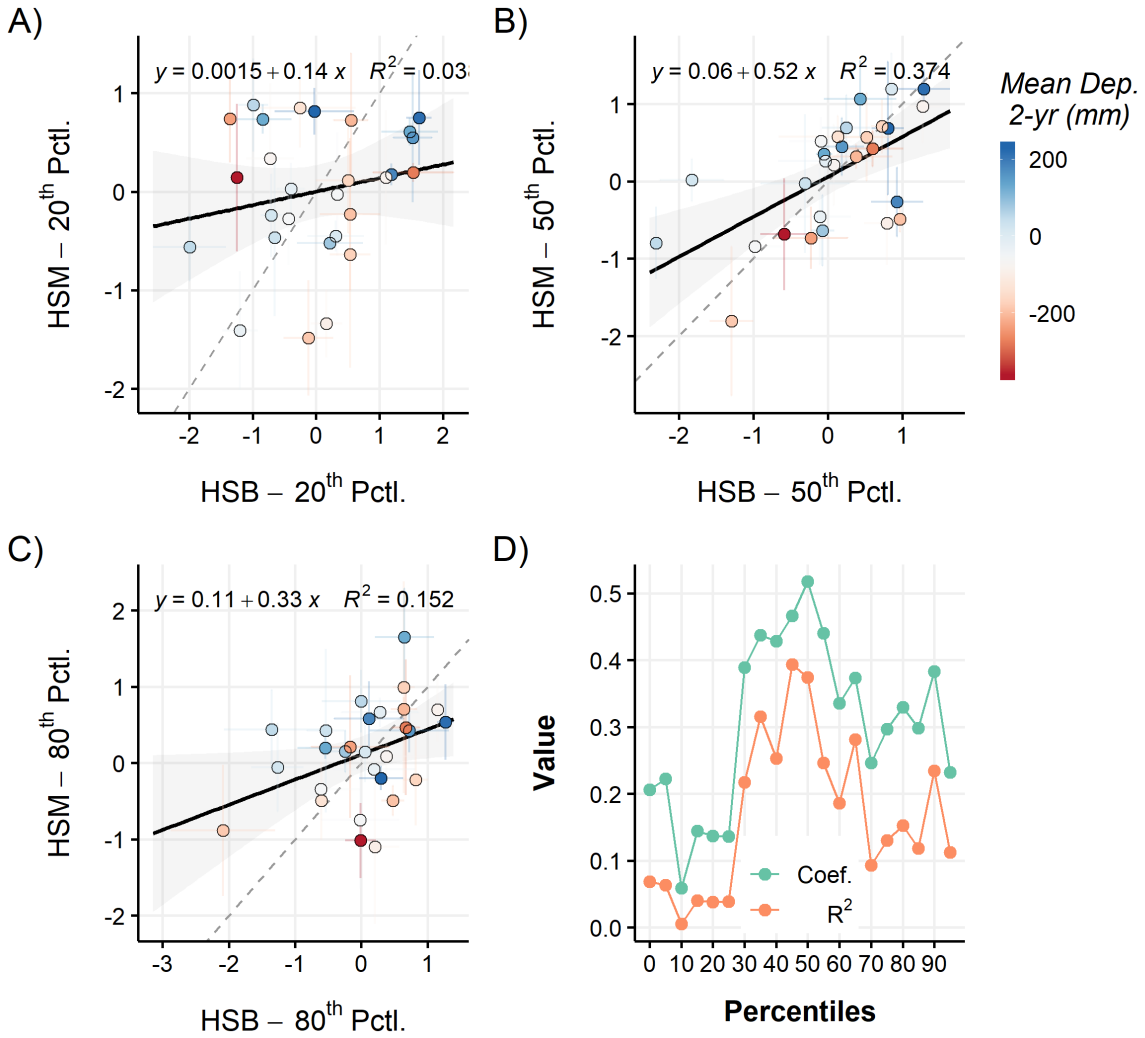

Figure 5.8: Similarity of lumen radial diameter across percentile positions between sites (HSB, HSM) for *P. glauca* based on OLS relationships. Panels A to C show exemplary relative positions (percentiles 20, 50 and 80) as well as OLS equations and coefficient of determination. Panel D features an overview across all positions with values corresponding to the OLS slopes ('Coef.') and respective R^2. Slopes represent Pearson's correlation coefficients, as the data was mean-centered and scaled to units of standard deviations. The dashed, gray line represents a 1:1 relationship. Note that, on average, moving along an annual ring (right to left, Panel D), lumen diameters become more similar toward central positions (e.g. 50, panel B), and are most dissimilar toward their senescence period (position 0).

5.4.2.2 Intra-annual time-scale

Magnitudes of correlations between P (summed over variable windows) and averaged sectors (based on relative position percentiles) of *P. glauca* are similar to those found for annual totals and mean P departures P (Fig. 5.9), as well as for RWI and running-window correlations (Fig. 5.6. The individual sectors, however, show considerably different patterns between sites, providing a more comprehensive and functionally-resolved image of xylogenesis through a given year. Individual sectors of HSB correlate less comprehensively and weaker than RWI, although indicating similar timing of positive association. Most notably, the first earlywood sector shows fairly extensive, yet diffuse, positive association between P during the previous winter (i.e. one year prior), the previous growing season, and the entire preceding autumn and winter (Fig. 5.6A), ranging from $r_{HSB} = 0.37$ to 0.48, which agrees with Fig. 5.7A; the highest observed correlation with $r_{HSB} = 0.49$ is for a window covering mid-August to September. For HSM, patterns indicate a positive association with previous-year P, as observed in Fig. 5.7A, with diffuse patterns and $r_{HSM} = 0.37$ to 0.47, similar to HSB. In the successive sectors, HSB displays far less-pronounced association (in time, as well as magnitude), than HSM, where correlations with P virtually cover the entire preceding year, the winter prior ring formation, as well as the early part of the growing season and range between $r_{HSM} = 0.37$ in all sectors to 0.56 in the middle to latter half of earlywood. There is some indication of a positive association during the early growing season (May - Jun) for HSB, of up to $r_{HSB} = 0.52$ for the sectors covering the 75^{th} to 26^{ts} percentile, as well as during the preceding year ($r_{HSB} = 0.37$ to 0.48 across both). The negative correlations beyond September are likely spurious, as the dominant process during the late phase of the growing season is likely lignification, rather than cell enlargement (leading to greater radial diameters).

Latewood correlations across HSB and HSM sectors are similar qualitatively, yet somewhat higher and more extensive temporally during the period of ring-formation

(Fig. 5.10). For HSM, the strongest association in the first latewood sector is with P occurring between January and August ($r_{HSM} = 0.52$), while additionally, positive correlations extending well into the growing season, covering May - Aug, were found also ($r_{HSM} = 0.37$ to 0.50). In the following sectors, associations were found increasingly limited to the previous growing season. For HSB, positive association was found in the spring immediately preceding ring formation, as well as during the previous growing season, ranging from $r_{HSB} = 0.37$ to 0.5. Additionally, a negative correlation persists through all latewood sectors at HSB, ranging from $r_{HSB} = -0.51$ to -0.44.

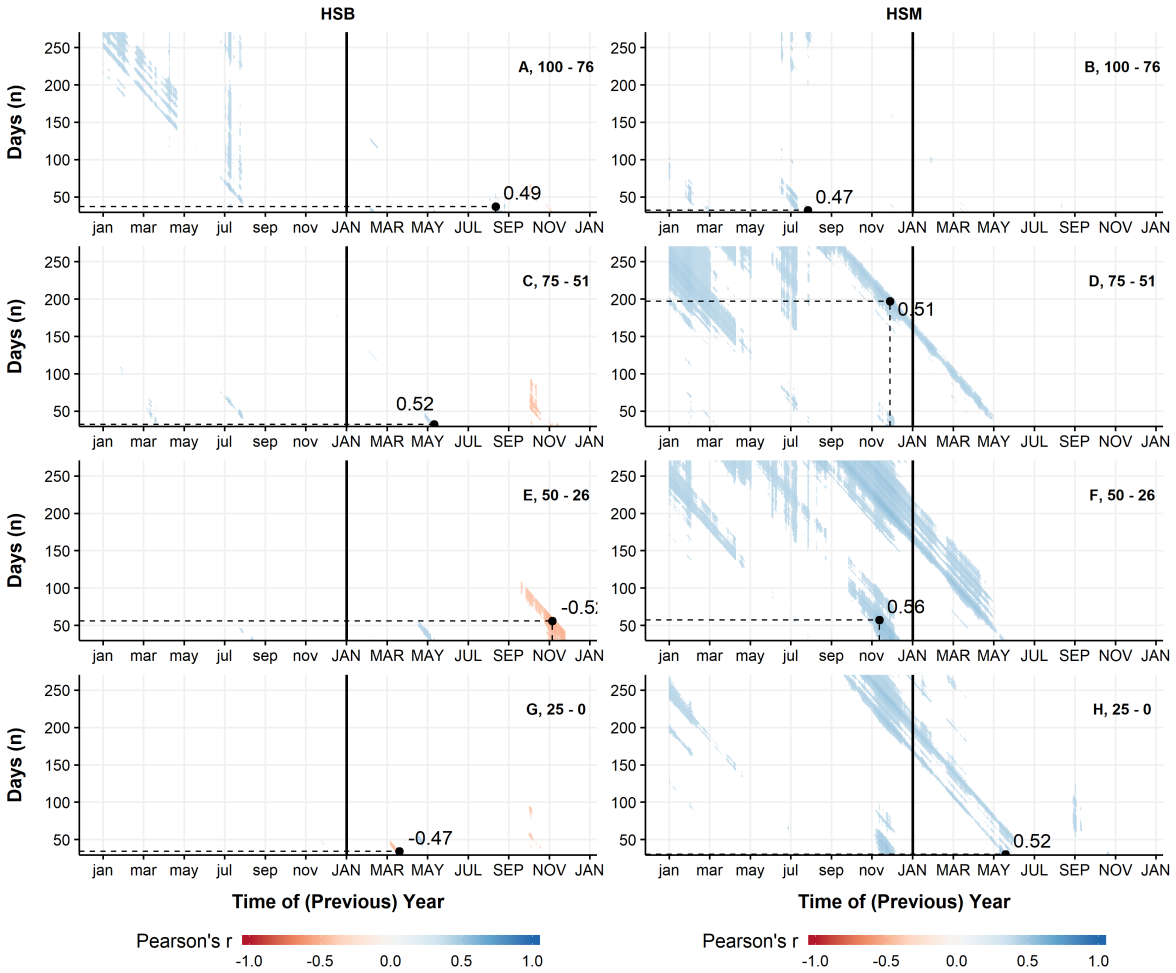

Figure 5.9: Pearson's correlations between earlywood lumen diameter averaged over relative positions of *P. glauca* and daily P in both sites (HSB, HSM) for running windows of variable length (y-axis) and starting periods (x-axis). Points are highest identified correlation, and only statiscially discernible $\alpha < 0.05$ values are shown.

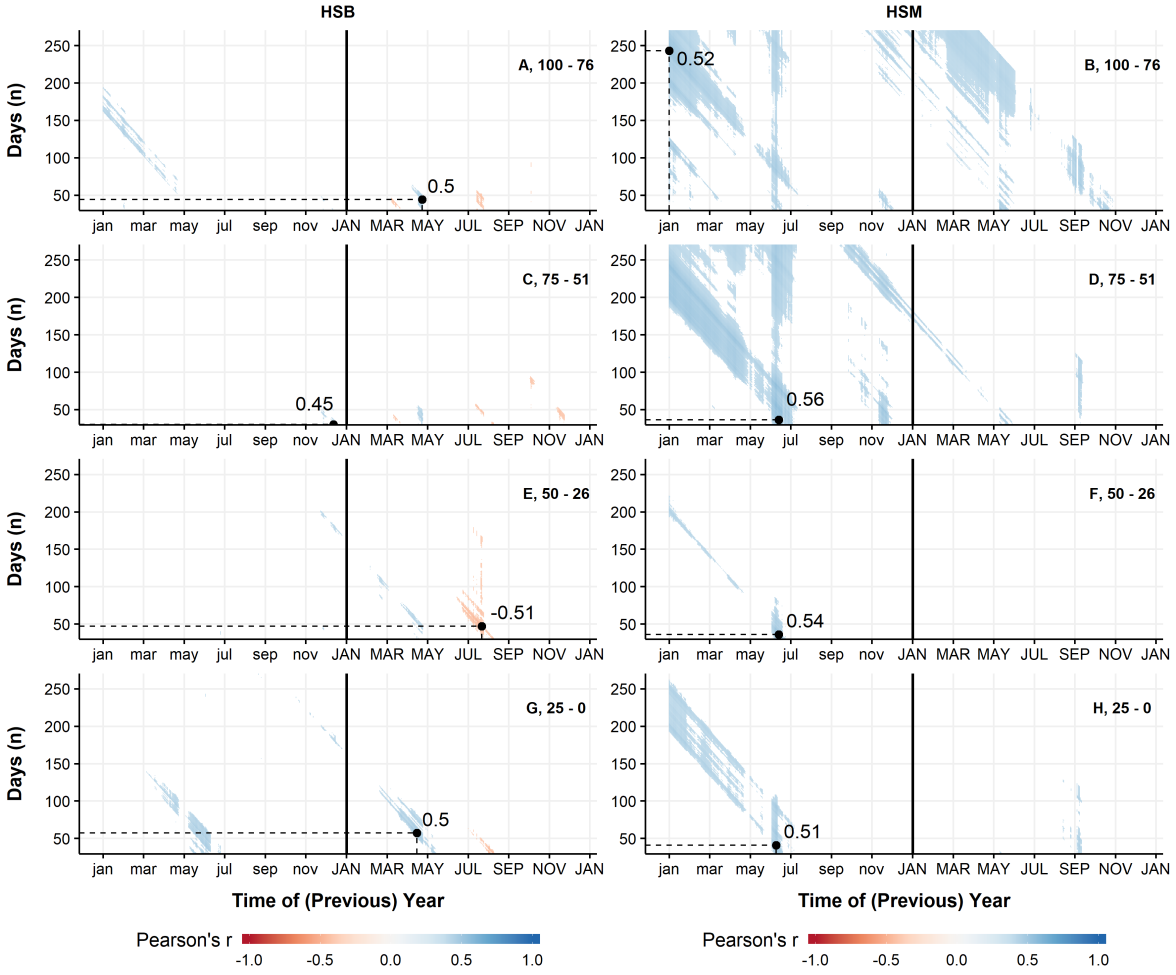

Figure 5.10: Pearson's correlations between latewood lumen diameter averaged over relative positions of *P. glauca* and daily P in both sites (HSB, HSM) for running windows of variable length (y-axis) and starting periods (x-axis). Points are highest identified correlation, and only statiscially discernible $\alpha < 0.05$ values are shown.

Additional running-window analyses for lumen diameter chronologies are found in the supplemental information, and drawn upon for discussion and contextualizing results further. See Fig. 5.S11 and Fig. 5.S12 for correlations with *vpd* of earlywood and latewood, respectively.

5.5 Discussion

This work constitutes, according to surveyed literature, the first to study the effect of hydrological position along a Boreal Plain hillslope with intermittent water supplementation by a forested swamp with an ephemeral hydrological regime on tree growth dynamics. Climate-growth relationships observed here agreed well with previous research on moisture-limited areas for *P. glauca*, while for *P. tremuloides* they showed intriguing divergence regarding precipitation (P), and good agreement for atmospheric controls. Site-specific differences for *P. glauca*, that could be related to hydrological position, were most evident when combining ring width with wood anatomy, indicating plasticity in hydraulic architecture between sites.

5.5.1 Climate-growth relationships and intra-specific differences

Climate-growth relationships with P sums on intra and inter-annual scales differed dramatically between species, and considerably between sites for *P. glauca*. *P. tremuloides* showed a remarkably low or even lack of sensitivity to P, warranting a separate section to discuss mechanisms that could account for the observed pattern (see Section 5.5.2).

P. glauca showed strikingly strong, positive correlations for annual growth increment with P totals on annual basis and cumulative mean departures, as well as for running-windows covering the immediately preceding winter and early spring ($r = 0.59 - 0.64$), which in all cases exceeded correlations for current-year P (totals, moving window) alone at both sites. The dependence on previous over current-year P dynamics is frequently found for *P. glauca* in a variety of moisture-limited regions such as the BP, ranging from interior Alaska, to southern Manitoba (Barber *et al.*, 2000; Chhin *et al.*, 2004b; Lloyd *et al.*, 2013), and moisture in general is reportedly one of the

dominant controls on tree productivity across Boreal Canada (Girardin *et al.*, 2016). Results further agree with broader assessments and understanding of forest ecosystems in the BP ecoregion (Hogg and Bernier, 2005; Price *et al.*, 2013). Additionally, in line with the studies mentioned above, the coincident negative correlation with spring and early summer temperatures of year(s) prior ring formation, indicates that trees at both sites were likely subject to heat-induced drought stress. These lagged responses on wood formation are common for many conifers, such as *P. glauca*, with evergreen canopies, where the amount of stored, non-structural carbohydrates in the previous growing season predetermines, to a large extent, the annual increment of the current year (Kozlowski and Pallardy, 1996).

Extensive vadose zone storage (i.e. soil moisture deficits) develops frequently in the BP resulting from interactions of climate, vegetation and soil texture (Devito *et al.*, 2005a; Ireson *et al.*, 2015) and can largely explain site-specific differences for *P. glauca* with a shallow, and spatially-limited root network (compared to *P. tremuloides*; Strong and Roi, 1983). Where storage capacity is large it can take multiple surplus years (i.e. positive mean departure or $P > pET$) for deficits to be replenished and/or to effect hydrological responses (Redding and Devito, 2008; Carrera-Hernández *et al.*, 2011; Smith and Redding, 2012). The wetland-upland hillslope continuum is underlain by a surface-near, low-permeability clay layer, rapidly reducing storage from the hillslope middle to its base (see Fig. 5.S14); this shallow storage causes frequent saturation in the wetland and flows toward the hillslope base. Hence, under equal P input, the hillslope base would frequently gain greater access to water across growing seasons, producing more positive ring width indices in relation to current-year P, as well as for totals and mean departures. Contrastingly, when soil moisture deficits are large up the hillslope, water availability during the growing season of the ring-forming year would be limited to atmospheric inputs alone, and stronger ring-width signals consequently would require greater (cumulative) P compared to the hillslope base.

The proposed, differential sensitivity to P is further expressed in the hydraulic architecture of *P. glauca*, showing less sensitivity of lumen radial diameter to water availability at the hillslope bottom. There, only the first quarter of earlywood showed sensitivity to P (previous year, 2-year mean departure, running windows), while, contrastingly, most earlywood (excluding first quarter) and all latewood sectors showed expressed signals in all correlation methods, with increasing strength toward later sectors, as well as increasing temporal coverage in running-windows. This is conceptually in line with discussion above if considering the hydrological position, as well as contrasting storage and access to water, and also agrees with wood formation theory: the water transporting system (i.e. tracheids) would establish itself to maximize transport from the roots to canopy, while minimizing the risk of xylem cavitation (Sperry *et al.*, 2006). Down or upscaling lumen diameter would be less required for hillslope base trees assuming groundwater supplementation, and hence frequently favorable conditions. Contrastingly, trees growing further along the hillslope would encounter conditions where soils accumulate water deficit across years, and hence allowing for higher sensitivity when developing water transporting cells would balance risks and benefits inherent in a more drought prone location, where soil water potentials become increasingly negative. This would also explain the stronger response of radial growth to *vpd* (i.e. down regulation of transpiration limiting excessive water loss and xylem cavitation) for the hillslope middle (Fig. 5.6F), as well as to sensitivity to *vpd* in later ring sectors when the larger hillslope storage becomes more depleted across the growing season (Fig. 5.S11). This assumption is further corroborated by consistently greater variance of lumen diameters for hillslope trees (see supporting information; Fig. 5.S13). An indication for this is further provided by comparing relative percentile positions directly (Fig. 5.8), where differences (i.e. low correlations) are strongest in the first and latest sections, representing early and late stages of the growing season, when the hillslope base would be wettest and the middle driest, respectively. During xylogenesis, the size of a tracheid is determined in the cell enlargement phase, which can be affected by

the availability of water to fill cells' cytoplasm (Cosgrove, 2005). High moisture variability across and within years therefore can affect the expression of plant and xylem traits relating to water transport, as well as drought (and frost) tolerance, and can lead to consistently larger vessels entailing higher hydraulic efficiency where moisture is abundant (von Arx *et al.*, 2012). A wet climate period from around the mid-1980s to mid-1990s (see Fig. 5.2) coincided with consistently larger radial diameters for the hillslope base (Fig. 5.S6). However, a potential growth release for *P. glauca* in the hillslope bottom from around 1980 to 2000, possibly due to a coincident aspen growth collapse following repeated defoliation and drought events between 1979 to 1983 (Hogg *et al.*, 2002), confounds direct comparisons of raw diameters. The detrending methods applied for the lumen diameter series, however, preserved high frequency variability (i.e. year-to-year), which gives higher confidence in the observed correlations and the dynamics argued to be operating here.

5.5.2 *P. tremuloides* growth dynamics and insensitivity to P

Direct comparison between both species indicates that aspen may fair better under dryer conditions (i.e. higher ring width indices during drier periods, see. Fig. 5.4A). The pervasive absence of P sensitivity for *P. tremuloides*, except for the interface site at the hillslope base (HSB), is striking, and largely contrasting previous work on aspen in the wider area (e.g., Hogg and Bernier, 2005). For example, Hogg *et al.* (2005) report that moisture deficit in a given year adversely affected radial increment, and lead to notably decreased growth for up to four successive years after excessive deficits. Similarly, Hogg *et al.* (2013) and Girardin *et al.* (2016) report aspen productivity closely tracking soil moisture dynamics on local and regional scales, respectively. By contrast, the only correlation found statistically different from zero was for previous-year P in the interface site. One possible explanation accounting for this may be provided by the mechanism of hydraulic redistribution, where root networks access water at one location

(or depth), and release it at another. In the case of *P. tremuloides*, the extensive root networks that develop through clonal growth (suckering) can provide individual stems with water from comparatively large distances (Snedden, 2013a). These networks can span from wetter areas, such as wetlands and/or their margins, up and along hillslopes (DesRochers and Lieffers, 2001). The deeper and larger root network, as compared to *P. glauca*'s shallow system, may allow for more extensive foraging (Strong and Roi, 1983) and, possibly, sustained supply on the hillslope. Indications for this have been given previously by Brown *et al.* (2014b) and Petrone *et al.* (2014), where soil moisture dynamics, as well as sustained transpiration indicated supply from (adjacent), wetter source areas, and via a direct assessment of *P. tremuloides* water sources along a hillslope (Depante *et al.*, 2019).

Research focusing on inferring long-term climate-growth relationships (e.g. Girardin *et al.*, 2016) would preferentially sample stands in which additional factors, such as hydrological position and/or edge effects, would likely be considered confounding and therefore avoided. Additionally, the spatial variability of water availability at small scales throughout the mixed-wood stand, driven by contrasting canopy phenology, may further aid in explaining the observed inter-specific differences (i.e. precipitation sensitivity). Throughfall and stemflow is considerably higher for deciduous-broad-leaf trees, as compared to coniferous species (Barbier *et al.*, 2009), with epiphytic cover on conifers causing even higher water retention (e.g. Pypker *et al.*, 2006). This may imply greater resources per unit area for *P. tremuloides*, enhanced by a greater "pedological" niche for soil water foraging due to its larger and deeper root network with lateral extents of up to 40 m (Jobling, 1990; Snedden, 2013b). If indeed a lateral redistribution mechanism is operating in addition, differences in precipitation sensitivity would be enhanced by the aforementioned dynamics.

Another possible explanation is that the indices applied in the work noted above (Hogg *et al.*, 2013; Girardin *et al.*, 2016) relied on climatic or soil water balances,

contrasting supply with demand (e.g. $P-pET$). Here, annual totals, as well as (cumulative) departures from long-term mean P were applied, of which the latter shows good agreement with landscape-scale hydrological dynamics (Hokanson *et al.*, 2018a), which may be a less suited indicator due to ecophysiological dynamics of *P. tremuloides*. *P. tremuloides* can regulate stomatal aperture, and therefore water loss, across a broad range of atmospheric demand (*vpd*; Hogg and Hurdle, 1997), with maximum daily transpiration rates being sensitive to pre-dawn *vpd* (Brown *et al.*, 2014b). Further, due to decreased rates of photosynthesis on hot days with high *vpd*, transpiration is down-regulated even during adequate supply of soil moisture (Dang *et al.*, 1997; Hogg *et al.*, 2000); this ensures the maintenance of adequate hydraulic potential from roots to the canopy, preventing cavitation of xylem conduits (Sperry *et al.*, 1998).

The applied P measures may indeed be less suitable for detecting water-related growth signals, as the coincidental strong and negative association of annual increment with *max.temp.* and *vpd* during the year prior ring formation do indicate down regulation of transpiration and hence productivity as discussed above (Dang *et al.*, 1997). In this case, autotrophic respiration may have exceeded the rate at which non-structural carbohydrates were stored, limiting and/or depleting what would be drawn upon for the succeeding year's growth (McDowell *et al.*, 2011). Re-analyses with other derived measures of water availability would shed additional light on effects of hydrological position, and warrants further pursuit for this site setting. However, correlations indicated that individuals at the hillslope base may show higher P sensitivity, which - as for *P. glauca* - could indicate greater positive influence of P due to wetland supplementation. Sample size and detrending method may also have masked responses (e.g. Peters *et al.*, 2015); however, chronology statistics were well within the range of typical dendroclimatological analyses (Fig. 5.S3), and indicated high signal-to-noise ratios, i.e. indicating sensitivity to climate (Tab. 5.S1). Employing wood anatomical analyses on vessel (i.e. water conduit) distribution and size may shed additional light here.

While climate-growth responses of *P. tremuloides* were similar between HSM and HSB, it is noteworthy that demographics differed considerably: interface (HSB) trees were recruited more recently (approximately past 30 to 60 years ago) and had lower maximum age over-all, as indicated by ring-width series (see Fig. 5.S1; trend also visually apparent on-site with size distribution as age proxy). This discrepancy may result from general stand dynamics (i.e. random stand demographics resulting in pattern), but other mechanisms could play a role. Disturbances that alter the hydrological regime (e.g. roads, drainage) of wetland-upland margins have been shown to affect vegetation community composition, turn-over and susceptibility to subsequent disturbance (Bauer *et al.*, 2009; Bocking *et al.*, 2017; Wilkinson *et al.*, 2018). An access road, cutting through the southern-end of the swamp reduced its effective water source area to a small extent, potentially leading to drier conditions further downgradient. This may have allowed *P. tremuloides* individuals to recruit closer to the swamp's edge of the ecotone due to its extensive lateral root network (Snedden, 2013b). While the exact construction date of the road is not know, it is likely that it has been expanded and reinforced with increased exploitation of natural resources (timber, oil, gas) in the area since the 1970's (personal communication), and may explain the observed age difference. However, conditions in the wetland-upland ecotone *per se* could also potentially cause higher individual turn-over rates by increasing the susceptibility to secondary stressors (i.e. linear disturbance not important driver of demographics). For example, extended saturated conditions during wet climate cycles (Mwale *et al.*, 2009) may weaken the rooting network and consequently structural integrity, increasing the likelihood of windthrow (e.g. Sanderson and Armstrong, 1978).

5.5.3 Landscape ecohydrological implications

Evidently, the direction and magnitude of growth modulation differs along wetland-upland hillslope continua, ranging from impedance through low soil temperature and

extended wet-periods on one end (e.g. Dang and Lieffers, 1989a, 1989b), to increasingly positive, but spatially limited, effects as one moves along the wetland-upland ecotone as indicated here. Further indications of this may also be inferred by an arguably deterministic expression of "lagg" ecotones along the interfaces of permanent wetlands (i.e. peatlands; Paradis *et al.*, 2015), as well as increased upland tree water use along drainage gradients (Loranty *et al.*, 2008; Angstmann *et al.*, 2012), and the previously discussed hydraulic redistribution (Depante *et al.*, 2019). In light of this, two interesting implications for BP landscapes are worth noting:

1) Storage contrasts, such as between the swamp and the adjacent hillslope do not only drive hydrological responses on regional scales (Devito *et al.*, 2005a, 2017), but also ecohydrological interactions at small scales. It is hence likely that low-storage, precipitation-fed systems (i.e. non-reliant on or disconnect from groundwater) would continue to display their current function under drier and warmer conditions predicted for the future (Price *et al.*, 2013), albeit at different spatial scales and magnitudes. Ultimately, this could entail altered interface vegetation communities in the future. However, given recent and future heat-induced drought stress and (predicted) pervasive mortality for trembling aspen (Hogg and Bernier, 2005; Michaelian *et al.*, 2011), the wetland water supplementation along its interface may act as thermal buffer (due to lower soil temperatures), and also provide conditions moist enough for continued white spruce reestablishment (following disturbance) (Hogg and Wein, 2005). Assessing growth-modulation across a range of wetland-upland physiographical settings and corresponding hydro-regimes could provide insight on how water source and sink functions may develop in the future; this is particularly important in areas that typically produce low runoff, but where downstream systems (e.g. terminal ponds) are highly dependent on intermittent flows.

2) If indeed hydraulic redistribution is driving the low or lack of P sensitivity for P.

tremuloides, other (clonal) aspen stems as well as sub-canopy and canopy species in the upland are likely to benefit to some extent, e.g. as argued by Brown *et al.* (2014b) for the maintenance of evapotranspiration rates from forest-floor communities in aspen forests. However, as mixed-wood stands mature, *P. tremuloides* is typically replaced by *P. glauca* in a gradual process due to episodic mortality, stem decay and a mixture of increasing shading and potentially decreasing soil temperatures (see Lieffers *et al.*, 2001 for detailed explanation). Hence, positive effects provided by hydraulic redistribution may diminish over time. Future warming and drying (Price *et al.*, 2013) may impede the establishment of *P. glauca*, and therefore assessing the extent and rate at which stands located in different hydrological settings undergo successional shifts may provide an interesting avenue of further work.

5.6 Conclusion

The assessed climate-growth relationships revealed stark differences between *P. glauca* and *P. tremuloides*, indicating that the latter may be less water limited in both the hillslope base and hillslope middle, and hence perform better under current climate in this setting. Modulating effects relatable to hydrological position and water supplementation were more strongly indicated for *P. glauca*, and were only fully revealed by considering running-windows (higher temporal resolution of climate vs. growth) and individual tree ring sectors representative of growth in distinct periods across a given growing season. This highlights the usefulness of including multiple proxies (Ziaco *et al.*, 2016), such as lumen radial diameter, to detect effects across small spatial or environmental gradients that are typically not considered sufficiently steep for dendroecological analyses (Fritts and Swetnam, 1989).

Wetland-upland interactions, as indicated and proposed here, may locally act as

moisture (and consequently thermal) buffers in the BP under future warming and drying (Price *et al.*, 2013), and hence maintain water source and sink dynamics (Devito *et al.*, 2017) similar to current conditions for longer. Additional work should focus on increasing the confidence in proposed wetland-upland ecohydrological interactions by identifying tree water sources, potential differences in nutrient availability and due to age-specific climate responses, increasing sample sizes and application of variance-partitioning methods that can provide further insight in the relative importance of pertinent climate factors (e.g. Lloyd *et al.*, 2013). Including wood-anatomical analyses of *P. tremuloides* across hydrological positions and physiographical settings also provide an exciting avenue of future work, especially in light of stand dynamics in the past and under future conditions, including competition for resources and space (Cortini *et al.*, 2012).

5.7 Supplemental Material

5.7.1 Figures

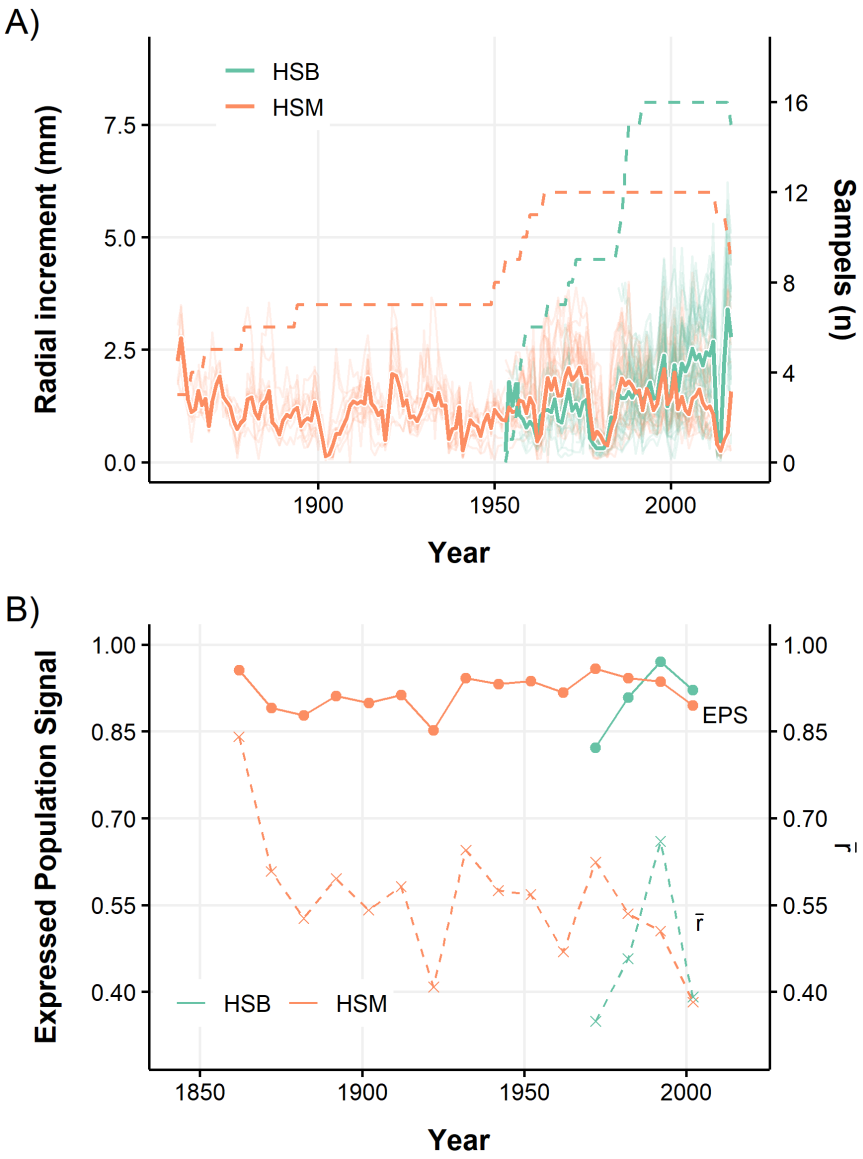

Figure 5.S1: A) Raw tree and averaged (thick line) site series for *P. tremuloides*, as well as sample depths (dashed lines), and B) corresponding chronology statistics.

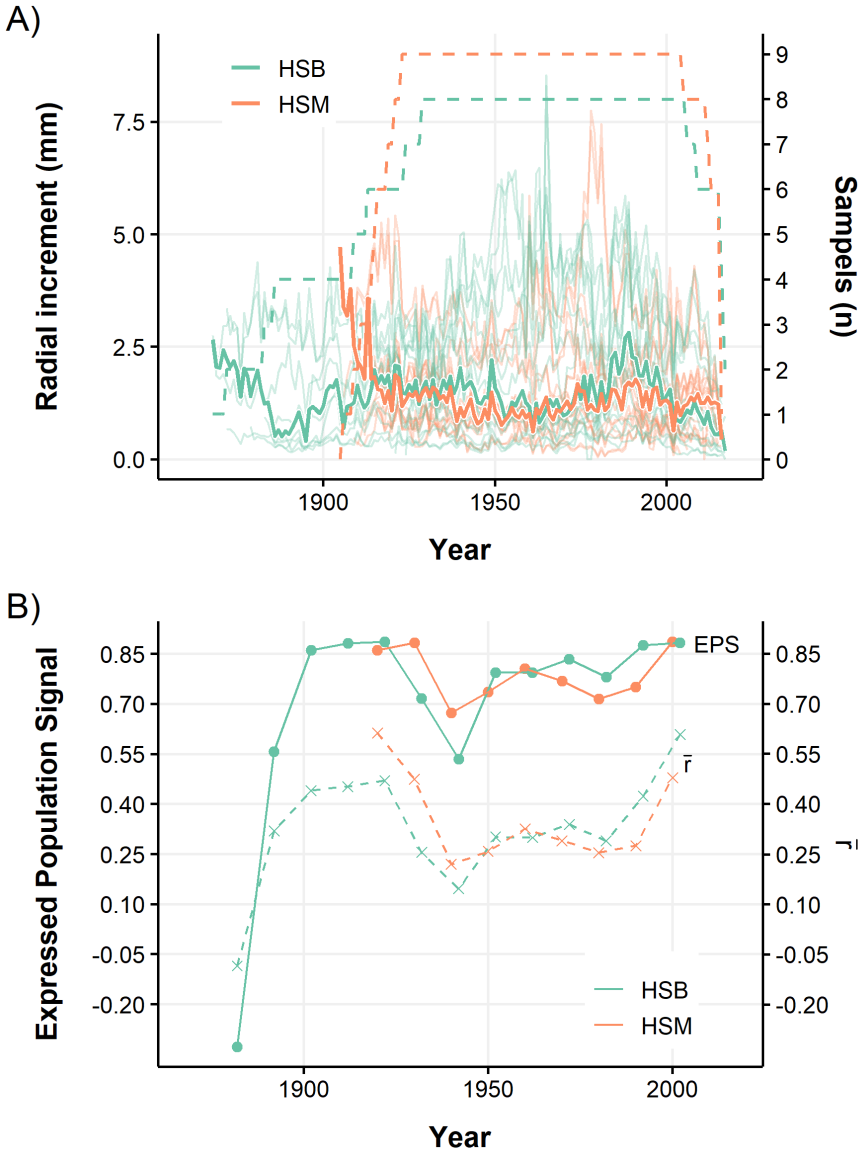

Figure 5.S2: A) Raw tree and averaged (thick line) site series for *P. glauca*, as well as sample depths (dashed lines), and B) corresponding chronology statistics.

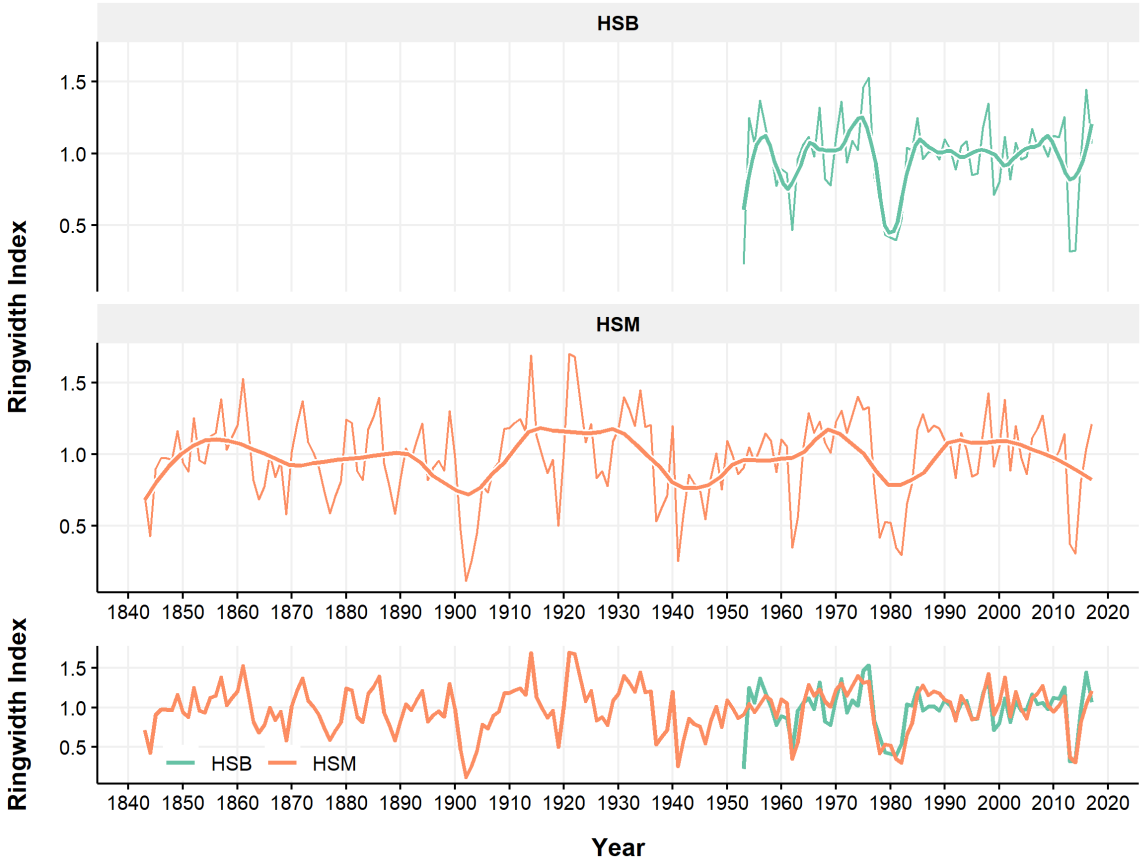

Figure 5.S3: Standardized chronologies for *P. tremuloides*. A) and B) show the ring width indices for for HSB and HSM, respectively, with fitted cubic splines visualizing longer-term trends. C) is for direct comparison between sites; note the strong agreement during known insect infestations (Hogg *et al.*, 2002) , e.g. in 1961 and 1981, as well as the shorter chronology for HSB.

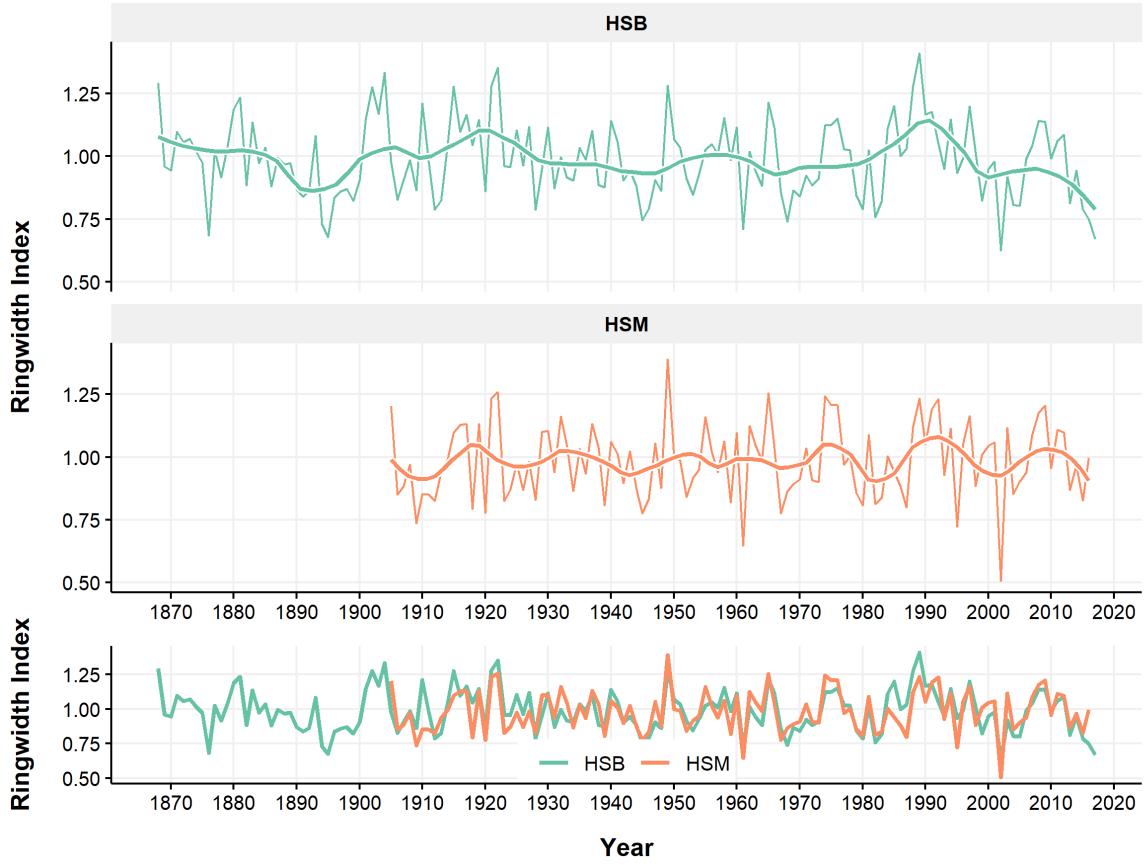

Figure 5.S4: Standardized chronologies for *P. glauca*. A) and B) show the ring width indices for HSB and HSM, respectively, with fitted cubic splines visualizing longer-term trends. C) is for direct comparison between sites; note the strong agreement of pattern for poor growth years, e.g. in 1961 and 2002, but difference in magnitude.

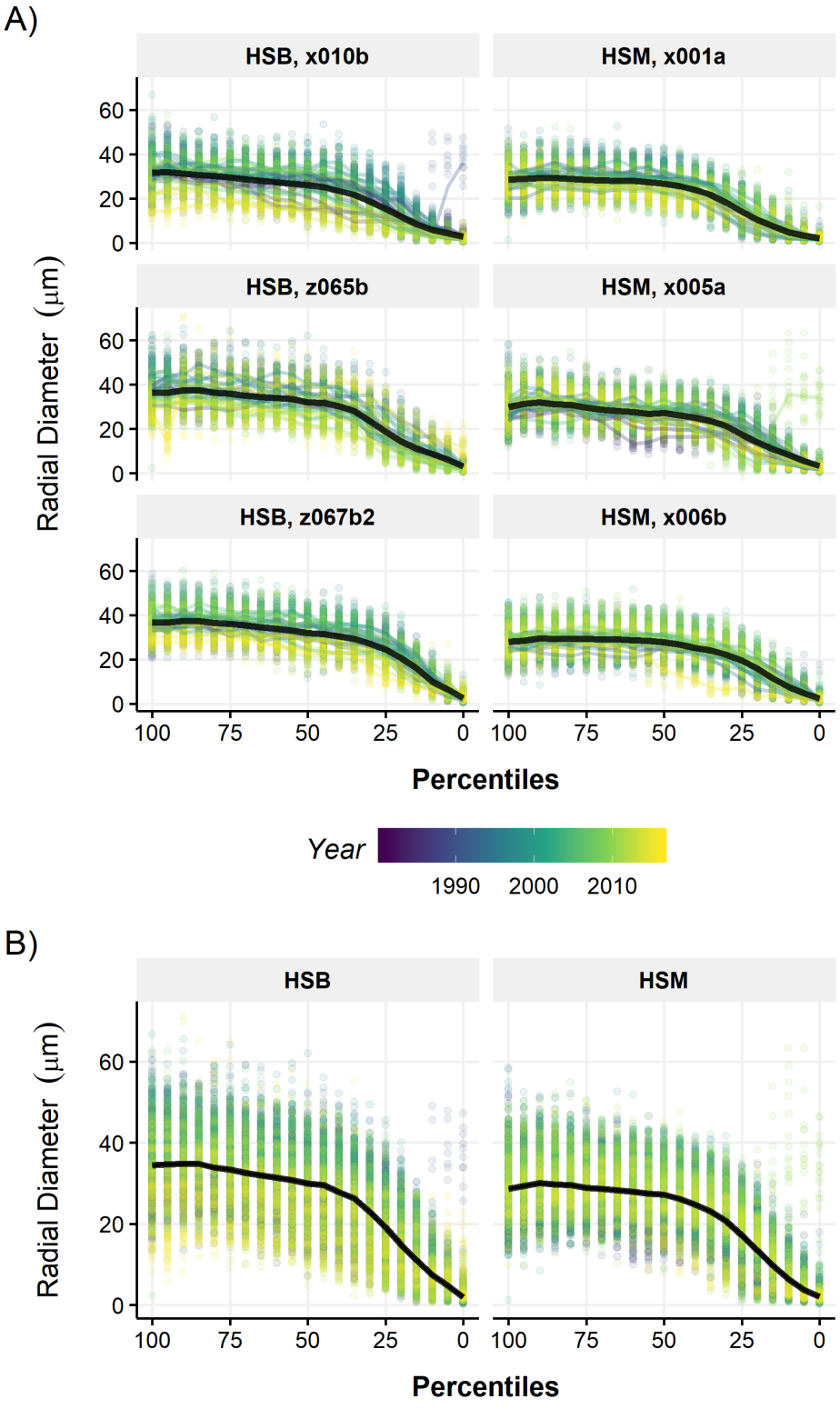

Figure 5.S5: A) Raw and averaged tree series of lumen radial diamter for *P. glauca*, and B) corresponding site-averaged series for relative position (percentiles). Averages were calculated using bi-weight robust means (Cook and Kairiukstis, 2013). Points represent annual variability across a relative position, colored lines are yearly means, and the thick, black line is for sample (A) or site (B) averages.

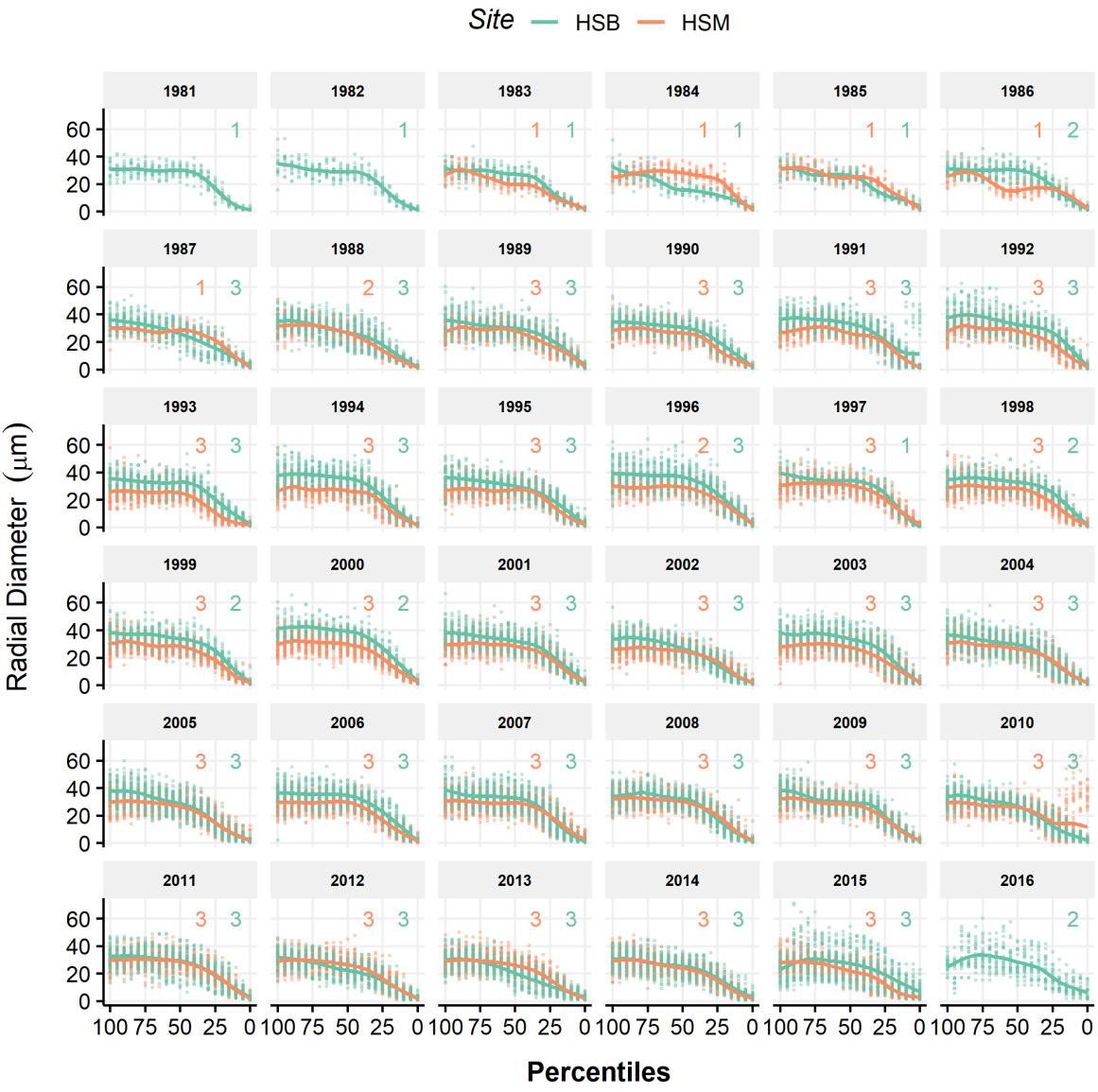

Figure 5.S6: Raw lumen diameter tracheidograms by relative (percentile) position, split by years. Numbers in panels are for sample depth.

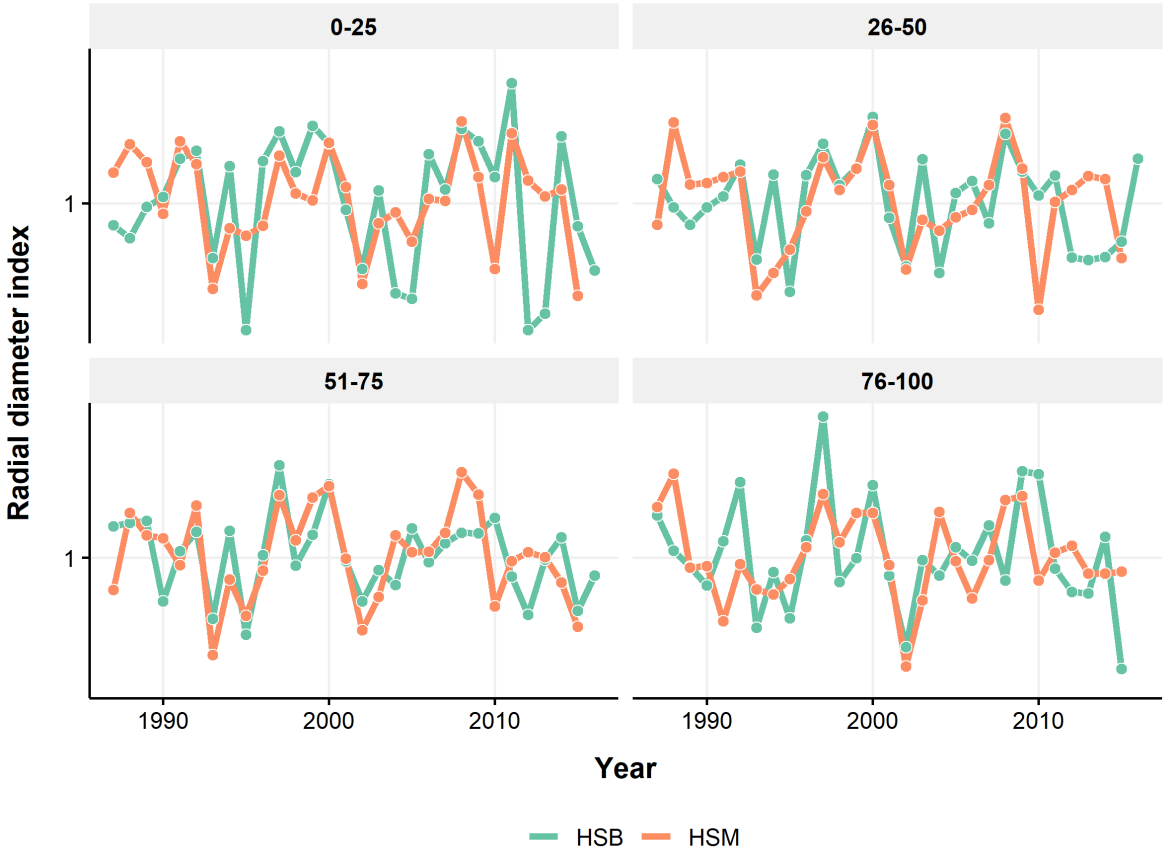

Figure 5.S7: Earlywood chronologies for *P. glauca* based on standardized and averaged percentile positions for both sites. Note, that 2016 was excluded from analyses as it represents an incomplete year for most individuals (August sampling).

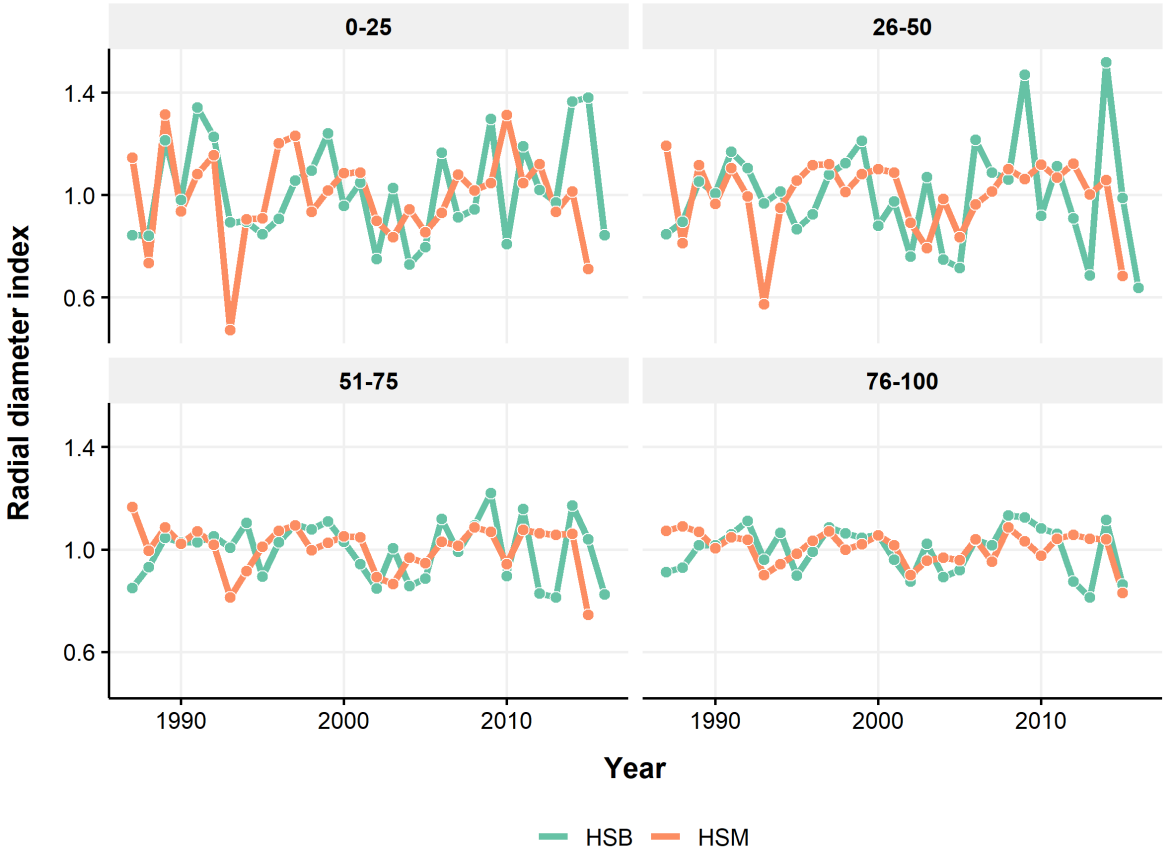

Figure 5.S8: Latewood chronologies for *P. glauca* based on standardized and averaged percentile positions for both sites. Note, that 2016 was excluded from analyses as it represents an incomplete year for most individuals (August sampling).

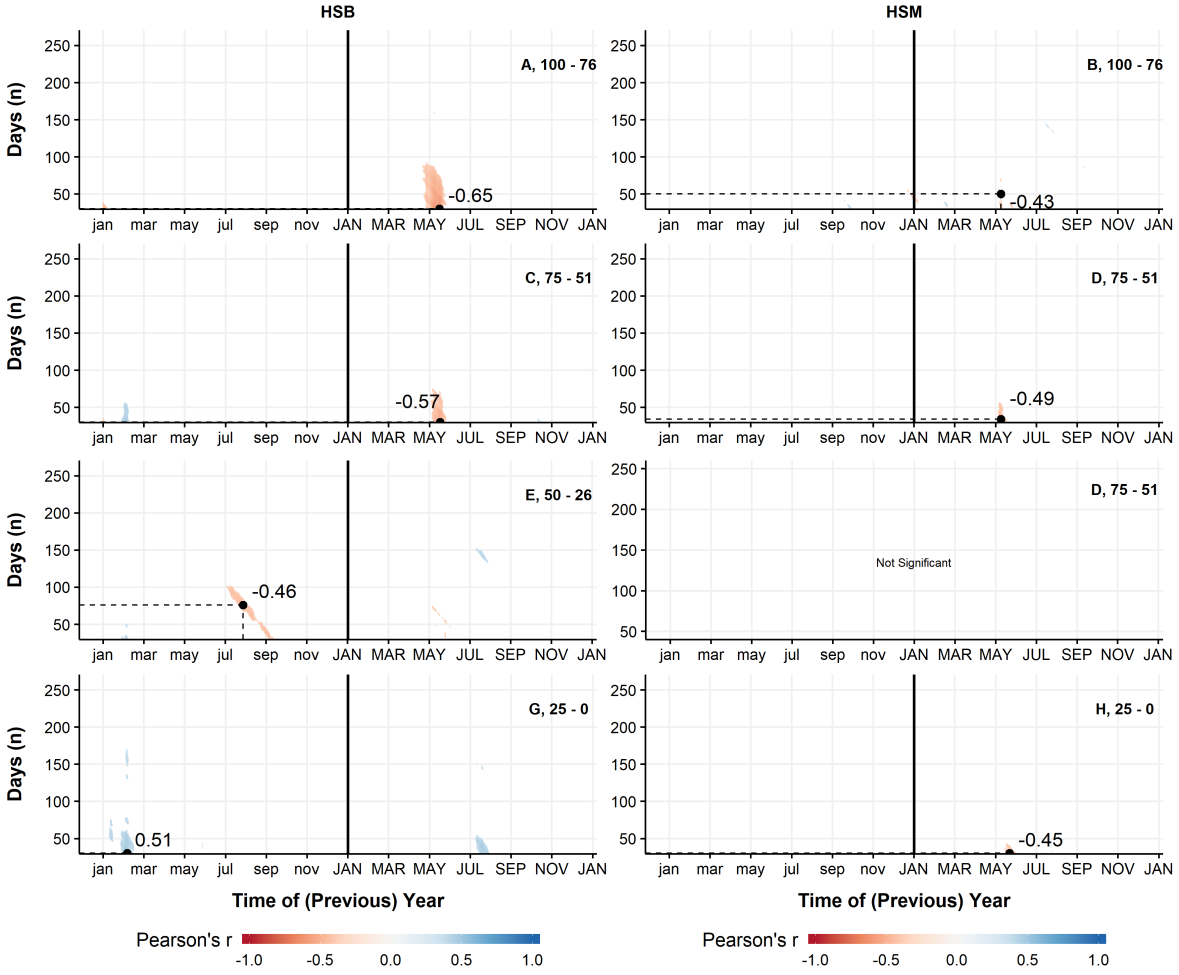

Figure 5.S9: Pearson's correlations between earlywood lumen diameter averaged over relative positions of *P. glauca* and daily *max. temp.* in both sites (HSB, HSM) for running windows of variable length (y-axis) and starting periods (x-axis). Points are highest identified correlation, and only statistically discernible $\alpha < 0.05$ values are shown.

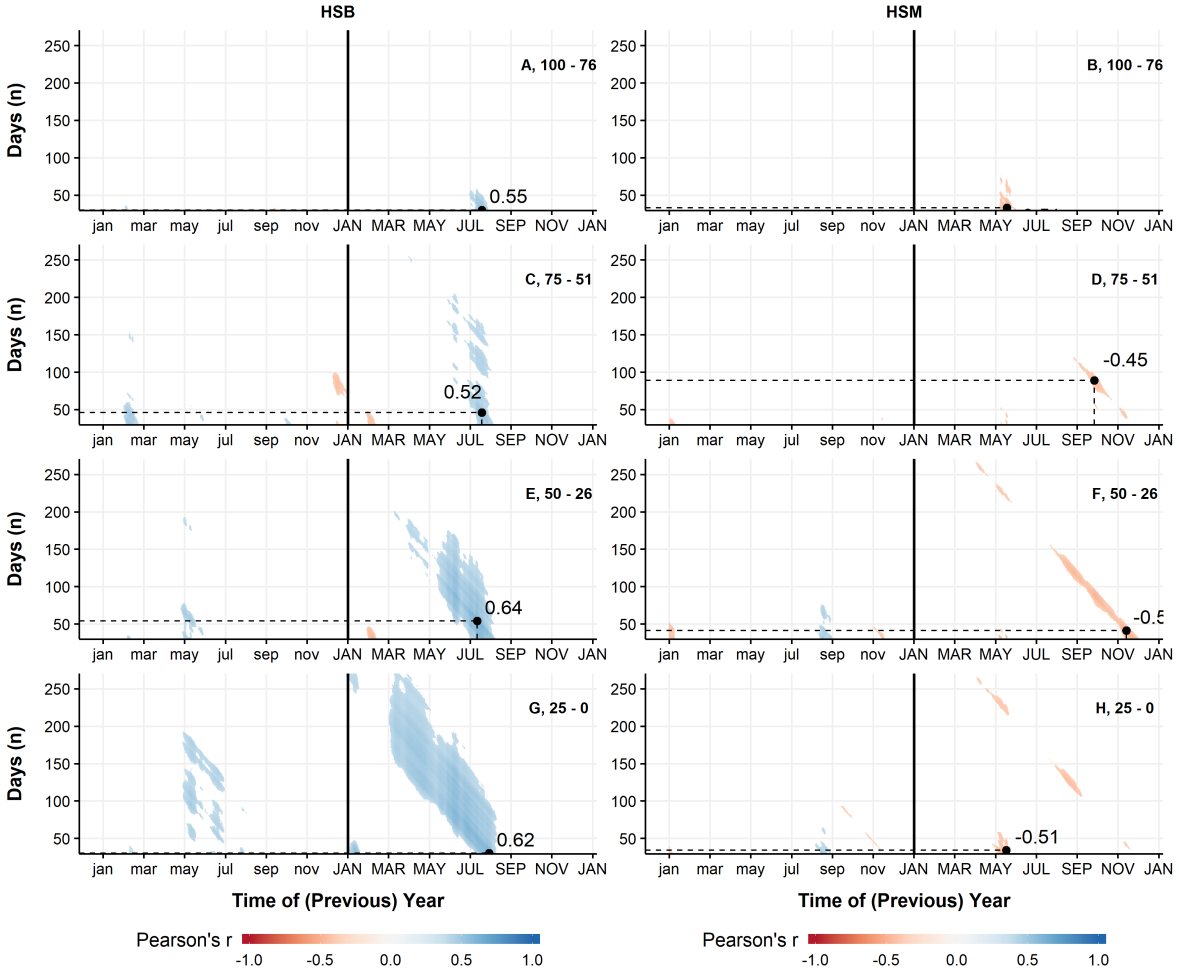

Figure 5.S10: Pearson's correlations between latewood lumen diameter averaged over relative positions of *P. glauca* and daily *max. temp.* in both sites (HSB, HSM) for running windows of variable length (y-axis) and starting periods (x-axis). Points are highest identified correlation, and only statistically discernible $\alpha < 0.05$ values are shown.

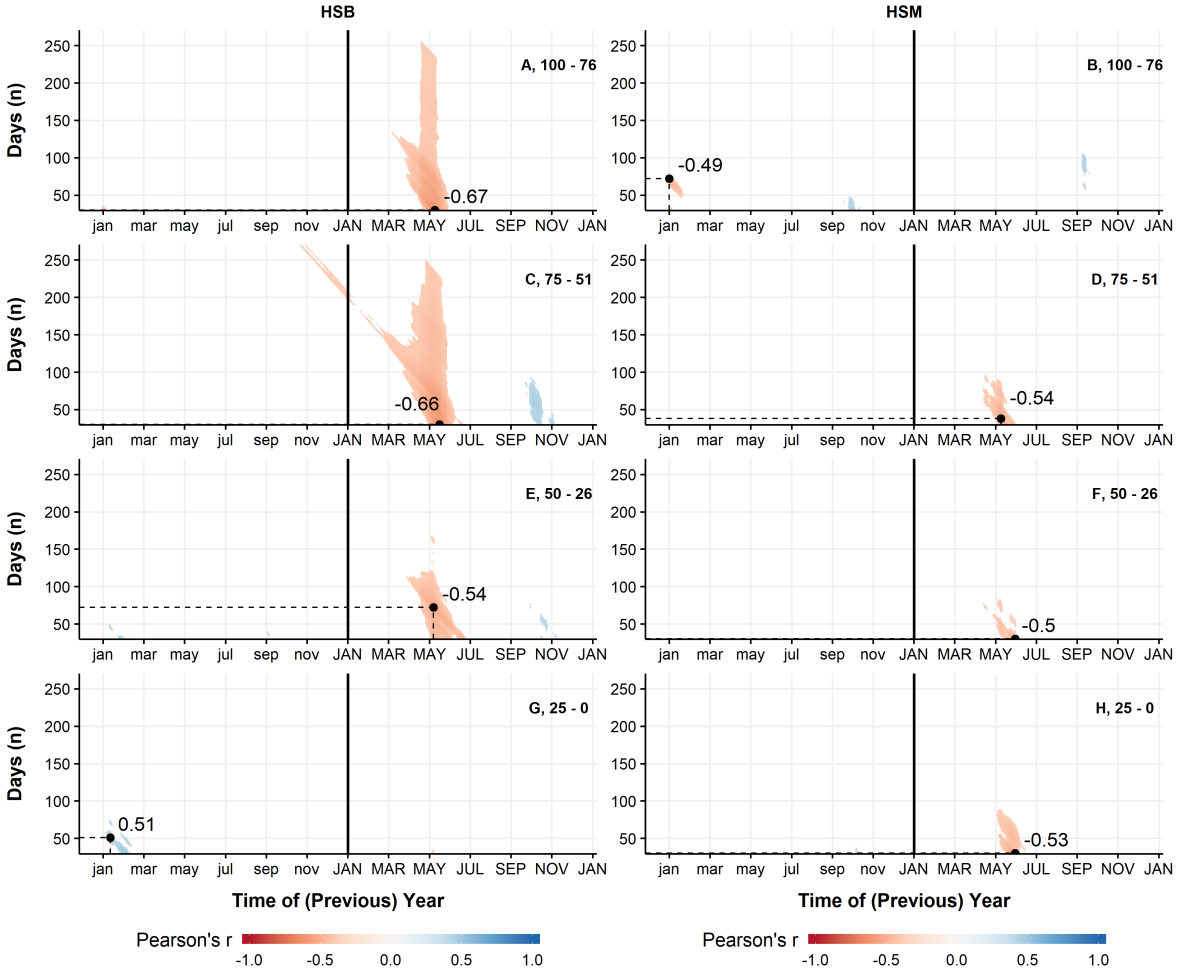

Figure 5.S11: Pearson's correlations between earlywood lumen diameter averaged over relative positions of *P. glauca* and daily *vpd* in both sites (HSB, HSM) for running windows of variable length (y-axis) and starting periods (x-axis). Points are highest identified correlation, and only statiscially discernible $\alpha < 0.05$ values are shown.

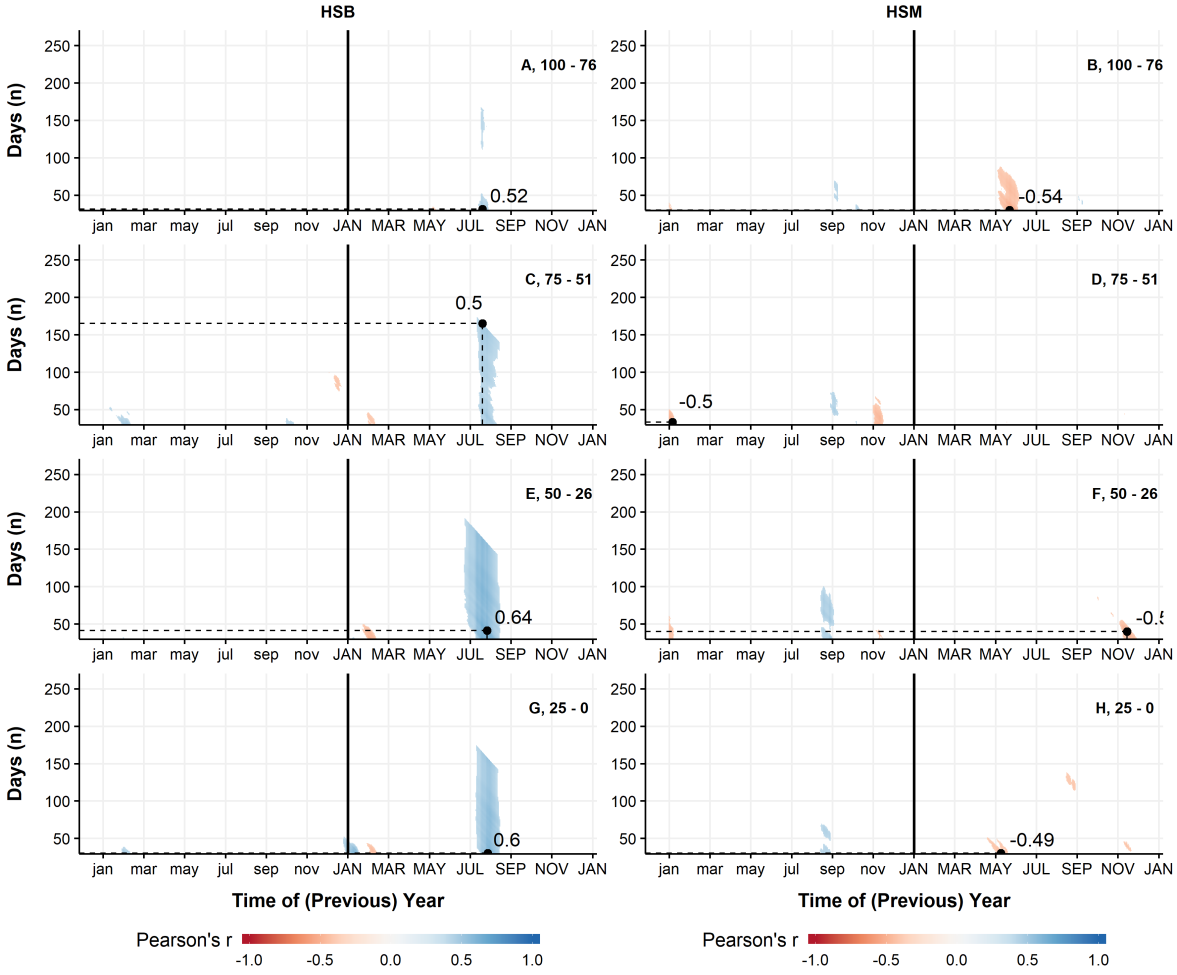

Figure 5.S12: Pearson's correlations between latewood lumen diameter averaged over relative positions of *P. glauca* and daily *vpd* in both sites (HSB, HSM) for running windows of variable length (y-axis) and starting periods (x-axis). Points are highest identified correlation, and only statiscially discernible $\alpha < 0.05$ values are shown.

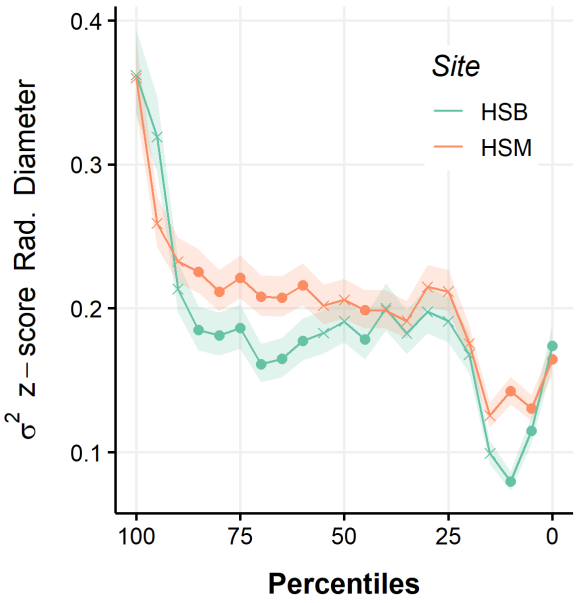

Figure 5.S13: Variance of all individual percentile chronologies over the period of 1987 to 2014. The bands are 95% CI for the variance point estimate and crosses indicate variance homogeneity at alpha = 0.05 (Levene's test). Variability of lumen radial appears to be greater for HSM for the majority of percentile positions (note confidence bands), and discernibly different predominantly for early and late percentiles.

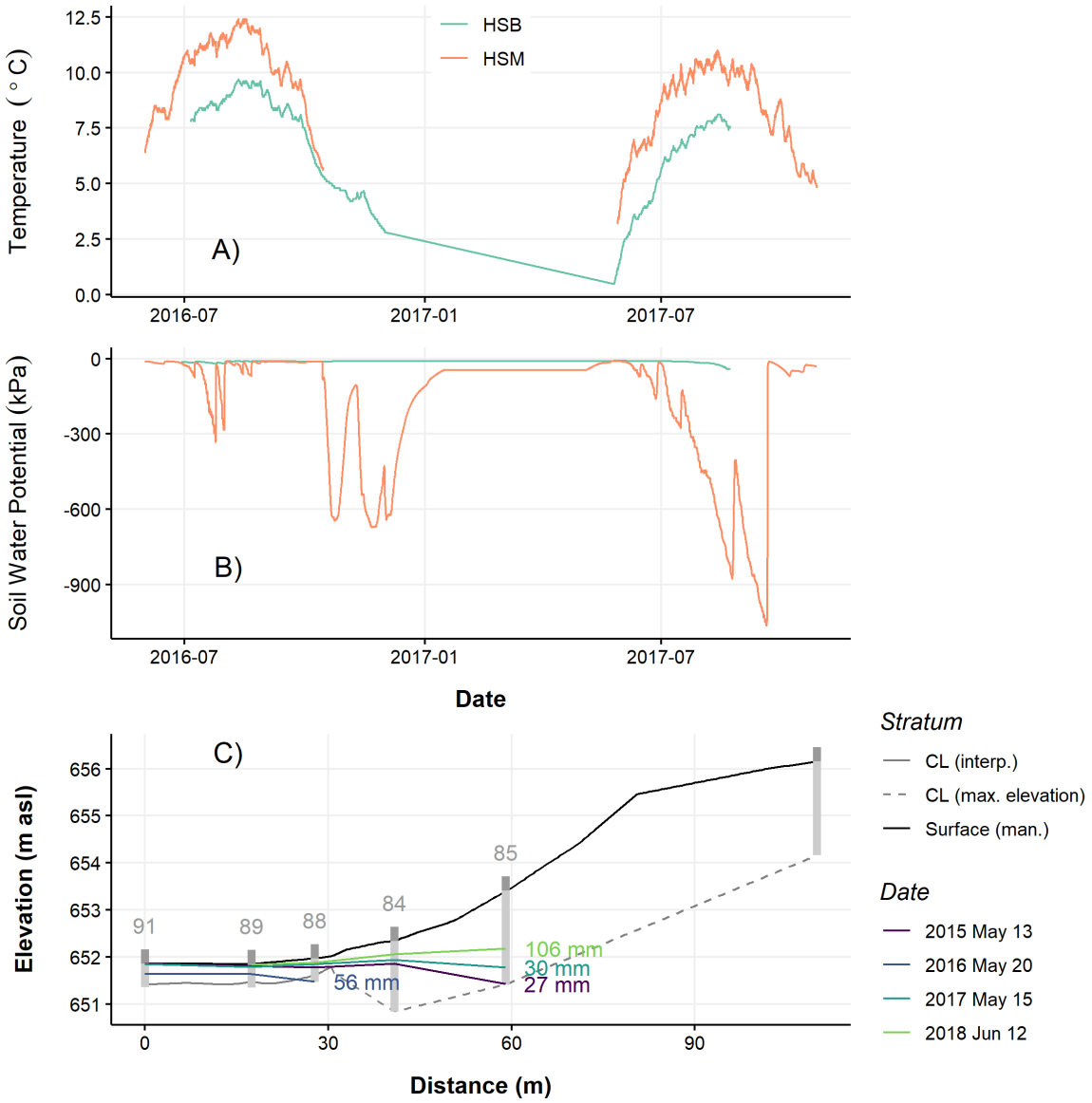

Figure 5.S14: Differences between rooting-zone conditions and water table configurations for typical HSB and HSM sites and the sampled wetland-upland transect show A) soil temperature B) soil water potential, and C) water tables based on measurements in a well transect in response to cumulative precipitation up to 10 days prior. Note, that the dashed line in C) represents a conservative estimate of low-permeability confining layer (CL), which likely drops off rapdily and to greater depths, as found for a nearby regional borehole in (Hokanson *et al.*, 2018a). HSB trees were sampled at heights equivalent to and above 84, and HSM trees were sampled at heights close to and above well 85.

5.7.2 Tables

Table 5.S1: Chronology statistics for both sites (HSB, HSM), and species (*P. glauca, P. tremuloides*), calculated for 30-year windows with 20-year overlap.

Year	$\bar{r}$	EPS	SNR
***P. tremuloides*, HSB**			
1953	-	-	-
1972	0.86	0.40	5.99
1982	0.91	0.46	9.96
1992	0.95	0.60	20.84
2002	0.94	0.50	15.89
2017	-	-	-
***P. tremuloides*, HSM**			
1843	-	-	-
1862	0.90	0.68	9.14
1872	0.83	0.48	4.91
1882	0.84	0.45	5.18
1892	0.91	0.59	10.05
1902	0.89	0.54	8.06
1912	0.91	0.60	10.57
1922	0.89	0.54	8.19
1932	0.94	0.69	16.64
1942	0.93	0.62	13.34
1952	0.93	0.59	13.83
1962	0.92	0.50	10.86
1972	0.96	0.66	22.44
1982	0.94	0.58	16.38
1992	0.94	0.59	17.05
2002	0.92	0.49	11.24
2017	-	-	-
***P. glauca*, HSB**			
1868	-	-	-
1920	0.80	0.37	4.10
1930	0.85	0.40	5.80
1940	0.82	0.34	4.66
1950	0.85	0.39	5.72
1960	0.88	0.44	7.11
1970	0.83	0.36	4.98
1980	0.83	0.34	4.73
1990	0.82	0.33	4.42
2000	0.82	0.35	4.59
2017	-	-	-
***P. glauca*, HSM**			
1905	-	-	-
1920	0.80	0.37	4.10
1930	0.85	0.40	5.80
1940	0.82	0.34	4.66
1950	0.85	0.39	5.72
1960	0.88	0.44	7.11
1970	0.83	0.36	4.98
1980	0.83	0.34	4.73
1990	0.82	0.33	4.42
2000	0.82	0.35	4.59
2016	-	-	-

Table 5.S2: Correlations between ring width indices for both species (*P. glauca, P. tremuloides*) in both sites (HSB, HSM) and precipitation indices. The latter were calculated based on hydrological years (Nov-Oct). Short-handles *dep* refer to cumulative departures from mean precipitation for 1 to 3 years. Statistics were calculated for 1980 to 2015; note, that 1981 - 1983, 2013 and 2014 were excluded for *P. tremuloides*. Degrees of freedom are 28 for *P. tremuloides*, and 34 for *P. glauca*.

Site	Species	Pearson's r	t-Statistic	p
previous				
HSM	*P. tremuloides*	0.31	1.72	0.097
HSB	*P. tremuloides*	0.42	2.48	**0.019**
HSM	*P. glauca*	0.43	2.75	**0.009**
HSB	*P. glauca*	0.53	3.65	**0.001**
current				
HSM	*P. tremuloides*	-0.26	-1.42	0.166
HSB	*P. tremuloides*	-0.20	-1.05	0.301
HSM	*P. glauca*	0.35	2.21	**0.034**
HSB	*P. glauca*	0.35	2.19	**0.036**
dep1a				
HSM	*P. tremuloides*	-0.26	-1.42	0.166
HSB	*P. tremuloides*	-0.20	-1.05	0.301
HSM	*P. glauca*	0.35	2.21	**0.034**
HSB	*P. glauca*	0.35	2.19	**0.036**
dep2a				
HSM	*P. tremuloides*	0.03	0.18	0.857
HSB	*P. tremuloides*	0.15	0.80	0.43
HSM	*P. glauca*	0.51	3.42	**0.002**
HSB	*P. glauca*	0.57	4.05	**0**
dep3a				
HSM	*P. tremuloides*	0.12	0.62	0.539
HSB	*P. tremuloides*	0.22	1.17	0.254
HSM	*P. glauca*	0.40	2.53	**0.016**
HSB	*P. glauca*	0.51	3.49	**0.001**

Table 5.S3: Correlations between relative position (percentile) indices of earlywood for 4 averaged sectors in both sites (HSB, HSM) and precipitation indices. The latter were calculated based on hydrological years (Nov-Oct). Short-handles *dep* refer to cumulative departures from mean precipitation for 1 to 3 years. Statistics were calculated for 1988 to 2015. Degrees of freedom are 26.

Index	Site	Pctl. position	Pearson's r	t-Statistic	p
current	HSB	0-25	0.01	0.05	0.964
	HSM	0-25	0.41	2.29	**0.031**
dep1a	HSB	0-25	0.01	0.05	0.964
	HSM	0-25	0.41	2.29	**0.031**
dep2a	HSB	0-25	0.10	0.53	0.602
	HSM	0-25	0.53	3.15	**0.004**
dep3a	HSB	0-25	0.18	0.91	0.37
	HSM	0-25	0.33	1.80	0.084
previous	HSB	0-25	0.15	0.79	0.436
	HSM	0-25	0.42	2.34	**0.027**
current	HSB	26-50	0.16	0.84	0.407
	HSM	26-50	0.40	2.26	**0.033**
dep1a	HSB	26-50	0.16	0.84	0.407
	HSM	26-50	0.40	2.26	**0.033**
dep2a	HSB	26-50	0.20	1.05	0.302
	HSM	26-50	0.52	3.08	**0.005**
dep3a	HSB	26-50	0.15	0.76	0.456
	HSM	26-50	0.36	1.95	0.063
previous	HSB	26-50	0.16	0.80	0.43
	HSM	26-50	0.41	2.29	**0.031**
current	HSB	51-75	0.13	0.66	0.512
	HSM	51-75	0.27	1.45	0.16
dep1a	HSB	51-75	0.13	0.66	0.512
	HSM	51-75	0.27	1.45	0.16
dep2a	HSB	51-75	0.29	1.53	0.139
	HSM	51-75	0.45	2.58	**0.016**
dep3a	HSB	51-75	0.25	1.30	0.204
	HSM	51-75	0.33	1.77	0.089
previous	HSB	51-75	0.32	1.74	0.094
	HSM	51-75	0.44	2.48	**0.02**

Table 5.S3: Correlations between relative position (percentile) indices of earlywood for 4 averaged sectors in both sites (HSB, HSM) and precipitation indices. The latter were calculated based on hydrological years (Nov-Oct). Short-handles *dep* refer to cumulative departures from mean precipitation for 1 to 3 years. Statistics were calculated for 1988 to 2015. Degrees of freedom are 26. *(continued)*

Index	Site	Pctl. position	Pearson's r	t-Statistic	p
current	HSB	76-100	0.16	0.82	0.418
	HSM	76-100	0.17	0.90	0.375
dep1a	HSB	76-100	0.16	0.82	0.418
	HSM	76-100	0.17	0.90	0.375
dep2a	HSB	76-100	0.40	2.20	**0.037**
	HSM	76-100	0.31	1.68	0.106
dep3a	HSB	76-100	0.33	1.77	0.088
	HSM	76-100	0.22	1.14	0.265
previous	HSB	76-100	0.47	2.68	**0.013**
	HSM	76-100	0.32	1.71	0.1

Table 5.S4: Correlations between relative position (percentile) indices of earlywood for 4 averaged sectors in both sites (HSB, HSM) and precipitation indices. The latter were calculated based on hydrological years (Nov-Oct). Short-handles *dep* refer to cumulative departures from mean precipitation for 1 to 3 years. Statistics were calculated for 1988 to 2015. Degrees of freedom are 26.

Index	**Site**	**Pctl. position**	**Pearson's r**	**t-Statistic**	**p**
annual	HSB	0-25	0.03	0.15	0.884
	HSM	0-25	0.18	0.91	0.371
dep1a	HSB	0-25	0.03	0.15	0.884
	HSM	0-25	0.18	0.91	0.371
dep2a	HSB	0-25	0.15	0.76	0.454
	HSM	0-25	0.34	1.87	0.073
dep3a	HSB	0-25	0.26	1.36	0.186
	HSM	0-25	0.19	0.99	0.331
previous	HSB	0-25	0.20	1.06	0.299
	HSM	0-25	0.37	2.01	0.055
annual	HSB	26-50	-0.11	-0.56	0.58
	HSM	26-50	0.17	0.90	0.374
dep1a	HSB	26-50	-0.11	-0.56	0.58
	HSM	26-50	0.17	0.90	0.374

Table 5.S4: Correlations between relative position (percentile) indices of earlywood for 4 averaged sectors in both sites (HSB, HSM) and precipitation indices. The latter were calculated based on hydrological years (Nov-Oct). Short-handles *dep* refer to cumulative departures from mean precipitation for 1 to 3 years. Statistics were calculated for 1988 to 2015. Degrees of freedom are 26. *(continued)*

Index	Site	Pctl. position	Pearson's r	t-Statistic	p
dep2a	HSB	26-50	0.10	0.52	0.608
	HSM	26-50	0.30	1.63	0.115
dep3a	HSB	26-50	0.24	1.24	0.227
	HSM	26-50	0.14	0.71	0.483
previous	HSB	26-50	0.27	1.43	0.166
	HSM	26-50	0.30	1.63	0.115
annual	HSB	51-75	-0.01	-0.06	0.953
	HSM	51-75	0.40	2.24	**0.034**
dep1a	HSB	51-75	-0.01	-0.06	0.953
	HSM	51-75	0.40	2.24	**0.034**
dep2a	HSB	51-75	0.13	0.66	0.513
	HSM	51-75	0.57	3.53	**0.002**
dep3a	HSB	51-75	0.26	1.36	0.187
	HSM	51-75	0.39	2.18	**0.039**
previous	HSB	51-75	0.21	1.12	0.272
	HSM	51-75	0.49	2.89	**0.008**
annual	HSB	76-100	-0.04	-0.23	0.821
	HSM	76-100	0.41	2.29	**0.03**
dep1a	HSB	76-100	-0.04	-0.23	0.821
	HSM	76-100	0.41	2.29	**0.03**
dep2a	HSB	76-100	0.19	1.01	0.323
	HSM	76-100	0.59	3.71	**0.001**
dep3a	HSB	76-100	0.28	1.47	0.154
	HSM	76-100	0.38	2.10	**0.046**
previous	HSB	76-100	0.35	1.91	0.067
	HSM	76-100	0.52	3.07	**0.005**

CHAPTER 6

Synthesis and Implications

This chapter provides a summary of key findings for each of the four studies (Chapters 2 through 5), and provides a synthesis which aims to contextualize results with current literature, highlight novel aspects and discuss their implications.

6.1 Chapter summary

Swamps are reportedly linked with water transmitting functions (Gibson *et al.*, 2015; Devito *et al.*, 2017), yet little research addressed their ecohydrological functioning and resulting interactions explicitly (Devito *et al.*, 2005a) or indirectly (Dixon *et al.*, 2017), despite their potential importance under dryer and more variable hydrometeorological regimes in the future (Price *et al.*, 2013; Ireson *et al.*, 2015). This thesis aimed to contribute mechanistic and conceptual understanding of small and likely ubiquitous forested swamps, as low-storage systems, on local to catchment-scales, as well as to provide the basis for translating this knowledge to other physiographical settings found in the BP in order to aid current and future watershed and land management under warming conditions.

The thesis applied a range of empirical and numerical methods to identify processes and interactions at different scales (individual tree/stands, wetland / point-scale, catchment) in four original studies, addressing the identified research gaps. **Chapter 2** (objective 1) assessed in detail the capacity (i.e. magnitude) and frequency at which a small, forested swamp generated (conditions necessary for) flows to downgradient or adjacent systems, and highlighted the strong controls of climate and contrasting (available) storage capacity in driving connectivity in the absence of appreciable external inputs. **Chapter 3** (objective 2) determined the influence of (absolute) water storage capacity and the dominant water loss pathway (evapotranspiration) on swamp hydrological regimes, and identified key periods under which flows may be generated, as well as climatic limitations of this function. **Chapter 4** (objective 3) provided an in-depth

assessment of the major negative flux component determining the swamp's hydrological regime, *viz.* sub-canopy evapotranspiration, and identified ecosystem structure and soil-plant-atmosphere feedbacks as prominent controls. **Chapter 5** (objective 4) aimed to assess the potential impact of water supplementation from a wetland with ephemeral hydrological regime to adjacent forests for two key tree species in the Boreal Plain and highlighted differences between absolute growth and water sensitivity based on hydrological position.

6.2 Main findings

This thesis provided an integrative, ecohydrological assessment of functions relating to water surplus generation and transmission (i.e. contributing and transmitting, *sensu* Black, 1997; Spence *et al.*, 2011), as well as their potential impacts on adjacent forests. Research conducted here was novel in that it 1) extended understanding of forested swamps with ephemeral hydrological regimes by focusing on processes and their interactions in glacial landforms (i.e. substrate types) that promote extensive, unsaturated zones, through all stages of the prevalent climate cycles (wet, mesic, dry), 2) it provided the first, detailed assessment of evapotranspiration from a deciduous swamp in the BP and highlighted (potential) feedback mechanisms that allow surplus generation, and 3) combined process-based and conceptual understanding with tree growth and wood-anatomical measurements to infer ecohydrological interactions between wetlands and adjacent forests. The main findings arrived at here are:

1. Storage contrasts (within / beyond wetland) control flow generation under the prevalent sub-humid climate. Flow generation can occur entirely through internal processes, and is dynamically controlled by available storage and near-surface ice dynamics within the wetland, which constituted only 4 % of total catchment area. As such, the swamp's hydrological behavior distinctly contrasted the surrounding

upland forests by generating flow even in markedly dry years. This indicates that low-storage areas - such as small, forested wetlands - are disproportionately important in defining catchment hydrological responses in all but the wettest years (with return periods above 25 years).

2. Sub-canopy ET was the dominant, negative water efflux from the small, forested wetland. Absolute storage capacity determines the sign and magnitude of the atmospheric water balance. Lower absolute storage results in frequent "shutdown" of evapotranspiration (ET) during high-demand periods (i.e. growing season), while simultaneously allowing for saturation in response to small precipitation (P) events throughout a given year, and even during dry years. Maximum attainable ET (annually) hence increased with storage, and the location of this peak shifted toward ever lower annual P totals (i.e. water input). Contrastingly, annual ET was close to P for unrestricted storage, indicating an optimal balance between demand and supply. This implies that absolute storage capacity at a given point (or an entire system) defines the optimal amount of P needed to maximize ET, which likely has strong control on swamp (i.e. small, forested wetland) initiation, productivity and permanence.

3. The sub-canopy environment of deciduous swamps is increasingly less conducive to sustaining high ET demand, as a result of phenology-driven and/or structural changes, i.e. leaf area increases in the overstory and sub-canopy during growing seasons. These increases further alter the relative importance of radiation and atmospheric demand (vapor pressure deficit, vpd) with a distinct shift to vpd-driven ET in mid-summer. Organic soils exhibited increasing tensions near the surface under extended periods of high demand, further limiting E losses. This indicates that forested swamps, of small extent, can develop distinct sub-canopy environments, which together with plant-physiological control on T, and tension-limited E, act to limit ET losses via the dominant efflux pathway (sub-canopy ET).

4. Marked differences were found between trembling aspen and white spruce growth dynamics regarding sensitivity to precipitation. Aspen stands showed little to no sensitivity to precipitation, potentially indicating adequate access to wetland water (supplements) via clonal root networks in low and high hydrological positions, or higher drought tolerance, while high temperature and especially high *vpd* indicated strong physiological control over water losses concomitant with decreased growth. Contrastingly, white spruce showed strikingly high correlations with winter P, as well as cumulative P anomalies in stands with and without access to wetland water. Hydraulic architecture in white spruce reflected availability to water, with frequent supplementation resulting in less variability in water-transporting conduits (i.e. tracheids), indicating marked plasticity between areas with and without supplementation. These differences are most pronounced early and late in growing seasons.

6.3 Synthesis

The research presented here was motivated by a high probability of future warming and drying to adversely affect ecohydrological functioning of the drought-prone Boreal Plain (Hogg and Bernier, 2005; Price *et al.*, 2013), a large region in Canada's Western Boreal Forest, likely leading to intensified disturbance regimes (Volney and Hirsch, 2005) and potentially causing a drastic state shift to ecosystems resembling the drier Aspen Parkland with only patchy forest cover (Hogg and Hurdle, 1995; Schneider *et al.*, 2016). Previous work on water redistribution mechanisms and functions from wetlands in the BP focused on topographically higher catchments with monthly P 55 % above BP averages (Wells *et al.*, 2017), or in low hydrological positions with considerable groundwater discharge (Goodbrand *et al.*, 2018). Similar to Devito *et al.* (2005a), this study aimed at assessing the functions provided by ephemeral systems as low storage areas, and conditions necessary for these to occur, in typical aspen-dominated

catchments, where extensive vadose zones form due to the high water demand (Devito *et al.*, 2012; Ireson *et al.*, 2015).

The exemplary, forested swamp acted like a swale once storage thresholds were overcome (Chapter 2, Chapter 3), intermittently establishing hydrological connectivity with an isolated pond via subsurface and surface flows (Chapter 2). The observed water surplus generating and transmitting functions (i.e. contributing and transmitting *sensu* Black, 1997; Spence *et al.*, 2011) were the expression of multiple interacting autogenic processes and characteristics, including their interactions.

Figure 6.1 gives a schematic representation of internal processes, and highlights those that were addressed here. Climatic variability, expressed through P and (drivers of) ET (Chapter 3, Chapter 4), interacted with absolute storage capacity (Chapter 3) to control saturation and thereby generate hydraulic heads in the swamp conducive for outward flows (Chapter 2, Thompson *et al.*, 2015a; Devito *et al.*, 1997) on frequent basis. Hillslope contributions were not required for these conditions; rather, water tables mirrored topography, indicating subsurface contributions toward hillslopes (Devito *et al.*, 2005b; Thompson *et al.*, 2015a). Storage contrasts within the wetland fundamentally governed the location of saturated areas, while the subsurface and surface topography determined when connectivity was established between them (Chapter 2, Ali *et al.*, 2011; Devito *et al.*, 2005a; Phillips *et al.*, 2011), slope permitting. Analyses of idealized systems (Chapter 3) further indicated that, saturation and positive atmospheric water balances (P - *actual* ET) occurred even during dry years under a range of absolute storage found in the swamp (Chapter 2). This higher potential for frequent saturation and runoff in the modelled system compared to the observed dynamics (Chapter 2) is reconciled by considering the range of processes and conditions governing the saturation and activation of areas within the wetland given the region's sub-humid climate (see above, also Buttle *et al.*, 2012; Spence, 2007). These include, amongst others, the spatio-temporal variability of ET (Kettridge *et al.*, 2013) and its

controls (e.g. energy balance dynamics including canopy light transmission as well as heat storage and transfer, Thompson *et al.*, 2015c; Nazarbakhsh *et al.*, 2020), and especially highlight water storage heterogeneity (e.g. through surface-near ice dynamics, Van Huizen *et al.*, 2020) as a governing principle for the catchment's (asynchronous) responses (Buttle *et al.*, 2012). Elaborating on work by Devito *et al.* (2005a), dry periods (annual basis) hence required the presence of solid ice as well as adequate snow water equivalent or P events in spring and early summer to overcome "gatekeeper" areas, i.e. with larger absolute and available storage, notably toward the wetland's outflow. Storage dynamics, governed by the timing of P, as well as variability of both winter P and temperatures (governing soil freeze-thaw cycles; Redding and Devito, 2011), will hence be decisive for controlling future magnitudes and frequencies of water redistribution from forested swamps and other wetland systems under future hydrometeorological regimes (Ireson *et al.*, 2015).

Both Chapters 3 and 4 give strong indication for feedbacks that maintain the currently observed water redistribution functions. Maximum annual ET was limited by and decreased with absolute storage, while requiring higher annual P for that maximum to be attained due to frequent dry-out. Note, that maxima were close to long-term mean annual P, likely indicating optimization between water availability and use by the swamp ecosystem. Climatic variability hence served to reduce maximum productivity under dry conditions, as well as under excessively wet ones, while promoting decomposition and accrual of organic matter (Rydin *et al.*, 2006), respectively. This provides further evidence for shallow-storage wetlands to be locked in low productivity states - maintaining their functioning (Dixon *et al.*, 2017). Such co-evolution of catchment (wetland) hydrological characteristics (i.e. storage) and vegetation water use has been hypothesized (Milly and Dunne, 1994), assessed in modelling exercises (Brolsma and Bierkens, 2007), and large-scale catchment comparisons (Gao *et al.*, 2014).

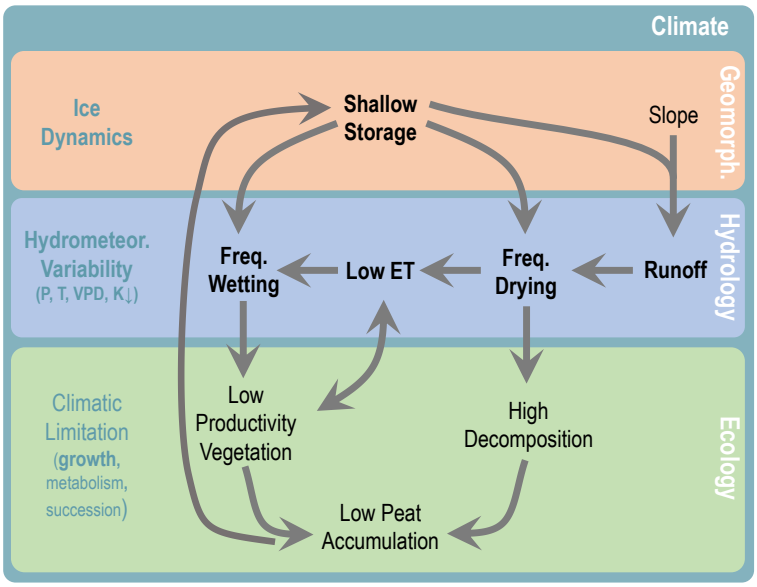

Figure 6.1: Concept of processes and characteristics that provide and maintain ephemeral hydrologic regimes and thereby swamp/wetland functioning in the Boreal Plain. Bold labels refer to topics assessed and discussed in detail throughout this thesis. The combination of sub-humid climate (as enveloping feature), local topography, geology and soils, as well as vegetation water use lead to a low-productivity loop. Climatic processes and dynamics that are considered a dominant control on the three major domains (geomorphology, hydrology, ecology) are given by text labels (color corresponding to climate envolope). Relationships depicted here are for geographically isolated systems after (Cohen *et al.*, 2016), and would be modified by extensive external inputs or effluxes (e.g. groundwater discharge or recharge under the wetland). Refer to the text for detailed discussion. Abbreviated variables are: P = precipitation, T = air temperature (2 m), VPD = vapor pressure deficit, $K\downarrow$ = incident radiation.

The partitioning of annual P into ET and water redistribution (runoff, subsurface flows) is hence also fundamentally linked to vegetation. While internal processes were the focus of this work here, external dynamics may also affect water supply and demand. Notably, press (long-term) and pulse (rapid) disturbances (Grosse *et al.*, 2018) could have strong effects on water use by changing vegetation composition and structure within the wetland, e.g. via long-term climate warming allowing for upland-tree encroachment (Waddington *et al.*, 2015) or by fire, logging or insect infestations that may remove structural elements that demote turbulent exchange and/or determine energy budgets (Bond-Lamberty *et al.*, 2009; Thompson *et al.*, 2014, 2015b). While the wetland does not receive or require appreciable inputs from adjacent uplands, disturbances there could equally impact turbulent dynamics between upland-wetland complexes, and enhance atmospheric water losses (Petrone *et al.*, 2007), as well as alter

energy budgets. Storage reduction, as absolute loss of soil or decrease in specific yields, due to e.g. prolonged drought or fire, would increase the frequency of saturation. Local conditions (hydrological regime, energy exchange) would then determine successional dynamics, as observed for peatland margins (Lukenbach *et al.*, 2017), which are often (similar to) low-storage swamps, and whether systems would return to an equivalent state. Unless pushed toward open-water wetlands with higher *ET* demand (Devito *et al.*, 2012, 2017), it is likely that water redistribution would remain as an emergent function. Yet, even in such cases, adequate build-up of organic material may allow for treed swamp systems to (re-) establish (Bauer *et al.*, 2003).

6.3.1 Catchment and landscape implications

On catchment-scale, wetlands exist in a continuum from fully connected to the drainage network to permanently lacking any exchange (Cohen *et al.*, 2016), reflecting the functions proposed by Black (1997) and Spence *et al.* (2011): storing (and/or losing), transmitting, and contributing water (i.e. internally generating flow). Low storage, forested wetlands, as saturating and actively contributing or transmitting areas, can be of disproportionate importance where their ephemeral hydrological regime is the sole driver of water redistributing functions (Chapter 2, Devito *et al.*, 2005a; Spence and Phillips, 2015). Indeed, ephemeral systems have been identified as a major component of drainage networks in the US (59 % of total length combining intermittent and ephemeral streams; Nadeau and Rains, 2007), and most likely constitute a large proportion of water-generating areas in headwater catchments throughout Canada (Buttle *et al.*, 2012), which has been indicated for the BP by Devito *et al.* (2017). Further, in the setting studied here, (conditions for) subsurface flow from saturated wetland areas toward forested uplands was frequently observed (Chapter 2, Riddell, 2008), and there was strong indication that this water supplementation facilitated tree growth and/or decreased water stress (Chapter 5), as found in other dry (i.e. semi-arid and

sub-humid) regions for wetlands and rivers with ephemeral regimes (see Thompson *et al.*, 2011 for detailed discussion). In the BP, forested swamps hence may act as local buffers or refugia (Raney *et al.*, 2016) under climate warming in the near future (Ireson *et al.*, 2015). The extent of such supplementation will be a function of local topography, hydrological position, soil stratification, and surficial geology (i.e. substrate type) modulating sub-surface flow rates, (Cohen *et al.*, 2016; Bourgault *et al.*, 2019). Figure 6.2 gives a schematic representation of how topographically-driven (Fig. 6.2A) and depressional (Fig. 6.2B) systems (with ephemeral regimes) may interact with adjacent upland forests, highlighting the role of their spatial distribution and geometry (Fig. 6.2C, Vanderhoof *et al.*, 2016; Shaw *et al.*, 2013).

Little-Devito *et al.* (2019) recently reported on ephemeral and potentially permanent wetlands forming opportunistically (i.e. unplanned) in reclaimed landscapes in the Athabasca Oil Sands region, where the sub-humid Boreal Plain climate and contrasting (overburden) deposits combined with climate change pose significant challenges to "mega-project reclamation" (Rooney *et al.*, 2015), most notably, balancing water security with ecosystem productivity (Devito *et al.*, 2012). Novel wetlands were identified in areas where storage was low, sheltered from dominant ET drivers (wind, radiation) and/or where effective catchment area was large enough to offset water deficits (i.e. through external contributions); similar functions, such as groundwater supplementation (e.g. indicated by willow rings, van der Kamp and Hayashi, 2009), are implied. This indicates that reclamation planning can utilize - and must account for - such wetland systems on their sites when developing catchment and landscape-scale water budgets. These systems, as well as small, forested swamps, based on their functioning observed here, may allow to balance water security via runoff generation - typically associated with wetlands with poor tree growth - with productive forests that generally entail low water yield (Chapter 2, Chapter 5, Devito *et al.*, 2012, 2017). Results presented here may therefore be useful to restoration planners as well

as land-managers. This is especially true where knowledge on the location, distribution and connectivity of ephemeral systems with other landscape units can prevent anthropogenical disturbances in key areas within or in the vicinity of the wetland or low-storage area in question. This could, for example, mean directing exploration for oil and gas via seismic lines away from frequently saturating and runoff-generating areas (Devito *et al.*, 2005a; Braverman and Quinton, 2016), or preventing the construction of roads through hydrologically connected and dependent areas (Miller *et al.*, 2015).

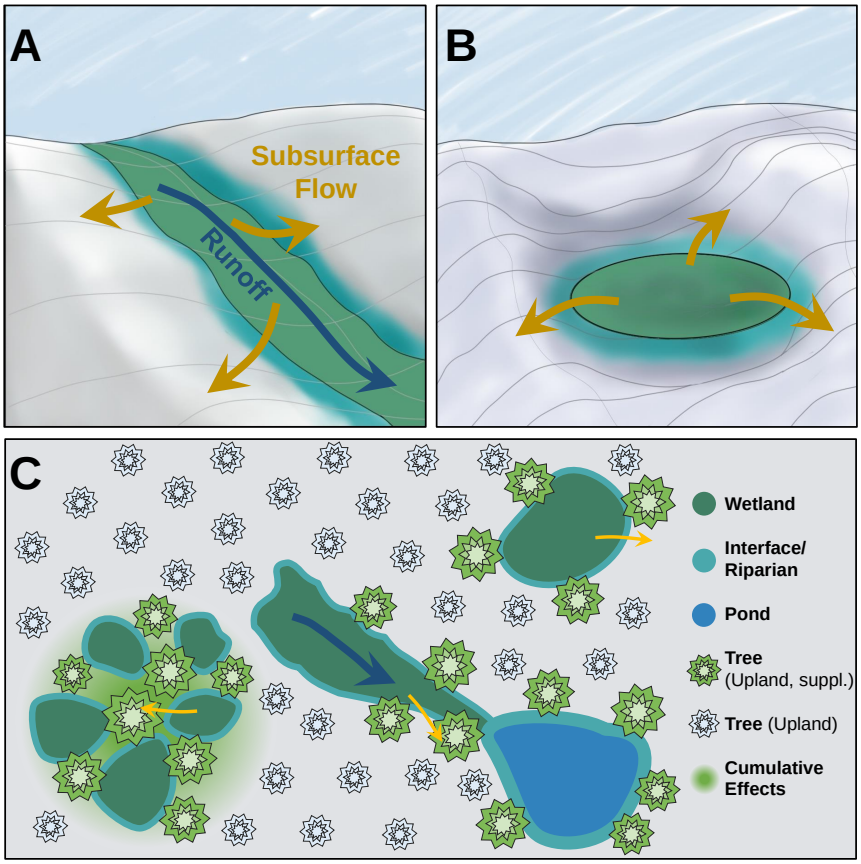

Figure 6.2: Wetland configuration and interactions with adjacent upland trees. The schematic features a A) topographically-driven system, B) depressional system and C) catchment with idealized representations of process impacts and spheres of interaction. Cumulative effects may be observed where the arrangement of ephemeral systems allows for a concentrated supplementation.

6.4 Future research avenues

The hydro(geo)logy of Boreal Plain is highly complex due to contrasting surficial geology on catchment and landscape-scales, a highly variable, sub-humid climate, low relief and complex ecohydrological interactions (Devito *et al.*, 2005a; Ireson *et al.*, 2015; Klaus *et al.*, 2015), which can have considerable impact on hydrological responses (Thompson *et al.*, 2011). As stated by Devito *et al.* (2017), process-based understanding of catchment or landscape unit functioning is required for ensuring water security in the Boreal Plain. With respect to wetlands with ephemeral regimes and their dynamics in this region, multiple avenues for further research were highlighted throughout Chapters 2 through 5, and those considered most stimulating and useful in an applied context are given below:

- Work herein and by others provided insight on wetland functioning under current climatic conditions (Devito *et al.*, 2005a; Wells *et al.*, 2017; Goodbrand *et al.*, 2018). Researchers may wish to investigate impacts of altered hydrometeorological regimes, most notably the temporal variability of P, including intensity, magnitude and type (snow *vs.* rain) on storage-threshold and storage-ET relationships under future conditions.

- Accordingly, investigating the impacts of altered P regimes, as well as climate warming, on the composition, structure and successional dynamics of vegetation communities is required to inform to which degree observed ecohydrological functioning and interactions display plasticity or when/if they would be compromised in the near future (Porporato *et al.*, 2002), e.g. due to physiological limitation. This understanding would also be useful for predicting community trajectories post-disturbance or after reclamation.

- The forested swamp studied here was located in a upland-wetland-pond complex with perched water tables (approximately 15 to 20 m above regional flow

system). Drier conditions in the future may result in the (periodic) loss of surface-groundwater connectivity for a range of landscape units across other glacial landforms, and hence low-storage systems/wetlands in these areas may become increasingly important. Assessing the spatial distribution of such units may provide important knowledge for land-managers in the near future, especially given the identified/indicated functioning here.

- Shape, size, topographic position and aspect of low-storage systems will indubitably affect the magnitude of influxes and losses, as well as drivers thereof (e.g. internal and external shading modulating energy budget). Researchers may wish to assess scale-limits (minimum, maximum size) to the observed functioning here, as to better inform restoration planning as well as for delineating priority areas/systems under current and future conditions.

6.5 Final remarks

Research presented in this thesis provides novel insight on the functioning that can be provided by small, forested swamps as low-storage areas in the hydro(geo)logically complex Boreal Plain by addressing four research gaps identified in Section 1.3. In particular, it improved understanding of hydrological responses in aspen-dominated catchments, and with a focus on climate and storage dynamics, may aid in inception of future research in and/or further inform conceptualization of the Boreal Plain. Identified and implied ecohydrological processes and interactions, most notably ET reduction and water supplementation to adjacent upland trees, may provide valuable information for land-managers aiming to decrease impacts of anthropogenical disturbance, or restoration planners designing landscapes with conflicting goals of water security (maintenance of flows) and forest productivity (requiring ET).

Bibliography

Abatzoglou JT, Dobrowski SZ, Parks SA, Hegewisch KC. 2018. TerraClimate, a high-resolution global dataset of monthly climate and climatic water balance from 19582015. *Scientific Data* **5**: 170191 DOI: 10.1038/sdata.2017.191

Abd Latif Z, Blackburn GA. 2010. The effects of gap size on some microclimate variables during late summer and autumn in a temperate broadleaved deciduous forest. *International Journal of Biometeorology* **54** (2): 119–129 DOI: 10.1007/s00484-009-0260-1

ABMI. 2017. The Status of Human Footprint in Alberta: Preliminary Report. The Alberta Biodiversity Monitoring Institute, Alberta, Edmonton, Canada.

Ali GA, L'Heureux C, Roy AG, Turmel M-C, Courchesne F. 2011. Linking spatial patterns of perched groundwater storage and stormflow generation processes in a headwater forested catchment. *Hydrological Processes* **25** (25): 3843–3857 DOI: 10.1002/hyp.8238

Allen RG, Pereira LS, Raes D, Smith M, others. 1998. Crop evapotranspiration-Guidelines for computing crop water requirements-FAO Irrigation and drainage paper 56. *Fao, Rome* **300** (9): D05109

Allen ST. 2016. Ecological-Hydrological Feedback in Forested Wetlands.LSU Doctoral Dissertations. 433, Louisiana State University; Agricultural; Mechanical College.

Allen ST, Edwards BL, Reba ML, Keim RF. 2016. Sub-canopy Evapotranspiration from Floating Vegetation and Open Water in a Swamp Forest. *Wetlands* **36** (4): 681–688 DOI: 10.1007/s13157-016-0778-z

Allen ST, Reba ML, Edwards BL, Keim RF. 2017. Evaporation and the subcanopy energy environment in a flooded forest. *Hydrological Processes* **31** (16): 2860–2871 DOI: 10.1002/hyp.11227

An N, Tang C-S, Xu S-K, Gong X-P, Shi B, Inyang HI. 2018. Effects of soil characteristics on moisture evaporation. *Engineering Geology* **239**: 126–135

Anderson AE, Weiler M, Alila Y, Hudson RO. 2010. Piezometric response in zones of a watershed with lateral preferential flow as a first-order control on subsurface flow. *Hydrological Processes* **24** (16): 2237–2247 DOI: 10.1002/hyp.7662

Anderson E. 1976. A point and mass balance model of a snow cover. NWS-19. US Department of Commerce, Washington, DC.

Angstmann JL, Ewers BE, Kwon H. 2012. Size-mediated tree transpiration along soil drainage gradients in a boreal black spruce forest wildfire chronosequence. *Tree physiology* **32** (5): 599–611

Atkinson SE, Woods RA, Sivapalan M. 2002. Climate and landscape controls on water balance model complexity over changing timescales. *Water Resources Research* **38** (12): 50–1–50–17 DOI: 10.1029/2002WR001487

Bachmair S, Weiler M. 2011. New dimensions of hillslope hydrology. In *Forest Hydrology and Biogeochemistry*Springer; 455–481.

Baldocchi D, Kelliher FM, Black TA, Jarvis P. 2000. Climate and vegetation controls on boreal zone energy exchange. *Global Change Biology* **6** (S1): 69–83 DOI: 10.1046/j.1365-2486.2000.06014.x

Baldocchi DD, Meyers TP. 1988. Turbulence structure in a deciduous forest. *Boundary-Layer Meteorology* **43** (4): 345–364 DOI: 10.1007/BF00121712

Barber VA, Juday GP, Finney BP. 2000. Reduced growth of Alaskan white spruce in the twentieth century from temperature-induced drought stress. *Nature* **405** (6787): 668–673 DOI: 10.1038/35015049

Barbier S, Balandier P, Gosselin F. 2009. Influence of several tree traits on rainfall partitioning in temperate and boreal forests: A review. *Annals of Forest Science* **66** (6): 602–602 DOI: 10.1051/forest/2009041

Barr AG, van der Kamp G, Black TA, McCaughey JH, Nesic Z. 2012. Energy balance closure at the BERMS flux towers in relation to the water balance of the White Gull Creek watershed 19992009. *Agricultural and Forest Meteorology* **153**: 3–13 DOI: 10.1016/j.agrformet.2011.05.017

Bauer IE, Bhatti JS, Swanston C, Wieder RK, Preston CM. 2009. Organic Matter Accumulation and Community Change at the PeatlandUpland Interface: Inferences from 14C and 210Pb Dated Profiles. *Ecosystems* **12** (4): 636–653 DOI: 10.1007/s10021-009-9248-2

Bauer IE, Gignac LD, Vitt DH. 2003. Development of a peatland complex in boreal western Canada: Lateral site expansion and local variability in vegetation succession and long-term peat accumulation. *Canadian Journal of Botany* **81** (8): 833–847 DOI: 10.1139/b03-076

Bedient PB, Huber WC, Vieux BE, others. 2008. Hydrology and floodplain analysis

Bishop K, Seibert J, Köhler S, Laudon H. 2004. Resolving the Double Paradox of rapidly mobilized old water with highly variable responses in runoff chemistry. *Hydrological Processes* **18** (1): 185–189 DOI: 10.1002/hyp.5209

Black PE. 1997. Watershed Functions. *JAWRA Journal of the American Water Resources Association* **33** (1): 1–11 DOI: 10.1111/j.1752-1688.1997.tb04077.x

Black T, Kelliher F. 1989. Processes controlling understorey evapotranspiration. *Philosophical Transactions of the Royal Society of London. B, Biological Sciences* **324** (1223): 207–231

Blume H-P, Brümmer GW, Horn R, Kandeler E, Kögel-Knabner I, Kretzschmar R, Stahr K, Wilke B-M. 2016. *Scheffer/schachtschabel: Lehrbuch der bodenkunde*. Springer-Verlag.

Bocking E, Cooper DJ, Price J. 2017. Using tree ring analysis to determine impacts of a road on a boreal peatland. *Forest Ecology and Management* **404** (Supplement C): 24–30 DOI: 10.1016/j.foreco.2017.08.007

Bond-Lamberty B, Peckham SD, Gower ST, Ewers BE. 2009. Effects of fire on regional evapotranspiration in the central Canadian boreal forest. *Global Change Biology* **15**

(5): 1242–1254 DOI: 10.1111/j.1365-2486.2008.01776.x

Bond-Lamberty B, Wang C, Gower ST. 2002. Aboveground and belowground biomass and sapwood area allometric equations for six boreal tree species of northern Manitoba. *Canadian Journal of Forest Research* **32** (8): 1441–1450

Bothe RA, Abraham C. 1993. *Evaporation and evapotranspiration in Alberta 1986 to 1992 addendum.* Surface Water Assessment Branch, Technical Services & Monitoring Division, Water Resources Services, Alberta Environmental Protection.

Bourgault M-A, Larocque M, Garneau M. 2019. How do hydrogeological setting and meteorological conditions influence water table depth and fluctuations in ombrotrophic peatlands? *Journal of Hydrology X* **4**: 100032 DOI: 10.1016/j.hydroa.2019.100032

Bourgeois B, Vanasse A, González E, Andersen R, Poulin M. 2016. Threshold dynamics in plant succession after tree planting in agricultural riparian zones. *Journal of Applied Ecology* **53** (6): 1704–1713 DOI: 10.1111/1365-2664.12675

Bracken LJ, Wainwright J, Ali GA, Tetzlaff D, Smith MW, Reaney SM, Roy AG. 2013. Concepts of hydrological connectivity: Research approaches, pathways and future agendas. *Earth-Science Reviews* **119**: 17–34 DOI: 10.1016/j.earscirev.2013.02.001

Brannen R, Spence C, Ireson A. 2015. Influence of shallow groundwaterSurface water interactions on the hydrological connectivity and water budget of a wetland complex. *Hydrological Processes* **29** (18): 3862–3877

Braverman M, Quinton WL. 2016. Hydrological impacts of seismic lines in the wetland-dominated zone of thawing, discontinuous permafrost, Northwest Territories, Canada. *Hydrological Processes* **30** (15): 2617–2627 DOI: 10.1002/hyp.10695

Brolsma RJ, Bierkens MFP. 2007. GroundwaterSoil waterVegetation dynamics in a temperate forest ecosystem along a slope. *Water Resources Research* **43** (1) DOI: 10.1029/2005WR004696

Brooks RT, Hayashi M. 2002. Depth-area-volume and hydroperiod relationships of ephemeral (vernal) forest pools in southern New England. *Wetlands* **22** (2): 247–255 DOI: 10.1672/0277-5212(2002)022[0247:DAVAHR]2.0.CO;2

Brown RL, Naeth MA. 2014. Woody Debris Amendment Enhances Reclamation after Oil Sands Mining in Alberta, Canada. *Restoration Ecology* **22** (1): 40–48 DOI: 10.1111/rec.12029

Brown SM, Petrone RM, Chasmer L, Mendoza CA, Lazerjan MS, Landhäusser SM, Silins U, Leach J, Devito KJ. 2014a. Atmospheric and soil moisture controls on evapotranspiration from above and within a Western Boreal Plain aspen forest. *Hydrological Processes* **28** (15): 4449–4462 DOI: 10.1002/hyp.9879

Brown SM, Petrone RM, Chasmer L, Mendoza C, Lazerjan MS, Landhäusser SM, Silins U, Leach J, Devito KJ. 2014b. Atmospheric and soil moisture controls on evapotranspiration from above and within a Western Boreal Plain aspen forest. *Hydrological Processes* **28** (15): 4449–4462 DOI: 10.1002/hyp.9879

Brown SM, Petrone RM, Mendoza C, Devito KJ. 2010. Surface vegetation controls on evapotranspiration from a sub-humid Western Boreal Plain wetland. *Hydrological Processes* **24** (8): 1072–1085 DOI: 10.1002/hyp.7569

Buckley TN. 2005a. The control of stomata by water balance: Tansley review. *New Phytologist* **168** (2): 275–292 DOI: 10.1111/j.1469-8137.2005.01543.x

Buckley TN. 2005b. The control of stomata by water balance. *New Phytologist* **168** (2): 275–292

Budyko MI, Miller DH, Miller DH. 1974. *Climate and life*. Academic press New York.

Bunn A, Korpela M, Biondi F, Campelo F, Mérian P, Qeadan F, Zang C. 2017. dplR: Dendrochronology Program Library in R. R package version 1.6.6

Burgess SS, Adams MA, Turner NC, Beverly CR, Ong CK, Khan AA, Bleby TM. 2001. An improved heat pulse method to measure low and reverse rates of sap flow in woody plants. *Tree physiology* **21** (9): 589–598

Buttle J, Boon S, Peters D, Spence C, van Meerveld H, Whitfield P. 2012. An overview of temporary stream hydrology in Canada. *Canadian Water Resources Journal* **37** (4): 279–310

Buttle J, Creed I, Moore R. 2009. Advances in Canadian forest hydrology, 2003-2007. *Canadian Water Resources Journal* **34** (2): 113–126

Carey SK, Woo M-k. 2001a. Spatial variability of hillslope water balance, wolf creek basin, subarctic yukon. *Hydrological Processes* **15** (16): 3113–3132 DOI: 10.1002/hyp.319

Carey SK, Woo M-k. 2001b. Slope runoff processes and flow generation in a subarctic, subalpine catchment. *Journal of Hydrology* **253** (1): 110–129 DOI: 10.1016/S0022-1694(01)00478-4

Carey SK, Tetzlaff D, Seibert J, Soulsby C, Buttle J, Laudon H, McDonnell J, McGuire K, Caissie D, Shanley J, et al. 2010. Inter-comparison of hydro-climatic regimes across northern catchments: Synchronicity, resistance and resilience. *Hydrological Processes* **24** (24): 3591–3602

Carrera-Hernández J, Mendoza CA, Devito KJ, Petrone RM, Smerdon BD. 2011. Effects of aspen harvesting on groundwater recharge and water table dynamics in a subhumid climate. *Water Resources Research* **47** (5)

Chhin S, Wang GG, Tardif J. 2004a. Dendroclimatic Analysis of White Spruce at its Southern Limit of Distribution in the Spruce Woods Provincial Park, Manitoba, Canada. *Tree-Ring Research* **60** (1): 31–43 DOI: 10.3959/1536-1098-60.1.31

Chhin S, Wang GG, Tardif J. 2004b. Dendroclimatic Analysis of White Spruce at its Southern Limit of Distribution in the Spruce Woods Provincial Park, Manitoba, Canada. *Tree-Ring Research* **60** (1): 31–43 DOI: 10.3959/1536-1098-60.1.31

Clark RB, Creed IF, Sass GZ. 2009. Mapping hydrologically sensitive areas on the Boreal Plain: A multitemporal analysis of ERS synthetic aperture radar data. *International Journal of Remote Sensing* **30** (10): 2619–2635 DOI: 10.1080/01431160802552819

Cohen MJ, Creed IF, Alexander L, Basu NB, Calhoun AJK, Craft C, D'Amico E, DeKeyser E, Fowler L, Golden HE, et al. 2016. Do geographically isolated wetlands influence landscape functions? *Proceedings of the National Academy of Sciences* **113** (8): 1978–1986

Condon LE, Maxwell RM. 2017. Systematic shifts in Budyko relationships caused by groundwater storage changes. *Hydrology and Earth System Sciences* **21** (2): 1117–1135 DOI: 10.5194/hess-21-1117-2017

Cook ER, Kairiukstis LA. 2013. *Methods of dendrochronology: Applications in the environmental sciences*. Springer Science & Business Media.

Cortini F, Comeau PG, Bokalo M. 2012. Trembling aspen competition and climate effects on white spruce growth in boreal mixtures of Western Canada. *Forest Ecology and Management* **277**: 67–73 DOI: 10.1016/j.foreco.2012.04.022

Cosgrove DJ. 2005. Growth of the plant cell wall. *Nature Reviews Molecular Cell Biology* **6** (11): 850–861 DOI: 10.1038/nrm1746

Creed IF, Sanford SE, Beall FD, Molot LA, Dillon PJ. 2003. Cryptic wetlands: Integrating hidden wetlands in regression models of the export of dissolved organic carbon from forested landscapes. *Hydrological Processes* **17** (18): 3629–3648

Dabros A, Pyper M, Castilla G. 2018. Seismic lines in the boreal and arctic ecosystems of North America: Environmental impacts, challenges, and opportunities. *Environmental Reviews* **26** (2): 214–229 DOI: 10.1139/er-2017-0080

Dalu T, Wasserman RJ, Dalu MTB. 2016. Agricultural intensification and drought frequency increases may have landscape-level consequences for ephemeral ecosystems. *Global Change Biology*

Dang QL, Lieffers VJ. 1989a. Climate and annual ring growth of black spruce in some Alberta peatlands. *Canadian Journal of Botany* **67** (6): 1885–1889 DOI: 10.1139/b89-239

Dang QL, Lieffers VJ. 1989b. Assessment of patterns of response of tree ring growth of black spruce following peatland drainage. *Canadian Journal of Forest Research* **19** (7): 924–929 DOI: 10.1139/x89-140

Dang QL, Margolis HA, Coyea MR, Sy M, Collatz GJ. 1997. Regulation of branch-level gas exchange of boreal trees: Roles of shoot water potential and vapor pressure difference. *Tree Physiology* **17** (8-9): 521–535 DOI: 10.1093/treephys/17.8-9.521

Davis TW, Kuo C-M, Liang X, Yu P-S. 2012. Sap Flow Sensors: Construction, Quality Control and Comparison. *Sensors* **12** (12): 954–971 DOI: 10.3390/s120100954

DeLancey ER, Kariyeva J, Bried JT, Hird JN. 2019. Large-scale probabilistic identification of boreal peatlands using Google Earth Engine, open-access satellite data, and machine learning. *PLOS ONE* **14** (6): e0218165 DOI: 10.1371/journal.pone.0218165

Denne MP. 1989. Definition of Latewood According to Mork (1928). *IAWA Journal* **10** (1): 59–62 DOI: 10.1163/22941932-90001112

Depante M, Morison MQ, Petrone RM, Devito KJ, Kettridge N, Waddington JM. 2019. Hydraulic redistribution and hydrological controls on aspen transpiration and establishment in peatlands following wildfire. *Hydrological Processes* **33** (21): 2714–2728 DOI: 10.1002/hyp.13522

DesRochers A, Lieffers VJ. 2001. The coarse-root system of mature Populus tremuloides in declining stands in Alberta, Canada. *Journal of Vegetation Science* **12** (3): 355–360 DOI: 10.2307/3236849

Devito KJ, Creed IF, Fraser CJD. 2005a. Controls on Runoff from a Partially Harvested Aspen-Forested Headwater Catchment, Boreal Plain, Canada. *Hydrological Processes* **19** (1): 3–25 DOI: 10.1002/hyp.5776

Devito KJ, Creed I, Gan T, Mendoza CA, Petrone R, Silins U, Smerdon B. 2005b. A framework for broad-scale classification of hydrologic response units on the Boreal Plain: Is topography the last thing to consider? *Hydrological Processes* **19** (8): 1705–1714 DOI: 10.1002/hyp.5881

Devito KJ, Dillon PJ, Lazerte BD. 1989. Phosphorus and nitrogen retention in five Precambrian shield wetlands. *Biogeochemistry* **8** (3): 185–204 DOI: 10.1007/BF00002888

Devito KJ, Hill A, Roulet N. 1996. Groundwater-surface water interactions in headwater forested wetlands of the Canadian Shield. *Journal of Hydrology* **181** (1): 127–147

Devito KJ, Hokanson KJ, Moore PA, Kettridge N, Anderson AE, Chasmer L, Hopkinson C, Lukenbach MC, Mendoza CA, Morissette J, et al. 2017. Landscape controls on long-term runoff in subhumid heterogeneous Boreal Plains catchments. *Hydrological Processes* **31** (15): 2737–2751 DOI: 10.1002/hyp.11213

Devito KJ, Mendoza CA, Petrone RM, Kettridge N, Waddington JM. 2016. Utikuma Region Study Area (URSA) Part 1: Hydrogeological and ecohydrological studies (HEAD). *The Forestry Chronicle* **92** (01): 57–61 DOI: 10.5558/tfc2016-017

Devito KJ, Mendoza CA, Qualizza C. 2012. Conceptualizing Water Movement in the Boreal Plains. Implications for Watershed Reconstruction. Synthesis Report Prepared for the Canadian Oil Sands Network for Research and Development, Environmental and Reclamation Research Group. 164 Pp.

Devito KJ, Waddington JM, Branfireun BA. 1997. Flow Reversals in Peatlands Influenced by Local Groundwater Systems. *Hydrological Processes* **11** (1): 103–110 DOI: 10.1002/(SICI)1099-1085(199701)11:1<103::AID-HYP417>3.0.CO;2-E

Dixon M, Johnson R. 1993. Interpretation of the dynamics of plant water potential. *Water transport in plants under climatic stress, Cambridge University Press, Cambridge*: 63–75

Dixon SJ, Kettridge N, Moore PA, Devito KJ, Tilak AS, Petrone RM, Mendoza CA, Waddington JM. 2017. Peat depth as a control on moss water availability under evaporative stress. *Hydrological Processes* **31** (23): 4107–4121 DOI: 10.1002/hyp.11307

Doss PK. 1993. The Nature of a Dynamic Water Table in a System of Non-Tidal, Freshwater Coastal Wetlands. *Journal of Hydrology* **141** (1): 107–126 DOI: 10.1016/0022-1694(93)90046-C

Ducks Unlimited Canada. 2000. Duck's unlimited's vision for the western boreal forest. Ducks Unlimited Canada, Western Boreal Forest Initiative, Stonewall, MB.

Ducks Unlimited Canada. 2011. Enhanced wetland classification inferred products users guide version 1.0

Dupont S, Patton EG. 2012. Momentum and scalar transport within a vegetation canopy following atmospheric stability and seasonal canopy changes: The CHATS experiment. *Atmospheric Chemistry and Physics* **12** (13): 5913–5935

Eamus D, Huete A, Yu Q. 2016. *Vegetation dynamics*. Cambridge University Press.

Elshorbagy A, Jutla A, Barbour L, Kells J. 2005. System dynamics approach to assess the sustainability of reclamation of disturbed watersheds. *Canadian Journal of Civil Engineering* **32** (1): 144–158 DOI: 10.1139/l04-112

Euliss NH, LaBaugh JW, Fredrickson LH, Mushet DM, Laubhan MK, Swanson GA, Winter TC, Rosenberry DO, Nelson RD. 2004. The wetland continuum: A conceptual framework for interpreting biological studies. *Wetlands* **24** (2): 448–458 DOI: 10.1672/0277-5212(2004)024[0448:TWCACF]2.0.CO;2

Eyles N, Boyce J, Barendregt R. 1999. Hummocky moraine; sedimentary record of stagnant Laurentide Ice Sheet lobes resting on soft beds; reply. *Sedimentary Geology* **129**: 169–171

Falkenmark M. 2013. Adapting to climate change: Towards societal water security in dry-climate countries. *International Journal of Water Resources Development* **29** (2): 123–136 DOI: 10.1080/07900627.2012.721714

Farmer D, Sivapalan M, Jothityangkoon C. 2003. Climate, soil, and vegetation controls upon the variability of water balance in temperate and semiarid landscapes: Downward approach to water balance analysis. *Water Resources Research* **39** (2) DOI: 10.1029/2001WR000328

Fatichi S, Pappas C. 2017. Constrained variability of modeled T:ET ratio across biomes. *Geophysical Research Letters* **44** (13): 6795–6803 DOI: 10.1002/2017GL074041

Fenton M, Waters E, Pawley S, Atkinson N, Utting D, Mckay K. 2013. Surficial Geology of Alberta. Map 601

Fenton MM, Paulen RC, Pawlowicz JG. 2005. Surficial Geology of the Lubicon Lake Area, Alberta (NTS 84B/SW)

Ferone JM, Devito KJ. 2004. Shallow groundwaterSurface water interactions in pond-Peatland complexes along a Boreal Plains topographic gradient. *Journal of Hydrology* **292** (1-4): 75–95 DOI: 10.1016/j.jhydrol.2003.12.032

Forsch KBC. 2014. Oil Sands Reclamation With Woody Debris Using LFH Mineral Soil Mix And Peat Mineral Soil Mix Cover Soils: Impacts On Select Soil And Vegetation Properties.MSc Thesis, University of Alberta, Edmonton, Alberta, Canada. DOI: 10.7939/R39G5GM3P

Frazer GW, Canham C, Lertzman K. 1999. Gap Light Analyzer (GLA), Version 2.0: Imaging software to extract canopy structure and gap light transmission indices from true-colour fisheye photographs, users manual and program documentation. *Simon Fraser University, Burnaby, British Columbia, and the Institute of Ecosystem Studies, Millbrook, New York* **36**

Freer J, McDonnell JJ, Beven KJ, Peters NE, Burns DA, Hooper RP, Aulenbach B, Kendall C. 2002. The role of bedrock topography on subsurface storm flow. *Water Resources Research* **38** (12): 5–1–5–16 DOI: 10.1029/2001WR000872

Frey BR, Lieffers VJ, Hogg E(, Landhäusser SM. 2004. Predicting landscape patterns of aspen dieback: Mechanisms and knowledge gaps. *Canadian Journal of Forest Research* **34** (7): 1379–1390 DOI: 10.1139/x04-062

Fritts HC, Swetnam TW. 1989. Dendroecology: A Tool for Evaluating Variations in Past and Present Forest Environments. *Advances in ecological research* **19**: 111–188

Gao H, Hrachowitz M, Schymanski SJ, Fenicia F, Sriwongsitanon N, Savenije HHG. 2014. Climate controls how ecosystems size the root zone storage capacity at catchment scale. *Geophysical Research Letters* **41** (22): 7916–7923 DOI: 10.1002/2014GL061668

Gärtner H, Nievergelt D. 2010. The core-microtome: A new tool for surface preparation on cores and time series analysis of varying cell parameters. *Dendrochronologia* **28** (2): 85–92 DOI: 10.1016/j.dendro.2009.09.002

Gibson JJ, Birks SJ, Yi Y, Vitt DH. 2015. Runoff to boreal lakes linked to land cover, watershed morphology and permafrost thaw: A 9-year isotope mass balance assessment: Boreal Lakes Isotope Mass Balance Assessment. *Hydrological Processes* **29** (18): 3848–3861 DOI: 10.1002/hyp.10502

Girardin MP, Bouriaud O, Hogg EH, Kurz W, Zimmermann NE, Metsaranta JM, de Jong R, Frank DC, Esper J, Büntgen U, et al. 2016. No Growth Stimulation of Canada's Boreal Forest under Half-Century of Combined Warming and CO2 Fertilization. *Proceedings of the National Academy of Sciences* **113** (52): E8406–E8414 DOI: 10.1073/pnas.1610156113

Goetz JD, Price JS. 2015. Role of morphological structure and layering of Sphagnum and Tomenthypnum mosses on moss productivity and evaporation rates. *Canadian Journal of Soil Science* **95** (2): 109–124 DOI: 10.4141/cjss-2014-092

Goodbrand A, Westbrook CJ, Kamp G van der. 2018. Hydrological Functions of a Peatland in a Boreal Plains Catchment. *Hydrological Processes* DOI: 10.1002/hyp.13343

Grayson RB, Western AW, Chiew FHS, Blöschl G. 1997. Preferred states in spatial soil moisture patterns: Local and nonlocal controls. *Water Resources Research* **33** (12): 2897–2908 DOI: 10.1029/97WR02174

Grosse G, Harden J, Turetsky M, McGuire AD, Camill P, Tarnocai C, Frolking S, Schuur EAG, Jorgenson T, Marchenko S, et al. 2018. Vulnerability of high-latitude soil organic carbon in North America to disturbance. *Journal of Geophysical Research: Biogeosciences* DOI: 10.1029/2010JG001507@10.1002/(ISSN)2169-8961.IMPACTNA1

Group CC on E(LCNWW, Warner BG, Rubec C. 1997. *The Canadian wetland classification system*. Wetlands Research Branch, University of Waterloo.

Hanson A, Swanson L, Ewing D, Grabas G, Meyer S, Ross L, Watmough M, Kirkby J. 2008. Wetland ecological functions assessment: An overview of approaches. *Canadian Wildlife Service Technical Report Series* **16** (2): 123–125

Hayashi M, van der Kamp G, Rudolph DL. 1998. Water and solute transfer between a prairie wetland and adjacent uplands, 1. Water balance. *Journal of Hydrology* **207** (1): 42–55

Heijmans MMPD, Arp WJ, Chapin FS. 2004. Controls on moss evaporation in a boreal black spruce forest. *Global Biogeochemical Cycles* **18** (2) DOI: 10.1029/2003GB002128

Hewlett JD, Hibbert AR. 1967. Factors affecting the response of small watersheds to precipitation in humid areas. *Forest hydrology* **1**: 275–290

Hogg EH, Bernier PY. 2005. Climate change impacts on drought-prone forests in western Canada. *The Forestry Chronicle* **81** (5): 675–682 DOI: 10.5558/tfc81675-5

Hogg EH, Hurdle PA. 1995. The aspen parkland in western Canada: A dry-climate analogue for the future boreal forest? *Water, Air, and Soil Pollution* **82** (1): 391–400 DOI: 10.1007/BF01182849

Hogg EH, Hurdle PA. 1997. Sap flow in trembling aspen: Implications for stomatal responses to vapor pressure deficit. *Tree Physiology* **17** (8-9): 501–509

Hogg EH, Wein RW. 2005. Impacts of drought on forest growth and regeneration following fire in southwestern Yukon, Canada. *Canadian Journal of Forest Research* **35** (9): 2141–2150 DOI: 10.1139/x05-120

Hogg EH, Barr AG, Black TA. 2013. A Simple Soil Moisture Index for Representing Multi-Year Drought Impacts on Aspen Productivity in the Western Canadian Interior. *Agricultural and Forest Meteorology* **178-179**: 173–182 DOI: 10.1016/j.agrformet.2013.04.025

Hogg EH, Brandt JP, Kochtubajda B. 2002. Growth and dieback of aspen forests in northwestern Alberta, Canada, in relation to climate and insects. *Canadian Journal of Forest Research* **32** (5): 823–832 DOI: 10.1139/x01-152

Hogg EH, Brandt JP, Kochtubajda B. 2005. Factors affecting interannual variation in growth of western Canadian aspen forests during 1951-2000. *Canadian Journal of Forest Research* **35** (3): 610–622 DOI: 10.1139/x04-211

Hogg EH, Saugier B, Pontailler J-Y, Black TA, Chen W, Hurdle PA, Wu A. 2000. Responses of trembling aspen and hazelnut to vapor pressure deficit in a boreal deciduous forest. *Tree Physiology* **20** (11): 725–734 DOI: 10.1093/treephys/20.11.725

Hokanson KJ, Mendoza CA, Devito KJ. 2018a. Interactions between regional climate, surficial geology, and topography: Characterizing shallow groundwater systems in sub-humid, low-relief landscapes. *Water Resources Research* DOI: 10.1029/2018WR023934

Hokanson KJ, Moore PA, Lukenbach MC, Devito KJ, Kettridge N, Petrone RM, Mendoza CA, Waddington JM. 2018b. A hydrogeological landscape framework to identify peatland wildfire smouldering hot spots. *Ecohydrology* **11** (4): e1942 DOI: 10.1002/eco.1942

Holecek G. 1988. Storage-effective drainage (SED) runoff model. *Journal of Hydrology* **98** (3-4): 295–314 DOI: 10.1016/0022-1694(88)90019-4

Hollinger DY, Kelliher FM, Schulze E-D, Köstner BMM. 1994. Coupling of tree transpiration to atmospheric turbulence. *Nature* **371** (6492): 60 DOI: 10.1038/371060a0

Holmes RL. 1983. Computer-assisted quality control in tree-ring dating and measurement

Hsiao TC, Acevedo E. 1975. Plant Responses to Water Deficits, Water-Use Efficiency, and Drought Resistance. In *Developments in Agricultural and Managed Forest Ecology*, Stone JF (ed.).Elsevier; 59–84. DOI: 10.1016/B978-0-444-41273-7.50012-X

Hufkens K, Basler D, Milliman T, Melaas EK, Richardson AD. 2018. An integrated phenology modelling framework in R: Modelling vegetation phenology with phenor. *Methods in Ecology & Evolution* **9**: 1–10

Hvorslev MJ. 1951. *Time lag and soil permeability in ground-water observations.* Corps of Engineers, U.S. Army, Waterways Experiment Station: Vicksburg.

Iida S, Ohta T, Matsumoto K, Nakai T, Kuwada T, Kononov AV, Maximov TC, van der Molen MK, Dolman H, Tanaka H, et al. 2009. Evapotranspiration from understory vegetation in an eastern Siberian boreal larch forest. *Agricultural and Forest Meteorology* **149** (6): 1129–1139 DOI: 10.1016/j.agrformet.2009.02.003

Immerzeel WW, Bierkens MFP. 2012. Asia's water balance. *Nature Geoscience* **5**: 841–842 DOI: 10.1038/ngeo1643

Ireson AM, Barr AG, Johnstone JF, Mamet SD, van der Kamp G, Whitfield CJ, Michel NL, North RL, Westbrook CJ, DeBeer C, et al. 2015. The changing water cycle: The Boreal Plains ecozone of Western Canada: The changing water cycle in the Boreal Plains ecozone. *Wiley Interdisciplinary Reviews: Water* **2** (5): 505–521 DOI: 10.1002/wat2.1098

Jackson RB, Jobbágy EG, Nosetto MD. 2009. Ecohydrology in a human-dominated landscape. *Ecohydrology* **2** (3): 383–389 DOI: 10.1002/eco.81

James LM. 2017. Formation and maintenance of permanent perched wetlands in the Boreal Plain of Western Canada.MSc Thesis, University of Alberta, Edmonton, Alberta, Canada. DOI: 10.7939/R3930P68H

Jencso KG, McGlynn BL, Gooseff MN, Wondzell SM, Bencala KE, Marshall LA. 2009. Hydrologic Connectivity between Landscapes and Streams: Transferring Reach- and Plot-Scale Understanding to the Catchment Scale. *Water Resources Research* **45** (4) DOI: 10.1029/2008WR007225

Jevsenak J, Levanic T. 2018. dendroTools: R package for studying linear and nonlinear responses between tree-rings and daily environmental data. *Dendrochronologia* **48**: 32–39 DOI: 10.1016/j.dendro.2018.01.005

Jobling J. 1990. Poplars for wood production and amenity. *Forestry Commission Bulletin (United Kingdom)*

Johnson EA, Miyanishi K, Weir JMH. 1998. Wildfires in the western Canadian boreal forest: Landscape patterns and ecosystem management. *Journal of Vegetation Science* **9** (4): 603–610 DOI: 10.2307/3237276

Jones B, Tardif J, Westwood R. 2004. Weekly xylem production in trembling aspen (*Populus Tremuloides*) in response to artificial defoliation. *Canadian Journal of Botany* **82** (5): 590–597 DOI: 10.1139/b04-032

Jones HG. 2013. *Plants and microclimate: A quantitative approach to environmental plant physiology*. Cambridge university press.

Jung M, Reichstein M, Ciais P, Seneviratne SI, Sheffield J, Goulden ML, Bonan G, Cescatti A, Chen J, de Jeu R, et al. 2010. Recent decline in the global land evapotranspiration trend due to limited moisture supply. *Nature* **467** (7318): 951–954 DOI: 10.1038/nature09396

Keddy PA. 2010. *Wetland ecology: Principles and conservation*. Cambridge University Press.

Kettridge N, Waddington J. 2014. Towards quantifying the negative feedback regulation of peatland evaporation to drought. *Hydrological Processes* **28** (11): 3728–3740

Kettridge N, Lukenbach MC, Hokanson KJ, Devito KJ, Petrone RM, Mendoza CA, Waddington JM. 2019. Severe wildfire exposes remnant peat carbon stocks to increased post-fire drying. *Scientific Reports* **9** (1): 3727 DOI: 10.1038/s41598-019-40033-7

Kettridge N, Lukenbach MC, Hokanson KJ, Hopkinson C, Devito KJ, Petrone RM, Mendoza CA, Waddington JM. 2017. Low Evapotranspiration Enhances the Resilience of Peatland Carbon Stocks to Fire. *Geophysical Research Letters* **44** (18): 9341–9349 DOI: 10.1002/2017GL074186

Kettridge N, Thompson DK, Bombonato L, Turetsky MR, Benscoter BW, Waddington JM. 2013. The ecohydrology of forested peatlands: Simulating the effects of tree shading on moss evaporation and species composition. *Journal of Geophysical Research: Biogeosciences* **118** (2): 422–435 DOI: 10.1002/jgrg.20043

Kettridge N, Turetsky MR, Sherwood JH, Thompson DK, Miller CA, Benscoter BW, Flannigan MD, Wotton BM, Waddington JM. 2015. Moderate Drop in Water Table Increases Peatland Vulnerability to Post-Fire Regime Shift. *Scientific Reports* **5** (1)

DOI: 10.1038/srep08063

Kirchner JW. 2009. Catchments as simple dynamical systems: Catchment characterization, rainfall-runoff modeling, and doing hydrology backward. *Water Resources Research* **45** (2) DOI: 10.1029/2008WR006912

Klaus J, McDonnell J, Jackson C, Du E, Griffiths N. 2015. Where does streamwater come from in low-relief forested watersheds? A dual-isotope approach. *Hydrology and Earth System Sciences* **19** (1): 125–135

Kozlowski TT, Pallardy SG. 1996. *Physiology of woody plants*. Elsevier.

Kuraś PK, Weiler M, Alila Y. 2008. The spatiotemporal variability of runoff generation and groundwater dynamics in a snow-dominated catchment. *Journal of Hydrology* **352** (1): 50–66 DOI: 10.1016/j.jhydrol.2007.12.021

Kurz WA, Shaw CH, Boisvenue C, Stinson G, Metsaranta J, Leckie D, Dyk A, Smyth C, Neilson ET. 2013. Carbon in Canada's boreal forest A synthesis. *Environmental Reviews* **21** (4): 260–292 DOI: 10.1139/er-2013-0041

Lafleur PM. 2008. Connecting Atmosphere and Wetland: Energy and Water Vapour Exchange. *Geography Compass* **2** (4): 1027–1057 DOI: 10.1111/j.1749-8198.2007.00132.x

Lafleur PM, Schreader CP. 1994. Water Loss from the Floor of a Subarctic Forest. *Arctic and Alpine Research* **26** (2): 152–158 DOI: 10.1080/00040851.1994.12003051

Lafleur PM, Hember RA, Admiral SW, Roulet NT. 2005. Annual and seasonal variability in evapotranspiration and water table at a shrub-covered bog in southern Ontario, Canada. *Hydrological Processes* **19** (18): 3533–3550 DOI: 10.1002/hyp.5842

Langlois MN, Price JS, Rochefort L. 2015. Landscape Analysis of Nutrient-Enriched Margins (Lagg) in Ombrotrophic Peatlands. *Science of The Total Environment* **505**: 573–586 DOI: 10.1016/j.scitotenv.2014.10.007

Laskin DN, McDermid GJ, Nielsen SE, Marshall SJ, Roberts DR, Montaghi A. 2019. Advances in phenology are conserved across scale in present and future climates. *Nature Climate Change* **9** (5): 419 DOI: 10.1038/s41558-019-0454-4

LaZerte SE, Albers S. 2018. Weathercan: Download and format weather data from Environment and Climate Change Canada. *J. Open Source Software* **3** (22): 571

Leibowitz SG, Brooks RT. 2008. Hydrology and landscape connectivity of vernal pools. *Science and conservation of vernal pools in northeastern North America. CRC, Boca Raton, Florida*

Lemprière T, Kurz W, Hogg E, Schmoll C, Rampley G, Yemshanov D, McKenney D, Gilsenan R, Beatch A, Blain D, et al. 2013. Canadian boreal forests and climate change mitigation. *Environmental Reviews* **21** (4): 293–321 DOI: 10.1139/er-2013-0039

Lieffers VJ, Landhäusser SM, Hogg EH. 2001. Is the Wide Distribution of Aspen a Result of Its Stress Tolerance? 14

Limpens J, Holmgren M, Jacobs CMJ, Zee SEATMV der, Karofeld E, Berendse F. 2014. How Does Tree Density Affect Water Loss of Peatlands? A Mesocosm Experiment. *PLOS ONE* **9** (3): e91748 DOI: 10.1371/journal.pone.0091748

Little-Devito M, Mendoza CA, Chasmer L, Kettridge N, Devito KJ. 2019. Opportunistic wetland formation on reconstructed landforms in a sub-humid climate: Influence of site and landscape-scale factors. *Wetlands Ecology and Management* DOI: 10.1007/s11273-019-09679-y

Lloyd AH, Duffy PA, Mann DH. 2013. Nonlinear responses of white spruce growth to climate variability in interior Alaska. *Canadian Journal of Forest Research* **43** (4): 331–343 DOI: 10.1139/cjfr-2012-0372

Locky DA, Bayley SE, Vitt DH. 2005. The vegetational ecology of black spruce swamps, fens, and bogs in southern boreal Manitoba, Canada. *Wetlands* **25** (3): 564–582 DOI: 10.1672/0277-5212(2005)025[0564:TVEOBS]2.0.CO;2

Loranty MM, Mackay DS, Ewers BE, Adelman JD, Kruger EL. 2008. Environmental Drivers of Spatial Variation in Whole-Tree Transpiration in an Aspen-Dominated Upland-to-Wetland Forest Gradient: SPATIAL TRANSPIRATION ACROSS AN ENVIRONMENTAL GRADIENT. *Water Resources Research* **44** (2) DOI: 10.1029/2007WR00627

Lu J, Sun G, McNulty SG, Amatya DM. 2005. A Comparison of Six Potential Evapotranspiration Methods for Regional Use in the Southeastern United States. *JAWRA Journal of the American Water Resources Association* **41** (3): 621–633 DOI: 10.1111/j.1752-1688.2005.tb03759.x

Lukenbach MC, Hokanson KJ, Devito KJ, Kettridge N, Petrone RM, Mendoza CA, Granath G, Waddington JM. 2017. Post-fire ecohydrological conditions at peatland margins in different hydrogeological settings of the Boreal Plain. *Journal of Hydrology* **548**: 741–753 DOI: 10.1016/j.jhydrol.2017.03.034

Mackay DS, Ewers BE, Cook BD, Davis KJ. 2007. Environmental drivers of evapotranspiration in a shrub wetland and an upland forest in northern Wisconsin. *Water Resources Research* **43** (3) DOI: 10.1029/2006WR005149

Malmström CM, Raffa KF. 2000. Biotic disturbance agents in the boreal forest: Considerations for vegetation change models. *Global Change Biology* **6** (S1): 35–48 DOI: 10.1046/j.1365-2486.2000.06012.x

Manabe S. 1969. Climate and the ocean circulation. *Monthly Weather Review* **97** (11): 739–774 DOI: 10.1175/1520-0493(1969)097<0739:CATOC>2.3.CO;2

Marshall I, Schut P, Ballard M. 1999. A national ecological framework for Canada: Attribute data. Ottawa, Ontario: Environmental Quality Branch, Ecosystems Science Directorate, Environment Canada and Research Branch. *Agriculture and Agri-Food Canada*

Mayner KM, Moore PA, Wilkinson SL, Petrone RM, Waddington JM. 2018. Delineating boreal plains bog margin ecotones across hydrogeological settings for wildfire risk management. *Wetlands Ecology and Management* **26** (6): 1037–1046 DOI: 10.1007/s11273-018-9636-5

McDonnell JJ. 2003. Where does water go when it rains? Moving beyond the variable source area concept of rainfall-runoff response. *Hydrological Processes* **17** (9): 1869–1875 DOI: 10.1002/hyp.5132

McDowell NG, Beerling DJ, Breshears DD, Fisher RA, Raffa KF, Stitt M. 2011. The interdependence of mechanisms underlying climate-driven vegetation mortality. *Trends in Ecology & Evolution* **26** (10): 523–532 DOI: 10.1016/j.tree.2011.06.003

McLeod MK, Daniel H, Faulkner R, Murison R. 2004. Evaluation of an enclosed portable chamber to measure crop and pasture actual evapotranspiration at small scale. *Agricultural Water Management* **67** (1): 15–34 DOI: 10.1016/j.agwat.2003.12.006

McNamara JP, Tetzlaff D, Bishop K, Soulsby C, Seyfried M, Peters NE, Aulenbach BT, Hooper R. 2011. Storage as a Metric of Catchment Comparison. *Hydrological Processes* **25** (21): 3364–3371 DOI: 10.1002/hyp.8113

McNaughton K, Jarvis P. 1983. Predicting effects of vegetation changes on transpiration and evaporation. *Water deficits and plant growth* **7**: 1–47

Meerveld HJT-v, McDonnell JJ. 2006. Threshold relations in subsurface stormflow: 2. The fill and spill hypothesis. *Water Resources Research* **42** (2) DOI: 10.1029/2004WR003800

Michaelian M, Hogg EH, Hall RJ, Arsenault E. 2011. Massive mortality of aspen following severe drought along the southern edge of the Canadian boreal forest. *Global Change Biology* **17** (6): 2084–2094 DOI: 10.1111/j.1365-2486.2010.02357.x

Millard SP. 2013. *EnvStats: An R package for environmental statistics*. Springer: New York.

Miller CA, Benscoter BW, Turetsky MR. 2015. The effect of long-term drying associated with experimental drainage and road construction on vegetation composition and productivity in boreal fens. *Wetlands Ecology and Management* **23** (5): 845 DOI: 10.1007/s11273-015-9423-5

Milly PCD. 1994. Climate, soil water storage, and the average annual water balance. *Water Resources Research* **30** (7): 2143–2156 DOI: 10.1029/94WR00586

Milly PCD, Dunne KA. 1994. Sensitivity of the Global Water Cycle to the Water-Holding Capacity of Land. *Journal of Climate* **7** (4): 506–526 DOI: 10.1175/1520-0442(1994)007<0506:SOTGWC>2.0.CO;2

Montaldo N, Oren R. 2018. Changing Seasonal Rainfall Distribution With Climate Directs Contrasting Impacts at Evapotranspiration and Water Yield in the Western Mediterranean Region. *Earth's Future* **6** (6): 841–856 DOI: 10.1029/2018EF000843

Muggeo VM. 2008. Segmented: An R package to fit regression models with broken-line relationships

Muggeo VMR. 2003. Estimating regression models with unknown break-points. *Statistics in Medicine* **22** (19): 3055–3071 DOI: 10.1002/sim.1545

Munro DS. 1979. Daytime energy exchange and evaporation from a wooded swamp. *Water Resources Research* **15** (5): 1259–1265 DOI: 10.1029/WR015i005p01259

Munro DS. 1986. On Forested Wetlands as Evaporators. *Canadian Water Resources Journal / Revue canadienne des ressources hydriques* **11** (1): 89–99 DOI: 10.4296/cwrj1101089

Mushet DM, Calhoun AJ, Alexander LC, Cohen MJ, DeKeyser ES, Fowler L, Lane CR, Lang MW, Rains MC, Walls SC. 2015. Geographically isolated wetlands: Rethinking a misnomer. *Wetlands* **35** (3): 423–431

Mwale D, Gan TY, Devito KJ, Mendoza CA, Silins U, Petrone R. 2009. Precipitation variability and its relationship to hydrologic variability in Alberta. *Hydrological Processes* **23** (21): 3040–3056 DOI: 10.1002/hyp.7415

Mwale D, Gan TY, Devito KJ, Silins U, Mendoza C, Petrone R. 2010. Regionalization of runoff variability of Alberta, Canada, by wavelet, independent component, empirical orthogonal function, and geographical information system analyses. *Journal of Hydrologic Engineering* **16** (2): 93–107

Nadeau T-L, Rains MC. 2007. Hydrological Connectivity Between Headwater Streams and Downstream Waters: How Science Can Inform Policy1. *JAWRA Journal of the American Water Resources Association* **43** (1): 118–133 DOI: 10.1111/j.1752-1688.2007.00010.x

Nazarbakhsh M, Ireson AM, Barr AG. 2020. Controls on evapotranspiration from jack pine forests in the Boreal Plains Ecozone. *Hydrological Processes* **34** (4): 927–940 DOI: 10.1002/hyp.13674

Noy-Meir I. 1973. Desert Ecosystems: Environment and Producers. *Annual Review of Ecology and Systematics* **4** (1): 25–51 DOI: 10.1146/annurev.es.04.110173.000325

Nwaishi F, Petrone RM, Price JS, Andersen R. 2015. Towards Developing a Functional-Based Approach for Constructed Peatlands Evaluation in the Alberta Oil Sands Region, Canada. *Wetlands* **35** (2): 211–225 DOI: 10.1007/s13157-014-0623-1

NWWG. 1997. *The Canadian Wetland Classification System.* National Wetlands Working Group. Wetlands Research Branch, University of Waterloo: Waterloo, Ont.

Oke TR. 1992. *Boundary Layer Climates.* Routledge: London; New York.

Padrón RS, Gudmundsson L, Greve P, Seneviratne SI. 2017. Large-Scale Controls of the Surface Water Balance Over Land: Insights From a Systematic Review and Meta-Analysis. *Water Resources Research* **53** (11): 9659–9678 DOI: 10.1002/2017WR021215

Pan Y, Birdsey RA, Phillips OL, Jackson RB. 2013. The Structure, Distribution, and Biomass of the World's Forests. *Annual Review of Ecology, Evolution, and Systematics* **44** (1): 593–622 DOI: 10.1146/annurev-ecolsys-110512-135914

Pangle LA, Gregg JW, McDonnell JJ. 2014. Rainfall seasonality and an ecohydrological feedback offset the potential impact of climate warming on evapotranspiration and groundwater recharge. *Water Resources Research* **50** (2): 1308–1321 DOI: 10.1002/2012WR013253

Paradis É, Rochefort L, Langlois M. 2015. The lagg ecotone: An integrative part of bog ecosystems in North America. *Plant Ecology* **216** (7): 999–1018

Park Y-I(, Spiecker H. 2005. Variations in the tree-ring structure of Norway spruce (Picea abies) under contrasting climates. *Dendrochronologia* **23** (2): 93–104 DOI: 10.1016/j.dendro.2005.09.002

Pasher J, Seed E, Duffe J. 2013. Development of boreal ecosystem anthropogenic disturbance layers for Canada based on 2008 to 2010 Landsat imagery. *Canadian Journal of Remote Sensing* **39** (1): 42–58 DOI: 10.5589/m13-007

Perez PJ, Castellvi F, Martínez-Cob A. 2008. A simple model for estimating the Bowen ratio from climatic factors for determining latent and sensible heat flux. *Agricultural and Forest Meteorology* **148** (1): 25–37 DOI: 10.1016/j.agrformet.2007.08.015

Peters RL, Balanzategui D, Hurley AG, von Arx G, Prendin AL, Cuny HE, Björklund J, Frank DC, Fonti P. 2018. RAPTOR: Row and position tracheid organizer in R. *Dendrochronologia* **47**: 10–16

Peters RL, Groenendijk P, Vlam M, Zuidema PA. 2015. Detecting long-term growth trends using tree rings: A critical evaluation of methods. *Global Change Biology* **21** (5): 2040–2054 DOI: 10.1111/gcb.12826

Petrone R, Devito K, Silins U, Mendoza C, Brown S, Kaufman S, Price J, others. 2008. Transient peat properties in two pond-peatland complexes in the sub-humid Western Boreal Plain, Canada. *Mires Peat* **3** (5): 1–13

Petrone R, Silins U, Devito K. 2007. Dynamics of evapotranspiration from a riparian pond complex in the Western Boreal Forest, Alberta, Canada. *Hydrological Processes* **21** (11): 1391–1401

Petrone RM, Chasmer L, Hopkinson C, Silins U, Landhäusser SM, Kljun N, Devito KJ. 2014. Effects of harvesting and drought on CO2 and H2O fluxes in an aspen-dominated western boreal plain forest: Early chronosequence recovery. *Canadian Journal of Forest Research* **45** (1): 87–100 DOI: 10.1139/cjfr-2014-0253

Pezeshki SR, DeLaune RD. 2012. Soil Oxidation-Reduction in Wetlands and Its Impact on Plant Functioning. *Biology* **1** (2): 196–221 DOI: 10.3390/biology1020196

Philben M, Kaiser K, Benner R. 2014. Does oxygen exposure time control the extent of organic matter decomposition in peatlands? *Journal of Geophysical Research: Biogeosciences* **119** (5): 897–909 DOI: 10.1002/2013JG002573

Phillips RW, Spence C, Pomeroy JW. 2011. Connectivity and runoff dynamics in heterogeneous basins. *Hydrological Processes* **25** (19): 3061–3075 DOI: 10.1002/hyp.8123

Pickell PD, Andison DW, Coops NC. 2013. Characterizations of anthropogenic disturbance patterns in the mixedwood boreal forest of Alberta, Canada. *Forest Ecology and Management* **304**: 243–253 DOI: 10.1016/j.foreco.2013.04.031

Plach JM, Petrone RM, Waddington JM, Kettridge N, Devito KJ. 2016. Hydroclimatic influences on peatland CO2 exchange following upland forest harvesting on the Boreal Plains. *Ecohydrology* **9** (8): 1590–1603 DOI: 10.1002/eco.1750

Porporato A, D'Odorico P, Laio F, Ridolfi L, Rodriguez-Iturbe I. 2002. Ecohydrology of water-controlled ecosystems. *Advances in Water Resources* **25** (8): 1335–1348

DOI: 10.1016/S0309-1708(02)00058-1

Price DT, Alfaro RI, Brown KJ, Flannigan MD, Fleming RA, Hogg EH, Girardin MP, Lakusta T, Johnston M, McKenney DW, et al. 2013. Anticipating the consequences of climate change for Canada's boreal forest ecosystems. *Environmental Reviews* **21** (4): 322–365 DOI: 10.1139/er-2013-0042

Price JS. 2003. Role and character of seasonal peat soil deformation on the hydrology of undisturbed and cutover peatlands. *Water Resources Research* **39** (9) DOI: 10.1029/2002WR001302

Pypker TG, Unsworth MH, Bond BJ. 2006. The role of epiphytes in rainfall interception by forests in the Pacific Northwest. II. Field measurements at the branch and canopy scale. *Canadian Journal of Forest Research* **36** (4): 819–832 DOI: 10.1139/x05-286

Rains MC, Leibowitz SG, Cohen MJ, Creed IF, Golden HE, Jawitz JW, Kalla P, Lane CR, Lang MW, McLaughlin DL. 2016. Geographically isolated wetlands are part of the hydrological landscape: Invited Commentary. *Hydrological Processes* **30** (1): 153–160 DOI: 10.1002/hyp.10610

Raney PA, Leopold DJ, Dovciak M, Beier CM. 2016. Hydrologic position mediates sensitivity of tree growth to climate: Groundwater subsidies provide a thermal buffer effect in wetlands. *Forest Ecology and Management* **379**: 70–80 DOI: 10.1016/j.foreco.2016.08.004

R Core Team. 2018. *R: A Language and Environment for Statistical Computing*. R Foundation for Statistical Computing: Vienna, Austria.

R Core Team. 2019. *R: A Language and Environment for Statistical Computing*. R Foundation for Statistical Computing: Vienna, Austria.

Redding T, Devito KJ. 2011. Aspect and soil textural controls on snowmelt runoff on forested Boreal Plain hillslopes. *Hydrology Research; London* **42** (4): 250–267 DOI: http://dx.doi.org.ezproxyd.bham.ac.uk/10.2166/nh.2011.162

Redding TE, Devito KJ. 2008. Lateral flow thresholds for aspen forested hillslopes on the Western Boreal Plain, Alberta, Canada. *Hydrological Processes* **22** (21): 4287–4300 DOI: 10.1002/hyp.7038

Redding TE, Devito KJ. 2010. Mechanisms and pathways of lateral flow on aspen-forested, Luvisolic soils, Western Boreal Plains, Alberta, Canada. *Hydrological Processes* **24** (21): 2995–3010 DOI: 10.1002/hyp.7710

Rice SK, Collins D, Anderson AM. 2001. Functional significance of variation in bryophyte canopy structure. *American Journal of Botany* **88** (9): 1568–1576 DOI: 10.2307/3558400

Riddell JT. 2008. Assessment of surface water-groundwater interaction at perched boreal wetlands, north-central Alberta.MSc Thesis, University of Alberta, Edmonton, Canada.

Rodriguez-Iturbe I. 2000. Ecohydrology: A hydrologic perspective of climate-soil-vegetation dynamies. *Water Resources Research* **36** (1): 3–9 DOI: 10.1029/1999WR900210

Rodriguez-Iturbe I, D'Odorico P, Laio F, Ridolfi L, Tamea S. 2007. Challenges in Humid Land Ecohydrology: Interactions of Water Table and Unsaturated Zone with Climate, Soil, and Vegetation. *Water Resources Research* **43** (9) DOI: 10.1029/2007WR006073

Rodriguez-Iturbe I, Porporato A, Laio F, Ridolfi L. 2001. Plants in water-controlled ecosystems: Active role in hydrologic processes and response to water stress: I. Scope and general outline. *Advances in Water Resources* **24** (7): 695–705 DOI: 10.1016/S0309-1708(01)00004-5

Rooney RC, Robinson DT, Petrone R. 2015. Megaproject reclamation and climate change. *Nature Climate Change* DOI: 10.1038/nclimate2719

Rosenberry DO, Winter TC. 1997. Dynamics of water-table fluctuations in an upland between two prairie-pothole wetlands in North Dakota. *Journal of Hydrology* **191** (1): 266–289 DOI: 10.1016/S0022-1694(96)03050-8

Rydin H, Jeglum JK, Hooijer A. 2006. *The biology of peatlands*. Oxford University Press: Oxford ; New York.

Sanderson PL, Armstrong W. 1978. Soil waterlogging, root rot and conifer windthrow: Oxygen deficiency or phytoxicity? *Plant and Soil* **49** (1): 185–190 DOI: 10.1007/BF02149920

Schneider RR, Devito K, Kettridge N, Bayne E. 2016. Moving beyond bioclimatic envelope models: Integrating upland forest and peatland processes to predict ecosystem transitions under climate change in the western Canadian boreal plain. *Ecohydrology* **9** (6): 899–908 DOI: 10.1002/eco.1707

Schulze E-D, Hall AE. 1982. Stomatal Responses, Water Loss and CO2 Assimilation Rates of Plants in Contrasting Environments. In *Physiological Plant Ecology II: Water Relations and Carbon Assimilation*, Lange OL„ Nobel PS„ Osmond CB„ Ziegler H (eds).Springer Berlin Heidelberg: Berlin, Heidelberg; 181–230. DOI: 10.1007/978-3-642-68150-9_8

Sevanto S, Mcdowell NG, Dickman LT, Pangle R, Pockman WT. 2014. How do trees die? A test of the hydraulic failure and carbon starvation hypotheses. *Plant, Cell & Environment* **37** (1): 153–161 DOI: 10.1111/pce.12141

Shaw DA, Pietroniro A, Martz LW. 2013. Topographic analysis for the prairie pothole region of Western Canada: TOPOGRAPHIC ANALYSIS FOR THE PRAIRIE POTHOLE REGION OF WESTERN CANADA. *Hydrological Processes*: n/a–n/a DOI: 10.1002/hyp.9409

Shaw DA, Vanderkamp G, Conly FM, Pietroniro A, Martz L. 2012. The Fill-Spill Hydrology of Prairie Wetland Complexes during Drought and Deluge. *Hydrological Processes* **26** (20): 3147–3156 DOI: 10.1002/hyp.8390

Shokri N, Lehmann P, Or D. 2009. Characteristics of evaporation from partially wettable porous media. *Water Resources Research* **45** (2) DOI: 10.1029/2008WR007185

Smerdon BD, Mendoza CA. 2010. Hysteretic freezing characteristics of riparian peatlands in the Western Boreal Forest of Canada. *Hydrological Processes* **24** (8): 1027–1038 DOI: 10.1002/hyp.7544

Smerdon BD, Devito KJ, Mendoza CA. 2005. Interaction of groundwater and shallow lakes on outwash sediments in the sub-humid Boreal Plains of Canada. *Journal of Hydrology* **314** (1): 246–262 DOI: 10.1016/j.jhydrol.2005.04.001

Smerdon BD, Mendoza CA, Devito KJ. 2008. Influence of subhumid climate and water table depth on groundwater recharge in shallow outwash aquifers. *Water Resources Research* **44** (8) DOI: 10.1029/2007WR005950

Smith R, Redding TE. 2012. Cumulative effects assessment: Runoff generation in snowmelt-dominated, montane and Boreal Plain catchments. *Streamline Watershed Management Bulletin* **15** (1): 24–34

Snedden JE. 2013a. The root distribution, architecture, transpiration and root sapflow dynamics of mature trembling aspen (Populus tremuloides) growing along a hillslope.PhD thesis, University of Alberta, Ann Arbor (Canada). DOI: 10.7939/R3N87374G

Snedden JE. 2013b. The root distribution, architecture, transpiration and root sapflow dynamics of mature trembling aspen (Populus tremuloides) growing along a hillslope. *ERA* DOI: 10.7939/R3N87374G

Soil Classification Working Group. 1998. *The Canadian System of Soil Classification.* Agriculture and Agri-Food Canada Publication.

Soja AJ, Tchebakova NM, French NHF, Flannigan MD, Shugart HH, Stocks BJ, Sukhinin AI, Parfenova EI, Chapin FS, Stackhouse PW. 2007. Climate-induced boreal forest change: Predictions versus current observations. *Global and Planetary Change* **56** (3): 274–296 DOI: 10.1016/j.gloplacha.2006.07.028

Speer JH. 2010. *Fundamentals of tree-ring research.* University of Arizona Press.

Spence C. 2007. On the relation between dynamic storage and runoff: A discussion on thresholds, efficiency, and function. *Water Resources Research* **43** (12) DOI: 10.1029/2006WR005645

Spence C. 2010. A paradigm shift in hydrology: Storage thresholds across scales influence catchment runoff generation. *Geography Compass* **4** (7): 819–833

Spence C, Phillips RW. 2015. Refining understanding of hydrological connectivity in a boreal catchment. *Hydrological Processes* **29** (16): 3491–3503 DOI: 10.1002/hyp.10270

Spence C, Woo M-k. 2003. Hydrology of Subarctic Canadian Shield: Soil-Filled Valleys. *Journal of Hydrology* **279** (1): 151–166 DOI: 10.1016/S0022-1694(03)00175-6

Spence C, Guan XJ, Phillips R. 2011. The Hydrological Functions of a Boreal Wetland. *Wetlands* **31** (1): 75–85 DOI: 10.1007/s13157-010-0123-x

Sperry JS, Adler FR, Campbell GS, Comstock JP. 1998. Limitation of plant water use by rhizosphere and xylem conductance: Results from a model. *Plant, Cell & Environment* **21** (4): 347–359 DOI: 10.1046/j.1365-3040.1998.00287.x

Sperry JS, Hacke UG, Pittermann J. 2006. Size and function in conifer tracheids and angiosperm vessels. *American Journal of Botany* **93** (10): 1490–1500 DOI: 10.3732/ajb.93.10.1490

Strilesky SL, Humphreys ER. 2012. A comparison of the net ecosystem exchange of carbon dioxide and evapotranspiration for treed and open portions of a temperate peatland. *Agricultural and Forest Meteorology* **153**: 45–53 DOI: 10.1016/j.agrformet.2011.06.006

Strong WL, Roi GHL. 1983. Root-system morphology of common boreal forest trees in Alberta, Canada. *Canadian Journal of Forest Research* **13** (6): 1164–1173 DOI: 10.1139/x83-155

Taylor CH, Pierson DC. 1985. The effect of a small wetland on runoff response during spring snowmelt. *Atmosphere-Ocean* **23** (2): 137–154 DOI: 10.1080/07055900.1985.9649219

Thompson C, Mendoza CA, Devito KJ. 2017. Potential influence of climate change on ecosystems within the Boreal Plains of Alberta. *Hydrological Processes* **31** (11): 2110–2124 DOI: 10.1002/hyp.11183

Thompson C, Mendoza CA, Devito KJ, Petrone RM. 2015a. Climatic controls on groundwater-surface water interactions within the Boreal Plains of Alberta: Field observations and numerical simulations. *Journal of Hydrology* **527** (Supplement C): 734–746 DOI: 10.1016/j.jhydrol.2015.05.027

Thompson D, Wotton B, Waddington J, others. 2015b. Estimating the heat transfer to an organic soil surface during crown fire. *International Journal of Wildland Fire* **24**: 120–129

Thompson DK, Baisley AS, Waddington JM. 2015c. Seasonal variation in albedo and radiation exchange between a burned and unburned forested peatland: Implications for peatland evaporation. *Hydrological Processes* **29** (14): 3227–3235 DOI: 10.1002/hyp.10436

Thompson DK, Benscoter BW, Waddington JM. 2014. Water balance of a burned and unburned forested boreal peatland. *Hydrological Processes* **28** (24): 5954–5964 DOI: 10.1002/hyp.10074

Thompson SE, Harman CJ, Troch PA, Brooks PD, Sivapalan M. 2011. Spatial scale dependence of ecohydrologically mediated water balance partitioning: A synthesis framework for catchment ecohydrology. *Water Resources Research* **47** (10) DOI: 10.1029/2010WR009998

Thornton PE, Thornton MM, Mayer BW, Wei Y, Devarakonda R, Vose RS, Cook RB. 2017. Daymet: Daily Surface Weather Data on a 1-km Grid for North America, Version 3. *ORNL DAAC* DOI: 10.3334/ORNLDAAC/1328

Timoney KP. 2003. The changing disturbance regime of the boreal forest of the Canadian Prairie Provinces. *The Forestry Chronicle* **79** (3): 502–516 DOI: 10.5558/tfc79502-3

Todd AK, Buttle JM, Taylor CH. 2006. Hydrologic dynamics and linkages in a wetland-dominated basin. *Journal of Hydrology* **319** (1-4): 15–35 DOI: 10.1016/j.jhydrol.2005.05.001

Tóth J. 1963. A theoretical analysis of groundwater flow in small drainage basins. *Journal of Geophysical Research (1896-1977)* **68** (16): 4795–4812 DOI: 10.1029/JZ068i016p04795

Tuck SL, Phillips HRP, Hintzen RE, Scharlemann JPW, Purvis A, Hudson LN. 2014. MODISTools downloading and processing MODIS remotely sensed data in R. *Ecology and Evolution* **4** (24): 4658–4668 DOI: 10.1002/ece3.1273

Vaganov E. 1990. The tracheidogram method in tree-ring analysis and its application. *Methods of dendrochronology* **63**: 67

Vanderhoof MK, Alexander LC, Todd MJ. 2016. Temporal and spatial patterns of wetland extent influence variability of surface water connectivity in the Prairie Pothole Region, United States. *Landscape Ecology* **31** (4): 805–824 DOI: 10.1007/s10980-015-0290-5

van der Kamp G, Hayashi M. 2009. Groundwater-wetland ecosystem interaction in the semiarid glaciated plains of North America. *Hydrogeology Journal* **17** (1): 203 DOI: 10.1007/s10040-008-0367-1

Van Gardingen P, Grace J. 1991. Plants and Wind. In *Advances in Botanical Research*, Callow JA (ed.).Academic Press; 189–253. DOI: 10.1016/S0065-2296(08)60023-3

Van Huizen B, Petrone RM, Price JS, Quinton WL, Pomeroy JW. 2020. Seasonal ground ice impacts on spring ecohydrological conditions in a western boreal plains peatland. *Hydrological Processes* **34** (3): 765–779 DOI: 10.1002/hyp.13626

Vitt DH, Halsey LA, Bauer IE, Campbell C. 2000. Spatial and temporal trends in carbon storage of peatlands of continental western Canada through the Holocene. *Canadian Journal of Earth Sciences* **37** (5): 683–693

Vogwill R. 2005. Hydrogeological map of the Lesser Slave Lake area, Alberta, NTS 83O. (Map 119)

Volney WJA, Hirsch KG. 2005. Disturbing forest disturbances. *The Forestry Chronicle* **81** (5): 662–668 DOI: 10.5558/tfc81662-5

von Arx G, Carrer M. 2014. ROXAS A new tool to build centuries-long tracheid-lumen chronologies in conifers. *Dendrochronologia* **32** (3): 290–293 DOI: 10.1016/j.dendro.2013.12.001

von Arx G, Archer SR, Hughes MK. 2012. Long-term functional plasticity in plant hydraulic architecture in response to supplemental moisture. *Annals of Botany* **109** (6): 1091–1100 DOI: 10.1093/aob/mcs030

Waddington J, Morris P, Kettridge N, Granath G, Thompson D, Moore P. 2015. Hydrological Feedbacks in Northern Peatlands. *Ecohydrology* **8** (1): 113–127

Wang Q, Adiku S, Tenhunen J, Granier A. 2005. On the relationship of NDVI with leaf area index in a deciduous forest site. *Remote Sensing of Environment* **94** (2): 244–255 DOI: 10.1016/j.rse.2004.10.006

Warren RK, Pappas C, Helbig M, Chasmer LE, Berg AA, Baltzer JL, Quinton WL, Sonnentag O. 2018. Minor contribution of overstorey transpiration to landscape evapotranspiration in boreal permafrost peatlands. *Ecohydrology* **11** (5): e1975 DOI: 10.1002/eco.1975

Wells C, Ketcheson S, Price J. 2017. Hydrology of a wetland-dominated headwater basin in the Boreal Plain, Alberta, Canada. *Journal of Hydrology* **547** (Supplement C): 168–183 DOI: 10.1016/j.jhydrol.2017.01.052

White JC, Wulder MA, Hermosilla T, Coops NC, Hobart GW. 2017. A nationwide annual characterization of 25years of forest disturbance and recovery for Canada using Landsat time series. *Remote Sensing of Environment* **194**: 303–321 DOI: 10.1016/j.rse.2017.03.035

Whitlow TH, Harris RW. 1979. Flood Tolerance in Plants: A State-of-the-Art Review. California Univ Davis Dept of Environmental Horticulture.

Whitson IR, Chanasyk DS, Prepas EE. 2004. Patterns of water movement on a logged Gray Luvisolic hillslope during the snowmelt period. *Canadian Journal of Soil Science* **84** (1): 71–82 DOI: 10.4141/S02-081

Wilkinson SL, Moore PA, Flannigan MD, Wotton BM, Waddington JM. 2018. Did enhanced afforestation cause high severity peat burn in the Fort McMurray Horse River wildfire? *Environmental Research Letters* **13** (1): 014018 DOI: 10.1088/1748-9326/aaa136

Willier CN. 2017. Changes in peatland plant community composition and stand structure due to road induced flooding and desiccation.MSc Thesis, University of Alberta, Edmonton, Alberta, Canada. DOI: 10.7939/R3F18SV1G

Wilmking M, D'Arrigo R, Jacoby GC, Juday GP. 2005. Increased temperature sensitivity and divergent growth trends in circumpolar boreal forests. *Geophysical Research Letters* **32** (15) DOI: 10.1029/2005GL023331

Wing MKC from J, Weston S, Williams A, Keefer C, Engelhardt A, Cooper T, Mayer Z, Kenkel B, Team the RC, Benesty M, et al. 2019. *Caret: Classification and Regression Training*.

Winter TC. 1988. A conceptual framework for assessing cumulative impacts on the hydrology of nontidal wetlands. *Environmental Management* **12** (5): 605–620

Winter TC. 1999. Relation of streams, lakes, and wetlands to groundwater flow systems. *Hydrogeology Journal* **7** (1): 28–45

Winter TC. 2001. The Concept of Hydrologic Landscapes. *JAWRA Journal of the American Water Resources Association* **37** (2): 335–349 DOI: 10.1111/j.1752-1688.2001.tb00973.x

Woo M-K, Winter TC. 1993. The role of permafrost and seasonal frost in the hydrology of northern wetlands in North America. *Journal of Hydrology* **141** (1): 5–31 DOI: 10.1016/0022-1694(93)90043-9

Zhang L, Hickel K, Dawes WR, Chiew FHS, Western AW, Briggs PR. 2004. A rational function approach for estimating mean annual evapotranspiration. *Water Resources Research* **40** (2) DOI: 10.1029/2003WR002710

Zhang Y, Chen JM, Miller JR. 2005. Determining digital hemispherical photograph exposure for leaf area index estimation. *Agricultural and Forest Meteorology* **133** (1-4): 166–181 DOI: 10.1016/j.agrformet.2005.09.009

Ziaco E, Biondi F, Heinrich I. 2016. Wood Cellular Dendroclimatology: Testing New Proxies in Great Basin Bristlecone Pine. *Frontiers in Plant Science* **7** DOI: 10.3389/fpls.2016.01602

Zweifel R, Zimmermann L, Zeugin F, Newbery DM. 2006. Intra-annual radial growth and water relations of trees: Implications towards a growth mechanism. *Journal of Experimental Botany* **57** (6): 1445–1459 DOI: 10.1093/jxb/erj125